

MHD Turbulence: A Biased Review

Alexander A. Schekochihin[†]

Rudolf Peierls Centre for Theoretical Physics, University of Oxford,
Clarendon Laboratory, Parks Road, Oxford OX1 3PU, UK

Merton College, Oxford OX1 4JD, UK

(compiled on 10 November 2021)

This (self-contained and aspiring to pedagogy) review of scaling theories of MHD turbulence aims to put the developments of the last few years in the context of the canonical time line (from Kolmogorov to Iroshnikov–Kraichnan to Goldreich–Sridhar to Boldyrev). It is argued that Beresnyak’s (valid) objection that Boldyrev’s alignment theory, at least in its original form, violates the RMHD rescaling symmetry can be reconciled with alignment if the latter is understood as an intermittency effect. Boldyrev’s scalings, a version of which is recovered in this interpretation, and the concept of dynamic alignment (equivalently, local 3D anisotropy) are thus an example of a qualitative, physical theory of intermittency in a turbulent system. The emergence of aligned structures naturally brings into play reconnection physics and thus the theory of MHD turbulence becomes intertwined with the physics of tearing, current-sheet disruption and plasmoid formation. Recent work on these subjects by Loureiro, Mallet et al. is reviewed and it is argued that we may, as a result, finally have a reasonably complete picture of the MHD turbulent cascade all the way to the dissipation scale. This picture appears to reconcile Beresnyak’s results advocating the Kolmogorov scaling of the dissipation cutoff (as $\text{Re}^{3/4}$) with Boldyrev’s aligned cascade. It turns out also that these ideas open the door to some progress in understanding MHD turbulence without a mean field—MHD dynamo—whose saturated state is argued to be controlled by reconnection and to contain, at small scales, a tearing-mediated cascade very similar to its strong-mean-field counterpart (this is a new result). On the margins of this core narrative, standard weak-MHD-turbulence theory is argued to require some adjustment—and a scheme for such an adjustment is proposed—to take account of the determining part that a spontaneously emergent 2D condensate plays in mediating the Alfvén-wave cascade from a weakly-interacting state to a strongly turbulent (critically balanced) one. This completes the picture of the MHD cascade at large scales. A number of outstanding issues are surveyed, most of them concerning variants of MHD turbulence featuring various imbalances: between the two Elsasser fields (“cross-helicity”) or between velocity and magnetic field (“residual energy”); subviscous and decaying regimes of MHD turbulence (where reconnection again features prominently) are also reviewed under this heading. Some new, if tentative, ideas about these regimes are proposed along the way. Finally, it is argued that the natural direction of research is now away from the fluid MHD theory and into kinetic territory—and then, possibly, back again. The review lays no claim to objectivity or completeness, focusing on topics and views that the author finds most appealing at the present moment and leaving fair and balanced coverage to more disinterested observers of the field.

[†] Email: alex.schekochihin@physics.ox.ac.uk

CONTENTS

| | |
|---|----|
| 1. Introduction | 5 |
| PART I. A LONG ROAD TO KOLMOGOROV | 7 |
| 2. K41, IK and GS95 | 7 |
| 2.1. K41 | 7 |
| 2.2. IK | 8 |
| 2.3. GS95 | 9 |
| 3. Reduced MHD | 11 |
| 4. Weak MHD Turbulence | 14 |
| 4.1. WT is Irrelevant | 14 |
| 4.2. A Sketch of WT Theory | 15 |
| 4.3. Imbalanced WT | 16 |
| 4.4. 2D Condensate | 17 |
| 5. Critical Balance, Parallel Cascade, and Anisotropy | 19 |
| 5.1. Critical Balance | 19 |
| 5.2. Parallel Cascade | 20 |
| 5.3. Local, Scale-Dependent Anisotropy | 21 |
| 6. Dynamic Alignment, Perpendicular Cascade, and Intermittency | 24 |
| 6.1. Boldyrev's Alignment Hypothesis | 25 |
| 6.2. Plot Thickens | 27 |
| 6.3. Revised Model of Aligned MHD Turbulence | 29 |
| 6.3.1. Dimensional and RMHD-Symmetry Constraints | 29 |
| 6.3.2. Intermittency Matters! | 31 |
| 6.4. 3D Anisotropy | 34 |
| 6.5. Higher-Order Statistics | 36 |
| 7. MHD Turbulence Meets Reconnection | 37 |
| 7.1. Disruption by Tearing | 39 |
| 7.2. Tearing-Mediated Turbulence in the Disruption Range | 40 |
| 7.2.1. Dissipation Scale | 41 |
| 7.2.2. Spectrum in the Disruption Range | 42 |
| 7.2.3. Alignment in the Disruption Range | 43 |
| 7.2.4. Parallel Cascade in the Disruption Range | 44 |
| 7.3. Plasmoid Chains and Fast Reconnection in Tearing-Mediated Turbulence | 44 |
| 7.3.1. How Much Reconnection? | 44 |
| 7.3.2. Turbulence in Reconnecting Sheets | 46 |
| 7.4. Is This the End of the Road? | 47 |
| PART II. IMBALANCES AND LOOSE ENDS | 50 |
| 8. Imbalanced MHD Turbulence | 50 |
| 8.1. Story So Far | 50 |
| 8.1.1. Numerical and Observational Evidence | 52 |
| 8.1.2. Geometry and Types of Alignment | 55 |
| 8.1.3. Lithwick <i>et al.</i> (2007) | 57 |
| 8.1.4. Perez & Boldyrev (2009) | 57 |
| 8.1.5. Parallel Scales and Two Flavours of CB | 58 |
| 8.2. Towards a New Theory of Imbalanced MHD Turbulence | 59 |
| 8.2.1. Two Semi-Local Cascades | 60 |
| 8.2.2. Perpendicular Spectra | 61 |

| | |
|--|------------|
| 8.2.3. Parallel Spectra | 62 |
| 8.2.4. Pinning | 62 |
| 8.2.5. Alignment, Intermittency, Reconnection | 63 |
| 9. Residual Energy in MHD Turbulence | 64 |
| 9.1. Observational and Numerical Evidence | 64 |
| 9.2. Old Theories | 64 |
| 9.3. New Theories: Residual Energy in Weak MHD Turbulence | 65 |
| 9.4. New Theories: Residual Energy in Strong MHD Turbulence | 66 |
| 9.5. Summary | 68 |
| 10. Subviscous MHD Turbulence | 68 |
| 10.1. Viscous Cutoff | 69 |
| 10.2. Magnetic Fields at Subviscous Scales | 69 |
| 10.3. Velocity Field at Subviscous Scales | 71 |
| 10.4. Disruption by Tearing | 72 |
| 11. Decaying MHD Turbulence | 73 |
| 11.1. Towards Elsasser States | 73 |
| 11.2. Evolution of Large Scales and the Role of Invariants | 74 |
| 11.3. Decaying Helical MHD Turbulence | 75 |
| 11.4. Reconnection Takes Over Again? | 77 |
| 11.4.1. “Dimensional Reduction”: Is 3D Like 2D? | 79 |
| 11.4.2. Decaying Non-Helical MHD Turbulence | 79 |
| 11.4.3. Helical MHD Turbulence Revisited | 80 |
| 11.5. Self-Similar Decay | 80 |
| 11.6. Self-Similar Spectra and Inverse Energy Transfer | 81 |
| 11.7. Self-Similar Decay in RMHD | 82 |
| 11.8. Inertial-Range Spectra | 83 |
| 11.9. Summary | 83 |
| 12. MHD Dynamo Meets Reconnection | 84 |
| 12.1. Old Arguments About Saturated Dynamo at Large Pm | 85 |
| 12.2. Numerical Evidence: Reconnection Strikes Again | 86 |
| 12.3. Towards a New Theory of Reconnecting Dynamo | 90 |
| 12.3.1. Kinematic Dynamo and Onset of Tearing | 90 |
| 12.3.2. Self-Similar Dynamo | 91 |
| 12.3.3. Reconnecting Dynamo: Universality Regained | 91 |
| 12.4. Saturation Scenarios | 94 |
| 12.4.1. Multiscale Folds? | 94 |
| 12.4.2. Magnetoelastic Turbulence? | 96 |
| 12.4.3. Inverse Magnetic-Energy Transfer via Sporadic Decay? | 98 |
| 12.4.4. Local Shear Dynamo? | 100 |
| 13. Next Frontier: Kinetic Turbulence | 101 |
| 13.1. Sundry Microphysics at Low Collisionality | 101 |
| 13.2. Failed Cascades | 103 |
| 13.3. Phase-Space Turbulence | 103 |
| 13.4. Macro- and Microphysical Consequences of Pressure Anisotropy | 104 |
| 14. Conclusion | 106 |
| APPENDICES | 107 |
| Appendix A. Successes and Failures of WT Theory | 107 |
| A.1. RMHD in Scalar Form | 107 |
| A.2. Classic WT Calculation | 108 |

| | |
|---|------------|
| A.3. Solution of WT Equation | 109 |
| A.4. Case of Broad-Band Forcing: Spectral Continuity | 110 |
| A.5. Residual Energy in WT | 112 |
| A.6. Imbalanced WT | 114 |
| Appendix B. 2D Spectra of RMHD Turbulence | 115 |
| B.1. Determining δ | 116 |
| B.2. Determining γ | 116 |
| B.3. Determining β | 116 |
| B.4. Determining α | 117 |
| B.5. 2D Spectrum of WT | 118 |
| Appendix C. A Reconnection Primer | 119 |
| C.1. Tearing Instability | 119 |
| C.1.1. Outer Solution | 120 |
| C.1.2. Scaling of Δ' | 120 |
| C.1.3. Inner Solution | 122 |
| C.1.4. Peak Growth Rate and Wavenumber | 123 |
| C.1.5. Case of Arbitrary Scaling of Δ' | 125 |
| C.2. Onset of Nonlinearity and Saturation of the Tearing Mode | 125 |
| C.3. Sweet–Parker Sheet | 126 |
| C.3.1. Sweet–Parker Reconnection | 126 |
| C.3.2. Plasmoid Instability | 128 |
| C.4. Formation and Disruption of Sheets | 129 |
| C.4.1. “Ideal Tearing” | 130 |
| C.4.2. Recursive Tearing | 132 |
| C.4.3. Variants of Recursive Tearing | 135 |
| C.5. Fast MHD Reconnection | 137 |
| C.6. Stochastic Reconnection and MHD Turbulence | 139 |
| C.6.1. Stochastic Reconnection and GS95 Turbulence | 141 |
| C.6.2. Stochastic Reconnection and Aligned Turbulence | 141 |

... Oft turning others' leaves, to see if thence would flow
 Some fresh and fruitful showers upon my sunburn'd brain.
 But words came halting forth, wanting invention's stay;
 Invention, Nature's child, fled step-dame Study's blows;
 And others' feet still seemed but strangers in my way.
 Thus great with child to speak and helpless in my throes,
 Biting my truant pen, beating myself for spite,
 "Fool," said my Muse to me, "look in thy heart, and write."

Sir Philip Sidney, *Astrophil and Stella*

Nothing is more usual and more natural for those, who pretend to discover any thing new to the world in philosophy and sciences, than to insinuate the praises of their own systems, by decrying all those, which have been advanced before them.

David Hume, *A Treatise of Human Nature*

1. Introduction

At times during the last two decades, watching furious debates about the theory of MHD turbulence raging over increasingly technical and/or unfalsifiable issues, or working hard on minute refinements to existing results, one might have been forgiven for gradually losing interest. Is MHD turbulence to follow hydrodynamic (isotropic, homogeneous, Kolmogorov) turbulence and become a boutique field, ever more disconnected from the excitements of “real” physics? This perhaps is the fate of any successful theory (what more is there to be done?) or indeed of one that stalls for too long after initial breakthroughs (all the low-hanging fruit already picked?).

Most of the reasons for which I now find myself writing this piece with a degree of renewed enthusiasm emerged or crystallised in and since 2016-17. Enough has happened in these recent years for this text to be entirely different than it would have been had it been written before 2017; I do not think I could have said the same in any of the 5, perhaps nearly 10, years before that. The last significant conceptual breakthrough predating 2017 was the dynamic-alignment theory of [Boldyrev \(2006\)](#) (see § 6.1), which updated the previous decade's paradigm-changing theory of [Goldreich & Sridhar \(1995\)](#) (§ 5) and was followed by a flurry of numerical activity, sustaining the field for nearly 10 years. Some of the furious debates alluded to above had to do with the validity of this work—but in the absence of a new idea as to what might be going on dynamically, the insistence in a series of papers by [Beresnyak \(2011, 2012a, 2014b\)](#) that Boldyrev's theory failed at small scales (meeting with casual dismissal from Beresnyak's opponents and with amused indifference from the rest of the community) appeared doomed to be kicked into the long grass, waiting for ever bigger computers.¹

Simultaneously, the community has been showing increasing interest and investing increasing resources into studying the dissipation mechanisms in MHD turbulence—in particular, the role of spontaneously formed current sheets and associated local reconnection processes (this was pioneered a long time ago by [Matthaeus & Lamkin 1986](#) and [Politano *et al.* 1989](#), but has only recently bloomed into an active field: see references

¹[Beresnyak \(2011\)](#) did put forward an unassailable, if formal, theoretical objection, discussed in § 6.2, to Boldyrev's original interpretation of dynamic alignment as an angular uncertainty associated with field-line wandering. This interpretation is not, however, essential for the dynamic alignment itself to remain a feasible feature of the turbulent cascade ([Chandran *et al.* 2015](#); [Mallet & Schekochihin 2017](#)). I will put Beresnyak's objection to good use in a slightly revised model of the aligned cascade in § 6.3.

in §7). The most intriguing question (which, however, remained mostly unasked—in print—until 2017) surely had to be this: if Boldyrev’s MHD turbulence consisted of structures that were ever more aligned and so ever more sheet-like at small scales, was a scale eventually to be reached, given a broad enough inertial range, where these sheets would become too thin to stay stable and the reconnection processes known to disrupt such sheets would kick in?

Like Boldyrev’s theory, the full/quantitative realisation that large-aspect-ratio current sheets cannot survive also dates back to the first decade of the century, if one accepts that the trigger was the paper by Loureiro *et al.* (2007) on the plasmoid instability (see appendix C.3.2; as always, in retrospect, one can easily identify early precursors, notably Bulanov *et al.* 1978, 1979, Biskamp 1982, 1986 and Tajima & Shibata 1997). This, however, did not translate into a clear understanding of the disruption of *dynamically forming* sheets until the papers by Pucci & Velli (2014) and Uzdensky & Loureiro (2016) (which, in fact, had been around in preprint form since 2014, while PRL was undertaking its characteristically thorough deliberations on the potential impact of publishing it). Once this result was out, it did not take long (even so, it took surprisingly long) to apply it to Boldyrev’s aligning structures—it is this calculation (see §7), published in the twin papers by Mallet *et al.* (2017*b*) and Loureiro & Boldyrev (2017*b*), that, in my view, has pushed the theory of MHD turbulence forward far enough that it is now both closer to a modicum of logical completeness and ripe for a new review. The outcome appears to be that the Beresnyak vs. Boldyrev controversy is resolved (both are right, in a sense: see §7.2.1), Kolmogorov’s dissipation scale is back, in a somewhat unusual way (see §7.2), reconnection and turbulence have joined hands, and the modellers in love with current sheets has been vindicated and offered further scope for their modelling.

While emphasising this development as conceptually the most exciting amongst the recent ones, I will also take the opportunity presented by this review to discuss, in §4 and appendix A, my reservations about the standard version of weak Alfvén-wave turbulence theory and some ideas for how to fix (or interpret) it; to summarise, in §6.3, what I view as a set of rather pretty new ideas on the intermittency of aligned turbulence (Mallet *et al.* 2015, 2016; Chandran *et al.* 2015; Mallet & Schekochihin 2017); to explore some old ideas, and propose some new ones, on various imbalanced regimes of MHD turbulence (with cross-helicity, with residual magnetic energy, subviscous, decaying: see §§8–11—in the case of decaying turbulence, reconnection steals the limelight again); to offer an updated, if tentative, perspective on the saturated state of MHD dynamo—i.e., MHD turbulence with no mean field, which turns out also to be intertwined with reconnection (§12); and to advocate (in §13) a number of lines of further investigation focusing on plasma effects—some of which have started emerging in a particularly intriguing way during the last few years.

Because the subject of this review, if not exactly young, is still an active one and no one narrative has been settled as definitive, my exposition will be chronological, rather than logical, viz., I will discuss ideas that have proved to be wrong or incomplete before getting to those that as yet have not—not least because the latter were strongly influenced by, and would not have emerged without, the former. One day, there will be a much shorter story told in textbooks, with all intermediate steps forgotten. The erudites who already know this history, are uninterested in my prose and just want to skim the essential points and check out the new bits can start by reading §§6.3, 7, 8.2, 9.4, 10, 11.4–11.7, 12.3–12.4, and appendices A.4, B, C.4.2, and C.6.2.

Before proceeding, I would like, by way of a disclaimer, to stress the point that is already made in the title of this piece: this is a thoroughly biased review. Rather than merely peddling the truism that there is no such thing as an unbiased review of anything,

I am apologising here for this one drawing particularly heavily on published papers in which I myself participated. I hope that I might nonetheless be forgiven on the grounds that the lion's share of the credit for those contributions in fact belongs to my co-authors. Leaving to more disengaged spectators the task of assigning to these works their true measure of (in)significance, perhaps as minor flecks of colour on the vast canvas of MHD turbulence theory, I will instead present this subject as I see it at the moment, with those flecks in the foreground.

PART I

A Long Road to Kolmogorov

Omnes autem, quae in rerum natura contingunt, mutationes ita sunt comparatae, ut si quid alicui rei accedit, id alteri derogetur. [...] Quae naturae lex cum sit universalis, ideo etiam ad regulas motus extenditur...

M. V. Lomonosov, *Letter to L. Euler, 5 July 1748*²

2. K41, IK and GS95

The basic starting point for this discussion is to imagine a static, homogeneous plasma or, more generally, a conducting continuous medium, threaded by a uniform magnetic field. We can think of this situation as describing some local patch of a larger system, in which the magnetic field and other equilibrium parameters (density, pressure, flow velocity) are large-scale and structured in some system-dependent way. We are not going to be concerned with the question of what this large-scale structure is or how it is brought about—locally, it always looks like our homogeneous patch. Within this patch, we shall consider perturbations whose time and length scales are short compared to any length scales associated with that large-scale structure. Of course, such a local approximation is not entirely universal: we are putting aside the cases of strong shear, various stratified or rotating systems, etc.—or, to be precise, we are excluding from consideration perturbations that are sufficiently extended in space and/or time to “feel” these background gradients. Arguably, in an ideal asymptotic world inhabited by theoretical physicists, one can always go to scales small enough for this restriction to be justified, without hitting dissipation/microphysical scales first (in a real world, this is, regrettably, not always true, but let us understand the asymptotically idealised reality first). The only large-scale feature that does not thus go away at small scales is the magnetic field. This is what makes MHD turbulence *a priori* different from, for example, rotating or stratified turbulence, which, at small enough scales, always reverts to the universal Kolmogorov state (Nazarenko & Schekochihin 2011).

2.1. K41

Let us recall with maximum brevity what this Kolmogorov state is. Assume that energy is being pumped into the system at large scales and at some fixed rate ε . Then, in the inertial range (i.e., at small enough scales so the system is locally homogeneous but not small enough for viscosity or any other microphysics to matter yet), this same ε is the

²“All changes in nature occur in such a way that if anything is added anywhere, the same amount is subtracted from somewhere else. [...] As this is a universal law of nature, it extends to the laws of motion. . . .”—Lomonosov (1748).

constant energy flux from scale to scale. Assuming that the cascade (i.e., the passing of energy from scale to scale) is local, the energy spectrum is, by dimensional analysis,

$$E(k) \sim \varepsilon^{2/3} k^{-5/3}, \quad (2.1)$$

the famous Kolmogorov spectrum (Kolmogorov 1941*b*; henceforth K41), or, in terms of typical velocity increments between points separated by a distance λ :

$$\delta u_\lambda \sim (\varepsilon \lambda)^{1/3}. \quad (2.2)$$

This is all obvious because the dimensions of the quantities involved are

$$[\varepsilon] = \frac{U^3}{L}, \quad \left[\int dk E(k) \right] = [\delta u_\lambda^2] = U^2, \quad [k] = [\lambda^{-1}] = L^{-1}, \quad (2.3)$$

where U is a unit of velocity and L of length. As we will be dealing with an incompressible medium (which is always achievable by going to small enough scales and so to sufficiently subsonic motions), its density is an irrelevant constant, which we will ignore.

2.2. IK

It was Kraichnan (1965) who appears to have been the first to realise clearly the point made above about the irreducibility of the magnetic field. He therefore argued that, if the background uniform magnetic field \mathbf{B}_0 , which in velocity units is called the Alfvén speed,

$$v_A = \frac{B_0}{\sqrt{4\pi\rho_0}} \quad (2.4)$$

(ρ_0 is the mass density of the conducting medium), was to have a persistent (at small scales) role in the energy transfer from scale to scale, then the energy spectrum in the inertial range must be, again by dimensional analysis,

$$E(k) \sim (\varepsilon v_A)^{1/2} k^{-3/2} \quad \Leftrightarrow \quad \delta u_\lambda \sim (\varepsilon v_A \lambda)^{1/4}. \quad (2.5)$$

This is known as the Iroshnikov–Kraichnan spectrum (henceforth IK; figure 1).³ The scaling exponent was fixed by the requirement, put forward with the trademark combination of deep insight and slightly murky argumentation that one often finds in Kraichnan’s papers, that the Alfvén time $\tau_A \sim 1/kv_A$ was the typical time during which interactions would occur (before build-up of correlations was arrested by perturbations propagating away from each other), so the energy flux had to be proportional to τ_A and, therefore, to $1/v_A$ —thus requiring them to enter in the combination εv_A .⁴

Kraichnan’s prediction was viewed as self-evidently correct for 30 years, then wrong for 10 years (§ 5), then correct again (in a different sense) for another 10 years (§ 6), then had to be revised again, at small enough scales (§ 7). His own interpretation of it (which was also Iroshnikov’s, arrived at independently) was certainly wrong, as it was based on the

³Iroshnikov (1963) got the same result slightly earlier, by what one might view as an early weak-turbulence calculation (before weak turbulence was properly invented), involving treatment of Alfvén waves as quasiparticles, opportune closure assumptions and, in the end, dimensional analysis. No one appears to have noticed his paper at the time and he disappeared into Soviet obscurity. In later years, he worked at the Institute of Oceanology and died in 1991, aged 54.

⁴Another argument for the IK spectrum, perhaps less cryptic (but still wrong), is to posit constant flux, $\delta u_\lambda^2/\tau_c \sim \varepsilon$, where the cascade time is $\tau_c \sim \tau_{nl}^2/\tau_A$ as in (4.5), but, assuming isotropy, $\tau_{nl} \sim \lambda/\delta u_\lambda$, $\tau_A \sim \lambda/v_A$, so $\tau_c \sim \lambda v_A/\delta u_\lambda^2$ and (2.5) follows. Thus, the IK theory is the isotropic version of WT for MHD.



R. S. Iroshnikov (1937-1991)



R. H. Kraichnan (1928-2008)



P. Goldreich



S. Sridhar

FIGURE 1. IK and GS (photo of R. S. Iroshnikov courtesy of N. Lipunova and K. Bychkov, Sternberg Astronomical Institute; photo of R. H. Kraichnan courtesy of the AIP Emilio Segrè Visual Archives).

assumption—natural for a true Kolmogorovian susceptible to the great man’s universalist notion of “restoration of symmetries” at small scales, but, in retrospect, illogical in the context of proclaiming the unwaning importance of \mathbf{B}_0 at those same small scales—that turbulence sufficiently deep in the inertial range would be isotropic, i.e., that there is only one k to be used in the dimensional analysis. In fact, one both can and should argue that, *a priori*, there is a k_{\parallel} and a k_{\perp} , which represent the variation of the turbulent fields along and across \mathbf{B}_0 and need not be the same. The presence of the dimensionless ratio k_{\parallel}/k_{\perp} undermines the dimensional inevitability of (2.5) and opens up space for much theorising, inspired or otherwise.

2.3. GS95

Intuitively, in a strong magnetic field, perturbations with $k_{\parallel} \ll k_{\perp}$ should be more natural than isotropic ones, as the field is frozen into the motions but hard to bend. It turns out that MHD turbulence is indeed anisotropic in this way, at all scales, however small. This was realised quite early on, when the first, very tentative, experimental and numerical evidence started to be looked at (Robinson & Rusbridge 1971; Montgomery & Turner 1981; Shebalin *et al.* 1983), but, interestingly, it took more than a decade after that for the IK theory to be properly revised.

Dynamically, the parallel variation (on scale $l_{\parallel} \sim k_{\parallel}^{-1}$) is associated with the propaga-

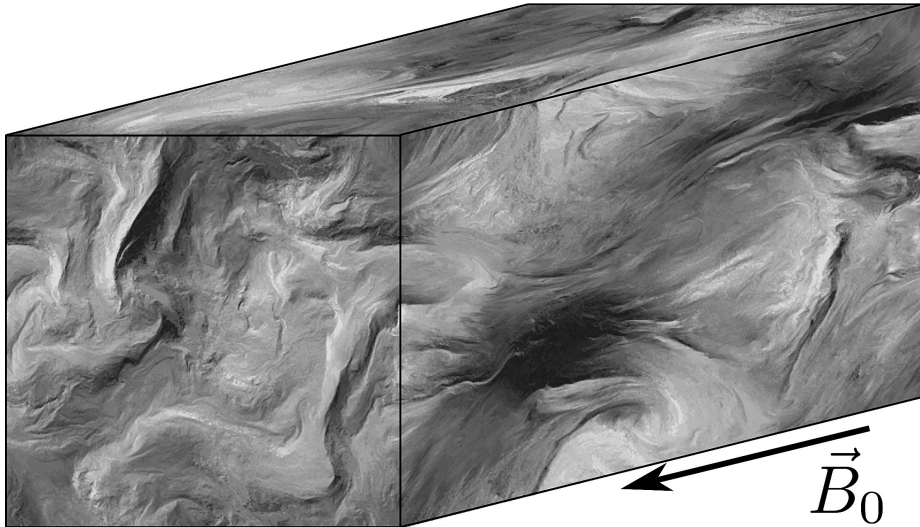


FIGURE 2. A visualisation of numerical RMHD turbulence, courtesy of A. Beresnyak (run R5 from Beresnyak 2012a, 1536³). The shades of grey represent the absolute value of $\mathbf{Z}_{\perp}^{+} = \mathbf{u}_{\perp} + \mathbf{b}_{\perp}$ (see §3).

tion of Alfvén (1942) waves, the wave period (or “propagation time”) being

$$\tau_A \sim \frac{l_{\parallel}}{v_A}, \quad (2.6)$$

and the perpendicular variation (on scale $\lambda \sim k_{\perp}^{-1}$) with nonlinear interactions, whose characteristic time is naïvely equal to

$$\tau_{\text{nl}} \sim \frac{\lambda}{\delta u_{\lambda}} \quad (2.7)$$

(we shall see in §6 why this is naïve). Here and below, δu_{λ} is used to represent the turbulent field on the grounds that, in Alfvénic perturbations, $\delta u_{\lambda} \sim \delta b_{\lambda}$, where δb is the magnetic perturbation in velocity units (see §3 for a discussion with equations). Declaring the two times comparable at all scales was an inspired conjecture by Goldreich & Sridhar (1995, 1997) (henceforth GS95; figure 1),⁵ which has come to be known as the *critical balance* (CB). I shall discuss the physical reasons for it properly in §§4 and 5, but here let me just postulate it. Then, naturally, the “cascade time” (i.e., the typical time to transfer energy from one perpendicular scale λ to the next) must be of the same order as either of the two other times:

$$\tau_c \sim \tau_A \sim \tau_{\text{nl}}. \quad (2.8)$$

If (2.7) is used for τ_{nl} , then (2.8) obviates the magnetic field and returns us to the K41 scaling (2.2), viz.,

$$\frac{\delta u_{\lambda}^2}{\tau_c} \sim \varepsilon, \quad \tau_c \sim \tau_{\text{nl}} \sim \frac{\lambda}{\delta u_{\lambda}} \quad \Rightarrow \quad \delta u_{\lambda} \sim (\varepsilon \lambda)^{1/3} \quad \Leftrightarrow \quad E(k_{\perp}) \sim \varepsilon^{2/3} k_{\perp}^{-5/3}. \quad (2.9)$$

This anisotropic version of K41 is known as the Goldreich–Sridhar (or GS95) spectrum.

⁵Anticipated, in fact, by Higdon (1984), who did not quite connect the dots, but, in retrospect, deserves more credit than he is getting.

Simultaneously, *along* the field,⁶ the velocity increments must satisfy

$$\frac{\delta u_{\parallel}^2}{\tau_c} \sim \varepsilon, \quad \tau_c \sim \tau_A \sim \frac{l_{\parallel}}{v_A} \quad \Rightarrow \quad \delta u_{\parallel} \sim \left(\frac{\varepsilon l_{\parallel}}{v_A} \right)^{1/2}. \quad (2.10)$$

Thus, \mathbf{B}_0 's influence does persist, but its size enters only the parallel scaling relations, not the perpendicular ones. Formally speaking, (2.9) is just the K41 dimensional argument for the perpendicular scale λ , with the CB conjecture used to justify not including v_A and l_{\parallel} amongst the local governing parameters. The assumption is that the sole role of \mathbf{B}_0 is to set the value of l_{\parallel} for any given λ : comparing (2.9) and (2.10), we get

$$l_{\parallel} \sim v_A \varepsilon^{-1/3} \lambda^{2/3}. \quad (2.11)$$

Physically, this l_{\parallel} is the distance that an Alfvénic pulse travels along the field, at speed v_A , over the time τ_{nl} , given by (2.7), that it takes a turbulent perturbation of size λ to break up nonlinearly. It is natural to argue, by causality, that this is the maximum distance over which any perturbation can remain correlated (Boldyrev 2005; Nazarenko & Schekochihin 2011).

This narrative arc brings us approximately to the state of affairs in mid-1990s, although the GS95 theory did not really become mainstream until the early years of this century—and soon had to be revised. Before I move on to discussing this revision (§6) and the modern state of the subject, I would like to put the discussion of what happens dynamically and how CB is achieved on a slightly less hand-waving basis than I have done so far. Indeed, why critical balance? *Pace* the causality argument, which sets the maximum l_{\parallel} , why can l_{\parallel} not be shorter? Is the nonlinear-time estimate (2.7), crucial for the scaling (2.9), justified? What happens dynamically?

From this point on, my exposition will be more sequential, I will avoid jumping ahead to the highlights and adopt a more systematic style, rederiving carefully some of the results reviewed in this section (an already well educated—or impatient—reader is welcome to skip or skim forward at her own pace).

3. Reduced MHD

The theoretical assumption (or numerical/observational evidence) that MHD turbulence consists of perturbations that have $k_{\perp} \gg k_{\parallel}$ but that their Alfvénic propagation remains important (so as to allow CB should the system want to be in it) leads to the following set of equations for these perturbations:

$$\partial_t \mathbf{Z}_{\perp}^{\pm} \mp v_A \nabla_{\parallel} \mathbf{Z}_{\perp}^{\pm} + \mathbf{Z}_{\perp}^{\mp} \cdot \nabla_{\perp} \mathbf{Z}_{\perp}^{\pm} = -\nabla_{\perp} p + \eta \nabla_{\perp}^2 \mathbf{Z}_{\perp}^{\pm} + \mathbf{f}^{\pm}. \quad (3.1)$$

These are evolution equations for the Elsasser (1950) fields $\mathbf{Z}_{\perp}^{\pm} = \mathbf{u}_{\perp} \pm \mathbf{b}_{\perp}$, where \mathbf{u}_{\perp} is the fluid velocity perpendicular to the equilibrium field \mathbf{B}_0 , and \mathbf{b}_{\perp} is the magnetic-field perturbation, also perpendicular to \mathbf{B}_0 and expressed in velocity units, i.e., scaled to $\sqrt{4\pi\rho_0}$. The total pressure p (which includes the magnetic pressure) is determined by the condition that $\nabla_{\perp} \cdot \mathbf{Z}_{\perp}^{\pm} = 0$, enforcing the solenoidality of the magnetic field and the incompressibility of the motions, the latter achieved at small enough scales by small enough perturbations. Namely, p is the solution of

$$\nabla_{\perp}^2 p = -\nabla_{\perp} \nabla_{\perp} : \mathbf{Z}_{\perp}^+ \mathbf{Z}_{\perp}^-, \quad (3.2)$$

⁶It turns out that this has to be along the exact, perturbed field rather than the mean field (Cho & Vishniac 2000; Maron & Goldreich 2001)—see §5.3.

which amounts to multiplying the nonlinear term on the left-hand side of (3.1) by a projection operator in Fourier space. I have, for simplicity, taken the kinematic viscosity and magnetic diffusivity η to be the same (but will relax this assumption from §6.3 onwards). The last term in equation (3.1), the body force \mathbf{f}^\pm , stands in for any energy-injection mechanism that this small-scale approximation might inherit from the non-universal large scales.

The *Reduced MHD equations* (3.1–3.2) (RMHD, first proposed by Strauss 1976, but, as often happened in those days, found independently by the Soviets, Kadomtsev & Pogutse 1974), which also have a compact scalar form (see appendix A.1), can be derived from the standard compressible MHD equations by ordering all perturbations of the equilibrium to be comparable to the Mach number and to $k_\parallel/k_\perp \ll 1$ and the rate of change of these perturbations to the Alfvén frequency $k_\parallel v_A$ (see Schekochihin & Cowley 2007 or Schekochihin 2020; a number of similar, if ever so subtly different, schemes exist: see review by Oughton *et al.* 2017 and references therein). These equations, apart from the visco-resistive terms, are, in fact, more general than the collisional MHD approximation and apply also to low-frequency, long-wavelength collisionless perturbations near a gyrotropic equilibrium (Schekochihin *et al.* 2009; Kunz *et al.* 2015),⁷ which makes them applicable to the solar wind (notable for being thoroughly measurable) and many other, more remote, astrophysical plasmas (only measurable with difficulty, but endlessly fascinating to large numbers of curious researchers in gainful employment).

While, like any nonlinear equations of serious consequence, they are impossible to solve except in trivial special cases, the RMHD equations possess a number of remarkable properties that form the basis for all theories of their turbulent solutions.

(i) The perturbations described by them, known as *Alfvénic*, are nonlinear versions of (packets of) Alfvén waves: perturbations of velocity and magnetic field transverse to \mathbf{B}_0 and propagating at speed v_A along it (\mathbf{Z}_\perp^+ in the \mathbf{B}_0 direction, \mathbf{Z}_\perp^- in the $-\mathbf{B}_0$ direction). They are entirely decoupled from all other perturbations (compressive in the case of fluid MHD, kinetic for a collisionless plasma; see Schekochihin *et al.* 2009 and Kunz *et al.* 2015) and can be considered in isolation from them. If evolved via full compressible MHD equations, these Alfvénic perturbations do not generate motions or fields that violate the $k_\parallel \ll k_\perp$ assumption (e.g., higher-frequency fast MHD waves), so RMHD appears to be well posed in the sense that it does not break the assumptions that it is based on (this was checked numerically by Cho & Lazarian 2002, 2003, who trod in the footsteps of Matthaeus *et al.* 1996).

(ii) Only counterpropagating fields interact, so the nonlinearity vanishes if either $\mathbf{Z}_\perp^+ = 0$ or $\mathbf{Z}_\perp^- = 0$, giving rise to the so-called Elsasser states ($\mathbf{u}_\perp = \mp \mathbf{b}_\perp$), exact nonlinear solutions that are arbitrary-amplitude, arbitrary-shape pulses travelling along \mathbf{B}_0 at the velocity $\mp v_A$.

(iii) The energies of the two Elsasser fields are conserved individually (apart from any injection and dissipation terms), viz.,

$$\frac{\partial}{\partial t} \frac{\langle |\mathbf{Z}_\perp^\pm|^2 \rangle}{2} = \varepsilon^\pm - \eta \langle |\nabla_\perp \mathbf{Z}_\perp^\pm|^2 \rangle. \quad (3.3)$$

The energy fluxes $\varepsilon^\pm = \langle \mathbf{Z}_\perp^\pm \cdot \mathbf{f}^\pm \rangle$ need not be the same and their ratio $\varepsilon^+/\varepsilon^-$ is, in general, a parameter of the problem—when it is different from unity, the turbulence is

⁷At high β , the amplitudes of these perturbations have to be small enough in order not to run afoul of some rather interesting and only recently appreciated spoiler physics (Squire *et al.* 2016, 2017*b*, *a*, 2019; Tenerani *et al.* 2017; Tenerani & Velli 2018)—§13.4.

called *imbalanced* (§ 8). Another way of framing (3.3) is by stating that RMHD has two invariants, the *total energy* and the *cross-helicity*:

$$\frac{\langle |\mathbf{u}_\perp|^2 + |\mathbf{b}_\perp|^2 \rangle}{2} = \frac{\langle |\mathbf{Z}_\perp^+|^2 + |\mathbf{Z}_\perp^-|^2 \rangle}{4}, \quad \langle \mathbf{u}_\perp \cdot \mathbf{b}_\perp \rangle = \frac{\langle |\mathbf{Z}_\perp^+|^2 - |\mathbf{Z}_\perp^-|^2 \rangle}{4}, \quad (3.4)$$

respectively (so imbalanced turbulence is turbulence with non-zero cross-helicity). The name of the second invariant has topological origins, alluding, in incompressible 3D MHD, to conservation of linkages between flux tubes and vortex tubes; in the context of small Alfvénic perturbations of a strong uniform mean field \mathbf{B}_0 , this does not appear to be a useful interpretation.

(iv) The amplitudes \mathbf{Z}_\perp^\pm , time and the gradients can be arbitrarily but simultaneously rescaled: $\forall \epsilon$ and a ,

$$\mathbf{Z}_\perp^\pm \rightarrow \epsilon \mathbf{Z}_\perp^\pm, \quad \mathbf{f}^\pm \rightarrow \frac{\epsilon^2}{a} \mathbf{f}^\pm, \quad \nabla_\perp \rightarrow \frac{1}{a} \nabla_\perp, \quad \nabla_\parallel \rightarrow \frac{\epsilon}{a} \nabla_\parallel, \quad t \rightarrow \frac{a}{\epsilon} t, \quad \eta \rightarrow \epsilon a \eta. \quad (3.5)$$

This means that \mathbf{Z}_\perp^\pm and ∇_\parallel are, formally speaking, infinitesimal compared to v_A and ∇_\perp , respectively (perpendicular and parallel distances in RMHD are measured “in different units,” as are the Alfvén speed and \mathbf{Z}_\perp^\pm). Any statistical scalings or heuristic theories must respect this symmetry (Beresnyak 2011, 2012a)—this requirement will feature prominently in § 6.3.

(v) Defining field increments

$$\delta \mathbf{Z}_\lambda^\pm = \mathbf{Z}_\perp^\pm(\mathbf{r} + \boldsymbol{\lambda}) - \mathbf{Z}_\perp^\pm(\mathbf{r}), \quad (3.6)$$

where $\boldsymbol{\lambda}$ is a point-separation vector in the perpendicular plane, assuming statistical isotropy in this plane and considering separations $\lambda = |\boldsymbol{\lambda}|$ belonging to the inertial range (i.e., smaller than the energy-injection scale but greater than the viscous/resistive scale), one finds, in a statistical steady state,⁸

$$\langle \delta Z_L^\mp | \delta \mathbf{Z}_\lambda^\pm|^2 \rangle = -2\epsilon^\pm \lambda, \quad (3.7)$$

where $\delta Z_L^\mp = \delta \mathbf{Z}_\lambda^\mp \cdot \boldsymbol{\lambda} / \lambda$ is the “longitudinal” increment. These exact laws are the RMHD version of the exact third-order laws that one always gets for turbulent systems with a convective nonlinearity, resembling the Kolmogorov (1941a) 4/5 law of hydrodynamic turbulence or (in fact, more closely) the Yaglom (1949) 4/3 law for a passive field (because in RMHD, \mathbf{Z}_\perp^+ advects \mathbf{Z}_\perp^- and vice versa). They were derived for incompressible MHD by Politano & Pouquet (1998a,b) assuming spatial isotropy and, isotropy having become untenable, adjusted to their RMHD form (3.7) by Boldyrev *et al.* (2009). They provide a useful (although not as restrictive as one might have hoped) analytical benchmark for any aspiring scaling theory of RMHD turbulence, weak or strong.

Everything in this review concerns turbulence that can be described by RMHD equations, the only exceptions being § 13, where the limitations of the fluid description and the importance of kinetic effects are discussed, parts of § 11, concerned with various types of decaying MHD turbulence, where energy-containing scales are the main object of study, and § 12, which deals with turbulent dynamo—a situation in which \mathbf{b}_\perp is

⁸Write an evolution equation for $\delta \mathbf{Z}_\lambda^\pm$ following directly from (3.1), take its scalar product with $\delta \mathbf{Z}_\lambda^\pm$ and average to get an evolution equation for the second-order structure function $\langle |\delta \mathbf{Z}_\lambda^\pm|^2 \rangle$, then throw out the viscous/resistive terms, assume steady state ($\partial_t = 0$), homogeneity (correlation functions depend on $\boldsymbol{\lambda}$ but not on \mathbf{r}) and isotropy in the perpendicular plane (scalar averaged quantities depend on $\lambda = |\boldsymbol{\lambda}|$ only), and, finally, integrate once with respect to λ .

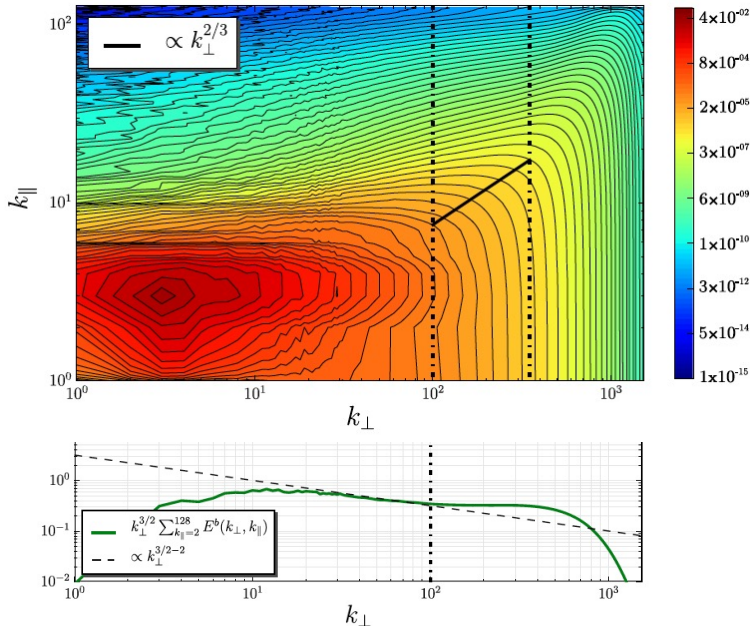


FIGURE 3. (Decaying) MHD simulation of transition from weak to strong turbulence by Meyrand *et al.* (2016): the upper panel shows the magnetic spectrum vs. k_{\parallel} and k_{\perp} (where k_{\parallel} is along the global mean field), the lower one the same integrated over k_{\parallel} and normalised by $k_{\perp}^{3/2}$ (see § 6 for why $k_{\perp}^{-3/2}$ rather than $k_{\perp}^{-5/3}$). A transition manifestly occurs from a k_{\perp}^{-2} to a $k_{\perp}^{-3/2}$ spectrum and, simultaneously, from a state with no k_{\parallel} cascade (and a relatively narrow-band parallel spectrum) to one consistent with a CB cascade (2D spectra of CB turbulence are worked out in appendix B).

emphatically not small compared to B_0 (there is no B_0) and so full MHD equations are needed.

4. Weak MHD Turbulence

Most theory in physics is perturbation theory. In turbulence, the available perturbation theory is the “weak-turbulence” (WT) approximation for wave-carrying systems. Its attraction is that it features a systematic derivation, an appealing interpretation of the turbulent system as a gas of weakly interacting quasiparticles, or “quantised” waves, and quantitative predictions for spectra, or occupation numbers, of these waves (see textbooks by Zakharov *et al.* 1992, Nazarenko 2011, Schekochihin 2020, or, for a quick recap, appendix A.2). Putting aside the question of whether the conditions necessary for it to hold are commonly (or ever) satisfied by natural turbulent systems, it is still interesting—and, arguably, also a matter of due diligence—to inquire whether such a regime, and such a theory, are relevant for our RMHD system. “Such a regime” means small amplitudes—small enough for the nonlinear interactions to occur very slowly compared to wave motion. One can certainly imagine, at least in principle, driving an RMHD system in a WT way, very gently.

4.1. WT is Irrelevant

On a broad-brush qualitative level, one can deal with this possibility as follows. Assume that in the energy-injection range, represented by some perpendicular scale L_{\perp} and some

parallel scale $L_{\parallel} = 2\pi/k_{\parallel}$, Alfvén waves are generated with amplitudes Z^{\pm} so small that

$$\omega_{\mathbf{k}}^{\pm} = \pm k_{\parallel} v_A = \frac{1}{\tau_A} \gg \frac{1}{\tau_{\text{nl}}^{\pm}} \sim \frac{Z^{\mp}}{L_{\perp}}. \quad (4.1)$$

If they are viewed as interacting quasiparticles (“+” can only interact with “−”, and vice versa), the momentum and energy conservation in a three-wave interaction require

$$\left. \begin{aligned} \mathbf{p} + \mathbf{q} &= \mathbf{k}, \\ \omega_{\mathbf{p}}^{\mp} + \omega_{\mathbf{q}}^{\pm} &= \omega_{\mathbf{k}}^{\pm} \end{aligned} \right\} \Rightarrow \quad q_{\parallel} = k_{\parallel}, \quad p_{\parallel} = 0. \quad (4.2)$$

Thus, three-wave interaction in fact involves a wave (\mathbf{q}) scattering off a 2D perturbation ($p_{\parallel} = 0$, not a wave) and becoming a wave (\mathbf{k}) with the same frequency ($k_{\parallel} = q_{\parallel}$) and a different perpendicular wavenumber ($\mathbf{k}_{\perp} = \mathbf{p}_{\perp} + \mathbf{q}_{\perp}$). Intuitively, there will be a cascade of the waves to higher k_{\perp} . If the amplitude of the waves does not fall off with k_{\perp} faster than k_{\perp}^{-1} , which is equivalent to their energy spectrum being less steep than k_{\perp}^{-3} , then the nonlinear-interaction time will become ever shorter with larger k_{\perp} , even as the waves’ k_{\parallel} and, therefore, their frequency stay the same. Eventually, at some perpendicular scale, which I shall call λ_{CB} , the condition $\tau_{\text{nl}} \gg \tau_A$ will be broken, so we end up with $\tau_{\text{nl}} \sim \tau_A$ and can return to considerations of the strong-turbulence regime, critical balance, etc. Numerically, this transition was first captured quite recently, by [Meyrand *et al.* \(2016\)](#), whose result is shown in figure 3.

The transition scale λ_{CB} is easy to estimate without the need for a specific WT theory. In view of (4.2), weak interactions cannot increase the characteristic parallel scale of the perturbations, which therefore remains L_{\parallel} . Then λ_{CB} is the perpendicular scale corresponding to $l_{\parallel} = L_{\parallel}$ in (2.11), viz.,

$$\lambda_{\text{CB}} \sim \varepsilon^{1/2} \left(\frac{L_{\parallel}}{v_A} \right)^{3/2}. \quad (4.3)$$

In fact, one does not even need to invoke the GS95 CB curve (2.11), because (4.3) is the only dimensionally correct possibility if one asks for a scale that depends on ε and $\tau_A \sim L_{\parallel}/v_A$ only [that L_{\parallel} and v_A must enter in this combination follows from the fact that ∇_{\parallel} and v_A only enter multiplying each other in the RMHD equations (3.1)].

A reader who is both convinced by this argument and regards it as grounds for dismissing the WT regime as asymptotically irrelevant, can at this point skip to §5. The rest of this section is for those restless souls who insist on worrying about what happens in weakly forced systems at $\lambda \gg \lambda_{\text{CB}}$.

4.2. A Sketch of WT Theory

A very simple heuristic WT calculation ([Ng & Bhattacharjee 1997](#); [Goldreich & Sridhar 1997](#))—a useful and physically transparent shortcut, and a good starting point for discussion—goes as follows.

Imagine two counterpropagating Alfvénic structures of perpendicular size λ and parallel coherence length L_{\parallel} (which cannot change in WT, as per the argument in §4.1) passing through each other and interacting weakly. Their transit time through each other is $\tau_A \sim L_{\parallel}/v_A$ and the change in their amplitudes during this time is

$$\Delta(\delta Z_{\lambda}^{\pm}) \sim \delta Z_{\lambda}^{\pm} \frac{\tau_A}{\tau_{\text{nl}}^{\pm}} \sim \frac{\delta Z_{\lambda}^{+} \delta Z_{\lambda}^{-}}{\lambda} \tau_A, \quad (4.4)$$

assuming $\tau_{\text{nl}}^{\pm} \sim \lambda/\delta Z_{\lambda}^{\mp}$. By definition of the WT regime, $\tau_{\text{nl}}^{\pm} \gg \tau_A$, so the amplitude

change in any one interaction is small, $\Delta(\delta Z_\lambda^\pm) \ll \delta Z_\lambda^\pm$, and many such interactions are needed in order to change the amplitude δZ_λ^\pm by an amount comparable to itself, i.e., to “cascade” the energy associated with scale λ to smaller scales. Suppose that interactions occur all the time and that the kicks (4.4) accumulate as a random walk. Then the cascade time is $\tau_c^\pm = N\tau_A$ if after N interactions the amplitude change is of order δZ_λ^\pm :

$$\Delta(\delta Z_\lambda^\pm)\sqrt{N} \sim \delta Z_\lambda^\pm \quad \Rightarrow \quad \frac{\tau_A}{\tau_{nl}^\pm} \sqrt{\frac{\tau_c^\pm}{\tau_A}} \sim 1 \quad \Rightarrow \quad \tau_c^\pm \sim \frac{(\tau_{nl}^\pm)^2}{\tau_A}. \quad (4.5)$$

The standard Kolmogorov constant-flux requirement gives

$$\varepsilon^\pm \sim \frac{(\delta Z_\lambda^\pm)^2}{\tau_c^\pm} \sim \frac{(\delta Z_\lambda^+)^2 (\delta Z_\lambda^-)^2 \tau_A}{\lambda^2}. \quad (4.6)$$

Assuming for the moment that $\varepsilon^+ \sim \varepsilon^-$ and, therefore, $\delta Z_\lambda^+ \sim \delta Z_\lambda^-$, gets us the classic WT scaling

$$\delta Z_\lambda \sim \left(\frac{\varepsilon}{\tau_A}\right)^{1/4} \lambda^{1/2} \quad \Leftrightarrow \quad E(k_\perp) \sim \left(\frac{\varepsilon}{\tau_A}\right)^{1/2} k_\perp^{-2}. \quad (4.7)$$

This scaling is indeed what one finds numerically (see figures 3 and 4)—it was first confirmed in early, semidirect simulations by Ng & Bhattacharjee (1997) and Bhattacharjee & Ng (2001), and then definitively by Perez & Boldyrev (2008) and Boldyrev & Perez (2009), leading the community to tick off WT as done and dusted.

As anticipated in § 4.1, with the scaling (4.7), the ratio of the time scales can only stay small above a certain finite scale:

$$\frac{\tau_A}{\tau_{nl}} \sim \frac{\tau_A \delta Z_\lambda}{\lambda} \sim \frac{\tau_A^{3/4} \varepsilon^{1/4}}{\lambda^{1/2}} \ll 1 \quad \Leftrightarrow \quad \lambda \gg \varepsilon^{1/2} \tau_A^{3/2} \sim \lambda_{CB}, \quad (4.8)$$

where λ_{CB} is transition scale anticipated in (4.3). For $\lambda \lesssim \lambda_{CB}$, turbulence becomes strong and, presumably, critically balanced. Thus, the WT cascade, by transferring energy to smaller scales, where nonlinear times are shorter, sows the seeds of its own destruction.

4.3. Imbalanced WT

What if $\varepsilon^+ \neq \varepsilon^-$, say, $\varepsilon^+ \gg \varepsilon^-$? (If $\varepsilon^+ > \varepsilon^-$ but both are of the same order, arguably the results obtained for $\varepsilon^+ \sim \varepsilon^-$ should still work, at least on the “twiddle” level.) Alas, (4.6) is obviously incapable of accommodating such a case, an embarrassment first noticed by Dobrowolny *et al.* (1980), who were attempting an IK-style, isotropic ($L_\parallel \sim \lambda$), imbalanced theory—quite wrong, as we now know (§ 2.3), but they correctly identified the issue with the imbalanced regime. They concluded that no imbalanced stationary state was possible except a pure Elsasser state. This may be true for (certain types of) decaying turbulence (see § 11.1), but is certainly not a satisfactory conclusion for a forced case where ε^\pm are externally prescribed.

A way out of this difficulty, various versions of which have been explored (Galtier *et al.* 2000; Lithwick & Goldreich 2003; Chandran 2008), is to accept (4.6) but notice that it allows the two Elsasser fields to have different scaling exponents, $\delta Z_\lambda^\pm \propto \lambda^{\gamma^\pm}$, as long as they satisfy $\gamma^+ + \gamma^- = 1$. The corresponding 2D spectra of the two fields are

$$E_{2D}^\pm(k_\perp, k_\parallel) = f^\pm(k_\parallel) k_\perp^{\mu^\pm}, \quad \mu^+ + \mu^- = -4, \quad (4.9)$$

because $\mu^\pm = -2\gamma^\pm - 1$ and, WT permitting no changes in k_\parallel , the scaling arguments of § 4.2 apply to each k_\parallel individually. One may then declare that the difference between ε^+ and ε^- is hidden in the prefactors $f^\pm(k_\parallel)$, which are non-universal, inaccessible to

“twiddle” scaling arguments about local interactions in the WT inertial range, and have to be fixed from outside it. At the large-scale end, one has to decide whether the outer scales for the two Elsasser fields are the same or different (Chandran 2008) and whether it is the fluxes ε^\pm or the fields’ energies at the outer scale(s) that it makes better sense to consider prescribed. At the dissipation scale, one has the option of “pinning” the spectra to the same value (an idea due to Grappin *et al.* 1983 and revived by Lithwick & Goldreich 2003), and it must also be decided whether the two fields are required to start feeling viscosity at the same scale or one can do so before the other (see discussion in Beresnyak & Lazarian 2008, and, for strong imbalanced turbulence, in §8.2.4). If WT breaks down before the dissipation scale is reached, some other set of *ad hoc* arrangements is required (see, e.g., Chandran 2008). Typically, the outcome is that the stronger field has a steeper spectrum than the weaker field, but their scalings are non-universal, i.e., they depend on the particular set up of the problem, at both macro- and micro-scales.

Another possibility is that (4.6) is wrong. Let me observe that the balanced ($\varepsilon^+ \sim \varepsilon^-$, $\delta Z_\lambda^+ \sim \delta Z_\lambda^-$) version of this scaling, i.e., the statement that the flux ε is proportional to the fourth power of the amplitude, is less likely to be wrong than any particular assignment of “+”s and “-”s to these amplitudes: all it says is that the flux is what it would have been in the case of strong interactions, $\sim \delta Z_\lambda^2 / \tau_{nl}$ [cf. (2.9)], times the first power of the expansion parameter τ_A / τ_{nl} , i.e., the lowest order that ε can be in a perturbation expansion in that parameter. Thus, one may doubt the validity of (4.6) for the imbalanced regime without rejecting the numerically confirmed k_\perp^{-2} scaling of the balanced spectra. For example, in the (heuristic) scheme proposed by Schekochihin *et al.* (2012),

$$\varepsilon^\pm \sim \frac{(\delta Z_\lambda^\pm)^3 \delta Z_\lambda^\mp \tau_A}{\lambda^2}, \quad (4.10)$$

which changes nothing for balanced WT, but leads to a very different situation in the imbalanced case than (4.6), allowing perfectly good k_\perp^{-2} spectra for both fields.

I do not go through all that in detail because, the WT regime being largely irrelevant (§4.1), it would also, if it really were non-universal, not be very interesting. If it is universal and something like (4.10) holds, that *is* interesting, but I do not know how to make much progress beyond Schekochihin *et al.* (2012), whose theory does not quite match simulations (see §4.4). I also do not know how to construct a theory of imbalanced WT that would connect smoothly to any believable theory of strong imbalanced turbulence (e.g., one presented in §8.2). An interested reader will find some further, equally unsatisfactory, observations in appendix A.6.

4.4. 2D Condensate

It follows from the discussion in §4.1 that the WT approximation in its standard form cannot, in fact, work for the turbulence of Alfvén waves, at least not formally, because in every three-wave interaction, one of the three waves is not a wave at all, but a zero-frequency 2D perturbation, for which the nonlinear interactions are the dominant influence. If such $k_\parallel = 0$ perturbations are forbidden, i.e., if displacements vanish at infinity, one must consider four-wave interactions (i.e., go to next order in τ_A / τ_{nl}), which gives rise to an apparently legitimate WT state, different from (4.7) (Sridhar & Goldreich 1994). There is no particular reason to think, however, that such a restriction on displacements is legitimate in a general physical situation (Ng & Bhattacharjee 1996) or, even if one starts with no energy at $k_\parallel = 0$, that such a state can be maintained, except in a box with field lines nailed down at the boundaries—failing such restrictions,

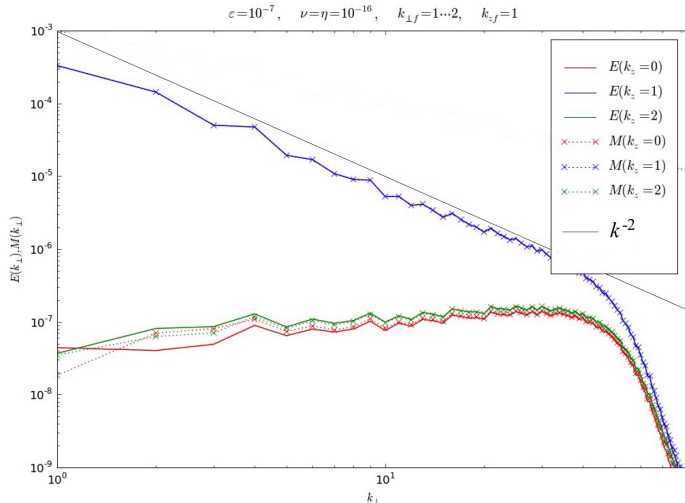


FIGURE 4. Kinetic (E , solid lines) and magnetic (M , dotted lines with crosses) energy spectra for $k_{\parallel} = 0$ (red), $k_{\parallel} = 2\pi/L_{\parallel}$ (blue) and $k_{\parallel} = 4\pi/L_{\parallel}$ (green) from an unpublished weak RMHD turbulence simulation by Yousef & Schekochihin (2009). The box size was $(L_{\perp}, L_{\parallel})$ in the parallel and perpendicular directions, respectively, and the forcing was narrow-band, at $k_{\parallel} = 2\pi/L_{\parallel}$ and $k_{\perp} = (1, 2) \times 2\pi/L_{\perp}$, deep in the WT regime ($L_{\perp} \gg \lambda_{\text{CB}}$). WT spectra for the case of broad-band forcing can be found in Perez & Boldyrev (2008) and Boldyrev & Perez (2009) and are discussed in appendix A.4.

a 2D “condensate” must emerge (and does, in numerical simulations: see Boldyrev & Perez 2009, Wang *et al.* 2011, Meyrand *et al.* 2015, 2016, and figure 4).

Mathematically, this becomes quite obvious if we represent the solutions to (3.1) as

$$\mathbf{Z}_{\perp}^{\pm}(t, \mathbf{r}) = \sum_{k_{\parallel}} \mathbf{Z}_{k_{\parallel}}^{\pm}(t, x, y) e^{ik_{\parallel}(z \pm v_{\text{A}} t)} \quad (4.11)$$

and separate the $k_{\parallel} = 0$ modes from the rest:

$$\partial_t \mathbf{Z}_0^{\pm} + \hat{\mathcal{P}} \mathbf{Z}_0^{\mp} \cdot \nabla_{\perp} \mathbf{Z}_0^{\pm} = - \sum_{k_{\parallel} \neq 0} \hat{\mathcal{P}} \mathbf{Z}_{k_{\parallel}}^{\mp} \cdot \nabla_{\perp} \mathbf{Z}_{-k_{\parallel}}^{\pm} e^{\mp i 2 k_{\parallel} v_{\text{A}} t}, \quad (4.12)$$

$$\partial_t \mathbf{Z}_{k_{\parallel}}^{\pm} + \hat{\mathcal{P}} \mathbf{Z}_0^{\mp} \cdot \nabla_{\perp} \mathbf{Z}_{k_{\parallel}}^{\pm} = - \sum_{p_{\parallel} \neq 0} \hat{\mathcal{P}} \mathbf{Z}_{p_{\parallel}}^{\mp} \cdot \nabla_{\perp} \mathbf{Z}_{k_{\parallel} - p_{\parallel}}^{\pm} e^{\mp i 2 p_{\parallel} v_{\text{A}} t}, \quad (4.13)$$

where $\hat{\mathcal{P}}$ is the projection operator that takes care of the pressure term [see (3.2)] and has been introduced for brevity; forcing and dissipation terms have been dropped. The first of these equations, (4.12), describes the condensate—two real fields $\mathbf{Z}_0^{\pm}(x, y)$ advecting each other in the 2D plane and subject to an oscillating “force” due to the mutual coupling of the Alfvén waves $\mathbf{Z}_{k_{\parallel}}^{\pm}$. These Alfvén waves, described by (4.13), are advected by the 2D field and also by each other, but the latter interaction has an oscillating factor and vanishes in the WT approximation. Even if only the Alfvén waves are forced and the condensate is not, the condensate will nevertheless be built up.

Returning to three-wave interactions then (where one of the waves is not a wave), the traditional approach has been to ignore the inapplicability of the WT approximation to the $k_{\parallel} = 0$ modes by conjecturing that the function $f^{\pm}(k_{\parallel})$ in (4.9) is flat around $k_{\parallel} = 0$ —the hypothesis of “spectral continuity”. One can then press on with putting

MHD through the WT analytical grinder, find an evolution equation for the spectra and show that it has steady-state, constant-flux solutions of the form (4.9). This is what was done in the now-classic paper by Galtier *et al.* (2000) (see appendices A.2 and A.3). In balanced turbulence, obviously, $\mu^+ = \mu^- = 2$, and we are back to (4.7).

Nazarenko (2007) argues that the hypothesis of spectral continuity is certainly false if the nonlinear broadening of the waves' frequencies, of order τ_{nl}^{-1} , is smaller than the linear frequency associated with the spacing of the k_{\parallel} "grid" ($= 2\pi/L_{\parallel}$, the inverse parallel "box" size)—i.e., if the Alfvénic perturbations at the longest finite parallel scale in the system are already in the WT limit (4.1), $v_A/L_{\parallel} \gg \tau_{\text{nl}}^{-1}$. He is right. Figure 4 is taken from a (sadly, unpublished) numerical study of weak RMHD turbulence by Yousef & Schekochihin (2009), who forced Alfvén waves at $k_{\parallel} = 2\pi/L_{\parallel}$, where L_{\parallel} was the box size. It shows that, while the k_{\perp}^{-2} scaling of the $k_{\parallel} = 2\pi/L_{\parallel}$ modes is undeniable, the spectra for all unforced modes ($k_{\parallel} = 0$ and $k_{\parallel} = \text{multiples of } 2\pi/L_{\parallel}$) are dramatically shallower. Similar spectra were reported by Bigot & Galtier (2011) and by Meyrand *et al.* (2015). Qualitatively similar spectra (and a simple mechanism for how they might form) were also proposed by Schekochihin *et al.* (2012)—but their theory fails quantitatively, with the spectra that it predicts for all unforced modes at least one power of k_{\perp} steeper than the numerical ones (e.g., their $k_{\parallel} = 0$ condensate has a $\propto k_{\perp}^{-1}$ spectrum, while simulations suggest $\propto k_{\perp}^0$).

Nazarenko (2007) expects that the conventional WT theory should survive when $k_{\parallel}v_A \gg \tau_{\text{nl}}^{-1} \gg v_A/L_{\parallel}$. This is a situation that should be realisable in a system that is weakly and randomly forced in a broad band of frequencies (and, therefore, parallel wavenumbers)—in appendix A.4, I discuss how, and in what sense, one might defend spectral continuity for such a system; I argue that the 2D condensate in this case is a strongly turbulent, critically balanced sub-system constantly fed by the weakly turbulent waves and developing a falsifiable set of scalings, which are, indeed, continuous with the WT scalings. While there are some indications (from the simulations by Wang *et al.* 2011; see appendix A.5) that these scalings might be right, I have not seen spectral continuity corroborated numerically in a definitive fashion, as even Perez & Boldyrev (2008) and Boldyrev & Perez (2009), who took great care to force in a broad band of k_{\parallel} to make sure the conventional WT theory did apply, saw a distinct dip in $f(k_{\parallel})$ at $k_{\parallel} = 0$, associated with an emergent condensate (which is magnetically dominated; see §9.3 and appendix A.5). The same was true in the decaying simulations of Meyrand *et al.* (2015, 2016, see upper panel of figure 3), where an initial small-amplitude (and so WT-compliant) state had the choice to evolve towards a continuous parallel spectrum, but refused to do so, again developing a $k_{\parallel} = 0$ condensate with dramatically distinct properties (including high degree of intermittency and a spectrum quite similar to figure 4).

Thus, the conventional WT theory is at best incomplete and at worst wrong. It is discussed further in appendix A, where I review the WT's derivation, speculate about the structure of the condensate, and discuss a number of other WT-related issues. Here, having flagged these issues, I want to halt this digression into matters that are, arguably, of little impact, and move on to the physics-rich core of the MHD-turbulence theory.

5. Critical Balance, Parallel Cascade, and Anisotropy

5.1. Critical Balance

Section 4 can be viewed as one long protracted justificatory piece in favour of critical balance: even if an ensemble of high-frequency Alfvén waves is stirred up very gently

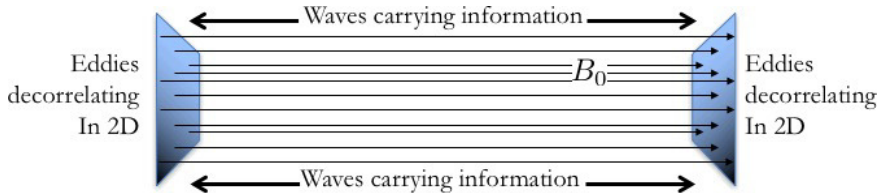


FIGURE 5. Critical balance in a (2+1)D system supporting both nonlinearity and waves (RMHD).

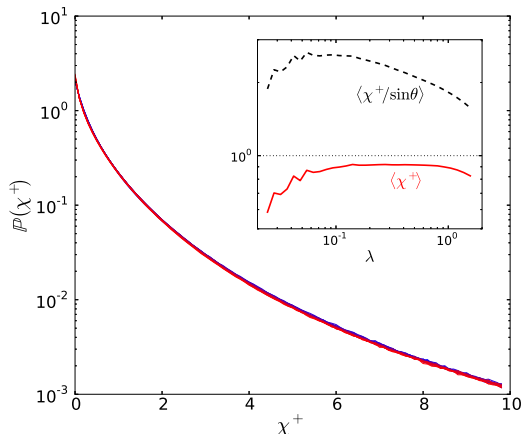


FIGURE 6. Refined critical balance: this figure, taken from Mallet *et al.* (2015), shows the probability density function (PDF) of the ratio $\chi^+ = \tau_A/\tau_{\text{nl}}^+$ with τ_{nl}^+ defined by (6.1). In fact, 17 PDFs are plotted here, taken at different scales within an approximately decade-wide inertial range (this was a 1024^3 RMHD simulation)—the corresponding lines are in colour shades from blue (smaller scales) to red (larger scales), but this is barely visible because the PDFs all collapse on top of each other. The inset shows that the self-similarity does not work if τ_{nl}^+ is defined without the alignment angle (see § 6).

($\tau_{\text{nl}} \gg \tau_A$), it will, at small enough scales, get itself into the strong-turbulence regime ($\tau_{\text{nl}} \sim \tau_A$). The opposite limit, a 2D regime with $\tau_{\text{nl}} \ll \tau_A$, is unsustainable for the very simple reason of causality: as information in an RMHD system propagates along \mathbf{B}_0 at speed v_A , no structure longer than $l_{\parallel} \sim v_A \tau_{\text{nl}}$ can be kept coherent and so will break up (see Boldyrev 2005, Nazarenko & Schekochihin 2011 and figure 5).

It is worth mentioning in passing that the CB turns out to be a very robust feature of the turbulence in the following interesting sense. With a certain appropriate definition of τ_{nl} (which will be explained in § 6.1), the ratio τ_A/τ_{nl} has been found (numerically) by Mallet *et al.* (2015) to have a scale-invariant distribution (figure 6), a property that they dubbed *refined critical balance (RCB)*. It gives a quantitative meaning to the somewhat vague statement $\tau_A/\tau_{\text{nl}} \sim 1$ —and becomes important in the (as it turns out, unavoidable) discussion of intermittency of MHD turbulence (§ 6.3.2).

5.2. Parallel Cascade

The most straightforward—and the least controversial—consequence of CB is the scaling of *parallel* increments. I have already derived this result in (2.10), but let me now restate it using Elsasser fields. If it is the case that the nonlinear-interaction time

and, therefore, the cascade time for Z_{\perp}^{\pm} are approximately the same as their propagation time $\tau_A \sim l_{\parallel}/v_A$, then the parallel increments $\delta Z_{l_{\parallel}}^{\pm}$ satisfy

$$\frac{(\delta Z_{l_{\parallel}}^{\pm})^2}{\tau_A} \sim \varepsilon^{\pm} \quad \Rightarrow \quad \delta Z_{l_{\parallel}}^{\pm} \sim \left(\frac{\varepsilon^{\pm} l_{\parallel}}{v_A} \right)^{1/2} \quad \Leftrightarrow \quad E^{\pm}(k_{\parallel}) \sim \frac{\varepsilon^{\pm}}{v_A} k_{\parallel}^{-2}. \quad (5.1)$$

Beresnyak (2012a, 2015) gives two rather elegant (and related) arguments in favour of the scaling (5.1), alongside robust numerical evidence presented in the latter paper.⁹ First, he argues that the scaling relation (5.1) can be obtained by dimensional analysis because the RMHD equations (3.1) stay invariant if v_A and $1/k_{\parallel}$ are scaled simultaneously [see (3.5)] and so these two quantities must always appear in the combination $k_{\parallel} v_A$ in scaling relations for any physical quantities—in the case of (5.1), energy, or field increment. Secondly, Beresnyak (2015) notes that following the structure of the fluctuating field (calculating its increments) along the field line (in the positive \mathbf{B}_0 direction) is the MHD equivalent of following its time evolution forward (for Z_{\perp}^{-}) or backward (for Z_{\perp}^{+}) in time and it should, therefore, be possible to infer the parallel spectrum (5.1) from the Lagrangian frequency spectrum of the turbulence. Estimating the energy flux as the rate of change of energy in a fluid element in the Lagrangian frame (i.e., excluding sweeping by large eddies), one obtains (Landau & Lifshitz 1987; Corrsin 1963)

$$\varepsilon^{\pm} \sim (\delta Z_{\tau}^{\pm})^2 \tau^{-1} \quad \Leftrightarrow \quad E^{\pm}(\omega) \sim \varepsilon^{\pm} \omega^{-2}, \quad (5.2)$$

where δZ_{τ}^{\pm} is the Lagrangian field increment over time interval τ . Then (5.1) is recovered from (5.2) by changing variables $\omega = k_{\parallel} v_A$ and letting $E^{\pm}(\omega) d\omega = E^{\pm}(k_{\parallel}) dk_{\parallel}$.

Thus, the parallel cascade and the associated scaling (5.1) appear to be a very simple and solid property of MHD turbulence. What happens in the perpendicular direction is a more complicated story.

5.3. Local, Scale-Dependent Anisotropy

Using instead of the parallel increments the perpendicular ones δZ_{λ}^{\pm} and substituting the nonlinear time

$$\tau_{\text{nl}}^{\pm} \sim \frac{\lambda}{\delta Z_{\lambda}^{\mp}} \quad (5.3)$$

for the cascade time, we recover (2.9):¹⁰

$$\begin{aligned} \frac{(\delta Z_{\lambda}^{\pm})^2}{\tau_{\text{nl}}^{\pm}} \sim \varepsilon^{\pm} &\Rightarrow \frac{\delta Z_{\lambda}^{+}}{\delta Z_{\lambda}^{-}} \sim \frac{\varepsilon^{+}}{\varepsilon^{-}}, \quad \delta Z_{\lambda}^{\pm} \sim (\tilde{\varepsilon}^{\pm} \lambda)^{1/3}, \quad \tilde{\varepsilon}^{\pm} \equiv \frac{(\varepsilon^{\pm})^2}{\varepsilon^{\mp}} \\ &\Rightarrow E^{\pm}(k_{\perp}) \sim (\tilde{\varepsilon}^{\pm})^{2/3} k_{\perp}^{-5/3}. \end{aligned} \quad (5.4)$$

⁹To be precise, the scaling he actually observes is closer to $k_{\parallel}^{-1.9}$, although he argues that this is a finite-resolution effect. Imperfect following of field lines might also conceivably be a factor. Meyrand *et al.* (2019), who followed field lines to a higher precision than that afforded by linear interpolation at every scale (see §5.3), found a rather good k_{\parallel}^{-2} scaling for the magnetic-field increments, but a slightly steeper slope for velocities—although that too may be a finite-resolution issue.

¹⁰Cf. Lithwick *et al.* (2007), the imbalanced version of the GS95 scalings (§8.1.3). This and especially whether the parallel correlations obey (5.5) is by no means uncontroversial. I am going to discuss these things in §8, but here I keep track of ε^{\pm} purely for future convenience and invite the reader to substitute $\varepsilon^{+} = \varepsilon^{-} = \tilde{\varepsilon}^{\pm} = \varepsilon$ whenever thinking of imbalance-related complications becomes too much to bear.

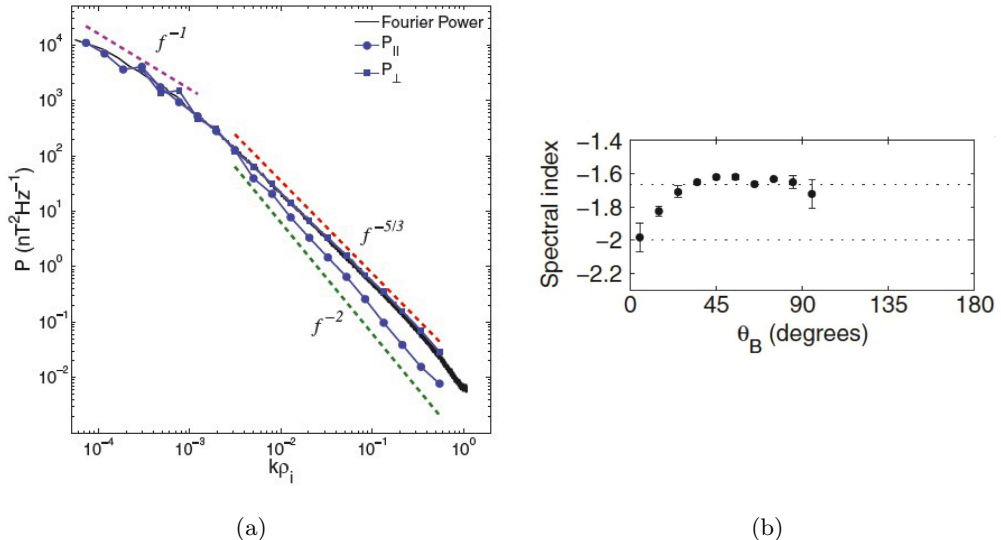


FIGURE 7. (a) Parallel (P_{\parallel}) and perpendicular (P_{\perp}) spectra (Fourier and wavelet) of the magnetic fluctuations in the solar wind, measured by the Ulysses spacecraft and computed by Wicks *et al.* (2010), with frequencies f converted to wavenumbers k using the Taylor hypothesis. (b) An earlier (historic, the first ever) measurement by Horbury *et al.* (2008) of the spectral index of these spectra as a function of angle to the local mean field.

Treating δZ_{λ}^{\pm} and $\delta Z_{l_{\parallel}}^{\pm}$ as increments for the same structure, but measured across and along the field, and setting them equal to each other, we find a relationship between the parallel and perpendicular scales—the scale-dependent anisotropy (2.11):

$$l_{\parallel}^{\pm} \sim v_A (\bar{\varepsilon}^{\mp})^{-1/3} \lambda^{2/3}. \quad (5.5)$$

The fact of scale-dependent anisotropy of MHD turbulence [if, in retrospect, not with the same confidence the scaling (5.5)] was confirmed numerically by Cho & Vishniac (2000) and Maron & Goldreich (2001) and, in a rare triumph of theory correctly anticipating measurement, observed in the solar wind by Horbury *et al.* (2008), followed by many others (e.g., Podesta 2009; Wicks *et al.* 2010; Luo & Wu 2010; Chen *et al.* 2011—a complete list is impossible here as this has now become an industry, as successful ideas do; see Chen 2016 for a recent review). Figure 7 shows some of the first of those results. An important nuance is that, in order to see scale-dependent anisotropy, one must measure the parallel correlations along the perturbed, rather than global, mean magnetic field.¹¹ The reason for this is as follows.

Both the causality argument (Boldyrev 2005; Nazarenko & Schekochihin 2011) and the Lagrangian-frequency one (Beresnyak 2015) that I invoked in §§ 5.1 and 5.2 to justify long parallel coherence lengths of the MHD fluctuations rely on the ability of Alfvénic perturbations to propagate along the magnetic field. Physically, a small such perturbation on any given scale does not know the difference between a larger perturbation on, say, a

¹¹This detail was first understood by Cho & Vishniac (2000) and Maron & Goldreich (2001), but still needed restating 10 years later (Chen *et al.* 2011) and, it seems, continues (or has until recently continued) to fail to be appreciated in some particularly die-hard sanctuaries where adherents of the old religion huddle for warmth before the dying fire of the isotropic IK paradigm (I will refrain from providing citations here—and will, in § 6, offer some comfort to admirers of Robert Kraichnan, who was, in a certain sense, less wrong than it appeared in the early 2000s).

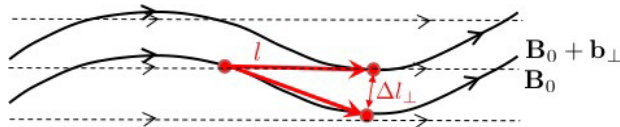


FIGURE 8. Measuring correlations along local vs. global mean field. True parallel correlations cannot be captured by a measurement along the global field \mathbf{B}_0 if the distance Δl_\perp [see (5.7)] by which the point-separation vector \mathbf{l} along \mathbf{B}_0 “slips” off the exact field line ($\mathbf{B}_0 + \mathbf{b}_\perp$) is greater than the perpendicular decorrelation length λ between “neighbouring” field lines.

few times its scale, and the “true” mean field (whatever that is, outside the ideal world of periodic simulation boxes). Thus, it will propagate along the local field and so it is along the local field that the arguments based on this propagation will apply. What if we instead measure correlations along the global mean field or, more generally, along some coarse-grained version of the exact field? Let that coarse-grained field be the average over all perpendicular scales at and below some L_\perp (to get the global mean field, make L_\perp the outer scale). Define Elsasser-field increments between pairs of points separated by a vector \mathbf{l} ,

$$\delta \mathbf{Z}_l^\pm = \mathbf{Z}_\perp^\pm(\mathbf{r} + \mathbf{l}) - \mathbf{Z}_\perp^\pm(\mathbf{r}), \quad (5.6)$$

and consider \mathbf{l} along the exact magnetic field vs. \mathbf{l} along our coarse-grained field. The *perpendicular* distance by which the latter vector will veer off the field line (figure 8) will be dominated by the magnetic perturbation at the largest scale that was not included in the coarse-grained field:

$$\Delta l_\perp \sim l \frac{\delta b_{L_\perp}}{v_A}. \quad (5.7)$$

If we are trying to capture parallel correlations corresponding to perturbations with perpendicular scale $\lambda \ll L_\perp$, then, using CB, $l/v_A \sim \tau_{nl}$, and (5.3) with $\delta Z_\lambda^\pm \sim \delta b_\lambda$, we conclude that

$$\Delta l_\perp \sim \lambda \frac{\delta b_{L_\perp}}{\delta b_\lambda} \gg \lambda, \quad (5.8)$$

i.e., in such a measurement, the parallel correlations are swamped by perpendicular decorrelation, unless, in fact, $\lambda \sim L_\perp$ or larger (there is no such problem with measuring perpendicular correlations: small changes in a separation vector \mathbf{l} taken perpendicular to the global vs. exact field make no difference).

Consequently, the easiest practical way to extract correlations along the local field from either observed or numerically simulated turbulence (Chen *et al.* 2011) is to measure field increments (5.6) for many different separation vectors \mathbf{l} and to calculate for each such increment the angle between \mathbf{l} and the “local mean field” \mathbf{B}_{loc} defined as the arithmetic mean of the magnetic field measured at the two points involved:

$$\cos \phi = \frac{\mathbf{l} \cdot \mathbf{B}_{loc}}{|\mathbf{l}| |\mathbf{B}_{loc}|}, \quad \mathbf{B}_{loc} = \mathbf{B}_0 + \frac{\mathbf{b}_\perp(\mathbf{r} + \mathbf{l}) + \mathbf{b}_\perp(\mathbf{r})}{2}. \quad (5.9)$$

This amounts to coarse-graining the field always at the right scale (just) for the correlations that are being probed. One can then measure (for example) perpendicular and parallel structure functions as conditional averages:

$$\langle (\delta Z_\lambda^\pm)^n \rangle = \langle |\delta \mathbf{Z}_l^\pm|^n | \phi = 90^\circ \rangle, \quad (5.10)$$

$$\langle (\delta Z_{l_\parallel}^\pm)^n \rangle = \langle |\delta \mathbf{Z}_l^\pm|^n | \phi = 0 \rangle, \quad (5.11)$$

and similarly for intermediate values of ϕ (as explained above, the difference between \mathbf{B}_0

and \mathbf{B}_{loc} matters only for small ϕ). Thus, in general, one measures

$$\langle |\delta \mathbf{Z}_l^\pm|^n | \phi \rangle \propto l^{\zeta_n(\phi)}. \quad (5.12)$$

Alternatively, in simulations, one can simply follow field lines to get $\delta Z_{l\parallel}^\pm$ (Cho & Vishniac 2000; Maron & Goldreich 2001) or, as was initially done in the solar wind, use local wavelet spectra (Horbury *et al.* 2008; Podesta 2009; Wicks *et al.* 2010).

It turns out (see references cited above and innumerable others) that, quite robustly, $\zeta_2(0) = 1$, consistent with (5.1), whereas $\zeta_2(90^\circ)$ is typically between 2/3 and 1/2, i.e., between GS95 and IK, in the solar wind, and rather closer to 1/2 in numerical simulations—although this, as I will discuss in §§ 6.2 and 6.3, has been hotly disputed by Beresnyak (2011, 2012a, 2014b, 2019), who may have a point.

Thus, while little doubt remains about the reality of scale-dependent anisotropy [although not necessarily of the specific scaling (5.5)] and of the k_{\parallel}^{-2} spectrum (5.1), both arising from the GS95 theory, the GS95 prediction for the perpendicular spectrum (5.4) has continued to be suspect and controversial.

6. Dynamic Alignment, Perpendicular Cascade, and Intermittency

Whereas solar-wind turbulence observations were, for a period of time, viewed to be consistent with a $-5/3$ spectrum,¹² leading ultimately to the GS95 revision of the IK paradigm, high-resolution numerical simulations of forced, incompressible MHD turbulence, starting with Maron & Goldreich (2001) and Müller *et al.* (2003), have consistently shown scaling exponents closer to $-3/2$ (while strongly confirming the local anisotropy; see also Cho & Vishniac 2000; Cho *et al.* 2002b). This undermined somewhat the then still young GS95 consensus and stimulated hard questioning of the assumptions underlying its treatment of nonlinear interactions. This focused on whether the nonlinearity in MHD turbulence might be depleted in a scale-dependent way by some form of alignment between \mathbf{Z}_\perp^+ and \mathbf{Z}_\perp^- and/or, perhaps, between the magnetic and velocity fields. Maron & Goldreich (2001) commented in passing on field alignment in their simulations and Beresnyak & Lazarian (2006) focused on “polarisation alignment” explicitly, putting it on the table as a key effect requiring revision of GS95.¹³ The same possibility was mooted by Boldyrev (2005) and a year later, he came up with a very beautiful (if, as we will see in § 6.2, flawed) argument based on the idea of what he called “dynamic alignment” (Boldyrev 2006), which set the direction of the field for the subsequent 10 years and which I am now going to discuss.

¹²Matthaeus & Goldstein (1982) were possibly the first to come out with this claim; see the monumental review by Bruno & Carbone (2013) for an exhaustive bibliography and Chen (2016) for the current state of the art ($-3/2$ is back; solar wind and simulations seem more or less in agreement: see Boldyrev *et al.* 2011). Interestingly, this $-5/3$ period intersected by more than 10 years with the undisputed reign of the IK theory, confirming that no amount of adverse evidence can dent a dominant theoretical paradigm—or, at any rate, it takes a while and a hungry new generation entering the field (Kuhn 1962). One wonders if, had simulations and observations showing a $-3/2$ spectrum been available at the time, IK might have survived forever.

¹³The first inklings of correlations naturally arising between the two fields and affecting scalings in a significant way appear to be traceable to Dobrowolny *et al.* (1980), Grappin *et al.* (1982, 1983), Matthaeus *et al.* (1983), and Pouquet *et al.* (1986, 1988), although there was perhaps no explicit clarity about any physical distinction between alignment and imbalance (local or global; cf. § 11.1)—and, of course, everybody was chained to the isotropic IK paradigm then.

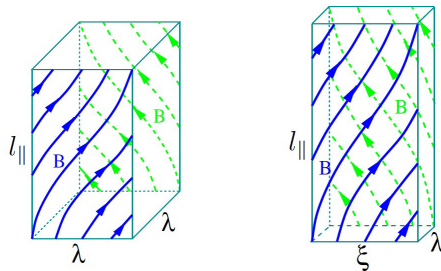


FIGURE 9. Cartoon of a GS95 eddy (left) vs. a Boldyrev (2006) aligned eddy (right). The latter has three scales: $l_{\parallel} \gg \xi \gg \lambda$ (along \mathbf{B}_0 , along \mathbf{b}_{\perp} , and transverse to both). This picture is adapted from Boldyrev (2006). In the context of my discussion, the fluctuation direction should, in fact, be thought of as along \mathbf{Z}_{\perp}^{\mp} (see figure 20).

6.1. Boldyrev’s Alignment Hypothesis

The Alfvén wave being the basic elemental MHD motion (and an exact solution), including at finite amplitudes, it stands to reason that perturbations of a strong magnetic field would “want” to resemble Alfvén waves as closely as possible—i.e., as consistent with sustaining a strong turbulent cascade. CB can be viewed as a manifestation of this principle: an Alfvénic perturbation decorrelates in roughly one wave period. Dynamic alignment is another such manifestation: in an Alfvén wave, \mathbf{u}_{\perp} and \mathbf{b}_{\perp} are the same, which is just a dynamical consequence of plasma flows dragging the field with them or the field accelerating the flows by relaxing under tension. Another angle at this is to think of the two Elsasser fields advecting each other and thus shearing each other into mutual alignment (Chandran *et al.* 2015).¹⁴

However, were the two fields actually parallel to each other, there would be no nonlinearity at all: indeed, considering the nonlinear term in (3.1), we see that we ought to replace the estimate (5.3) of the nonlinear time with

$$\tau_{\text{nl}}^{\pm} \sim \frac{\xi}{\delta Z_{\lambda}^{\mp}} \sim \frac{\lambda}{\delta Z_{\lambda}^{\mp} \sin \theta_{\lambda}}. \quad (6.1)$$

Here ξ is the scale of variation of \mathbf{Z}_{\perp}^{\pm} in the direction of \mathbf{Z}_{\perp}^{\mp} , taken at scale λ , which is the scale of its variation in the direction perpendicular both to itself and to \mathbf{B}_0 (all interactions are still assumed local in scale). Then θ_{λ} is the angle between the two Elsasser fields taken at scale λ , or, equivalently, $\sin \theta_{\lambda}$ is the aspect ratio of the field structures in the perpendicular 2D plane, in which a local anisotropy is now posited (see figure 9):

$$\sin \theta_{\lambda} \sim \frac{\lambda}{\xi}. \quad (6.2)$$

¹⁴Matthaeus *et al.* (2008) confirm numerically a fast dynamical tendency for the velocity and magnetic field to align locally, in patches, and discuss it in terms of the local evolution of the cross-helicity density $\mathbf{u}_{\perp} \cdot \mathbf{b}_{\perp}$, noting a formal analogy with the velocity–vorticity alignment in hydrodynamic turbulence. I want to alert the reader here that alignment of \mathbf{u}_{\perp} and \mathbf{b}_{\perp} , on which Matthaeus *et al.* (2008) or Boldyrev and his coworkers focused, is not, mathematically, the same thing as alignment of \mathbf{Z}_{\perp}^{+} and \mathbf{Z}_{\perp}^{-} advocated by Chandran *et al.* (2015), Mallet *et al.* (2015), and Mallet & Schekochihin (2017). In practice, both types of alignment occur (Mallet *et al.* 2016). I shall discuss these matters more carefully in § 8.1.2.

Thus, the fields must be misaligned in some minimal way in order to allow strong turbulence (i.e., in order for τ_{nl}^{\pm} to be finite). A version of Boldyrev’s argument¹⁵ is to conjecture that this minimal degree of misalignment would be set by a kind of uncertainty principle: since the direction of the local magnetic field along which these perturbations propagate can itself only be defined within a small angle $\sim \delta b_{\lambda}/v_A$, the two Elsasser fields (or the velocity and the magnetic field) cannot be aligned any more precisely than this and so

$$\sin \theta_{\lambda} \sim \theta_{\lambda} \sim \frac{\delta b_{\lambda}}{v_A} \ll 1. \quad (6.3)$$

By being vague about which quantities might be different for the two different Elsasser fields, I have effectively put aside any attempt at a general argument valid for imbalanced, as well as balanced, turbulence. Since alignment and local imbalance can be related in a nontrivial way and there are several possibilities as to exactly how they are related, I do not wish be distracted and so will postpone the discussion of that to § 8.1.2. Thus, from here till § 8, I shall assume

$$\varepsilon^+ \sim \varepsilon^- \quad \Rightarrow \quad \delta Z_{\lambda}^+ \sim \delta Z_{\lambda}^- \sim \delta u_{\lambda} \sim \delta b_{\lambda}. \quad (6.4)$$

This allows (6.3) to be combined with (6.1) and yield

$$\tau_{\text{nl}} \sim \frac{\lambda v_A}{\delta Z_{\lambda}^2}. \quad (6.5)$$

The constancy of flux then implies immediately¹⁶

$$\frac{\delta Z_{\lambda}^2}{\tau_{\text{nl}}} \sim \varepsilon \quad \Rightarrow \quad \delta Z_{\lambda} \sim (\varepsilon v_A \lambda)^{1/4} \quad \Leftrightarrow \quad E(k_{\perp}) \sim (\varepsilon v_A)^{1/2} k_{\perp}^{-3/2}. \quad (6.6)$$

In dimensional terms, this has brought us back to the IK spectrum (2.5), except the wavenumber is now the perpendicular wavenumber and both anisotropy and CB are retained, although the relationship between the parallel and perpendicular scales changes:

$$\tau_{\text{nl}} \sim \frac{l_{\parallel}}{v_A} \quad \Rightarrow \quad l_{\parallel} \sim v_A^{3/2} \varepsilon^{-1/2} \lambda^{1/2}. \quad (6.7)$$

Since CB remains in force, the parallel cascade stays the same as discussed in § 5.2.

If one embraces (6.6), one could argue that Kraichnan’s dimensional argument was actually right, but it should have been used with k_{\perp} , rather than with k , because k_{\parallel}

¹⁵His actual original argument looked somewhat more complicated than this, but in the end amounted to the same thing. In later papers (Perez *et al.* 2012, 2014b), he does appear to embrace implicitly something more compatible with the line of thinking that I will advocate in § 6.3.1.

¹⁶A perceptive reader might protest at this point that $\delta Z_{\lambda} \propto \lambda^{1/4}$ looks rather suspicious in view of the exact law (3.7), which seems to hint at a $\lambda^{1/3}$ scaling. In fact, there is no contradiction: since one of the three Elsasser increments in the exact law (3.7) is the *longitudinal* one, the alignment angle successfully insinuates its way in, and (3.7) should be viewed as saying that $\delta Z_{\lambda}^{\mp} (\delta Z_{\lambda}^{\pm})^2 \sin \theta_{\lambda} \sim \varepsilon^{\pm} \lambda$ (Boldyrev *et al.* 2009). This tells us nothing new, other than that the estimate (6.1) for the nonlinear time is reasonable. Indeed, if the right way to turn (3.7) into a “twiddle” constant-flux relation of the form $(\delta Z_{\lambda}^{\pm})^2 \sim \varepsilon^{\pm} \tau_{\text{nl}}^{\pm}$ is by interpreting λ in (3.7) as being in the direction perpendicular to $\delta \mathbf{Z}_{\lambda}^{\mp}$ (the direction of the fastest variation of the fields; see figure 20), then one might argue that the exact law (3.7) provides a good reason to view specifically the angle between the two Elsasser fields as the relevant quantity affecting τ_{nl}^{\pm} . Such an approach is different and, in general, not equivalent, to Boldyrev’s original focus on the alignment between the velocity and the magnetic perturbation. This difference will become important in the context of imbalanced turbulence—see § 8.1.2.

is not a “nonlinear” dimension. This is the style of reasoning that Kraichnan himself might have rather liked. We are about to see, however, that the result (6.6) also runs into serious trouble and needs revision.

For imminent use in what follows, let us compute the extent of the inertial range that this aligned cascade is supposed to span. Comparing the nonlinear cascade time (6.5) with the Ohmic diffusion time (assuming, for convenience that the magnetic diffusivity η is either the same or larger than the kinematic viscosity of our MHD fluid), we find

$$\tau_{\text{nl}} \sim \left(\frac{v_A \lambda}{\varepsilon} \right)^{1/2} \ll \tau_\eta \sim \frac{\lambda^2}{\eta} \Leftrightarrow \lambda \gg \eta^{2/3} \left(\frac{v_A}{\varepsilon} \right)^{1/3} \equiv \lambda_\eta, \quad (6.8)$$

where λ_η is the cutoff scale—the Kolmogorov scale for this turbulence. For comparison, note that the same calculation based on the GS95 scalings (5.3) and (5.4) gives

$$\tau_{\text{nl}}^{\text{GS95}} \sim \varepsilon^{-1/3} \lambda^{2/3} \ll \tau_\eta \sim \frac{\lambda^2}{\eta} \Leftrightarrow \lambda \gg \eta^{3/4} \varepsilon^{-1/4} \equiv \lambda_\eta^{\text{GS95}}, \quad (6.9)$$

where $\lambda_\eta^{\text{GS95}}$ is the classic Kolmogorov scale.

6.2. Plot Thickens

This is a very appealing theory, whose main conclusions were rapidly confirmed by a programme of numerical simulations undertaken by Boldyrev’s group—in particular, the angle between velocity and magnetic field, measured in a certain opportune way,¹⁷ was reported to scale according to $\theta_\lambda \propto \lambda^{1/4}$, as implied by (6.6) and (6.3) (Mason *et al.* 2006, 2008, 2011, 2012; Perez *et al.* 2012, 2014b). The same papers confirmed the earlier numerical results on the spectrum of MHD turbulence indeed scaling as $k_\perp^{-3/2}$ (figure 10a). However, the legitimacy of this conclusion was contested by Beresnyak (2011, 2012a, 2014b, 2019), who disputed that those spectra were converged and argued that systematic convergence tests in fact favoured a trend towards a $k_\perp^{-5/3}$ spectrum at small enough scales. His point was that convergence of spectra with increasing resolution ought to be checked from the dissipative end of the inertial interval and that rescaling the spectra in his simulations to the Kolmogorov scale (6.9) gave a better data collapse than rescaling them to Boldyrev’s cutoff scale (6.8) (figure 10b). Despite the sound and fury of the ensuing debate about the quality of the two competing sets of numerics (Perez *et al.* 2014a; Beresnyak 2013, 2014a), it would not necessarily be obvious to anyone who took a look at their papers that their raw numerical results themselves were in fact all that different—certainly not as different as their interpretation by their authors. Without dwelling on either, however, let me focus instead on a conceptual wrinkle in Boldyrev’s original argument that Beresnyak (2011) spotted and that cannot be easily dismissed.

In the RMHD limit (whose applicability to MHD turbulence at sufficiently small scales we have no reason to doubt), $\delta b_\lambda / v_A$ is an arbitrarily small quantity, and so must then

¹⁷They focused on one particular measure of alignment, $\sin \theta_\lambda = \langle |\delta \mathbf{u}_\lambda \times \delta \mathbf{b}_\lambda| \rangle / \langle |\delta \mathbf{u}_\lambda| |\delta \mathbf{b}_\lambda| \rangle$, which indeed turns out to scale as $\lambda^{1/4}$ in a certain range of scales. Obviously, one can invent other proxies for the alignment angle, involving different fields ($\delta \mathbf{Z}_\lambda^\pm$) and/or different powers of the fields’ increments under the averages. This game produces many different scalings (Beresnyak & Lazarian 2009b; Mallet *et al.* 2016) (some of which can be successfully theorised about: see Chandran *et al.* 2015), and it is not *a priori* obvious which of these should be most representative of the “typical” alignment that figures in the “twiddle” theories of §6.1 or §6.3.1. Perhaps a better handle on the scaling of the alignment is obtained when one studies the full distribution of the “RMHD ensemble” (see §6.3.2 and Mallet & Schekochihin 2017) and/or the 3D-anisotropic statistics (see §6.4 and papers by Chen *et al.* 2012a, Mallet *et al.* 2016 and Verdini *et al.* 2018, 2019).

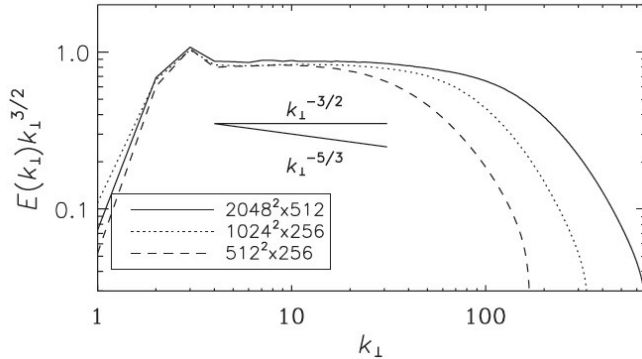
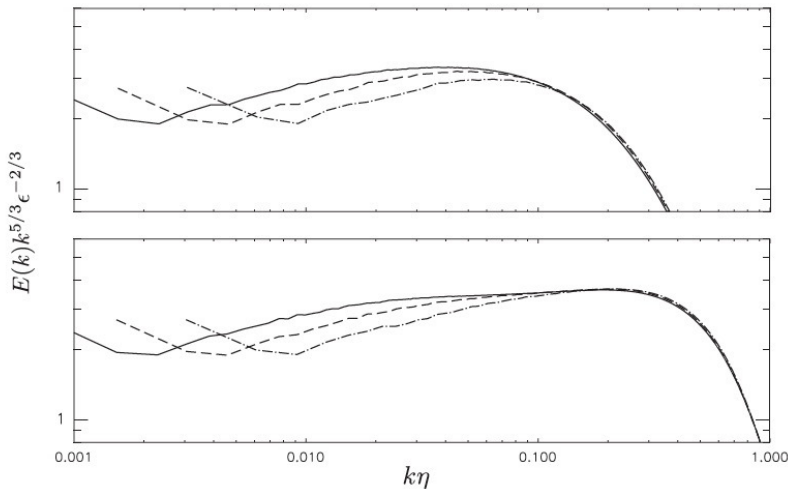
(a) Perez *et al.* (2012)(b) Beresnyak (2014*b*)

FIGURE 10. The best-resolved currently available spectra of RMHD turbulence. (a) From simulations by Perez *et al.* (2012) (their figure 1), with Laplacian viscosity and resolution up to $2048^2 \times 512$. (b) From simulations by Beresnyak (2014*b*) (his figure 1), with Laplacian viscosity (top panel) and with 4th-order hyperviscosity (bottom panel); the resolution for the three spectra is 1024^3 , 2048^3 and 4096^3 . His spectra are rescaled to Kolmogorov scale (6.9) (which he denotes η). He finds poorer convergence (see his figure 2) when he rescales to Boldyrev’s scale (6.22). Perez *et al.* (2012) appear to get a somewhat better outcome (see their figure 8) if they plot their spectra vs. $k_{\perp} \lambda_{\eta}$ where λ_{η} is given by (6.22) with λ_{CB} computed in each simulation as the normalisation constant in the scaling (6.20) of $\sin \theta_{\lambda}$ (in their analysis, however, this is the angle between velocity and magnetic perturbations, not the Elsasser fields).

be, according to (6.3), the alignment angle $\sin \theta_{\lambda}$. Introducing such a large depletion of the nonlinearity into (3.1) would abolish it completely in the RMHD ordering and render the system linear. The only way to keep the nonlinearity while assuming a small angle θ_{λ} is to take the angle to be small but still ordered as unity in the RMHD ordering—in other words, it cannot scale with ϵ under the RMHD rescaling symmetry (3.5). The same rescaling symmetry implies that any physical scaling that involves v_A and l_{\parallel} (and no other scales) must involve them in the combination l_{\parallel}/v_A (see § 5.2 and Beresnyak 2012*a*), which (6.7) manifestly does not. All this flies in the face of the fact that a substantial body of numerical evidence supporting aligned MHD turbulence was obtained by means

of RMHD simulations (Mason *et al.* 2011, 2012; Perez *et al.* 2012; Beresnyak 2012a; Mallet *et al.* 2015, 2016)—complemented by explicit evidence that full MHD simulations produce quantitatively the same alignment—so the standard recourse to casting a cloud of suspicion on the validity of an asymptotic approximation is not available in this case.

In a further blow to the conjecture (6.3), it turns out that the alignment angle between the Elsasser fields at any given scale is *anticorrelated* with their amplitudes (Mallet *et al.* 2015), supporting the view that the dynamical alignment is indeed *dynamical*, being brought about by the mutual shearing of the Elsasser fields (Chandran *et al.* 2015), rather than by the uncertainty principle (6.3) (which would imply, presumably, a positive correlation between θ_λ and δZ_λ).

On the other hand, the (numerical) evidence of alignment is real.¹⁸ While numerical simulations at currently feasible resolutions cannot definitively verify or falsify Beresnyak’s expectation that it is but a transient feature that disappears at small scales, they certainly show aligned, locally 3D-anisotropic turbulence over a respectable inertial subrange at least one order of magnitude wide, and probably two. This is approaching the kind of scale separations that actually exist in Nature, e.g., in the solar wind, and we cannot be casually dismissive of a physical regime, even if transient, that occupies most of the phase space that we are able to measure!

6.3. Revised Model of Aligned MHD Turbulence

6.3.1. Dimensional and RMHD-Symmetry Constraints

Let me make the restrictions implied by Beresnyak’s objection more explicit. Under the RMHD rescaling symmetry (3.5),

$$\delta Z_\lambda \rightarrow \epsilon \delta Z_\lambda, \quad \epsilon \rightarrow \frac{\epsilon^3}{a} \epsilon, \quad v_A \rightarrow v_A, \quad \lambda \rightarrow a\lambda. \quad (6.10)$$

Therefore, the scaling relation (6.6) becomes $\epsilon \delta Z_\lambda \sim \epsilon^{3/4} (\epsilon v_A \lambda)^{1/4}$, which is obviously a contradiction. Indeed, trialling

$$\delta Z_\lambda \sim \epsilon^\mu v_A^\nu \lambda^\gamma \quad (6.11)$$

and mandating both the symmetry (6.10) and dimensional consistency, one finds that the GS95 solution (5.4), $\nu = 0$ and $\gamma = \mu = 1/3$, is the only possibility, which was Beresnyak’s point.

It seems obvious that the only way to rescue alignment is to allow another parameter—and the (almost) obvious choice is L_\parallel , the parallel outer scale, which transforms as

¹⁸Just to make it all more confusing, the real (observational) evidence is far from conclusive: in the solar wind, Podesta *et al.* (2009) and Wicks *et al.* (2013a) see scale-dependent alignment, but only for fluctuations at large scales—larger than what is normally viewed as the outer scale/the start of the inertial range (in the solar wind, this shows up as a break between f^{-1} and $f^{-5/3 \dots -3/2}$ slopes in the frequency spectrum). Osman *et al.* (2011) also report alignment, on the outer scale, as far as I can tell. Chen *et al.* (2012a) see alignment across the inertial range, but, to the best of their measurement, it is not scale-dependent. Most recently, Verdini *et al.* (2018, 2019) have managed to extract structure functions in three field-dependent directions (see §6.4) that scale in a way that is consistent with scale-dependent alignment, but all measures of the alignment angle θ_λ that they tried had much shallower (but not flat!) scalings than $\lambda^{1/4}$. This appears to be the first time that scale-dependent alignment at small scales has (still quite timidly) shown itself in the solar wind. Theoreticians must live in hope that, as both instruments and analysis techniques become more refined, definite and universal scalings will eventually emerge from this sea of uncertainty—there is some recent history of this happening, e.g., with the turbulence spectra in the kinetic range (Alexandrova *et al.* 2009; Chen *et al.* 2012b, 2013b; Sahraoui *et al.* 2013; Huang *et al.* 2014), so these hopes are perhaps not entirely foolish.

$L_{\parallel} \rightarrow (a/\epsilon)L_{\parallel}$. Then

$$\delta Z_{\lambda} \sim \varepsilon^{\mu} v_{\text{A}}^{\nu} \lambda^{\gamma} L_{\parallel}^{\delta} = \varepsilon^{(1+\delta)/3} \left(\frac{L_{\parallel}}{v_{\text{A}}} \right)^{\delta} \lambda^{(1-2\delta)/3}, \quad (6.12)$$

where the second expression is the result of imposing on the first the RMHD symmetry (6.10) and dimensional correctness; $\delta = 0$ returns us to GS95.¹⁹ The same argument applied to the scaling of l_{\parallel} with ε , v_{A} , λ and L_{\parallel} gives

$$l_{\parallel} \sim \varepsilon^{(\sigma-1)/3} v_{\text{A}}^{1-\sigma} L_{\parallel}^{\sigma} \lambda^{2(1-\sigma)/3}, \quad (6.13)$$

where σ is a free parameter. Note that both (6.12) and (6.13) manifestly contain the parallel scales and v_{A} in the solely allowed combinations $l_{\parallel}/v_{\text{A}}$ and $L_{\parallel}/v_{\text{A}}$. A reassuring consistency check is to ask what perpendicular scale $\lambda = L_{\perp}$ corresponds to $l_{\parallel} = L_{\parallel}$: this turns out to be

$$L_{\perp} \sim \varepsilon^{1/2} \left(\frac{L_{\parallel}}{v_{\text{A}}} \right)^{3/2} \sim \lambda_{\text{CB}}, \quad (6.14)$$

the very same λ_{CB} , given by (4.3), at which weak turbulence becomes strong—thus seamlessly connecting any strong-turbulence theory expressed by (6.12) and (6.13) with the WT cascade discussed in §4.²⁰ Notably, if we applied such a test to (6.7), we would find the price of consistency to be $L_{\perp} = L_{\parallel}$, which is allowed but does not have to be the case in MHD and certainly cannot be the case in RMHD.

Finally, since the parallel-cascade scaling (5.1) remains beyond reasonable doubt and, as can be readily checked, respects the rescaling symmetry (3.5) (Beresnyak 2015), combining it with (6.13) and (6.12) fixes

$$\sigma = 2\delta. \quad (6.15)$$

Alas, CB does not help with determining δ because, in aligned turbulence, the nonlinear time (6.1) contains the unknown scale ξ , or, equivalently, the alignment angle $\theta_{\lambda} \sim \lambda/\xi$. If we did know δ , CB would let us determine this angle:

$$\frac{l_{\parallel}}{v_{\text{A}}} \sim \tau_{\text{nl}} \sim \frac{\lambda}{\delta Z_{\lambda} \sin \theta_{\lambda}} \quad \Rightarrow \quad \sin \theta_{\lambda} \sim \left(\frac{\lambda}{\lambda_{\text{CB}}} \right)^{2\delta}, \quad (6.16)$$

where λ_{CB} is given by (6.14). The answer that we want to get—keeping Boldyrev’s scalings of everything with λ but not with ε or v_{A} —requires

$$\delta = \frac{1}{8}. \quad (6.17)$$

Then, instead of (6.6), we end up with

$$\delta Z_{\lambda} \sim \varepsilon^{3/8} \left(\frac{L_{\parallel}}{v_{\text{A}}} \right)^{1/8} \lambda^{1/4}, \quad l_{\parallel} \sim \varepsilon^{-1/4} v_{\text{A}}^{3/4} L_{\parallel}^{1/4} \lambda^{1/2}, \quad \sin \theta_{\lambda} \sim \varepsilon^{-1/8} \left(\frac{v_{\text{A}}}{L_{\parallel}} \right)^{3/8} \lambda^{1/4}, \quad (6.18)$$

¹⁹The weak-turbulence spectrum (4.7) corresponds to $\delta = -1/4$.

²⁰If we had included L_{\perp} with some unknown exponents into (6.12) and (6.13), we would have found that L_{\perp} had to satisfy (6.14) and so could not be treated as an independent quantity. What, might one ask, will then happen if I attempt to inject energy at some L_{\perp} that does not satisfy (6.14)? If this $L_{\perp} > \lambda_{\text{CB}}$, then the cascade set off at the outer scale will be weak and transition to the strong-turbulence regime at λ_{CB} as described in §4; if $L_{\perp} < \lambda_{\text{CB}}$, then I am effectively forcing 2D motions, which should break up by the causality argument (§5.1) and it is L_{\parallel} that will be determined by (6.14). Thus, λ_{CB} can be treated without loss of generality as the perpendicular outer scale of the CB cascade.

and the dissipation cutoff scale (6.8) is corrected as follows:

$$\tau_{\text{nl}} \sim \left(\frac{L_{\parallel}}{\varepsilon v_A} \right)^{1/4} \lambda^{1/2} \ll \tau_{\eta} \sim \frac{\lambda^2}{\eta} \quad \Leftrightarrow \quad \lambda \gg \eta^{2/3} \left(\frac{L_{\parallel}}{\varepsilon v_A} \right)^{1/6} \equiv \lambda_{\eta}. \quad (6.19)$$

Note that, since $\lambda_{\eta} \propto \eta^{2/3}$ still, this does not address Beresnyak’s numerical evidence on the convergence of the spectra (§ 6.2); this problem will be dealt with in § 7.

For future convenience, let me recast all these scalings in a somewhat simpler form:

$$\delta Z_{\lambda} \sim \left(\frac{\varepsilon L_{\parallel}}{v_A} \right)^{1/2} \left(\frac{\lambda}{\lambda_{\text{CB}}} \right)^{1/4}, \quad \frac{l_{\parallel}}{L_{\parallel}} \sim \left(\frac{\lambda}{\lambda_{\text{CB}}} \right)^{1/2}, \quad \sin \theta_{\lambda} \sim \left(\frac{\lambda}{\lambda_{\text{CB}}} \right)^{1/4}. \quad (6.20)$$

Defining the magnetic Reynolds number based on the CB scale (6.14) and the fluctuation amplitude at this scale,

$$\text{Rm} = \frac{\delta Z_{\lambda_{\text{CB}}} \lambda_{\text{CB}}}{\eta} \sim \frac{\varepsilon}{\eta} \left(\frac{L_{\parallel}}{v_A} \right)^2, \quad (6.21)$$

allows the dissipation scale (6.19) to be recast as follows:

$$\frac{\lambda_{\eta}}{\lambda_{\text{CB}}} \sim \left(\frac{\text{Rm}}{1 + \text{Pm}} \right)^{-2/3} = \widetilde{\text{Re}}^{-2/3}, \quad \text{Pm} = \frac{\nu}{\eta}, \quad \widetilde{\text{Re}} = \frac{\delta Z_{\lambda_{\text{CB}}} \lambda_{\text{CB}}}{\nu + \eta}. \quad (6.22)$$

I have restored the possibility that viscosity ν might be larger than the magnetic diffusivity η : if that is the case, one must replace the latter with the former in the calculation of the dissipative cutoff, whereas if $\text{Pm} \lesssim 1$, it does not matter, hence the appearance of the magnetic Prandtl number Pm in the combination $(1 + \text{Pm})$ in (6.22).

Yet another way to write the first of the scaling relations (6.18) is

$$\delta Z_{\lambda} \sim \varepsilon^{1/3} \lambda_{\text{CB}}^{1/12} \lambda^{1/4} \quad \Leftrightarrow \quad E(k_{\perp}) \sim \varepsilon^{2/3} \lambda_{\text{CB}}^{1/6} k_{\perp}^{-3/2}. \quad (6.23)$$

This is effectively the prediction for the spectrum that Perez *et al.* (2012, 2014b) used in their numerical convergence studies. Thus, they and I are on the same page as to what the spectrum of aligned turbulence is expected to be, although the question remains why it should be that if Boldyrev’s uncertainty principle (6.3) can no longer be used.

A set of RMHD-compatible scalings (6.18), or (6.23), is also effectively what was deduced by Chandran *et al.* (2015) and by Mallet & Schekochihin (2017) from a set of plausible conjectures about the dynamics and statistics of RMHD turbulence (they did not explicitly discuss the issue of the RMHD rescaling symmetry, but used normalisations that enforced it automatically). The two papers differed in their strategy for determining the exponent δ ; my exposition here will be a “heuristic” version of Mallet & Schekochihin (2017).

6.3.2. Intermittency Matters!

The premise of both Chandran *et al.* (2015) and Mallet & Schekochihin (2017) is that in order to determine the scalings of everything, including the energy spectrum, one must have a working model of intermittency, i.e., of the way in which fluctuation amplitudes and their scales lengths in all three directions— λ , ξ and l_{\parallel} —are distributed in a turbulent MHD system. It may be disturbing to the reader, or viewed by her as an unnecessary complication, that we must involve “rare” events—as this is what the theory of intermittency is ultimately about—in the mundane business of the scaling of the energy spectra, which are usually viewed as made up from the more “typical” fluctuations. These doubts might be alleviated by the following observation. The appearance of the outer scale L_{\parallel} in (6.12) suggests that the self-similarity is broken—this is somewhat analogous

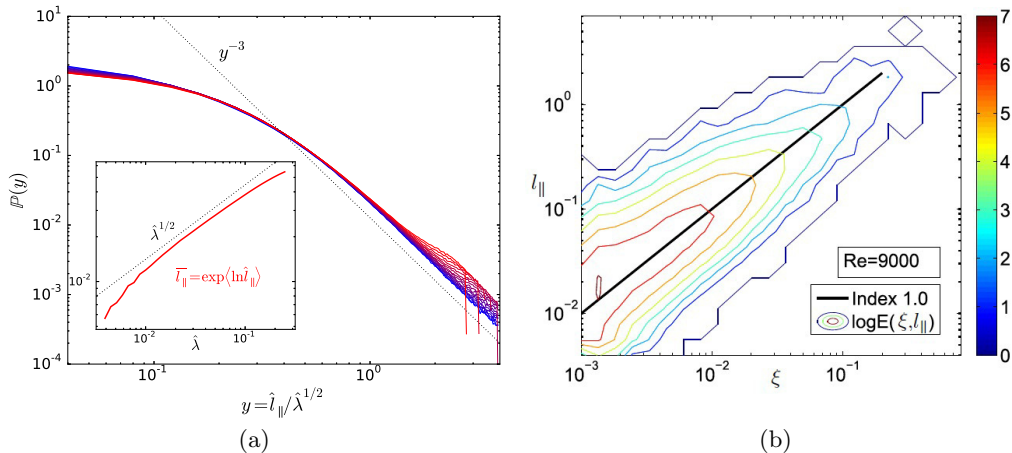


FIGURE 11. (a) Probability distribution of $l_{\parallel}/\lambda^{1/2}$ in a 1024^3 RMHD simulation (the shades of colour from blue to red correspond to PDFs at increasing scales within the inertial range). This plot is taken from Mallet & Schekochihin (2017) (where the reader will find a discussion—somewhat inconclusive—of the slope of this PDF) and illustrates how good (or otherwise) is the assumption that $l_{\parallel}/\lambda^{\alpha}$ has a scale-invariant distribution (the assumption is not as good as RCB, illustrated in figure 6 based on data from the same simulation). (b) Joint probability distribution for the length l_{\parallel} and width ξ (in my notation) of the most intense dissipative structures (adapted from Zhdankin *et al.* 2016b). This shows that $\xi \propto l_{\parallel}$, in line with (6.27). Independent simulations by J. M. Stone (private communication, 2018) support this scaling.

to what happens in hydrodynamic turbulence, where corrections to the K41 scaling (2.2) come in as powers of λ/L (Kolmogorov 1962; Frisch 1995). We may view δ as just such a correction to the self-similar GS95 result, and alignment as the physical mechanism whereby this intermittency correction arises. The main difference with the hydrodynamic case is that δ is not all that small (MHD turbulence is “more intermittent” than the hydrodynamic one), the mechanism responsible for it has important consequences (§ 7), and so we care.

I shall forgo a detailed discussion of the intermittency model that Mallet & Schekochihin (2017) proposed; for my purposes here, a vulgarised version of their argument will suffice. They consider the turbulent field as an ensemble of structures, or fluctuations, each of which has some amplitude and three scales: parallel l_{\parallel} , perpendicular λ and fluctuation-direction ξ (they call this the “RMHD ensemble”). They make certain conjectures about the joint probability distribution of these quantities, which then allow them to fix scalings. The most crucial (and perhaps also the most arbitrary) of these conjectures is, effectively, that for all structures, $l_{\parallel} \sim \lambda^{\alpha}$ with the same exponent α , i.e., that the quantity $l_{\parallel}/\lambda^{\alpha}$ has a scale-invariant distribution (this appears to be confirmed by numerical evidence: see figure 11a). They then determine the exponent α by considering “the most intense structures”²¹—because it is possible to work out what the probability of encountering them is as a function both of λ and of l_{\parallel} .

They conjecture that the most intense structures in the RMHD ensemble are sheets transverse to the local perpendicular direction. Therefore, if one looks for their probability (filling fraction) in any perpendicular plane as a function of the perpendicular scale λ ,

²¹Often an object of particular importance in intermittency theories (e.g., She & Leveque 1994; Dubrulle 1994; She & Waymire 1995; Grauer *et al.* 1994; Müller & Biskamp 2000; Boldyrev 2002; Boldyrev *et al.* 2002).

one expects it to scale as

$$P \propto \lambda. \quad (6.24)$$

If, on the other hand, one is interested in their filling fraction in the plane locally tangent to a flux sheet (i.e., defined by the local mean field and the direction of the fluctuation vector), it is

$$P \propto \xi l_{\parallel}. \quad (6.25)$$

The next conjecture is the “refined critical balance” (RCB, already advertised in §5.1), stating that not only is $\tau_{\text{nl}} \sim \tau_A$ in some vague “typical” sense, but the quantity

$$\chi = \frac{\delta Z l_{\parallel}}{\xi v_A} \sim \frac{\tau_A}{\tau_{\text{nl}}} \quad (6.26)$$

has a scale-invariant distribution in the RMHD ensemble—this was discovered by Mallet *et al.* (2015) to be satisfied with truly remarkable accuracy in numerically simulated RMHD turbulence (figure 6).²² If this is true for all structures, it is true for the most intense ones—and a further assumption about those is that their amplitude δZ_{max} is not a function of scale but is simply equal to some typical outer-scale value (i.e., the most intense structures are formed by the largest perturbations collapsing, or being sheared, into sheets without breaking up into smaller perturbations; see Chandran *et al.* 2015). This, together with (6.25), implies that for those structures,

$$\xi \sim l_{\parallel} \frac{\delta Z_{\text{max}}}{v_A} \Rightarrow P \propto l_{\parallel}^2 \quad (6.27)$$

(Zhdankin *et al.* 2016*b* confirm that $\xi \propto l_{\parallel}$ for the most intense dissipative structures: see figure 11*b*). Comparing (6.27) with (6.24), we conclude that $l_{\parallel} \propto \lambda^{1/2}$ for the most intense structures and, therefore, for everyone else—by the conjecture of scale invariance of $l_{\parallel}/\lambda^{\alpha}$, where we now know that $\alpha = 1/2$. Comparing this with (6.13), we see that $\alpha = 2(1 - \sigma)/3$, whence

$$\sigma = \frac{1}{4} \Rightarrow \delta = \frac{1}{8}, \quad (6.28)$$

the latter by virtue of (6.15). Q.e.d.: we now have the scalings (6.18).

I do not know if the reader will find this quasi-intuitive argument more (or less) convincing than the formal-looking conjectures and corollaries in Mallet & Schekochihin (2017). There is no need to repeat their algebra here, but hopefully the above sheds some (flickering) light—if not, perhaps a better argument will be invented one day, but all I can recommend for now is reading their paper. Notably, in their more formal treatment, not just the energy spectrum but the two-point structure functions of all orders are predicted—and turn out to be a decent fit to numerical data as it currently stands.²³ The same is true about the model proposed in the earlier paper by Chandran *et al.* (2015). Their approach is based on a much more enthusiastic engagement with dynamics: a careful analysis of how aligned and non-aligned structures might form and interact. They get $\delta \approx 0.108$, which leads to $\delta Z_{\lambda} \propto \lambda^{0.26}$ —not a great deal of difference with (6.18),

²²Note that it makes sense then that the alignment angle $\sin \theta_{\lambda} \sim \lambda/\xi$ should be anticorrelated with the fluctuation amplitude δZ_{λ} at any given scale λ (stronger fluctuations are more aligned—the strongest of them are the sheets being discussed here), as I mentioned in §6.2 and as Mallet *et al.* (2015) indeed found.

²³The key tenet of their theory—a log-Poisson distribution of field increments, which follows from arguments analogous to those advanced in the hydrodynamic-turbulence theory (She & Leveque 1994; Dubrulle 1994; She & Waymire 1995)—also appears to be at least consistent with numerical evidence (Zhdankin *et al.* 2016*a*; Mallet & Schekochihin 2017).

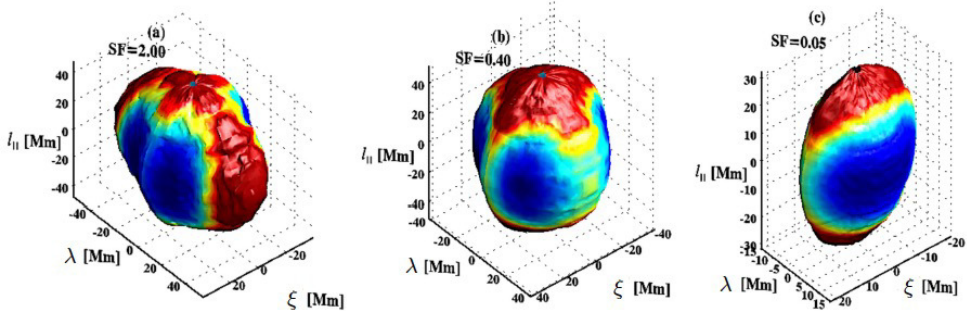
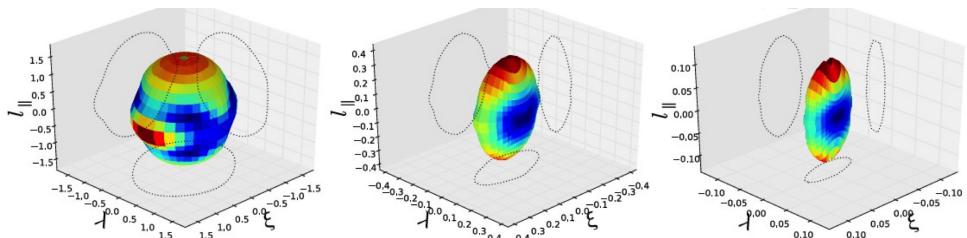
(a) Solar wind (adapted from Verdini *et al.* 2018, data from *Wind* spacecraft)(b) RMHD simulation (from Mallet *et al.* 2016)

FIGURE 12. Locally 3D-anisotropic structures in the (a) solar wind and (b) numerical simulations (here l_{\parallel} is normalised to $L_{\parallel}/2\pi$ and λ and ξ to $L_{\perp}/2\pi$, hence apparent isotropy at the outer scale). These are surfaces of constant second-order structure function of the magnetic field (a) or one of the Elsasser fields (b). The three images correspond to successively smaller fluctuations and so successively smaller scales (only the last of the three is firmly in the universal inertial range). In both cases, the emergence of statistics with $l_{\parallel} \gg \xi \gg \lambda$ is manifest. In the solar wind, the route to this aligned state that turbulence takes appears to depend quite strongly on the solar-wind expansion, which distorts magnetic-field component in the radial direction compared to the azimuthal ones (Verdini & Grappin 2015; Vech & Chen 2016). The data shown in panel (a) was carefully selected to minimise this effect; without such selection, one sees structures most strongly elongated in the ξ direction at the larger scales ($\xi > l_{\parallel} > \lambda$), although they too tend to the universal aligned regime at smaller scales (Chen *et al.* 2012a).

considering that all of this is very far from being exact science. Their approach does have the distinction, however, of emphasising particularly strongly the dynamic nature of the dynamic alignment, which arises as Elsasser fields shear each other into sheet-like structures.

6.4. 3D Anisotropy

Before moving on, I would like to re-emphasise the 3D anisotropy of the aligned MHD turbulence—and the fact that this anisotropy is local, associated at every point with the three directions that themselves depend on the fluctuating fields: parallel to the magnetic field (l_{\parallel}), along the vector direction of the perturbed field \mathbf{Z}_{\perp}^{\mp} that advects the field \mathbf{Z}_{\perp}^{\pm} whose correlations we are measuring (ξ), and the third direction perpendicular to the other two (λ). This local 3D anisotropy is measurable²⁴ and has indeed been

²⁴A sophisticated reader interested in how this can be done, might wonder whether the prescription given in §5.3 and based on defining the local field \mathbf{B}_{loc} at each scale according to (5.9) is still valid for aligned turbulence: indeed, would the distance (5.7) by which the point-separation vector \mathbf{l} veered off the exact field line not be $\Delta l_{\perp} \gg \lambda$ even when the coarse-graining scale is $L_{\perp} \sim \lambda$, because in (5.7), $l/v_A \sim \lambda/\delta b_{\lambda} \sin \theta_{\lambda}$? In fact, since Δl_{\perp} is clearly

observed both in the solar wind (Chen *et al.* 2012a; Verdini *et al.* 2018, 2019) and in numerical simulations (Verdini & Grappin 2015; Mallet *et al.* 2016)—both are illustrated by figure 12. The main point of discrepancy between the true and virtual reality is the scale dependence of the anisotropy: confirmed solidly in simulations but only very tentatively in the solar wind (see footnote 18). However, progress never stops, and one can hope for better missions (Chen *et al.* 2020) and even more sophisticated analysis.

The scaling of the energy spectrum in the parallel direction (§ 5.2) was arguably the most robust and uncontroversial of the results reviewed thus far. We then occupied ourselves with the scalings of the Elsasser-field increments and of l_{\parallel} vs. the perpendicular scale λ , culminating in § 6.3 with a theory that one (hopefully) can believe in. The scalings with the third, fluctuation-direction coordinate ξ are very easy to obtain because the nonlinear time of the aligned cascade (6.1) has the same dependence on ξ as it did on λ in the unaligned, GS95 theory: see (5.3). Therefore,

$$\delta Z_{\xi} \sim (\varepsilon \xi)^{1/3}, \quad \xi \sim \varepsilon^{1/8} \left(\frac{L_{\parallel}}{v_A} \right)^{3/8} \lambda^{3/4} \sim \lambda_{\text{CB}}^{1/4} \lambda^{3/4} \quad (6.29)$$

with the latter formula following from (6.2) and (6.18) or (6.20). Thus, Elsasser fields' spectra have exponents -2 in the l_{\parallel} direction, $-3/2$ in the λ direction and $-5/3$ in the ξ direction (see the $n = 2$ exponents in figure 13a). Let me note in passing that the ‘‘Kolmogorov’’ scaling (6.29) will play a key part in my discussion, in appendix C.6, of why the Lazarian & Vishniac (1999) notion of ‘‘stochastic reconnection’’ does not automatically invalidate the aligned cascade and return us to GS95, as an erudite reader might have been worried it would.

A good way of thinking of the inevitability of 3D anisotropy is to note that, from (6.1) and CB,

$$\xi \sim l_{\parallel} \frac{\delta Z_{\lambda}}{v_A} \sim l_{\parallel} \frac{\delta b_{\lambda}}{v_A}, \quad (6.30)$$

i.e., ξ is the typical displacement of a fluid element and also the typical perpendicular distance a field line wanders within a structure coherent on the parallel scale l_{\parallel} . Fluctuations must therefore preserve coherence in their own direction at least on the scale ξ . They are not constrained in this way in the third direction λ and the fluctuation direction itself has an angular uncertainty of the order of the angle θ_{λ} between the two fields, so it makes sense that the aspect ratio of the structures in the perpendicular plane should satisfy (6.2).

The dependence of the anisotropy on the local direction of the fluctuating fields makes the connection between anisotropy, alignment and intermittency more obvious: when we follow perturbed field lines to extract parallel correlations or measure one Elsasser field's decorrelation along the direction of another Elsasser field, we are clearly not calculating second-order statistics in the strict sense—and so, in formal terms, local scale-dependent anisotropy always involves correlation functions of (all) higher orders.²⁵ Thus, it makes a certain natural sense to speak of the alignment-induced departure of MHD-

in the direction of \mathbf{b}_{\perp} , the fluctuation direction, all we need to do in order to preserve parallel correlations is to ensure $\Delta l_{\perp} \ll \xi$. This is indeed marginally satisfied when $L_{\perp} \sim \lambda$ because, in (5.7), $l/v_A \sim \xi/\delta b_{\lambda}$. Chen *et al.* (2012a) and Verdini *et al.* (2018, 2019) observationally and Mallet *et al.* (2016) numerically used this method with apparent success.

²⁵It is easy to show that a Gaussian field cannot have scale-dependent alignment—although a solenoidal field will naturally have some modest scale-independent one (Chen *et al.* 2012a; Mallet *et al.* 2016). Note also the paper by Matthaeus *et al.* (2012), where the role of higher-order statistics in locally parallel correlations is examined with great punctiliousness.

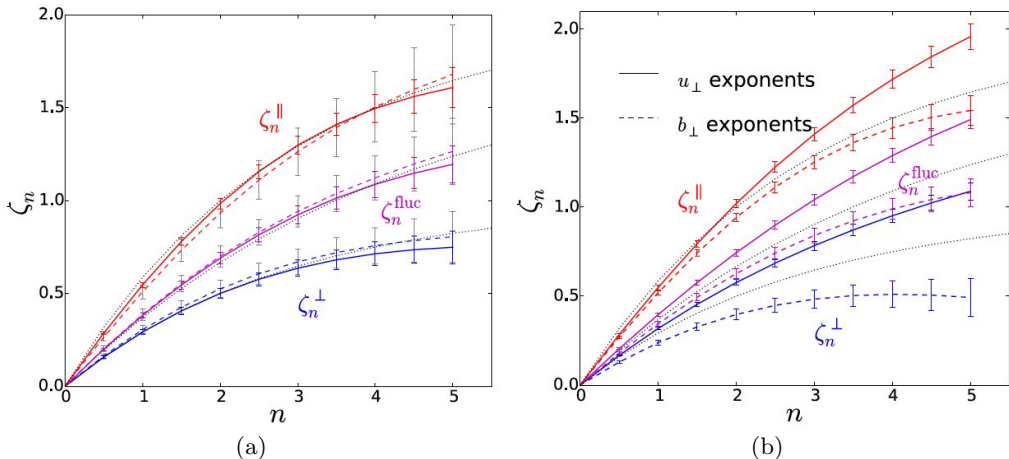


FIGURE 13. Scaling exponents of the structure functions in RMHD turbulence simulated by Mallet *et al.* (2016) (the plot is from Mallet & Schekochihin 2017). (a) Structure functions of the Elsasser-field increments (5.6): by definition, $\langle |\delta \mathbf{Z}_l^+|^n \rangle \propto l^{\zeta_n}$ and ζ_n^{\perp} , ζ_n^{fluc} , ζ_n^{\parallel} are exponents for $l = \lambda, \xi, l_{\parallel}$, respectively (i.e., all structure functions are conditional on the point separation being in one of the three directions of local 3D anisotropy; see §§ 5.3 and 6.4). The solid lines are for a 1024^3 simulation (with hyperviscosity), the dashed ones are for a 512^3 simulation, indicating how converged, or otherwise, the exponents are, and the dotted lines, in both (a) and (b), are the theoretical model by Mallet & Schekochihin (2017). (b) Similarly defined structure functions of the velocity (solid lines) and magnetic-field (dashed lines) increments from the same 1024^3 simulation. The magnetic field is “more intermittent” than the Elsasser fields and the latter more so than velocity. An early (possibly first) numerical measurement of this kind, highlighting the differences between scalings of different fields and in different local directions, was done by Cho *et al.* (2003).

turbulence spectrum from the Kolmogorovian GS95 scaling and of the 3D anisotropy of the underlying fluctuation field as an intermittency effect, as I have done here.

6.5. Higher-Order Statistics

In several places (e.g., in §§ 5.3 and 6.3.2), I have brushed against the more formal task of the intermittency theory—the calculation of the scaling exponents of higher-order structure functions or, equivalently, of the probability distributions of field increments—and recoiled every time, opting for “twiddle” algebra and statements about spectra. A fair amount of information on these matters is available from simulations and from the solar-wind measurements: what intermittency looks like in the former is illustrated by figure 13 (a survey of previous measurements of structure functions, both in simulations and in the solar wind, can be found in Chandran *et al.* 2015). Some of what is known is perhaps understood, but much remains a mystery: for example, we do not know why the higher-order scaling exponents are generally not the same for velocity, Elsasser and magnetic fields, with the latter “more intermittent” than the former, as is evident in figure 13(b) (see, however, the discussion in § 9.4 of the possible connexion between intermittency and negative “residual energy”—an asymmetry between the magnetic and velocity spectra seen both in numerical simulations and in the solar wind).

Interesting as it is, I will now leave the problem of higher-order statistics alone. We know from the (ongoing) history of hydrodynamic-turbulence theory that once this becomes *the* unsolved problem that everyone is working on, the scope for abstract theorising expands to fill all available space (and time) while attention paid by the

outside world diminishes.²⁶ This said, I hasten to dispel any possible impression that I do not consider intermittency of MHD turbulence an important problem: in fact, as I have argued above, intermittency as a physical phenomenon appears to be so inextricably hard-wired into the structure of MHD turbulence that any workable theory of the latter has to be a theory of its intermittency.

Finally, let me jump ahead of myself and mention also that we know nothing at all of the intermittency in “tearing-dominated turbulence,” which is about to be introduced (§ 7), and very little of the intermittency in the variants of MHD turbulence surveyed in §§ 8–12. In particular, the relationship between intermittency and Elsasser imbalance, local or global, appears to me to be a promising object for theoreticians’ scrutiny (see § 8.1).

7. MHD Turbulence Meets Reconnection

Finally, we wonder if it is possible that Sweet’s mechanism might modify somewhat the diffusion and dissipation of the magnetic field in hydromagnetic turbulence.

Last sentence of [Parker \(1957\)](#)

If we accept that MHD turbulence in the inertial range—or, at least, in some subrange of the inertial range immediately below the outer scale—has a tendency to organise itself into fettuccine-like structures whose aspect ratio in the 2D plane perpendicular to the mean magnetic field increases as their size decreases, we are opting for a state of affairs that is not sustainable at ever smaller scales. These structures are mini-sheets, and sheets in MHD tend to be tearing-unstable. Thus, just like WT, strong aligned turbulence too carries the seeds of its own destruction, making an eventual transition to some new state inevitable at sufficiently small scales.²⁷

The notion that current sheets will spontaneously form in a turbulent MHD fluid is not new ([Matthaeus & Lamkin 1986](#); [Politano *et al.* 1989](#)) and the phenomenology of these structures has been studied (numerically) quite extensively, most notably, over the last decade, by [Servidio *et al.* \(2009, 2010, 2011a,b\)](#) in 2D and by [Zhdankin *et al.* \(2013, 2014, 2015, 2016b\)](#) in 3D (see also [Wan *et al.* 2014](#)), while solar-wind measurements ([Retinò *et al.* 2007](#); [Sundkvist *et al.* 2007](#); [Osman *et al.* 2014](#); [Greco *et al.* 2016](#)) provided motivation and, perhaps, vindication. However, theoretical discussion of these results appeared to focus on the association between current sheets in MHD turbulence and its intermittent nature, identifying spontaneously forming current sheets as the archetypal

²⁶Let me qualify this by mentioning a recent paper by [Mallet *et al.* \(2019\)](#) where abstract theory of intermittency is converted into insights into particle-heating physics in the solar wind (more of the [Chandran *et al.* 2010](#) stochastic heating in the more intense, intermittent patches), which some might view as a more “practical” (in the astrophysical sense) preoccupation.

²⁷That this transition can and, generally speaking, will happen *within the inertial range* is made obvious by the following rather apt observation due to [Uzdensky & Boldyrev \(2006\)](#). The aspect ratio of an aligned sheet-like structure at Boldyrev’s cutoff scale (6.22) is $\xi/\lambda \sim \text{Rm}^{1/6}(1 + \text{Pm})^{-1/6}$, using (6.29) for ξ and setting $\lambda = \lambda_\eta$. The Lundquist number at this scale is $S_\xi = \delta Z_{\lambda_\eta} \xi/\eta \sim \text{Rm}^{1/3}(1 + \text{Pm})^{2/3}$. Therefore, $\xi/\lambda \sim S_\xi^{1/2}(1 + \text{Pm})^{-1/2}$. Apart from the Pm dependence, this is the aspect ratio of a Sweet–Parker (SP) current sheet, which is $S_\xi^{1/2}(1 + \text{Pm})^{-1/4}$ (see appendix C.3.1). But, provided S_ξ is large enough and Pm is not too large, such a sheet will be violently (i.e., high above threshold) unstable to the plasmoid instability, which is a variety of tearing mode and has a growth rate that is much larger than the nonlinear rate at which the sheet is formed (see appendix C.3.2). Therefore, tearing should muscle its way into turbulent dynamics already at some scale that is larger than λ_η .

intermittent events—and effectively segregating this topic from the traditional questions about the turbulence spectrum and the “typical” structures believed to be responsible for it, viz., Alfvénic perturbations, aligned or otherwise.²⁸

In fact, as we saw in §§ 6.3.2 and 6.4, it is difficult and indeed unnatural to separate the physics of alignment from that of intermittency. Dynamic alignment produces sheet-like structures that measurably affect the energy spectrum but are also the intermittent fluctuations that can perhaps collapse into proper current sheets. The likelihood that they will do so—or, more generally, that aligned structures can survive at all—hinges on whether the nonlinear cascade time τ_{nl} at a given scale λ is longer or shorter than the typical time scale on which a tearing mode can be triggered, leading to the break up of the dynamically forming sheets into islands (Uzdensky & Loureiro 2016). Since the growth rate of the tearing mode in resistive MHD is limited by resistivity and would be zero in the limit of infinitely small η , the aligned turbulent cascade should be safe from tearing above a certain scale that must be proportional to some positive power of η . However, this need not be the same as Boldyrev’s cutoff scale (6.19) that arises from the competition between the cascade rate and vanilla Ohmic (or viscous) diffusion (τ_{nl} vs. τ_η)—and so, at the very least, the cutoff scale of the aligned cascade may not be what you might have thought it was, and what happens below that scale may be more interesting than the usual dull exponential petering out of the energy spectrum in the dissipation range.

This possibility was explored by Mallet *et al.* (2017b) and Loureiro & Boldyrev (2017b) (unaware of each other’s converging preoccupations), leading to a new scaling for the aligned cascade’s cutoff and to a model for the tail end of the MHD turbulence spectrum—mitigating some of the unsatisfactory features of the aligned-turbulence paradigm and thus providing a kind of glossy finish to the overall picture (despite their rather esoteric nature, the two papers appear to have become instant classics—so much so as to merit logarithmic corrections being derived to their scaling predictions: Comisso *et al.* 2018). While the key idea in the two papers is the same, their takes on its consequences for the “tearing-mediated turbulence” are different—here I will side with Mallet *et al.* (2017b), but present their results in a somewhat simpler, if less general, form.²⁹

Before I proceed, let me alert an erudite reader that the profound alteration of the

²⁸In the minds of some current-sheet enthusiasts, the distinction between the sheets (“structures”) and critically balanced Alfvénic perturbations (“waves”) has become a dichotomy between two allegedly incompatible conceptions of how energy is dissipated in MHD turbulence (based on the incorrect interpretation of the CB theory as requiring turbulence to be an ensemble of random-phased Alfvén waves, similar to WT). No such dichotomy, of course, exists: while Alfvénic perturbations retain certain properties associated with the linear-wave response, their turbulence is strong (§ 5) and the tendency to form sheets dynamic (§ 6). In the recent literature, the most systematic discussion of the “waves vs. structures” issue can be found in Grošelj *et al.* (2019) (although their focus is on the kinetic, rather than MHD, range of scales).

²⁹Namely, I will ignore the nuance that, in an intermittent ensemble, fluctuations of different strengths that are always present even at the same scale will be affected by reconnection to a different degree and so more intense structures will be disrupted at larger scales than the less intense ones. This means that there is, in fact, not a single “disruption scale” but rather a “disruption range.” I will also not present scalings that follow from the theory of the aligned cascade by Chandran *et al.* (2015), focusing for simplicity exclusively on the model by Mallet & Schekochihin (2017) (which is the same as Boldyrev’s original theory if the latter is interpreted as explained in § 6.3). In this sense, my exposition in § 7.1 is closer in style to Loureiro & Boldyrev (2017b) than the paper by Mallet *et al.* (2017b) was. The material difference between the two arises in § 7.2 and concerns the spectrum of the tearing-mediated turbulence. This is now moot, however, as the follow-up paper by Boldyrev & Loureiro (2017) embraced the Mallet *et al.* (2017b) spectrum, if not quite the physical model that led to it (see § 7.2.2).

MHD cascade by reconnection that I will discuss here has nothing at all to do with the concept of stochastic reconnection in MHD turbulence associated with the names of Lazarian, Vishniac, and Eyink—this is explained carefully in appendix C.6.

7.1. Disruption by Tearing

The scale at which the aligned structures will be disrupted by tearing can be estimated very easily by comparing the nonlinear time (6.1) of the aligned cascade with the growth time of the fastest tearing mode that can be triggered in an MHD sheet of a given transverse scale λ . That this growth time is a good estimate for the time that reconnection needs to break up a sheet forming as a result of ideal-MHD dynamics is not quite as obvious as it might appear, but it is true and was carefully shown to be so by Uzdensky & Loureiro (2016). The maximum tearing growth rate is

$$\gamma \sim \frac{v_{Ay}}{\lambda} S_\lambda^{-1/2} (1 + \text{Pm})^{-1/4}, \quad S_\lambda = \frac{v_{Ay}\lambda}{\eta}, \quad \text{Pm} = \frac{\nu}{\eta}. \quad (7.1)$$

How to derive this is reviewed in appendix C.1 [see (C31)]. Here v_{Ay} is the Alfvén speed associated with the perturbed magnetic field at scale λ , S_λ is the corresponding Lundquist number and Pm is the magnetic Prandtl number, which only matters if the viscosity ν is larger than the magnetic diffusivity η . In application to our aligned Alfvénic structures, we should replace $v_{Ay} \sim \delta Z_\lambda$. Then, using the scalings (6.20) to work out τ_{nl} , we find that the aligned cascade is faster than tearing as long as

$$\gamma\tau_{\text{nl}} \sim \frac{S_\lambda^{-1/2}(1 + \text{Pm})^{-1/4}}{\sin\theta_\lambda} \ll 1 \quad \Leftrightarrow \quad \lambda \gg \text{Rm}^{-4/7}(1 + \text{Pm})^{-2/7}\lambda_{\text{CB}} \equiv \lambda_{\text{D}}, \quad (7.2)$$

where $\text{Rm} \sim S_{\lambda_{\text{CB}}}$, as defined in (6.21). At scales $\lambda \lesssim \lambda_{\text{D}}$, aligned sheet-like structures can no longer retain their integrity against the onslaught of tearing.³⁰

The new *disruption scale* λ_{D} , upon comparison with the putative resistive cutoff (6.22) of the aligned cascade turns out to supersede it provided Pm is not too large:

$$\frac{\lambda_{\text{D}}}{\lambda_\eta} \sim \left[\frac{\text{Rm}}{(1 + \text{Pm})^{10}} \right]^{2/21} \gg 1. \quad (7.3)$$

In view of the ridiculous exponents involved, this means that in a system with even moderately large Pm and/or not a truly huge Rm, the aligned cascade will happily make it to the dissipation cutoff (6.22) and no further chapters are necessary in this story.³¹ However, I do want to tell the story in full and so will focus on situations in which the condition (7.3) is satisfied.

I shall turn to the question of what happens at scales below λ_{D} in § 7.2, but to do that, it is necessary first to ask what becomes of the aligned structures that are disrupted at λ_{D} .

³⁰This is equivalent to the idea of Pucci & Velli (2014) that one can determine the maximum allowed aspect ratio of sheets in MHD by asking when the tearing time scale in the sheet becomes comparable to its ideal-MHD dynamical evolution time (see appendix C.4.1). Careful examination of semi-forgotten ancient texts reveals that nothing is new under the Moon and the idea that tearing would disrupt the MHD cascade in fact appeared first in an early paper by Carbone *et al.* (1990), who derived the disruption scale (7.2) (without Pm) by comparing the tearing growth rate (7.1) with the cascade time taken from the IK theory—this gives the same scaling, $\lambda_{\text{D}} \propto \text{Rm}^{-4/7}$, because the IK spectrum has the same scaling as Boldyrev’s spectrum.

³¹This is, in fact, not quite true: at $\text{Pm} \gg 1$, interesting things can happen between the viscous and resistive cutoffs—see § 10. In particular, if the tearing disruption fails to occur in the inertial range, it may still occur at subviscous scales (§ 10.4).

The tearing instability that disrupts them, the so called Coppi mode, or (the fastest-growing) resistive internal kink mode (Coppi *et al.* 1976), has the wavenumber [see (C 31)]

$$k_* \sim \frac{1}{\lambda} S_\lambda^{-1/4} (1 + \text{Pm})^{1/8} \sim \frac{1}{\lambda_{\text{CB}}} \text{Rm}^{-1/4} (1 + \text{Pm})^{1/8} \left(\frac{\lambda}{\lambda_{\text{CB}}} \right)^{-21/16}, \quad (7.4)$$

where (6.20) has been used to substitute for δZ_λ inside S_λ . Therefore, at the disruption scale ($\lambda = \lambda_{\text{D}}$),

$$k_* \sim \frac{1}{\lambda_{\text{CB}}} \text{Rm}^{1/2} (1 + \text{Pm})^{1/2}. \quad (7.5)$$

If referred to the length of the sheet ξ_{D} , which depends on λ_{D} via (6.29), this wavenumber gives us an estimate for the number of islands in the growing perturbation:

$$N \sim k_* \xi_{\text{D}} \sim \text{Rm}^{1/14} (1 + \text{Pm})^{2/7} \gg 1. \quad (7.6)$$

As this is always large, the mode fits comfortably into the sheet that it is trying to disrupt.³²

What happens to these islands? When the tearing mode enters the nonlinear regime, the island width is (see appendix C.2)

$$w \sim k_* \lambda_{\text{D}}^2, \quad (7.7)$$

which is smaller than λ_{D} and so, technically speaking, the aligned structures need not be destroyed by these islands. Uzdensky & Loureiro (2016) (followed by Mallet *et al.* 2017*b* and by Loureiro & Boldyrev 2017*b*) argue that, after the tearing mode goes nonlinear, the X -points between the islands will collapse into current sheets on the same time scale (7.1) as the mode grew. The outcome is a set of N islands, which can be assumed to have circularised. Their width is then $(wk_*^{-1})^{1/2} \sim \lambda_{\text{D}}$ and so they do disrupt the aligned structure (ideal-MHD sheet) that spawned them. The argument leading to this conclusion (which is not specific to MHD turbulence) is rehearsed more carefully in appendices C.2 and C.4, but the key point for us here is that at the disruption scale, the aligned structures that cascade down from the inertial range are broken up by reconnection into flux ropes that are *isotropic* in the perpendicular plane. This is a starting point for a new kind of cascade, which we shall now proceed to consider.

7.2. Tearing-Mediated Turbulence in the Disruption Range

If you accept the argument at the end of §7.1 that the disruption by tearing of an aligned structure at the scale λ_{D} leads to its break-up into a number of unaligned flux ropes, then the natural conclusion is that λ_{D} now becomes a kind of “outer scale” for a new cascade. There need not be anything particularly different about this cascade compared to the standard aligned cascade except the alignment angle is now reset to being order unity. As these “disruption-range” structures interact with each other and break up into smaller structures, the latter should develop the same tendency to align as their inertial-range predecessors did. For a while, the structures in this new cascade are safe from tearing as their aspect ratio is not large enough, but eventually (i.e., at

³²Based on (7.4), we see that this would be the case for tearing perturbations of any inertial-range structure with $\lambda \lesssim \text{Rm}^{-4/9} (1 + \text{Pm})^{2/9} \lambda_{\text{CB}}$. At larger scales than this, the fastest tearing mode that fits into the sheet is the FKR mode (Furth *et al.* 1963) with \sim one growing island of size $\sim \xi$ [see (C 33) and the discussion at the end of appendix C.1.4]. However, both this mode and the secular Rutherford (1973) evolution that succeeds it are always slower than the Coppi mode and, therefore, than the nonlinear ideal-MHD evolution of the sheet, so there is no danger of disruption at those scales.

small enough scales), they too will become sufficiently aligned to be broken up by tearing modes. This leads to another disruption, another iteration of an aligned “mini-cascade,” and so on. Thus, if we rebaptise our critical-balance scale as $\lambda_{\text{CB}} = \lambda_0$, the disruption scale as $\lambda_{\text{D}} = \lambda_1$, and the subsequent disruption scales as λ_n , we can think of the MHD cascade as consisting of a sequence of aligned cascades interrupted by disruption episodes.

7.2.1. Dissipation Scale

Let us calculate the disruption scales λ_n , following Mallet *et al.* (2017b). Since the “mini-cascades” that connect them are just the same as the aligned cascade whose disruption we analysed in §7.1, we can use (7.2) to deduce a recursion relation

$$\lambda_{n+1} \sim S_{\lambda_n}^{-4/7} (1 + \text{Pm})^{-2/7} \lambda_n \quad (7.8)$$

(remembering that Rm was defined as the Lundquist number at scale $\lambda_{\text{CB}} = \lambda_0$). To work out the Lundquist number S_{λ_n} at scale λ_n , notice that there must be a downward jump in the amplitude of the turbulent fluctuations at any disruption scale: indeed, if the alignment angle θ_λ just below λ_n is reset to being order unity, the nonlinear time (6.1) shortens significantly compared to what it was in the aligned cascade just above λ_n , and the cascade accelerates. Since it still has to carry the same energy flux,³³ we have, for amplitudes just below the disruption scale (λ_n^-),

$$\frac{(\delta Z_{\lambda_n^-})^3}{\lambda_n} \sim \varepsilon \quad \Rightarrow \quad \delta Z_{\lambda_n^-} \sim (\varepsilon \lambda_n)^{1/3}. \quad (7.9)$$

Therefore,

$$S_{\lambda_n} \sim \frac{\delta Z_{\lambda_n^-} \lambda_n}{\eta} \sim \frac{\varepsilon^{1/3} \lambda_n^{4/3}}{\eta} \sim \text{Rm} \left(\frac{\lambda_n}{\lambda_{\text{CB}}} \right)^{4/3}. \quad (7.10)$$

In combination with (7.8), this gives us

$$\frac{\lambda_n}{\lambda_{\text{CB}}} \sim \left[\text{Rm}^{-4/7} (1 + \text{Pm})^{-2/7} \right]^{\frac{21}{16} \left[1 - \left(\frac{5}{21} \right)^n \right]} \rightarrow \text{Rm}^{-3/4} (1 + \text{Pm})^{-3/8}, \quad n \rightarrow \infty. \quad (7.11)$$

Apart from the Pm dependence, which we shall discuss in a moment, we are back to the Kolmogorov scale (6.9), where Achilles catches up with the tortoise and the cascade terminates.

Let us confirm that this is indeed the final dissipation scale. For each “mini-cascade” starting at λ_n , we can calculate the dissipative cutoff by replacing Rm with S_{λ_n} in (6.22):

$$\begin{aligned} \frac{\lambda_{\eta,n}}{\lambda_{\text{CB}}} &\sim S_{\lambda_n}^{-2/3} (1 + \text{Pm})^{2/3} \frac{\lambda_n}{\lambda_{\text{CB}}} \sim \text{Rm}^{-\frac{3}{4} + \frac{1}{12} \left(\frac{5}{21} \right)^n} (1 + \text{Pm})^{\frac{5}{8} + \frac{1}{24} \left(\frac{5}{21} \right)^n} \\ &\rightarrow \text{Rm}^{-3/4} (1 + \text{Pm})^{5/8}. \end{aligned} \quad (7.12)$$

Thus, this too converges to the Kolmogorov scale as long as $\text{Pm} \lesssim 1$. In fact, it converges to the Kolmogorov scale also at $\text{Pm} \gg 1$. From (7.12), we see that the cascade will, in fact, terminate at a finite n for which $\lambda_{\eta,n} \sim \lambda_n$, or $S_{\lambda_n} \sim 1 + \text{Pm}$. In other words, the cutoff occurs when either Rm or Re associated with the λ_n -scale structures is order

³³As we saw in (7.3) and as we shall see in (7.12), λ_n is always larger than the corresponding dissipation scale $\lambda_{\eta,n}$. This means that the amount of energy dissipation at λ_n is negligible, so it makes sense to assume that reconnection at the disruption scale(s) converts the energy of aligned structures into that of the flux ropes, while dissipating very little of it.

unity. Via (7.10), this condition gives us

$$\lambda_{\eta,n} \sim \lambda_{\text{CB}} \left(\frac{\text{Rm}}{1 + \text{Pm}} \right)^{-3/4} = \lambda_{\text{CB}} \widetilde{\text{Re}}^{-3/4} \sim \frac{(\nu + \eta)^{3/4}}{\varepsilon^{1/4}}, \quad (7.13)$$

where $\widetilde{\text{Re}}$, defined in (6.22), is Rm when $\text{Pm} \lesssim 1$ and Re when $\text{Pm} \gg 1$. Thus, Kolmogorov's scaling of the dissipative cutoff is rehabilitated: the scale (7.13) is just that, due to viscosity or resistivity, whichever is larger. It is easy to check that the condition for the range $[\lambda_{\text{D}}, \lambda_{\eta,n}]$ to be non-empty is less stringent than (7.3), so it is always satisfied if the disruption occurs in the first place.

It is interesting to note that it is the Kolmogorov scaling at the dissipation scales that was the strongest claim made by Beresnyak (2011, 2012a, 2014b, 2019) on the basis of a convergence study of his numerical spectra (see §6.2 and figure 10b). While he inferred from that an interpretation of these spectra as showing a $-5/3$ scaling in the inertial range, it is their convergence at the dissipative end of the resolved range that appeared to be the least negotiable feature of his work. He may well have been right.

7.2.2. Spectrum in the Disruption Range

In the picture that I have described above, the disruption-range cascade looks like a ladder (figure 14), with amplitude dropping at each successive disruption scale as structures become unaligned. In between the disruption scales, there are aligned “mini-cascades” of the same kind as the original one discussed in §6.3. This means that the overall scaling of the turbulent fluctuation amplitudes can be constrained between their scaling just below each disruption scale (λ_n^-) and just above it (λ_n^+). We already have the former: it is the Kolmogorov (or GS95) scaling (7.9). The scaling of the amplitudes of the structures just before they get disrupted can be inferred from the fact that for these structures, the tearing growth rate (7.1) is the same as the nonlinear interaction (cascade) rate: letting $v_{Ay} \sim \delta Z_{\lambda_n^+}$ in (7.1), we get

$$\tau_{\text{nl}}^{-1} \sim \gamma \sim (\delta Z_{\lambda_n^+})^{1/2} \lambda_n^{-3/2} \eta^{1/2} (1 + \text{Pm})^{-1/4} \quad (7.14)$$

and, therefore,

$$\begin{aligned} \frac{(\delta Z_{\lambda_n^+})^2}{\tau_{\text{nl}}} \sim \varepsilon &\Rightarrow \delta Z_{\lambda_n^+} \sim \varepsilon^{2/5} \eta^{-1/5} (1 + \text{Pm})^{1/10} \lambda_n^{3/5} \\ &\sim \left(\frac{\varepsilon L_{\parallel}}{v_A} \right)^{1/2} \left(\frac{\lambda_{\text{D}}}{\lambda_{\text{CB}}} \right)^{1/4} \left(\frac{\lambda_n}{\lambda_{\text{D}}} \right)^{3/5}. \end{aligned} \quad (7.15)$$

The last expression puts this result explicitly in contact with the inertial-range scaling (6.20). Thus, the disruption-range spectrum is (Mallet *et al.* 2017b)³⁴

$$\varepsilon^{2/3} k_{\perp}^{-5/3} \lesssim E(k_{\perp}) \lesssim \varepsilon^{4/5} \eta^{-2/5} (1 + \text{Pm})^{1/5} k_{\perp}^{-11/5}. \quad (7.16)$$

Since the $-11/5$ upper envelope is steeper than the $-5/3$ lower one, the two converge and eventually meet at

$$\lambda_{\infty} \sim \eta^{3/4} \varepsilon^{-1/4} (1 + \text{Pm})^{-3/8} \sim \lambda_{\text{D}}^{21/16} \lambda_{\text{CB}}^{-5/16}, \quad (7.17)$$

which is, of course, the cutoff scale (7.11) obtained in the limit $n \rightarrow \infty$. An attentive reader will recall that, for $\text{Pm} \gg 1$, this is, in fact, superseded by the true Kolmogorov cutoff (7.13), while at $\text{Pm} \lesssim 1$, the two are the same.

³⁴Boldyrev & Loureiro (2017) have a somewhat differently phrased derivation of the $k_{\perp}^{-11/5}$ spectrum, which will be discussed in §7.3.1.

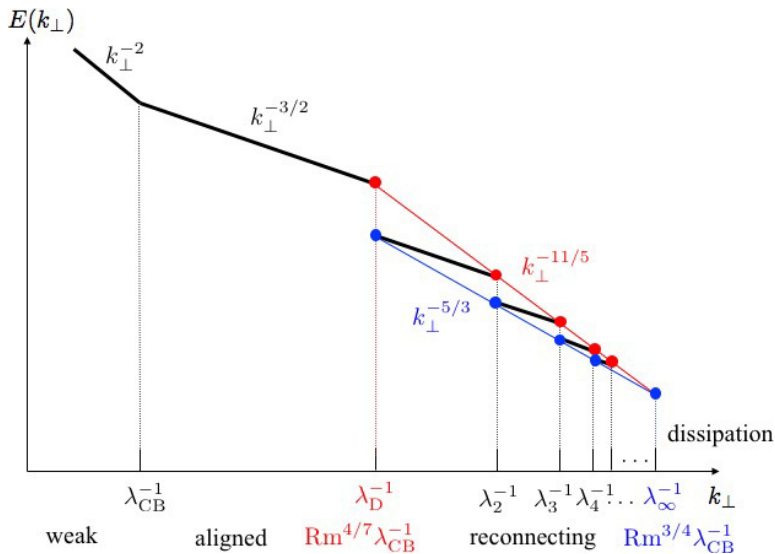


FIGURE 14. Spectrum of MHD turbulence and transition to tearing-mediated cascade [see (7.16)] in the disruption range (adapted from Mallet *et al.* 2017b). The width of the disruption range is, of course, exaggerated in this cartoon.

While in the above construction, the disruption-range spectrum is pictured as a succession of “steps” representing the “mini-cascades” that connect the successive disruption scales (figure 14), the reality will almost certainly look more like some overall power-law spectrum with a slope for which the upper $-11/5$ bound (7.16) seems to be a good estimate. Indeed, the tearing disruptions will be happening within intermittently distributed aligned structures of different amplitudes and sizes, on which the disruption scales will depend (Mallet *et al.* 2017b). Thus, each scale λ_n will in fact be smeared over some range and, as the successive intervals $(\lambda_n, \lambda_{n+1})$ become narrower, this smear can easily exceed their width. Pending a detailed theory of intermittency in the disruption range, perhaps the best way to think of the spectrum and other scalings in this range is, therefore, in a “coarse-grained” sense, focusing on the characteristic dependence of all interesting quantities on λ_n , treated as a continuous variable.

7.2.3. Alignment in the Disruption Range

The structures corresponding to the lower (Kolmogorov) envelope (7.9) are unaligned, whereas the alignment corresponding to the upper envelope (7.15) is the tightest alignment sustainable in the disruption range and achieved by each aligned “mini-cascade” just before it is disrupted by tearing at the scale λ_n . This is (cf. Boldyrev & Loureiro 2017)

$$\sin \theta_{\lambda_n^+} \sim \frac{\lambda / \delta Z_{\lambda_n^+}}{\tau_{nl}} \sim \left(\frac{\lambda_D}{\lambda_{CB}} \right)^{1/4} \left(\frac{\lambda_n}{\lambda_D} \right)^{-4/5}. \quad (7.18)$$

Equivalently, the fluctuation-direction coherence scale is

$$\xi_n \sim \frac{\lambda_n}{\sin \theta_{\lambda_n^+}} \sim \lambda_{CB} \left(\frac{\lambda_D}{\lambda_{CB}} \right)^{3/4} \left(\frac{\lambda_n}{\lambda_D} \right)^{9/5}. \quad (7.19)$$

The corresponding spectral exponent is again $-5/3$, which is automatically the case given the definitions of τ_{nl} , θ_λ and ξ [see (6.1) and § 6.4].

Thus, the smallest possible alignment angle, having reached its minimum at λ_D , gets larger through the disruption range, according to (7.18), until it finally becomes order unity at the cutoff scale (7.17). To the (doubtful) extent that existing numerical evidence can be considered to be probing this regime, perhaps we can take heart from the numerical papers by both Beresnyak and by Boldyrev’s group cited in §6.2 all reporting that alignment fades away at the small-scale end of the inertial range—although this may also be just a banal effect of the numerical resolution cutoff.

7.2.4. Parallel Cascade in the Disruption Range

As ever, CB should be an enduring feature of our turbulence. This means that the parallel spectrum (5.1) will not notice the disruption scale and blithely extend all the way through the disruption range. Since the “isotropic” flux ropes produced in the wake of the disruption of aligned structures have a shorter decorrelation time than their aligned progenitors, they should break up in the parallel direction. The resulting parallel coherence scale, the same as the scale (5.5) in the GS95 theory, is the lower bound on l_{\parallel} at each λ_n . The upper bound can be inferred by equating the nonlinear time (7.14) at λ_n to the Alfvén time l_{\parallel}/v_A . The result is

$$v_A \varepsilon^{-1/3} \lambda_n^{2/3} \lesssim l_{\parallel} \lesssim v_A \varepsilon^{-1/5} \eta^{-2/5} (1 + \text{Pm})^{1/5} \lambda_n^{6/5} \sim L_{\parallel} \left(\frac{\lambda_D}{\lambda_{\text{CB}}} \right)^{1/2} \left(\frac{\lambda_n}{\lambda_D} \right)^{6/5}. \quad (7.20)$$

Thus, the upper bound on the parallel anisotropy *decreases* with scale in this range. The lower and upper bounds meet at the final cutoff scale (7.17):

$$l_{\parallel} \sim v_A \varepsilon^{-1/2} \eta^{1/2} (1 + \text{Pm})^{-1/4} \sim L_{\parallel} \text{Rm}^{-1/2} (1 + \text{Pm})^{-1/4} \quad \text{at} \quad \lambda \sim \lambda_{\infty}. \quad (7.21)$$

Dividing (7.20) and (7.21) by v_A gives us the scaling and the cutoff value, respectively, for the nonlinear (cascade) time τ_{nl} (and so also the frequency cutoff).

7.3. Plasmoid Chains and Fast Reconnection in Tearing-Mediated Turbulence

In what until recently was a separate strand of research, much interest has focused on stochastic plasmoid chains that arise in current sheets susceptible to the plasmoid instability (a sub-species of tearing), where a lively population of islands (plasmoids) are born, grow, travel along the sheet with Alfvénic outflows, occasionally eat each other (coalesce),³⁵ and, as shown by [Uzdensky *et al.* \(2010\)](#), cause reconnection in the sheet that they inhabit to be fast (independent of η as $\eta \rightarrow +0$)—a derivation of the plasmoid instability, as well as a long list of references on stochastic plasmoid chains (and, in figure 41, an example of one) can be found in appendix C.3.2 and the [Uzdensky *et al.* \(2010\)](#) argument in appendix C.5. A stochastic chain can be viewed as a kind of “1D turbulence”, and has some distinctive statistical properties. Should one imagine the disrupted aligned structures spawning multiple instances of such a turbulence, and does the simple theory outlined in §7.2 describe this situation or does it need to be revised to represent a superposition of many fast-reconnecting, plasmoid-infested sheets (as attempted in three different ways by [Loureiro & Boldyrev 2017b, 2020](#) and [Tenerani & Velli 2020b](#))?

7.3.1. How Much Reconnection?

In order to consider this question, one must first decide what the “disruption” of the aligned structures actually consists of. There are two lines of thinking on this, articulated

³⁵Possibly, in the process of coalescence, giving rise to transverse secondary current sheets and plasmoid chains: see [Bárta *et al.* \(2011\)](#).

most explicitly by Mallet *et al.* (2017b) and Boldyrev & Loureiro (2017), of which I have so far stuck with the former. Namely, at the end of § 7.1, I followed Uzdensky & Loureiro (2016), Mallet *et al.* (2017b) and Loureiro & Boldyrev (2017b) in invoking the collapse of the X -points separating the tearing-mode islands as a means of circularising these islands and thus consummating the disruption of the aligned structures—the theory of the disruption-range cascade in § 7.2 was then presented as a corollary of this view.

The collapse of inter-island X -points is actually the first step in the formation of a stochastic chain. A quick comparison of the X -point collapse rate (with $\text{is} \sim$ the tearing growth rate γ) with the growth rate of a *secondary* tearing instability of the same X -point shows that the latter is always greater than the former (at asymptotically large Lundquist numbers). Therefore, the collapse may itself be disrupted by tearing, producing more islands and more X -points, followed by a collapse of those, also disrupted, and so on. This recursive tearing is worked out in detail in appendix C.4.2 (different versions of it that have been proposed are discussed, with attribution, in appendix C.4.3). I argue there that the smaller-scale islands that are produced in this process are not energetically relevant and so need not modify the “one-level” picture of tearing disruption that I have put forward so far.

The recursive tearing proceeds until inter-island current sheets are short enough to be stable, at which point the true nonlinear plasmoid chain can form, involving not just multiple tearings, but also plasmoid circularisation, coalescence, and ejection from the sheet. While the statistics of such a chain may be different from that of a tearing-mediated cascade that I described in § 7.2, I assumed there that it cannot exist for a long time, if at all: indeed, the characteristic time scale of the process of fully forming the sheet out of an aligned structure is the tearing time, and the time to reconnect most of the flux associated with the structure is either of the same order or shorter (if we are in the asymptotic regime where reconnection is fast). If this is true, the “mother sheet” (aligned structure) breaks apart entirely shortly after (or even before) fully forming and releases its plasmoids (flux ropes) into the general turbulent wilderness, where they are free to interact with each other or with anything else that comes along and are thus no different from turbulent fluctuations of a particular size generically splashing around in a large nonlinear system. This gives rise to the disruption-range “mini-cascades” in § 7.2, with the overall $k_{\perp}^{-11/5}$ spectral envelope (7.16).

Boldyrev & Loureiro (2017) also derive the $-11/5$ spectrum by using (7.14) as the operational prescription for the cascade time ($\tau_{\text{nl}} \sim \gamma^{-1}$ at each scale in the disruption range). However, they have a different narrative about what happens dynamically: they do not believe that inter-island X -points ever collapse, but that, rather, the tearing mode upsets alignment by order unity, changing the effective nonlinear cascade rate to the tearing rate. This is based on the (correct) observation that the alignment angle at the disruption scale (7.2)

$$\sin \theta_{\lambda_{\text{D}}} \sim S_{\lambda_{\text{D}}}^{-1/2} (1 + \text{Pm})^{-1/4} \quad (7.22)$$

is the same (at least for $\text{Pm} \lesssim 1$) as the angular distortion of the field line caused by the tearing perturbation at the onset of the nonlinear regime: indeed, using (7.7) and (7.4) at $\lambda = \lambda_{\text{D}}$,

$$\theta_{\text{tearing}} \sim wk_* \sim (k_* \lambda_{\text{D}})^2 \sim S_{\lambda_{\text{D}}}^{-1/2} (1 + \text{Pm})^{1/4}. \quad (7.23)$$

They think that this is enough to make the aligned structure to “cascade,” in some unspecified manner, without much reconnection, production of flux ropes, etc.

In Loureiro & Boldyrev (2020), they revise this a little and allow that, since the collapse time, the tearing time and, therefore, the cascade time are comparable to each other, *some*

aligned structures might, in fact, collapse into sheets. They then conjecture that those will only host significant reconnection if Rm is large enough for reconnection to be fast and for the rate of that fast reconnection to be greater than the tearing growth rate. They expect these reconnection sites to dissipate a lot of energy and thus modify the nature of the turbulent cascade, making it more intermittent, and the spectrum steeper.³⁶ Presumably, these reconnecting sheets will also modify its nature because they must host stochastic plasmoid chains etc. While these suppositions are not numerically falsifiable for resistive MHD because the lower bound on the required Rm turns out to be humongous, it also turns out that the “nonlinear-reconnecting” regime (as opposed to reconnecting by linear tearing) might be easily accessible in certain kinetic settings.

It is hard to say whether the two pictures outlined above represent a disagreement in substance or merely in the style of presentation. While in the Mallet *et al.* (2017b) interpretation, the collapse of the inter-island X -points *is* the way in which the distortion of alignment caused by tearing leads to faster nonlinear break-up of the aligned structures, Loureiro & Boldyrev (2020) think this is not necessary but does happen with some finite probability. This does not seem to be sufficiently quantifiable a difference to be testable.

7.3.2. Turbulence in Reconnecting Sheets

It is nevertheless an interesting question whether, in a turbulent environment, we should expect to see fully formed stochastic chains of the kind theorised and simulated in the literature quoted in appendix C.3.2.

It is worth stressing that much of that literature describes 2D simulations, and there is only a handful of papers dedicated to unstable sheets in 3D (Oishi *et al.* 2015; Huang & Bhattacharjee 2016; Beresnyak 2017; Kowal *et al.* 2017; Stanier *et al.* 2019). In all of these numerical experiments, a large-scale reconnecting configuration (a macroscopic sheet) is set up, (as an initial condition and/or driven by inflows/outflows from/to the boundaries of the domain), then goes violently unstable, much more so than in 2D, and ends up looking like a strip of vigorous turbulence, rather than a quasi-1D chain.³⁷

³⁶They seem to think that the tearing-mediated cascade can only be a constant-flux cascade if it did not involve much reconnection because reconnection is dissipative—hence the spectrum steepening if reconnection did set in. Is there really a contradiction between significant reconnection and constant flux? First, it is not inevitable that reconnection must always involve large dissipation. Secondly, if collapse and reconnection of an aligned structure of scale λ do lead to significant dissipation, that dissipation does not, in fact, occur at scale λ , but at much smaller scales—the scales of the inter-island sheets and outflows. Transfer of energy to those scales could arguably be viewed as part of the tearing-mediated cascade. Thirdly, the proponents of “stochastic reconnection” (Lazarian *et al.* 2020, and references therein) would at this point say that reconnection in a turbulent environment is always fast, and every cascaded eddy always gets a significant amount of reconnection (but not dissipation). As explained in appendix C.6, this is plausible, and does not preclude either aligned or tearing-mediated turbulence. It does seem though that stochastic reconnection could claim to obviate, or sideline, the particular mechanism of fast reconnection in collapsed sheets on which the paper of Loureiro & Boldyrev (2020) is specially focused.

³⁷According to Kowal *et al.* (2020), this turbulence is driven primarily by Kelvin–Helmholtz instability, not tearing—at least at large scales, long times, and in the outflow regions (for a theory of KH instability in reconnecting sheets, see Loureiro *et al.* 2013a). However, the simulations by Kowal *et al.* (2017) from which that conclusion was drawn had an anti-parallel, reconnecting field 10 times larger than the guide field. This is the opposite of the RMHD regime that one expects to find locally in the kind of MHD turbulence that I have discussed so far, where the in-plane field is always small, $b_{\perp} \ll B_0$. Of the rest of the papers cited here, Oishi *et al.* (2015) had $B_0 = 0$, and the others $b_{\perp} \sim B_0$. I have not seen a 3D study of a reconnecting sheet in RMHD, which would be more directly relevant to aligned structures that arise in the inertial range of MHD turbulence.

There does not appear to be any reason for such a configuration to stay together without external help, so it is likely that what we are witnessing in these numerical simulations is a version of a tearing-mediated cascading event, possibly prolonged by the bespoke numerical set-up.

If this is true, then such reconnection-driven MHD turbulence and turbulence in a homogeneous box into which turbulent energy is injected by a body force are different only inasmuch as any two different outer-scale, system-specific arrangements for stirring up turbulence are different. In the spirit of universality, it is hard to believe that small patches of a turbulent sheet would look any different in close-up than a generic box of MHD turbulence. At a stretch, one can imagine that, due to the macroscopic “reconnection forcing” of the turbulence in a sheet, it starts off at the outer scale already in a highly aligned, or even tearing-dominated, regime (Walker *et al.* 2018 was an explicit attempt to exploit this idea). Indeed, both Bárta *et al.* (2011) and Huang & Bhattacharjee (2016) see spectra somewhat steeper than -2 , perhaps consistent with $-11/5 = -2.2$, although, in contrast, Beresnyak (2017) and Kowal *et al.* (2017) report small-scale statistics very similar to those found in standard MHD turbulence. Tenerani & Velli (2020*b*) find the same at a sufficient distance from the neutral line, whereas close to it, they see interesting anisotropic scalings dependent on the (component of) the field and the direction in which its variation is probed vis-à-vis the orientation of the sheet. They then speculate about the spectrum of a turbulence entirely dominated by such reconnecting sheets filling a scale-dependent fraction of the volume and arrive at $k_{\perp}^{-11/5}$ by an entirely different route, perhaps a coincidence. Loureiro & Boldyrev (2020), in pursuit of the same idea, but with somewhat different assumptions, amend $k_{\perp}^{-11/5}$ to $k_{\perp}^{-12/5}$.

I will let the subject drop at this point, with the parting message that the last word might not have been written on intermittency corrections and the role of fast plasmoid reconnection in tearing-mediated turbulence.

7.4. *Is This the End of the Road?*

It never quite is (see the following sections), but the story looks roughly complete for the first time in years. The aligned cascade (§6) gave one an impression of unfinished business, both in the sense that it gave rise to a state that appeared unsustainable at asymptotically small scales and in view of the objections, physical and numerical, raised by Beresnyak (2011, 2012*a*, 2014*b*, 2019). With the revised interpretation of alignment as an intermittency effect (§6.3) and with the disruption-range cascade connecting the larger-scale aligned cascade to the Kolmogorov cutoff (7.13), these issues appear to be satisfactorily resolved. In what is also an aesthetically pleasing development, the tearing-mediated accelerated cascade emerges as an ingenious way in which MHD turbulence contrives to thermalise its energy while shedding the excessive alignment that ideal-MHD dynamics cannot help producing in the inertial range. This development joins together in a most definite way the physics of turbulence and reconnection—arguably, this was always inevitable and it is good that we now know the specifics.

Is this a falsifiable theory? Probably not any time soon.

Numerically, anything like a definite confirmation will require formidably large simulations: the condition (7.3) demands $Rm \sim 10^5$ at least (estimated via the frivolous but basically sound principle that the smallest large number is 3)—and probably much larger if one is to see the scaling of the disruption-range spectrum (7.16). However, as was mooted above, an optimist might find cause for optimism in the evidence of the MHD turbulence cutoff appearing to obey the Kolmogorov scaling (7.13) or in the alignment

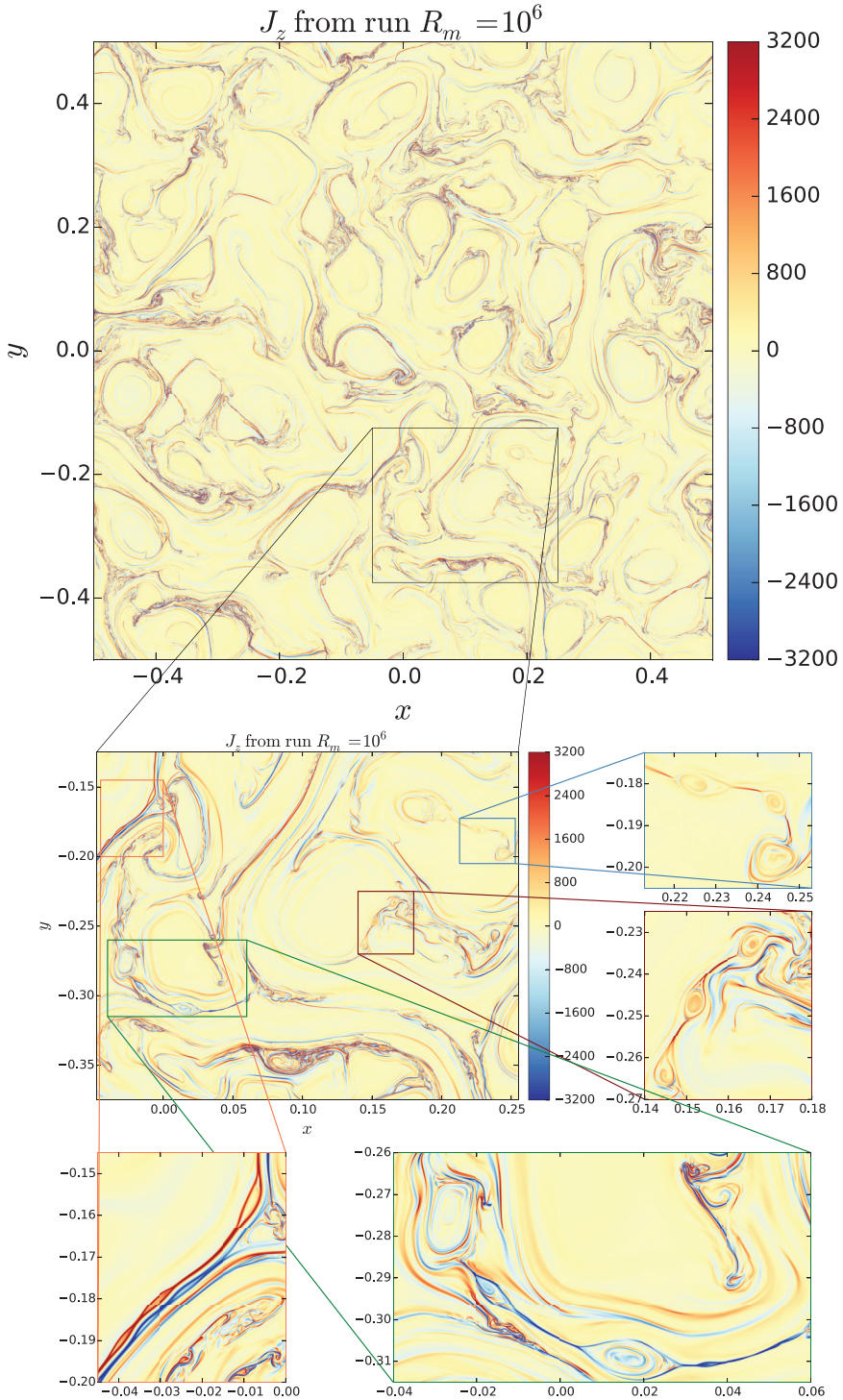


FIGURE 15. A snapshot of current density (j_z) from a 2D, $R_m = 10^6$ ($64,000^2$) MHD simulation by [Dong et al. \(2018\)](#) (I am grateful to C. Dong for letting me have the original figure file). Zoomed areas show sheets broken up into plasmoids.

petering out at the small-scale end of the inertial range, making §7.2.3 seem at least reasonable. While the trouble to which I have gone to keep track of the Pm dependence of the disruption-range quantities did not yield anything qualitatively spectacular, there is perhaps an opportunity here for numerical tests: e.g., can one obtain Boldyrev’s scaling (6.22) of the dissipation cutoff in the limit of large Pm?—which, in view of (7.3), is unlikely to need to be very large to take over and shut down tearing.

One way to circumvent the need for getting into a hyper-asymptotic regime is to simulate directly the dynamics of structures that resemble Alfvénic sheets deep in the inertial range. Such a study by Walker *et al.* (2018), in 2D, of the decay of an Alfvénic “eddy” highly anisotropic in the perpendicular plane, has shown it breaking up promisingly into plasmoids and giving rise to a steeper spectrum than exhibited by a larger-Rm case where tearing was too slow. Dong *et al.* (2018) went further and actually demonstrated a spectral break at the disruption scale and a $k_{\perp}^{-11/5}$ spectrum below it, with sheets in a turbulent system very vividly breaking up into plasmoids (figure 15)—but still in 2D. So far so good.

Observationally, our best bet for fine measurements of turbulence is the solar wind and the terrestrial magnetosphere (e.g., the magnetosheath). However, these are collisionless environments, so, before any triumphs of observational confirmation can be celebrated, all the resistive reconnection physics on which the disruption-range cascade depends needs to be amended for the cornucopia of kinetic effects that await at the small-scale end of the cascade (see §13.1). Once the tearing disruption in MHD was proposed, such generalisations were ripe, low-hanging fruit and so quite a lot of it was immediately picked (Mallet *et al.* 2017a; Loureiro & Boldyrev 2017a; Boldyrev & Loureiro 2019; see also Loureiro & Boldyrev 2018 where these ideas were ported to pair plasmas).

Finally, it would be fair to spell out what can go catastrophically wrong with this picture on the conceptual level. Arguably, it is still subject to verification (perhaps at inaccessible resolutions) that alignment is not a transient, large-scale feature, as Beresnyak (2019) would have it. It seems to me that we do know, however, that if we stir up unaligned turbulence, it will get aligned at smaller scales, so its possible transient nature can only be due to instability of the aligned structures. The picture presented above relied on this instability being the tearing instability—but it is not entirely impossible that it is, in fact, an ideal MHD instability, viz., some version of Kelvin–Helmholtz instability. The difference is that tearing required resistivity and so the disruption scale $\lambda_D \propto \eta^{4/7}$ was asymptotically separated from the outer scale λ_{CB} [see (7.2)], whereas the KH instability would kick in at some $\lambda \sim$ a finite fraction of λ_{CB} . The usual expectation is that KH instability is quenched by the magnetic field (and indeed hence perhaps the statistical preponderance of current sheets over shear layers; see §9.4), but this can in principle turn out to be wrong. If it does, ideal MHD will take care of limiting alignment and, presumably, we will be back to GS95 (in which case I apologise to my readers for having wasted their time with this review).

Pending all this validation and verification, the disruption-range tearing-mediated cascade remains a beautiful fantasy—but one must be grateful that after half a century of scrutiny, MHD turbulence still has such gifts to offer.

PART II

Imbalances and Loose Ends

As we know,
 There are known knowns.
 There are things we know we know.
 We also know
 There are known unknowns.
 That is to say
 We know there are some things
 We do not know.
 But there are also unknown unknowns,
 The ones we don't know
 We don't know.

D. H. Rumsfeld,
U.S. Department of Defense News Briefing,
12 February 2002

In the remainder of this review, I will survey some of what has been done, what remains to be done, and what, in my view, is worth doing regarding the regimes of MHD turbulence in which there is an imbalance either between the energies of the two Elsasser fields or between the kinetic and magnetic energy. Such situations are relevant (and indeed often more relevant) in many astrophysical contexts but remain much less (or even less) well understood, than the nice (and somewhat fictional) case in which one can just assume $\delta Z_\lambda^+ \sim \delta Z_\lambda^- \sim \delta b_\lambda \sim \delta u_\lambda$. Not only the cases of Elsasser (§ 8) and Alfvénic (§ 9) imbalance can be put in this class but also the distinct regimes of MHD turbulence that arise below the viscous scale (assuming large Pm; § 10), or when the turbulence is allowed to decay freely (§ 11), or when no mean field is imposed (the saturated MHD dynamo; § 12).

8. Imbalanced MHD Turbulence

8.1. *Story So Far*

Since both incompressible MHD and RMHD conserve two invariants—the total energy and the cross-helicity,—each of the two Elsasser fields \mathbf{Z}_\perp^\pm has its own conserved energy [see (3.3)]. The energy fluxes ε^\pm of these fields are, therefore, independent parameters of MHD turbulence. Setting them equal to each other makes arguments simpler, but does not, in general, correspond to physical reality, for a number of reasons.

First, everyone's favourite case of directly measurable MHD turbulence is the solar wind, where the Alfvénic perturbations propagating away from the Sun are launched from the Sun (Roberts *et al.* 1987), while the counterpropagating ones have to be supplied by some mechanism that is still under discussion and probably involves Alfvén-wave reflection as plasma density decreases outwards from the Sun (see Chandran & Perez 2019 and references therein). The counterpropagating component is usually energetically smaller, especially in the fast wind (Bruno & Carbone 2013; Chen *et al.* 2020).

Secondly—and, for a theoretical physicist interested in universality, more importantly—it is an intrinsic property of MHD turbulence to develop *local* imbalance. This can be understood dynamically as a desire to evolve towards an Elsasser state, $\mathbf{Z}_\perp^+ = 0$ or $\mathbf{Z}_\perp^- = 0$, which is an exact solution of RMHD equations (confirmed in simulations of decaying MHD turbulence; see § 11), or statistically as a tendency for the local dissipation rates ε^\pm to fluctuate in space—a mainstay of intermittency theories since Landau's

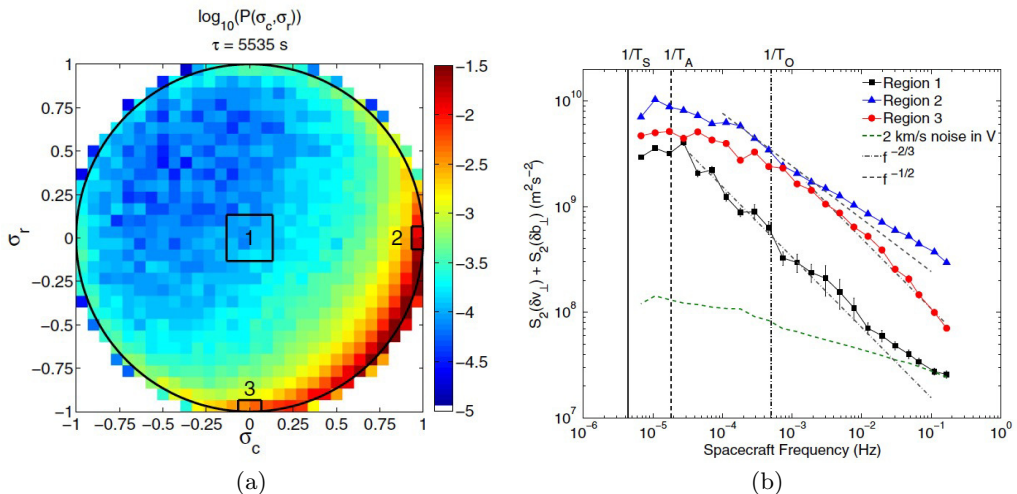


FIGURE 16. (a) Distribution of normalised cross-helicity (σ_c) and residual energy (σ_r) [see (8.4)] in an interval of fast-solar-wind data taken by Wind spacecraft and analysed by Wicks *et al.* (2013b), from whose paper both plots in this figure are taken. (b) Structure functions corresponding to the total energy (sum of kinetic and magnetic) conditioned on values of σ_c and σ_r and corresponding to Regions 1 (balanced), 2 (Elsasser-imbalanced) and 3 (Alfvénically imbalanced towards magnetic perturbations), indicated in panel (a). The $f^{-2/3}$ slope corresponds to a $k_{\perp}^{-5/3}$ spectrum, the $f^{-1/2}$ slope to a $k_{\perp}^{-3/2}$ one.

famous objection (see Frisch 1995) to Kolmogorov (1941b) and the latter’s response in the form of the refined similarity hypothesis, accepting a fluctuating ε (Kolmogorov 1962). In this context, a complete intermittency theory for MHD turbulence must incorporate whatever local modification (if any) of the MHD cascade is caused by $\varepsilon^+ \neq \varepsilon^-$, something that no existing theory has as yet accomplished or attempted.

That an intimate connection must exist between any verifiable theory of MHD turbulence and local imbalance is well illustrated (in figure 16) by the following piece of observational analysis, rather noteworthy, in my (not impartial) view. Wicks *et al.* (2013b) took a series of measurements by Wind spacecraft of magnetic and velocity perturbations in fast solar wind and sorted them according to the amount of imbalance, both Elsasser and Alfvénic (§ 9), at each scale. They then computed structure functions conditional on these imbalances. While the majority of perturbations were imbalanced one way or the other (or both), there was a sub-population with $\delta Z_{\lambda}^+ \sim \delta Z_{\lambda}^- \sim \delta b_{\lambda} \sim \delta u_{\lambda}$. Interestingly, the structure function restricted to this population had what seemed to be a robust GS95 scaling (corresponding to a $k_{\perp}^{-5/3}$ spectrum), even though the structure functions of the imbalanced perturbations—and also of all perturbations averaged together—were consistent with Boldyrev’s $k_{\perp}^{-3/2}$ aligned-cascade scaling and indeed exhibited some alignment, unlike the GS95 population (see Wicks *et al.* 2013a; Podesta & Borovsky 2010 reported analogous results, conditioning on the presence of cross-helicity only). It is important to recognise that imbalance and alignment do not automatically imply each other, so balanced fluctuations are not absolutely required to be unaligned, or aligned fluctuations to be imbalanced (see § 8.1.2). However, as I argued in § 6.3.2, dynamical alignment is an intermittency effect and so there may be a correlation between the emergence of imbalanced patches at ever smaller scales and Elsasser fields shearing each other into alignment (cf. Chandran *et al.* 2015).

Intuitively then, since patches of mild imbalance are locally ubiquitous even in globally

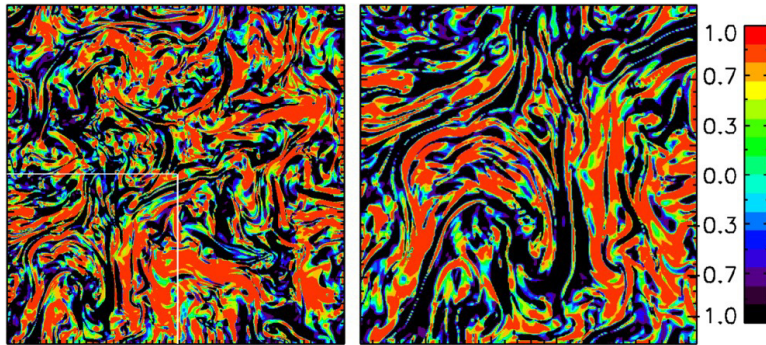


FIGURE 17. Cosine of the angle between increments $\delta\mathbf{u}_\lambda$ and $\delta\mathbf{b}_\lambda$ in the (x, y) plane, for $\lambda = L_\perp/6$ (left) and $\lambda = L_\perp/12$ (right, corresponding to the region demarcated by the white square within the left panel) in a balanced RMHD simulation by Perez & Boldyrev (2009), whence this figure was taken. Since $\delta\mathbf{u}_\lambda \cdot \delta\mathbf{b}_\lambda = (|\delta Z_\lambda^+|^2 - |\delta Z_\lambda^-|^2)/4$, this is an illustration of patchy local imbalance, as well as of local alignment between the velocity and magnetic field.

balanced turbulence (Perez & Boldyrev 2009; see figure 17) and since the theory of balanced turbulence described in §6.3 incorporates intermittency effects in the form of alignment, we might expect that this allows for local imbalance—and, therefore, that mildly imbalanced turbulence might look largely similar to the balanced one. Indeed, how would perturbations in the middle of inertial range “know” that the local imbalance they “see” is local rather than global? Obviously, on average, there will not be an imbalance and so the results for δZ_λ that one derives for balanced turbulence (§§6 and 7) are effectively averaged over the statistics of the stronger and weaker Elsasser fields—which of δZ_λ^+ and δZ_λ^- is which depends on time and space.

If we now allow $\varepsilon^+ > \varepsilon^-$ on average, it becomes reasonable to expect $\delta Z_\lambda^+ > \delta Z_\lambda^-$ nearly everywhere or, at least, typically—unless $\varepsilon^+/\varepsilon^-$ is close enough to unity that fluctuations of local imbalance overwhelm the overall global one. In the latter case, presumably imbalance does not matter—at any rate, in the balanced considerations of §§6 and 7, we only ever required $\varepsilon^+ \sim \varepsilon^-$, rather than $\varepsilon^+ = \varepsilon^-$ exactly. What I am driving at here, perhaps with too much faffing about, is the rather obvious point that it is only the limit of strong imbalance, $\varepsilon^+ \gg \varepsilon^-$, that can be expected to be physically distinct, in a qualitative manner, from the balanced regime.

8.1.1. Numerical and Observational Evidence

As usual, it is this most interesting limit that is also the hardest to resolve numerically and so we have little definitive information as to what happens in the strongly imbalanced regime. As in the case of the spectra of balanced turbulence, the debate about the numerical evidence regarding the imbalanced cascade and its correct theoretical interpretation has been dominated by the antagonistic symbiosis of Beresnyak and Boldyrev, so it is from their papers (Beresnyak & Lazarian 2008, 2009b, 2010; Beresnyak 2019; Perez & Boldyrev 2009, 2010a,b) that I derive much of the information reviewed below. Perez & Boldyrev (2010a,b) argue that large imbalances are unresolvable and refuse to simulate them. Beresnyak & Lazarian (2009b, 2010) do not necessarily disagree with this, but believe that useful things can still be learned from strongly imbalanced simulations. Based on both groups’ simulations, imbalanced MHD turbulence appears to exhibit the following distinctive features (which I recount with a degree of confidence as they have been reproduced in two sets of independent, unpublished RMHD simulations by Mallet & Schekochihin 2011 and by Meyrand & Squire 2020).

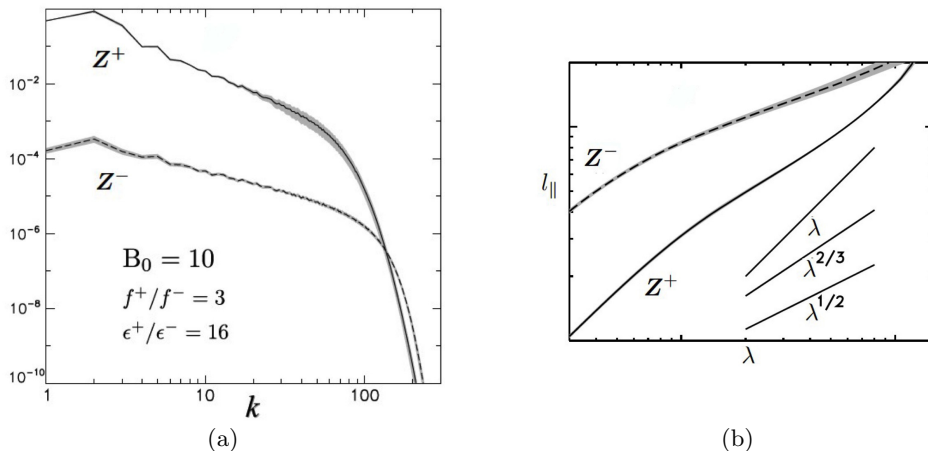


FIGURE 18. A typical MHD simulation with large imbalance: (a) spectra, (b) anisotropy, l_{\parallel}^{\pm} vs. λ . These plots are adapted from Beresnyak & Lazarian (2009b). Mallet & Schekochihin (2011) and Meyrand & Squire (2020) have qualitatively similar results (although the difference in slopes between the weaker and the stronger fields’ spectra is smaller in the higher-resolution simulations of Meyrand & Squire 2020—see an example of that in Fig. 5c of Meyrand *et al.* 2020).

(i) The stronger field has a steeper spectrum than the weaker one, with the former steeper and the latter shallower than the standard balanced-case spectra (figure 18a). However, it is quite likely that these spectra are not converged with resolution: as resolution is increased, the tendency appears to be for the spectral slopes to get a little closer to each other, both when the imbalance is weak (Perez & Boldyrev 2010a) and when it is strong (Mallet & Schekochihin 2011). This led Perez & Boldyrev (2010a) to argue that numerical evidence was consistent with the two fields having the same spectral slope in the asymptotic limit of infinite Reynolds numbers. There is no agreement as to whether the two fields’ spectra might be pinned to each other at the dissipation scale: yes in weakly imbalanced simulations of Perez & Boldyrev (2010a), no in the strongly imbalanced ones of Beresnyak & Lazarian (2009b).³⁸

(ii) The ratio of stronger to weaker field’s energies, a crude outer-scale quantity that Beresnyak & Lazarian (2008, 2009b, 2010) argue (reasonably, in my view) to be more likely to be numerically converged than inertial-range scalings, scales very strongly with ϵ^+/ϵ^- : it increases at least as fast as $\langle |Z_{\perp}^+|^2 \rangle / \langle |Z_{\perp}^-|^2 \rangle \sim (\epsilon^+/\epsilon^-)^2$ and possibly faster (which is inconsistent with the theory of Perez & Boldyrev 2009, another *casus belli* for the two groups; see § 8.1.4). Mallet & Schekochihin (2011, see figure 19) and Meyrand & Squire (2020) found the same scaling in their simulations for values of ϵ^+/ϵ^- up to 10 (simulations with much higher imbalances are numerically suspect).

³⁸Whereas the question of pinning may be subject to nontrivial discussion (Lithwick & Goldreich 2003; Chandran 2008) in application to MHD turbulence with a viscous or resistive cutoff at small scales, it would appear that it is more straightforward in a collisionless plasma, e.g., in the solar wind. Indeed, there, the decoupling between the two Elsasser fields breaks down at the ion Larmor scale, where they are allowed to exchange energy (Schekochihin *et al.* 2009; Kunz *et al.* 2015) and, presumably, will not have very different typical amplitudes. Thus, an imbalanced turbulence theory with Larmor-scale pinning might be a desirable objective. If and when such an outcome proves impossible, this can have interesting implications for the very viability of a constant-flux cascade (and, at low beta, does, according to Meyrand *et al.* 2020: see § 13.2).

(iii) According to Beresnyak & Lazarian (2008, 2009b) and Meyrand & Squire (2020), the stronger field is less anisotropic than the weaker one, in the sense that $l_{\parallel}^{+} < l_{\parallel}^{-}$ and l_{\parallel}^{+} drops faster with λ than l_{\parallel}^{-} (figure 18b). Beresnyak (2019) notes that this is true in his simulations even though he forces the two fields with the same parallel scale, i.e., given an opportunity to keep $l_{\parallel}^{+} = l_{\parallel}^{-}$, the system refuses to do so.

(iv) Mallet & Schekochihin (2011, see figure 19) found that the parallel spectrum of the weaker field was very robustly k_{\parallel}^{-2} —to be precise, the exponent varied between -1.9 and -2.1 , but in a manner that evinced no systematic dependence on $\varepsilon^{+}/\varepsilon^{-}$. For the stronger field, they found a gradual steepening of the parallel spectrum with higher imbalance.

(v) Beresnyak & Lazarian (2009b) found that the alignment angle between the Elsasser fields, defined as $\sin \theta$ in (8.1), with numerator and denominator averaged separately, decreased with scale roughly as $\lambda^{0.1}$, independently of the degree of imbalance. Mallet & Schekochihin (2011) measured the same exponent, quite robustly for a wide range of imbalances, but noticed also that the scaling exponent depended on the definition of the “alignment angle”: e.g., if root-mean-square numerator and denominator were used, the scaling was $\lambda^{0.2\dots 0.25}$, closer to the familiar theory (6.18). This is not special to the imbalanced cases—the same is true in balanced turbulence (Mallet *et al.* 2016).

(vi) The observational picture is only just emerging. A steeper scaling for the stronger field noted in item (i) appears to be consistent with the structure functions measured in the fast solar wind by, e.g., Wicks *et al.* (2011), although, besides this, they also exhibit low Alfvén ratio (see § 9), which simulations do not, and a rather-hard-to-interpret (or, possibly, to trust) scale dependence of the anisotropy. In contrast, Podesta & Borovsky (2010) report a scale-independent Elsasser ratio and $k^{-3/2}$ spectra for both fields in a number of reasonably imbalanced cases of solar-wind turbulence at 1 AU. The same result has been reported by Chen *et al.* (2020) from the very recent measurements by the Parker Solar Probe made closer to the Sun, where the imbalance gets larger ($\langle |Z^{+}|^2 \rangle / \langle |Z^{-}|^2 \rangle \approx 15$)—this may be damning for any theory or simulation where the two fields’ spectra scale differently, at least inasmuch as these theories or simulations aspire to apply to the solar wind.

(vii) As the solar wind offers practically the only chance of observational testing of theory—a chance greatly enhanced by the launch of the Parker Solar Probe,—there is a growing industry of direct numerical modelling of the generation of inward-propagating (Z^{-}) perturbations by reflection of the outward-propagating ones (Z^{+}), which is what is supposed to happen in the expanding solar wind. The latest and most sophisticated study of this kind is Chandran & Perez (2019) (who also provide an excellent overview of previous work). Their results appear to be quite different from the idealised periodic-box, artificially-forced studies discussed above: the stronger field’s spectrum is actually *shallower* than the weaker one’s (sometimes as shallow as k^{-1}), but both asymptote towards $k^{-3/2}$ with increasing heliocentric distance—good news for modelling, in view of what Chen *et al.* (2020) have found. Chandran & Perez (2019) acknowledge, however, that they can break these results by fiddling with how their turbulence is forced in the photosphere. Thus, the nature of large-scale energy injection appears to matter,³⁹ at least at finite resolutions, perhaps reinforcing the doubts expressed above about the convergence of even the more idealised simulations.

³⁹Chandran & Perez (2019) have a theory as to why that is, which will be explained in § 8.1.3.

| $\varepsilon^+/\varepsilon^-$ | μ_{\perp}^+ | μ_{\parallel}^+ | μ_{\perp}^- | μ_{\parallel}^- | R_E |
|-------------------------------|-----------------|---------------------|-----------------|---------------------|-------|
| 1 | -1.6 | -1.9 | -1.6 | -1.9 | 1 |
| 2 | -1.6 | -1.9 | -1.5 | -2.0 | 5 |
| 5 | -1.8 | -2.0 | -1.5 | -2.0 | 35 |
| 8 | -1.8 | -2.1 | -1.5 | -2.0 | 45 |
| 10 | -1.9 | -2.2 | -1.4 | -2.1 | 110 |
| 100 | -2.3 | -2.3 | -1.4 | -2.0 | 2200 |
| 1000 | -2.5 | -2.6 | -1.3 | -2.0 | 13000 |

FIGURE 19. Scalings found in (unpublished) 512^3 RMHD numerical simulations by [Mallet & Schekochihin \(2011\)](#): perpendicular (parallel) spectral indices μ_{\perp} (μ_{\parallel}) (inferred from structure functions calculated as explained in §5.3) for both fields, denoted by the \pm superscripts. In terms of the scaling exponents $\gamma_{\perp,\parallel}^{\pm}$ of the field increments ($\delta Z_{\lambda}^{\pm} \propto \lambda^{\gamma_{\perp}^{\pm}}$, $\delta Z_{i\parallel}^{\pm} \propto l_{\parallel}^{\gamma_{\parallel}^{\pm}}$), these are $\mu_{\perp,\parallel}^{\pm} = -2\gamma_{\perp,\parallel}^{\pm} - 1$. The last column shows the overall Elsasser ratio $R_E = \langle |\mathbf{Z}_{\perp}^+|^2 \rangle / \langle |\mathbf{Z}_{\perp}^-|^2 \rangle$. The parallel scalings of the weaker field were converged with resolution, while the perpendicular scalings of the stronger (weaker) field at $\varepsilon^+/\varepsilon^- = 10$ became shallower (steeper) as resolution was increased from 256^3 to 512^3 to $1024^2 \times 512$. Simulations with $\varepsilon^+/\varepsilon^- = 100, 1000$ should be viewed as numerically suspect.

For a short while still, the field appears set to remain open to enterprising theoreticians.

8.1.2. Geometry and Types of Alignment

Let me now deal with a topic to which I have alluded several times but thus far avoided discussing carefully: the formal relationship between imbalance and (various kinds of) alignment. The first salient fact is purely geometric: the two alignment angles (defined for a particular pair of field increments)

$$\sin \theta = \frac{|\delta \mathbf{Z}_{\lambda}^+ \times \delta \mathbf{Z}_{\lambda}^-|}{|\delta \mathbf{Z}_{\lambda}^+| |\delta \mathbf{Z}_{\lambda}^-|}, \quad \sin \theta^{ub} = \frac{|\delta \mathbf{u}_{\lambda} \times \delta \mathbf{b}_{\lambda}|}{|\delta \mathbf{u}_{\lambda}| |\delta \mathbf{b}_{\lambda}|}, \quad (8.1)$$

and the Elsasser and Alfvén ratios

$$R_E = \frac{|\delta \mathbf{Z}_{\lambda}^+|^2}{|\delta \mathbf{Z}_{\lambda}^-|^2}, \quad R_A = \frac{|\delta \mathbf{u}_{\lambda}|^2}{|\delta \mathbf{b}_{\lambda}|^2} \quad (8.2)$$

are related (see figure 20) by the following equations

$$\sin^2 \theta = \frac{\sin^2 \theta^{ub}}{\sin^2 \theta^{ub} + (1 - R_A)^2 / 4R_A}, \quad \sin^2 \theta^{ub} = \frac{\sin^2 \theta}{\sin^2 \theta + (1 - R_E)^2 / 4R_E}, \quad (8.3)$$

so only two of these quantities are independent. Equivalently, in terms of the normalised local cross-helicity and residual energy

$$\sigma_c = \frac{|\delta \mathbf{Z}_{\lambda}^+|^2 - |\delta \mathbf{Z}_{\lambda}^-|^2}{|\delta \mathbf{Z}_{\lambda}^+|^2 + |\delta \mathbf{Z}_{\lambda}^-|^2} = \frac{R_E - 1}{R_E + 1}, \quad \sigma_r = \frac{|\delta \mathbf{u}_{\lambda}|^2 - |\delta \mathbf{b}_{\lambda}|^2}{|\delta \mathbf{u}_{\lambda}|^2 + |\delta \mathbf{b}_{\lambda}|^2} = \frac{R_A - 1}{R_A + 1}, \quad (8.4)$$

the alignment angles are

$$\cos \theta = \frac{\sigma_r}{\sqrt{1 - \sigma_c^2}}, \quad \cos \theta^{ub} = \frac{\sigma_c}{\sqrt{1 - \sigma_r^2}}. \quad (8.5)$$

This means that, generally speaking, alignment between the velocity and magnetic field is not the same thing as alignment between the Elsasser variables, and it is a nontrivial

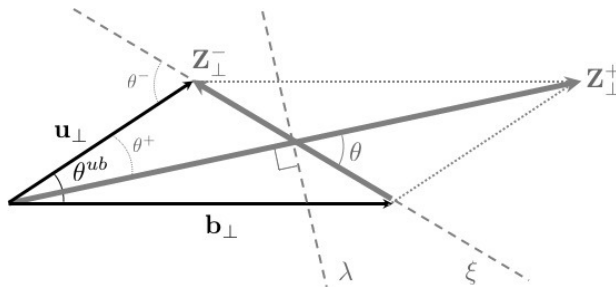


FIGURE 20. Geometry of velocity, magnetic and Elsasser fields. All four fields are aligned: the angles θ , θ^{ub} , θ^\pm are all small (although they do not have to be). Also shown are the axes along which the λ and ξ scales in (6.1) are meant to be calculated (perpendicular to \mathbf{Z}_\perp^+ and along \mathbf{Z}_\perp^- , respectively). The angle between these axes is $\phi = \pi/2 - \theta$ and so $\cos \phi = \sin \theta$.

decision which of these you think matters for the determination of τ_{nl}^\pm . As I noted in § 6.1, my answer to this question is different from Boldyrev’s: I prefer the alignment of Elsasser variables, while he favours that of \mathbf{u}_\perp and \mathbf{b}_\perp —hence my use of $\sin \theta$ in (6.1). In this, I follow Chandran *et al.* (2015) and Mallet *et al.* (2015), who think of alignment as a result of mutual shearing of Elsasser fields—then it makes sense that it is the alignment of \mathbf{Z}_\perp^+ and \mathbf{Z}_\perp^- that leads to the depletion of the $\mathbf{Z}_\perp^\mp \cdot \nabla_\perp \mathbf{Z}_\perp^\pm$ nonlinearity in (3.1).⁴⁰

This kind of alignment does not have to be directly related to the local dynamics enhancing the cross-helicity $\mathbf{u}_\perp \cdot \mathbf{b}_\perp$ (Matthaeus *et al.* 2008) or to the latter’s statistical tendency to cascade to small scales, together with the energy (Perez & Boldyrev 2009). Consider a strongly (locally) imbalanced situation, where $R_E \gg 1$, i.e., the cross-helicity is large ($\sigma_c \approx 1$). Then (8.3) gives us

$$\sin^2 \theta^{ub} \approx \frac{4 \sin^2 \theta}{R_E} \ll 1, \quad (1 - R_A)^2 \approx \frac{16 \cos^2 \theta}{R_E} \ll 1. \quad (8.6)$$

Mallet & Schekochihin (2011) found, unsurprisingly, that these inequalities were extremely well satisfied in their imbalanced RMHD simulations. Thus, local imbalance implies that \mathbf{u}_\perp and \mathbf{b}_\perp are both closely aligned and have nearly the same amplitude (this is geometrically obvious from figure 20), but whether or not the Elsasser fields are aligned is up to the turbulence to decide. It does seem to decide to align them [see § 8.1.1, item (v)], hence the way in which I drew the field increments in figure 20.

If R_E (equivalently, σ_c) is independent of scale in the inertial range, as reported for the solar wind by Podesta & Borovsky (2010) and Chen *et al.* (2020), then the first relation in (8.6) implies that θ^{ub} and θ should have the same scaling. In numerical simulations, they appear to do so, approximately, in balanced turbulence (Mallet *et al.* 2016), which, of course, is patch-wise imbalanced, but not in the strongly imbalanced cases studied by Beresnyak & Lazarian (2009b) and Mallet & Schekochihin (2011) (see § 8.1.1). Accordingly, Mallet & Schekochihin (2011) found the dependence of θ^{ub} on λ getting shallower with increased imbalance, as R_E vs. λ got steeper and θ stayed the

⁴⁰This approach is circumstantially supported by the “refined critical balance” (Mallet *et al.* 2015; see figure 6)—the remarkable self-similarity shown by the ratio $\tau_A/\tau_{\text{nl}}^\pm$, with τ_{nl}^\pm defined by (6.1), using the angle between the Elsasser fields. Arguably, this says that it is this τ_{nl}^\pm that τ_A (and, therefore, l_\parallel^\pm) “knows” about, so it is this τ_{nl}^\pm that should be viewed as the cascade time of the decorrelating eddies. Another argument that I wish to turn to my advantage in this context is one involving the exact law (3.7): see footnote 16. Finally, the presence of negative residual energy in MHD turbulence also supports Elsasser alignment: see § 9.4.

same. Alas, those simulations are in all probability not in the asymptotic regime. Bigger, better simulations, as well as bigger, better ideas, are much overdue in this area.

8.1.3. *Lithwick et al. (2007)*

In view of the discussion in § 8.1.2, I shall stick with my use of the Elsasser-field alignment angle θ in the expression (6.1) for τ_{nl}^{\pm} . This angle is obviously the same for both fields, so

$$\tau_{\text{nl}}^{\pm} \sim \frac{\lambda}{\delta Z_{\lambda}^{\mp} \sin \theta_{\lambda}} \Rightarrow \frac{\tau_{\text{nl}}^{+}}{\tau_{\text{nl}}^{-}} \sim \frac{\delta Z_{\lambda}^{+}}{\delta Z_{\lambda}^{-}} > 1, \quad (8.7)$$

i.e., the cascade of the stronger field is slower (because it is advected by the weaker field). Assuming nevertheless that both cascades are strong, we infer immediately

$$\frac{(\delta Z_{\lambda}^{\pm})^2}{\tau_{\text{nl}}^{\pm}} \sim \varepsilon^{\pm} \Rightarrow \frac{\delta Z_{\lambda}^{+}}{\delta Z_{\lambda}^{-}} \sim \frac{\varepsilon^{+}}{\varepsilon^{-}}. \quad (8.8)$$

Thus, the two fields' increments have the same scaling with λ (the same k_{\perp} spectra) and the ratio of their energies is $\sim (\varepsilon^{+}/\varepsilon^{-})^2$. This is the conclusion at which *Lithwick et al. (2007, henceforth LGS07)* arrives—they considered unaligned GS95-style turbulence ($\sin \theta \sim 1$), but that does not affect (8.8) [note that this result already appeared in (5.4)].

Things are, however, not as straightforward as they might appear. LGS07 point out that it is, in fact, counterintuitive that the weaker δZ_{λ}^{-} perturbation, which is distorted by δZ_{λ}^{+} on a shorter time scale τ_{nl}^{-} , can nevertheless coherently distort δZ_{λ}^{+} for a longer time τ_{nl}^{+} . Their solution to this is to argue that, while the weaker field is strongly distorted *in space* by the stronger one, it remains correlated *in time* for as long as the stronger field does (coherence time of the long-correlated advector inherited by the advectee). In other words, during its (long) correlation time τ_{nl}^{+} , the stronger field (in its reference frame travelling at v_{Λ}) sees a weak field that has been rendered multiscale by the spatial variation of the stronger field, but remains approximately constant for a time τ_{nl}^{+} and so can keep distorting the stronger field in a time-coherent way.

Chandran & Perez (2019) argue that such a scheme, which they call the “coherence assumption,” while not justifiable in general, is fine if the weaker field is forced at the outer scale with the same correlation time as the cascade time of the stronger field. This is great for them as, in their model, the weaker field is generated by the reflection of the stronger one as the latter propagates outwards in an expanding solar wind, and so one should indeed expect the two fields to be tightly correlated at the outer scale. Their endorsement of LGS07—perhaps with an amendment that θ_{λ} should have some scaling with λ determined by alignment/intermittency (§ 6.3.2)—is backed up by their numerical results, where both fields' spectra approach $k_{\perp}^{-3/2}$ (and their alignment increases) with increasing heliocentric distance.

8.1.4. *Perez & Boldyrev (2009)*

Perez & Boldyrev (2009) disagree with the entire approach leading to (8.8): they think that the two Elsasser fields should have two different alignment angles θ_{λ}^{\pm} , both small, and posit that those ought to be the angles that they make with the velocity field.⁴¹

⁴¹*Podesta & Bhattacharjee (2010)* base their theory on the same assumption (also unexplained), but have a different scheme for generalising Boldyrev's aligned cascade to the imbalanced regime. Their picture of the geometric configuration of the fields assumes that $|\delta \mathbf{u}_{\lambda}| = |\delta \mathbf{b}_{\lambda}|$ and, consequently, that $\delta \mathbf{Z}_{\lambda}^{+}$ and $\delta \mathbf{Z}_{\lambda}^{-}$ are perpendicular to each other. This does not appear to be

Why that should be the case they do not explain, but if one takes their word for it, then (as is obvious from the geometry in figure 20)

$$\delta Z_\lambda^+ \sin \theta_\lambda^+ \sim \delta Z_\lambda^- \sin \theta_\lambda^- \quad \Rightarrow \quad \tau_{\text{nl}}^+ \sim \tau_{\text{nl}}^- \sim \frac{\lambda}{\delta Z_\lambda^\pm \sin \theta_\lambda^\pm} \quad \Rightarrow \quad \frac{\delta Z_\lambda^+}{\delta Z_\lambda^-} \sim \sqrt{\frac{\varepsilon^+}{\varepsilon^-}}. \quad (8.9)$$

The last result follows from the first relation in (8.8) with $\tau_{\text{nl}}^+ \sim \tau_{\text{nl}}^-$. The equality of cascade times also conveniently spares them having to deal with the issue, discussed above, of long-time correlatedness, or otherwise, of the weaker field (or with $l_\parallel^+ \neq l_\parallel^-$; see § 8.1.5).

Perez & Boldyrev (2009, 2010*a,b*) are not forthcoming with any detailed tests of this scheme (viz., either of the details of alignment or of the energy-ratio scaling), while Beresnyak & Lazarian (2010) present numerical results that contradict very strongly the expectation of the energy ratio scaling as $\varepsilon^+/\varepsilon^-$ [as implied by (8.9)] and possibly support $(\varepsilon^+/\varepsilon^-)^2$ [i.e., (8.8)].⁴² Perez & Boldyrev (2010*b*) reply that (8.9) should only be expected to hold for local fluctuating values of the amplitudes and of ε^\pm and not for their box averages. It is not impossible that this could make a difference for cases of weak imbalance ($\varepsilon^+/\varepsilon^- \sim 1$), with local fluctuations of energy fluxes superseding the overall imbalance, although it seems to me that if it does, we are basically dealing with balanced turbulence anyway: I do not see any fundamental physical difference between $\varepsilon^+ = \varepsilon^-$ and $\varepsilon^+ \sim \varepsilon^-$ on the level of “twiddle” arguments by which everything is done in these theories. At strong imbalance, (8.8) seems to work better (Beresnyak & Lazarian 2009*b*, 2010) for the overall energy ratio, but not for spectra, which do not have the same slope (figure 18*a*). Perez & Boldyrev (2010*a,b*) argue that such cases in fact cannot be properly resolved, the limiting factor being the weaker field providing too slow a nonlinearity to compete with dissipation and produce a healthy inertial range. If so, the interesting case is inaccessible and the accessible case is uninteresting, we know nothing.

8.1.5. Parallel Scales and Two Flavours of CB

By the CB conjecture (§ 5.1), the parallel coherence lengths of the two fields are, in the “naïve” theory leading to (8.8),

$$l_\parallel^\pm \sim v_A \tau_{\text{nl}}^\pm \quad \Rightarrow \quad \frac{l_\parallel^+}{l_\parallel^-} \sim \frac{\varepsilon^+}{\varepsilon^-} > 1, \quad (8.10)$$

whereas in the Perez & Boldyrev (2009) theory (8.9), the equality of cascade times implies $l_\parallel^+ \sim l_\parallel^-$, end of story. LGS07 argue that, in fact, also (8.10) should be replaced by

$$l_\parallel^+ \sim l_\parallel^- \sim v_A \tau_{\text{nl}}^- \quad (8.11)$$

what actually happens, at least in simulations [see § 8.1.1, item (v)]. Podesta & Bhattacharjee (2010) also inherit from Boldyrev’s original construction the incompatibility of their scalings with the RMHD symmetry (see § 6.3.1). There is an interesting angle in their paper though: they notice, in solar-wind observations, that the probabilities with which aligned or anti-aligned (in the sense of the sign of $\delta \mathbf{u}_\lambda \cdot \delta \mathbf{b}_\lambda$) perturbations occur are independent of scale throughout the inertial range; they then use the ratio of these probabilities as an extra parameter in the theory. This is a step in the direction of incorporating patchy imbalance into the game—something that seems important and inevitable.

⁴²Podesta (2011) collated both groups’ data and concluded that the results of Perez & Boldyrev (2010*b*) were entirely compatible with Beresnyak & Lazarian (2010) and with $(|\mathbf{Z}_\perp^+|^2)/(|\mathbf{Z}_\perp^-|^2) \approx (\varepsilon^+/\varepsilon^-)^2$.

because \mathbf{Z}_\perp^+ perturbations separated by distance l_\parallel^- in the parallel direction are advected by completely spatially decorrelated \mathbf{Z}_\perp^- perturbations, which would then imprint their parallel coherence length on their stronger cousins (the parallel coherence length of the short-correlated advector imprinted on the advectee).

Furthermore, if one accepts the LGS07 argument that the correlation time of the \mathbf{Z}_\perp^- field is τ_{nl}^+ , not τ_{nl}^- (see § 8.1.3), then $l_\parallel^- \sim v_A \tau_{\text{nl}}^-$ must be justified not by temporal (causal) decorrelation but by the weaker field being spatially distorted beyond recognition on the scale l_\parallel^- , even if remaining temporally coherent. This is more or less what Beresnyak & Lazarian (2008) call “propagation CB” (the other CB being “causality CB”). They note that the typical uncertainty in the parallel gradient of any fluctuating field at scale λ is

$$\delta k_\parallel \sim \frac{\mathbf{b}_\perp \cdot \nabla_\perp}{v_A} \sim \frac{\delta b_\lambda}{\xi_\lambda v_A}. \quad (8.12)$$

In balanced turbulence, $\delta k_\parallel^{-1} \sim v_A \tau_{\text{nl}} \sim l_\parallel$ [cf. (6.30)], so this is just a consistency check. In imbalanced turbulence,

$$\delta b_\lambda \sim \delta Z_\lambda^+ \quad \Rightarrow \quad \delta k_\parallel^{-1} \sim \frac{\xi_\lambda v_A}{\delta Z_\lambda^+} \sim v_A \tau_{\text{nl}}^-, \quad (8.13)$$

where τ_{nl}^- , given by (8.7), is the spatial-distortion time of δZ_λ^- , not necessarily its correlation time. The parallel scale of any field will be the shorter of δk_\parallel^{-1} and whatever is implied by the causality CB. In the LGS07 theory, the latter is $v_A \tau_{\text{nl}}^+$ for both fields. Since $\tau_{\text{nl}}^+ \gg \tau_{\text{nl}}^-$, we must set $l_\parallel^+ \sim l_\parallel^- \sim \delta k_\parallel^{-1}$, which is the same as (8.11).

Thus, we end up with both Elsasser fields having $\tau_A \sim l_\parallel^- / v_A$ that is smaller than their correlation time τ_{nl}^+ (even though the weaker field has a shorter spatial distortion time $\tau_{\text{nl}}^- \sim \tau_A$), but their cascades are nevertheless strong. Whatever you think of the merits of the above arguments, neither (8.10) nor (8.11) appear to be consistent with any of the cases reported by Beresnyak & Lazarian (2009b), weakly or strongly imbalanced, which all have $l_\parallel^+ < l_\parallel^-$ (see, e.g., figure 18b). No other numerical evidence on the parallel scales in imbalanced turbulence is, as far as I know, available in print.

8.2. Towards a New Theory of Imbalanced MHD Turbulence

The Beresnyak & Lazarian (2008) argument was, in fact, more complicated than presented in § 8.1.5, because they did not agree with LGS07 about the long correlation time of the weaker field, assumed the stronger field to be weakly, rather than strongly, turbulent, and were keen to accommodate $l_\parallel^+ < l_\parallel^-$. Their key innovation was to allow interactions to be nonlocal. I will not review their theory here, because it depends on a number of *ad hoc* choices that I do not know how to justify, and does not, as far as I can tell, lead to a fully satisfactory set of predictions, but I would like to seize on their idea of nonlocality of interactions, although in a way that is somewhat different from theirs. The resulting scheme captures most of the properties of imbalanced turbulence observed in numerical simulations (§ 8.1.1) and reduces to the already established theory for the balanced case when $\varepsilon^+ / \varepsilon^- \sim 1$, so perhaps it deserves at least some benefit of the doubt.

8.2.1. *Two Semi-Local Cascades*

Let me assume *a priori* that, as suggested by numerics (Beresnyak & Lazarian 2009b; Beresnyak 2019), $l_{\parallel}^+ \ll l_{\parallel}^-$ in the inertial range, viz.,

$$\frac{l_{\parallel\lambda}^+}{l_{\parallel\lambda}^-} \sim \left(\frac{\lambda}{L_{\perp}} \right)^{\alpha}, \quad (8.14)$$

where $\alpha > 0$ and L_{\perp} is the perpendicular outer scale (so the two Elsasser fields are assumed to have the same parallel correlation length, L_{\parallel} , at the outer scale—e.g., by being forced in such a way).

This implies that, at the same λ , the stronger field δZ_{λ}^+ oscillates much faster than the weaker field δZ_{λ}^- . I shall assume therefore that the interaction between the two fields local to the scale λ is not efficient: even though δZ_{λ}^- is buffeted quite vigorously by the stronger field δZ_{λ}^+ , most of this cancels out. Rather than attempting to pick up a contribution arising for the resulting weak interaction, let me instead posit that the dominant, strong nonlinear distortion of δZ_{λ}^- will be due to the stronger field $\delta Z_{\lambda'}^+$ at a scale $\lambda' > \lambda$ such that

$$l_{\parallel\lambda'}^+ \sim l_{\parallel\lambda}^-. \quad (8.15)$$

In other words, the interaction is nonlocal in λ but local in l_{\parallel} .⁴³ The constancy of the flux of the weaker field then requires

$$\frac{(\delta Z_{\lambda}^-)^2 \delta Z_{\lambda'}^+}{\xi_{\lambda'}} \sim \varepsilon^-, \quad (8.16)$$

where $\xi_{\lambda'}$ has been introduced to account for a possible depletion of the nonlinearity due to alignment:

$$\frac{\xi_{\lambda'}}{L_{\perp}} \sim \left(\frac{\lambda'}{L_{\perp}} \right)^{\beta}. \quad (8.17)$$

In the absence of alignment, $\beta = 1$. For aligned, balanced, locally cascading ($\lambda' \sim \lambda$) turbulence, $\beta = 3/4$ [see (6.29)]. By the usual CB argument, the parallel coherence scale of the weaker field is

$$l_{\parallel\lambda}^- \sim \frac{v_A \xi_{\lambda'}}{\delta Z_{\lambda'}^+}. \quad (8.18)$$

Note that, in the terminology of § 8.1.5, this is both the causality CB and the propagation CB, because δk_{\parallel} for δZ_{λ}^- is determined by the propagation of the latter along the “local mean field” $\delta b_{\lambda'}$ [see (8.12)].

Now consider the cascading of the stronger field by the weaker one. Since $l_{\parallel\lambda}^+ \ll l_{\parallel\lambda}^-$, the δZ_{λ}^- fluctuations are, from the point of view of the δZ_{λ}^+ ones, slow and quasi-2D, and so the weaker field can cascade the strong one locally, in the same way as it does in any of the theories described in § 8.1:

$$\frac{(\delta Z_{\lambda}^+)^2 \delta Z_{\lambda}^-}{\xi_{\lambda}} \sim \varepsilon^+. \quad (8.19)$$

Causality CB would imply $l_{\parallel\lambda}^+ \sim v_A \xi_{\lambda} / \delta Z_{\lambda}^-$, but that is long compared to $\delta k_{\parallel}^{-1}$ given

⁴³Beresnyak & Lazarian (2008) proposed the same, but to describe *weak* cascading of $\delta Z_{\lambda'}^+$ by δZ_{λ}^- . Thus, their cascade of the stronger field is weak and nonlocal and that of the weaker field is strong and local. In the scheme I am proposing here, both cascades are strong and it is the weaker field’s one that is nonlocal.

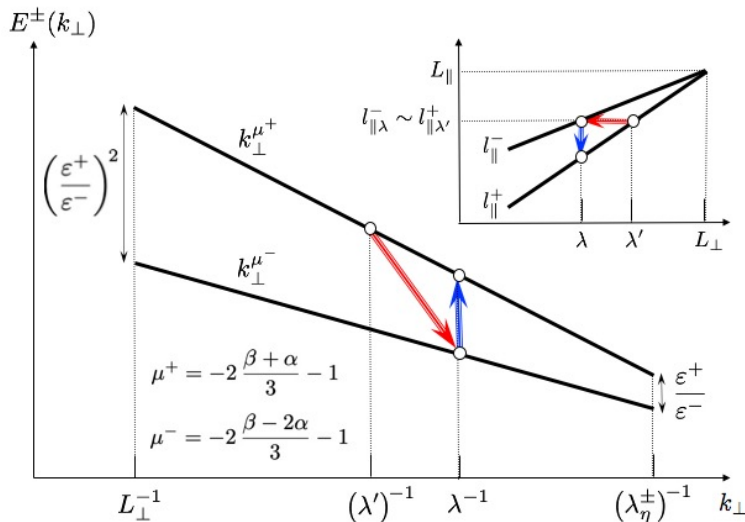


FIGURE 21. Cartoon of the spectra of imbalanced turbulence. The interactions are shown by arrows: red (advection of the weaker field by the stronger field, nonlocal in λ but local in l_{\parallel}) and blue (advection of the stronger field by the weaker field, local in λ but nonlocal in l_{\parallel}). The inset shows the parallel scales l_{\parallel}^{\pm} vs. the perpendicular scale λ .

by (8.12), so I shall use propagation CB instead, just like LGS07 and Beresnyak & Lazarian (2008) did:

$$l_{\parallel\lambda}^+ \sim \frac{v_A \xi_{\lambda}}{\delta Z_{\lambda}^+}. \quad (8.20)$$

Reassuringly, this choice immediately clicks into consistency with the requirement of parallel locality (8.15) if $l_{\parallel\lambda}^-$ is given by (8.18).

There are two nuances here. First, in order for the δZ_{λ}^- field to be able to distort δZ_{λ}^+ according to (8.19), it needs to remain coherent for a time $\sim \xi_{\lambda}/\delta Z_{\lambda}^-$. To make it do so, let me invoke the LGS07 argument already rehearsed in § 8.1.3: according to (8.16), δZ_{λ}^- stays coherent as long as $\delta Z_{\lambda'}^+$ does, which, according to (8.19) with $\lambda = \lambda'$ is $\xi_{\lambda'}/\delta Z_{\lambda'}^-$ —long enough!

Secondly, in (8.19), I used the same the fluctuation-direction scale ξ_{λ} as in (8.16), except at λ , rather than at λ' . This may be a somewhat simplistic treatment of alignment in local vs. nonlocal interactions, but I do not know how to do any better, and the scalings that I get this way will have all the right properties. A reader who finds this unconvincing may assume $\xi_{\lambda} \sim \lambda$ and treat what follows as a GS95-style theory that ignores alignment altogether.

To summarise, I am considering here an imbalanced turbulence that consists of two “semi-local” cascades: that of the stronger field, local in λ but not in l_{\parallel} , and that of the weaker one, local in l_{\parallel} but not in λ (figure 21).

8.2.2. Perpendicular Spectra

In view of (8.18) and (8.20), (8.16) can be rewritten as follows:

$$\frac{(\delta Z_{\lambda}^-)^2 \delta Z_{\lambda}^+}{\xi_{\lambda}} \sim \varepsilon^- \frac{\xi_{\lambda'} \delta Z_{\lambda}^+}{\xi_{\lambda} \delta Z_{\lambda'}^+} \sim \varepsilon^- \frac{l_{\parallel\lambda}^-}{l_{\parallel\lambda}^+} \sim \varepsilon^- \left(\frac{\lambda}{L_{\perp}} \right)^{-\alpha}, \quad (8.21)$$

the last step being a recapitulation of the assumption (8.14). Dividing (8.19) by (8.21), one gets

$$\frac{\delta Z_\lambda^+}{\delta Z_\lambda^-} \sim \frac{\varepsilon^+}{\varepsilon^-} \left(\frac{\lambda}{L_\perp} \right)^\alpha. \quad (8.22)$$

Thus, the ratio of the energies at the outer scale ($\lambda = L_\perp$) is $(\varepsilon^+/\varepsilon^-)^2$, likely the correct scaling [see § 8.1.1, item (ii) and § 8.1.4], and the spectrum of the stronger field is steeper than that of the weaker field, also in agreement with numerics [§ 8.1.1, item (i)].

Now, by using (8.19), (8.22) and the alignment assumption (8.17), it becomes possible to determine the scalings of both fields:

$$\delta Z_\lambda^+ \sim \left[\frac{(\varepsilon^+)^2}{\varepsilon^-} L_\perp \right]^{1/3} \left(\frac{\lambda}{L_\perp} \right)^{(\beta+\alpha)/3}, \quad \delta Z_\lambda^- \sim \left[\frac{(\varepsilon^-)^2}{\varepsilon^+} L_\perp \right]^{1/3} \left(\frac{\lambda}{L_\perp} \right)^{(\beta-2\alpha)/3}. \quad (8.23)$$

Comparing the first of these with (8.16), one can also work out how nonlocal the interactions are:

$$\frac{\lambda}{\lambda'} \sim \left(\frac{\lambda}{L_\perp} \right)^{3\alpha/(2\beta-\alpha)}. \quad (8.24)$$

At $\alpha = 0$ and $\beta = 1$, we are back with GS95 (§ 5.3), and at $\beta = 3/4$, with the aligned theory of § 6.3.

8.2.3. Parallel Spectra

Now, from (8.20), (8.17), (8.23), and (8.14), the parallel scales are

$$\frac{l_{\parallel\lambda}^+}{L_{\parallel}} \sim \left(\frac{\lambda}{L_\perp} \right)^{(2\beta-\alpha)/3}, \quad \frac{l_{\parallel\lambda}^-}{L_{\parallel}} \sim \left(\frac{\lambda}{L_\perp} \right)^{2(\beta-2\alpha)/3}, \quad (8.25)$$

where the parallel outer scale is [cf. (6.14)]

$$L_{\parallel} = v_A L_\perp^{2/3} \left[\frac{(\varepsilon^+)^2}{\varepsilon^-} \right]^{-1/3}. \quad (8.26)$$

Combining (8.25) with (8.23) gives us the parallel scalings of the field increments:

$$\delta Z_{l_{\parallel}}^+ \sim \left[\frac{(\varepsilon^+)^2 L_{\parallel}}{\varepsilon^- v_A} \right]^{1/2} \left(\frac{l_{\parallel}}{L_{\parallel}} \right)^{(\beta+\alpha)/(2\beta-\alpha)}, \quad \delta Z_{l_{\parallel}}^- \sim \left(\frac{\varepsilon^- l_{\parallel}}{v_A} \right)^{1/2}. \quad (8.27)$$

Whereas the stronger field's scaling is (for small α , slightly) steeper than $l_{\parallel}^{1/2}$, the weaker one's is exactly that, corresponding to a k_{\parallel}^{-2} spectrum, as is indeed seen in numerical simulations [§ 8.1.1, item (iv)]. This makes sense because the weaker field was assumed to have a local parallel cascade with the usual CB conjecture, so the standard arguments for its parallel spectrum given in § 5.2 remain valid.

8.2.4. Pinning

It turns out that it is possible to determine α by considering what happens at the dissipation scale(s). The dissipation cutoffs λ_η^\pm for the two Elsasser fields can be worked out by balancing their fluxes with their dissipation rates:

$$\varepsilon^\pm \sim \frac{\nu + \eta}{(\lambda_\eta^\pm)^2} \left(\delta Z_{\lambda_\eta^\pm}^\pm \right)^2. \quad (8.28)$$

Using (8.23) to work out the field amplitudes at λ_η^\pm , one gets

$$\frac{\lambda_\eta^+}{L_\perp} \sim \left(\frac{\varepsilon^-}{\varepsilon^+} \widetilde{\text{Re}} \right)^{-3/2(3-\beta-\alpha)}, \quad \frac{\lambda_\eta^-}{L_\perp} \sim \widetilde{\text{Re}}^{-3/2(3-\beta+2\alpha)}, \quad \widetilde{\text{Re}} = \frac{\delta Z_{L_\perp}^+ L_\perp}{\nu + \eta}, \quad (8.29)$$

where, as before, $\widetilde{\text{Re}}$ is the smaller of Re and Rm . Since $\alpha > 0$ and (assuming) $\beta < 3$, λ_η^- scales with $1/\widetilde{\text{Re}}$ raised a smaller power than λ_η^+ does. Therefore, allowing $\widetilde{\text{Re}}$ to be asymptotically large while $\varepsilon^+/\varepsilon^-$ is merely large (i.e., $\widetilde{\text{Re}}$ is greater than any finite power of $\varepsilon^+/\varepsilon^-$), one would expect $\lambda_\eta^+ < \lambda_\eta^-$. But this is, in fact, impossible: if the weaker field is cut off at λ_η^- , there is nothing to cascade the stronger field at $\lambda < \lambda_\eta^-$ (locally in λ , as I assumed in §8.2.1). In order to avoid a bottleneck, with too much stronger-field energy arriving at λ_η^- and finding nothing to push it to smaller scales at the right rate, the system must adjust to dissipate this field at λ_η^- , i.e., to set

$$\lambda_\eta^+ \sim \lambda_\eta^- \quad \Rightarrow \quad \alpha \approx \left(1 - \frac{\beta}{3}\right) \frac{\ln(\varepsilon^+/\varepsilon^-)}{\ln \widetilde{\text{Re}}}. \quad (8.30)$$

Thus, $\alpha \rightarrow 0$ as $\widetilde{\text{Re}} \rightarrow \infty$, but very slowly, with larger $\widetilde{\text{Re}}$ needed to achieve a modicum of asymptoticity at larger imbalances.

Arguably, this is a rather attractive theory: asymptotically, the spectra are parallel, interactions are local, etc., but in any finite-width inertial range, there are finite- $\widetilde{\text{Re}}$ logarithmic corrections to scalings, locality, etc., accounting for all of the distinctive features of imbalanced turbulence seen in non-asymptotic simulations (§8.1.1).

Finally, let me observe, with Beresnyak & Lazarian (2008), that if $\lambda_\eta^+ \sim \lambda_\eta^-$, (8.28) implies immediately that, at the dissipation scale,

$$\frac{\delta Z_{\lambda_\eta^+}}{\delta Z_{\lambda_\eta^-}} \sim \sqrt{\frac{\varepsilon^+}{\varepsilon^-}}. \quad (8.31)$$

Thus, while what I have proposed above is a kind of “pinning,” it is not the conventional pinning of the amplitudes of the two fields to each other at the dissipation scale that has been one of the tenets of the theory of weak imbalanced turbulence (§4.3).

8.2.5. Alignment, Intermittency, Reconnection

Like in balanced turbulence, alignment is likely related to intermittency in imbalanced turbulence as well. Since, for imbalanced turbulence, we are still litigating such basic things as spectra, there is not much we know about its intermittency—and I do not propose to engage with this topic here any more than I have done already with a few throw-away comments in §8.1. The argument in §6.3.2 that led to $\beta = 3/4$ depended on assumptions about the most intense structures being sheets and on the “refined critical balance” (Mallet *et al.* 2015, see figure 6). It seems a worthwhile project to check whether, and in what sense, these features survive in imbalanced turbulence.

Since reconnection playing an important role at the small-scale end of the inertial range depended on alignment, the equivalent of §7 for imbalanced turbulence must wait for a better understanding of alignment. If tearing disruption does occur at some scale in (strongly) imbalanced turbulence, the pinning scheme proposed in §8.2.4 has to be redesigned. Incidentally, it also has to be redesigned (according to Meyrand *et al.* 2020, redesigned quite dramatically) for natural plasmas like the solar wind, where the cutoff of the RMHD inertial range is accomplished by kinetic effects rather than by Laplacian viscosity—but these matters are outside the scope of this review (see §§13.1 and 13.2).

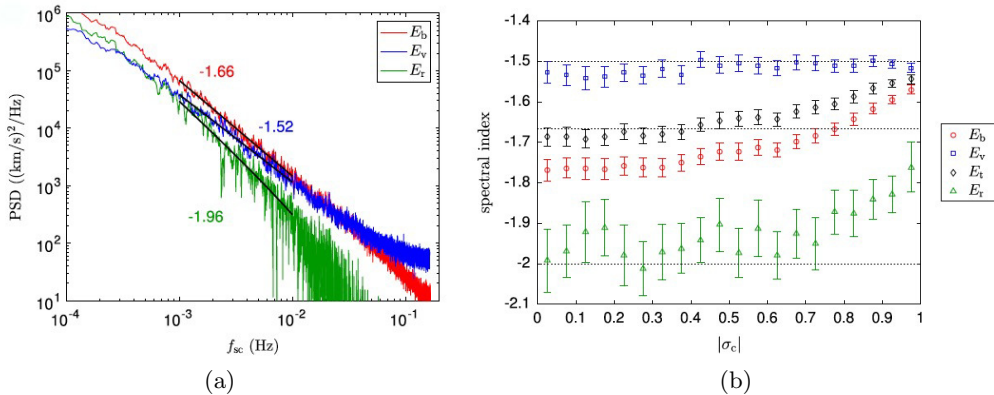


FIGURE 22. Spectra of magnetic (red), kinetic (blue), total (black) and residual (green) energies measured by [Chen *et al.* \(2013a\)](#) (figures taken from [Chen 2016](#)): (a) typical spectra; (b) average spectral indices vs. normalised cross-helicity σ_c [defined in (8.4)].

9. Residual Energy in MHD Turbulence

9.1. Observational and Numerical Evidence

Going back to figure 16(a), we see that real MHD turbulence observed in the solar wind is distributed between cases with a local Elsasser imbalance (cross-helicity) and those with an Alfvénic one—specifically, in favour of the magnetic field. Thus, the imbalanced cascades are only half of the story. According to the second relation in (8.6), in imbalanced turbulence ($|\sigma_c| \approx 1$), it is a geometric inevitability that $|\sigma_r| \ll 1$, as illustrated by figure 16(a) and confirmed directly in the statistical study of solar-wind data by [Bowen *et al.* \(2018\)](#). In contrast, when the cross-helicity is not large (i.e., when σ_c is not close to ± 1), there is flexibility for the perturbations to have finite residual energy: in the event, $\sigma_r < 0$. The definitive observational paper on this is [Chen *et al.* \(2013a\)](#), confirming negative σ_r over a large data set obtained in the solar wind. They also report that residual energy has a spectrum consistent with k_{\perp}^{-2} or perhaps a little shallower, but certainly steeper than either the kinetic- or magnetic-energy spectra: the scalings of all three are reproduced in figure 22. This seems to be in agreement with earlier observational and numerical evidence ([Müller & Grappin 2005](#); [Boldyrev *et al.* 2011](#), figure 23).

Obviously, it cannot be true at asymptotically small scales that, as the data suggests, the magnetic- and kinetic-energy spectra scale as $k_{\perp}^{-5/3}$ and $k_{\perp}^{-3/2}$, respectively, while their difference scales as k_{\perp}^{-2} —the \mathbf{b} and \mathbf{u} spectra must meet somewhere, as they indeed do in figure 22(a). The residual energy appears to peter out at the same scale (although that is also where the noise effects kick in)—but it would not be asymptotically impossible for it to retain the k_{\perp}^{-2} scaling as a subdominant correction to the approximately equipartitioned \mathbf{b} and \mathbf{u} spectra (as suggested by [Boldyrev *et al.* 2011](#)). I will discuss a possible origin of this correction in §9.4, but first some history.

9.2. Old Theories

The first awakening of the MHD turbulence community to the turbulence’s tendency for residual-energy generation dates back to the dawn of time ([Pouquet *et al.* 1976](#); [Grappin *et al.* 1982, 1983](#)), when theories and simulations based on isotropic EDQNM⁴⁴ closure models of MHD turbulence predicted a negative residual energy (i.e., an excess of magnetic energy) scaling as a k^{-2} correction to the dominant $k^{-3/2}$ IK spectrum (see

⁴⁴Eddy-Damped Quasi-Normal Markovian. You don’t want to know.

§ 2.2). While the isotropic IK theory certainly cannot be relevant to MHD turbulence with a strong mean field (see § 2), the modern evidence (§ 9.1) looks very much like those old results, with k replaced by k_{\perp} . This led Müller & Grappin (2005) to claim a degree of vindication for the EDQNM-based theory. This vindication cannot, however, be any stronger than the vindication of IK provided by Boldyrev’s theory (§ 6.1) and its cousins (§ 6.3): same scaling, different physics.

Below the turgid layers of EDQNM formalism, the basic physical idea (best summarised by Grappin *et al.* 2016) is that residual energy is generated from the total energy by nonlinear interactions that favour magnetic-field production (the “dynamo effect”)⁴⁵ and removed by the “Alfvén effect,” which tends to equalise \mathbf{u}_{\perp} and \mathbf{b}_{\perp} perturbations. A balance of these two effects leads to a prediction for the residual-energy spectrum in the form

$$E_{\text{res}} \sim \frac{\tau_A}{\tau_b} E \sim \left(\frac{\tau_A}{\tau_{\text{nl}}} \right)^{\alpha} E, \quad (9.1)$$

where E is the total-energy spectrum, τ_b is the characteristic time scale of the generation of excess magnetic energy at a given scale, τ_A and τ_{nl} are our old friends Alfvén and nonlinear times, and the exponent α depends on one’s theory of how τ_b is related to these two basic times. For example, in the IK theory, $\tau_b \sim \tau_{\text{nl}}^2/\tau_A$ [because IK turbulence is weak; cf. (4.5) and footnote 4], so $\alpha = 2$. Using the IK scalings (2.5) and $\tau_A/\tau_{\text{nl}} \sim \delta u_{\lambda}/v_A$, one gets from (9.1)

$$E_{\text{res}}(k) \sim \frac{\varepsilon}{v_A} k^{-2}. \quad (9.2)$$

I know of no unique or obvious way of adjusting this promising (but necessarily wrong because IK-based) result to fit a critically balanced cascade: indeed, the CB requires $\tau_A \sim \tau_{\text{nl}}$, implying $E_{\text{res}} \sim E$, i.e., a scale-independent ratio between the residual and total energy (this was also the conclusion of Gogoberidze *et al.* 2012, who undertook the heroic but thankless task of constructing an EDQNM theory of anisotropic, critically balanced MHD turbulence). Neither solar wind nor MHD simulations appear to agree with this (§ 9.1).

Obviously, once we enter the realm of intermittent scalings of the kind described in § 6.3.1, i.e., allow the outer scale to matter, there is a whole family of possibilities admitted by the RMHD symmetry and dimensional analysis: by exactly the same argument as led to (6.12), we must have

$$E_{\text{res}}(k_{\perp}) \sim \varepsilon^{2(1+\delta)/3} \left(\frac{L_{\parallel}}{v_A} \right)^{2\delta} k_{\perp}^{-(5-4\delta)/3}, \quad (9.3)$$

where δ is some exponent, in order to determine which, we must input some physical or mathematical insight.

9.3. New Theories: Residual Energy in Weak MHD Turbulence

An interesting step in this direction was made in yet another characteristically clever contribution by Boldyrev’s group. They showed that even weak interactions of AW packets mathematically lead to growth of excess magnetic energy and thus of negative residual energy—Boldyrev *et al.* (2012) by analysing weak interaction of two model

⁴⁵That they do favour magnetic-field production and thus promote $\sigma_r < 1$ is confirmed quantitatively within the closure theory (Grappin *et al.* 1982, 1983; Gogoberidze *et al.* 2012). Physically, it is possible to argue that simple Alfvén-wave interactions will produce residual energy (Boldyrev *et al.* 2012); see further discussion in §§ 9.3 and 9.4. I am not enthusiastic about dragging the dynamo effect into this.

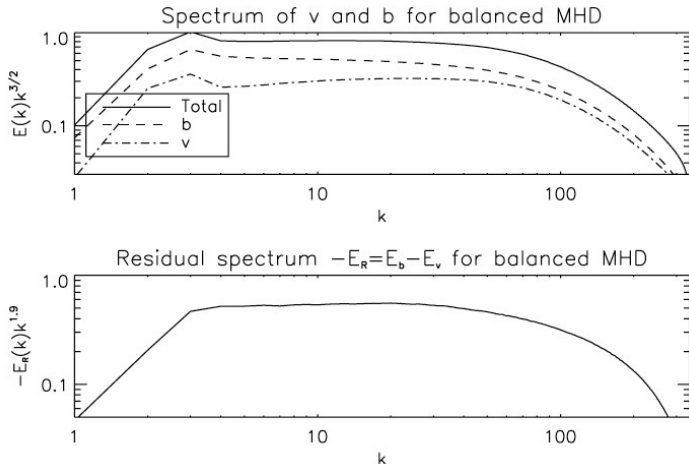


FIGURE 23. Spectra of total, magnetic, kinetic (upper panel, solid, dashed and dot-dashed lines, respectively, compensated by $k_{\perp}^{3/2}$) and residual energy (lower panel, compensated by $k_{\perp}^{1.9}$) in an RMHD simulation by Boldyrev *et al.* (2011).

AW packets and Wang *et al.* (2011) within the framework of traditional WT theory. However, all the action in their derivation was in the $k_{\parallel} = 0$ modes, which hosted the excess magnetic energy generated by AW interactions—the 2D magnetic condensate whose awkward relationship with WT theory I discussed in §4.4.

A version of the appropriate derivation is laid out in appendix A.5. Quantitatively, it cannot be right because the WT approximation does not apply to the condensate, which is strongly turbulent (see appendix A.4). Qualitatively, the outcome of the WT calculation—growth of excess magnetic energy at $k_{\parallel} = 0$ —can be understood as follows. Growth of positive (negative) residual energy is the same as growth of (anti)correlation between \mathbf{Z}_{\perp}^{+} and \mathbf{Z}_{\perp}^{-} :

$$\langle \mathbf{Z}_{\perp}^{+} \cdot \mathbf{Z}_{\perp}^{-} \rangle = \langle |\mathbf{u}_{\perp}|^2 \rangle - \langle |\mathbf{b}_{\perp}|^2 \rangle. \quad (9.4)$$

These correlations are created with particular ease at $k_{\parallel} = 0$, where \mathbf{Z}_0^{+} and \mathbf{Z}_0^{-} are forced by the interaction of the same pairs of AWs, $\mathbf{Z}_{k_{\parallel}}^{+}$ and $\mathbf{Z}_{k_{\parallel}}^{-}$ (which themselves are allowed to be uncorrelated): this is obvious from (4.12). The result is that a magnetic condensate emerges at $k_{\parallel} = 0$, giving rise to net negative residual energy—that it should be negative is not obvious, but the WT calculation says it is, as, perhaps more convincingly, does a qualitative argument that I shall now explain.

9.4. New Theories: Residual Energy in Strong MHD Turbulence

In the strong-turbulence regime, no quantitative calculation exists, as usual, but a reasonably compelling physical case can be made.

Emergence of negative residual energy here must be discussed in very different terms than in §9.3. As I repeatedly stated in §6, my preferred picture of alignment is one in which Elsasser fields dynamically shear each other into intermittent structures where they are nearly parallel to each other (Chandran *et al.* 2015). That, of course, means that they become strongly correlated: and indeed, alignment between Elsasser fields is mathematically impossible without non-zero residual energy, as is obvious from the first formula in (8.5) or from figure 20. That δb should be larger than δu in the resulting sheet-like structures is both a selection effect and the result of dynamics. First, the structures that have $\delta u > \delta b$ —shear layers, rather than current sheets—are prone to be destroyed by

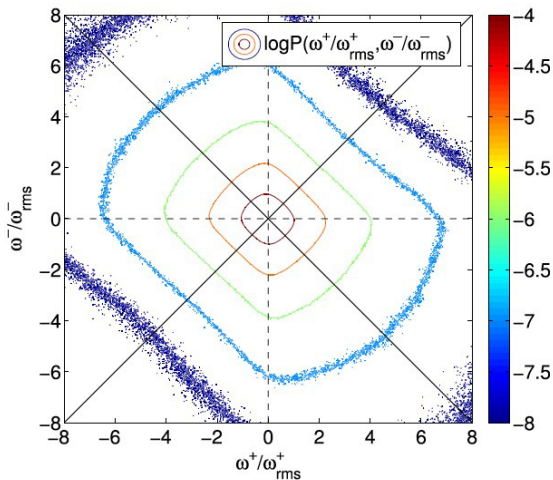


FIGURE 24. Joint probability distribution of Elsasser vorticities $\omega^\pm = \hat{z} \cdot (\nabla_\perp \times \mathbf{Z}_\perp^\pm)$ in an RMHD simulation by Zhdankin *et al.* (2016b) (whence this plot is taken). The contours are elongated in the SE-NW direction, indicating $\langle \omega^+ \omega^- \rangle < 0$ and thus a preponderance of current sheets over shear layers.

the Kelvin–Helmholtz instability and to curl up into vortices, as they do in hydrodynamic turbulence, whereas in the current sheets, the instability is happily stabilised by the magnetic field (at least before it all hits the disruption scale and current sheets become unstable as well; see appendix C and Loureiro *et al.* 2013a). Secondly, there is a dynamical tendency in RMHD that favours current sheets over shear layers: the nonlinearity pushes the “Elsasser vorticities” $\omega^+ = \hat{z} \cdot (\nabla_\perp \times \mathbf{Z}_\perp^+)$ and $\omega^- = \hat{z} \cdot (\nabla_\perp \times \mathbf{Z}_\perp^-)$ in opposite directions—this becomes obvious from the evolution equations (A 2) for these vorticities, where the nonlinear vortex-stretching terms have opposite signs for the two Elsasser fields. The result is a negative correlation between ω^+ and ω^- , viz., $\langle \omega^+ \omega^- \rangle < 0$, and thus a preference for current sheets over shear layers (Zhdankin *et al.* 2016b, see figure 24).

Let us now imagine that this effect is strongest in the most intense structures, which in § 6.3.2 were all assumed to have the same, scale-independent amplitude. If they are current sheets with $\delta Z_{\max} \sim \delta b \gg \delta u$, they would, if they were alone in the world, have a spectrum of k_\perp^{-2} because they are just an ensemble of step functions in \mathbf{b}_\perp .⁴⁶ In fact, there are many other fluctuations around, whose net spectrum is $k_\perp^{-3/2}$ and in which $\delta b \sim \delta u$. However, if the excess magnetic energy is dominated by the most intense sheets, one might imagine that the residual-energy spectrum would have a k_\perp^{-2} scaling.

An attentive reader who still remembers figure 13(b) might have wondered all through my discussion of residual energy how steeper magnetic than velocity spectra seen in numerical simulations (figure 23) could be compatible with structure functions of the magnetic field having *smaller* scaling exponents than those of the velocity field. How indeed? One possibility is that a sub-population of highly local step-like discontinuities will produce a highly nonlocal k_\perp^{-2} signature in the wavenumber space, with the power-law spectral scaling having little to do with any local scaling of a structure function: e.g., any structure function of a single step-like discontinuity is just a scale-independent constant, but the spectrum of such a discontinuity is k_\perp^{-2} (it is also the spectrum of

⁴⁶That current sheets naturally forming in a turbulent MHD system do indeed have this spectrum was shown by Dallas & Alexakis (2013a, 2014), although they only looked at decaying, no-mean-field MHD turbulence with a certain class of initial conditions.

many random steps: see footnote 49). In this context, the mystery of magnetic field being “more intermittent,” highlighted in §6.5, might count as circumstantial evidence in favour of the interpretation of residual energy in the inertial range as arising from magnetic discontinuities. The fact that obtaining a k_{\perp}^{-2} spectrum consistent with the RMHD symmetry requires $\delta = -1/4$ in (9.3) and, therefore, the presence of the outer scale L_{\parallel} in the expression for $E_{\text{res}}(k_{\perp})$, confirms that we must again be dealing with an intermittency effect. Encouragingly, recent analysis of solar-wind data by Bowen *et al.* (2018) directly established a positive correlation between the most intense, intermittent magnetic structures and residual energy.

Admittedly, all this is less than a theory, but it is something.

9.5. Summary

Perhaps speaking of an “Alfvénically imbalanced regime” of MHD turbulence is misleading. Residual energy is not an RMHD invariant, so this is not something that can be viewed as a parameter in the same way as the net Elsasser imbalance can be. It is, rather, what appears to be a necessary feature of any (approximately balanced) MHD turbulent state.

This feature has so far presented itself in two seemingly distinct manifestations. The first one is the tendency for sheet-like structures in the inertial range of strong MHD turbulence to be current sheets rather than shear layers and thus to have an excess of magnetic energy—it may be possible to argue that the most extreme of these structures are responsible for a subdominant k_{\perp}^{-2} spectrum of residual energy, which is observed numerically and in the solar wind (§9.4). The second one is the emergence of a 2D magnetic condensate in weak MHD turbulence (§9.3).

Are these two different phenomena? Not necessarily: in the WT context, all the residual energy is generated within the 2D condensate, which is, in fact, strongly turbulent (see appendices A.4 and A.5). Being strongly turbulent, it is strongly intermittent and appears to be dominated by sheet-like structures (Meyrand *et al.* 2015), so the physical mechanism whereby an excess of magnetic energy develops in it is likely to be the same as in strong MHD turbulence.

10. Subviscous MHD Turbulence

Let me now turn to an interesting, if somewhat boutique, regime of MHD turbulence that occurs at scales below the viscous cutoff when $\text{Pm} \gg 1$. This was first studied by Cho *et al.* (2002a, 2003) and Lazarian *et al.* (2004), and recently picked up again by Xu & Lazarian (2016, 2017), on the grounds that it is relevant to partially ionised interstellar medium, where viscosity is heavily dominated by the neutral atoms.⁴⁷ This is a limit in which viscous dissipation takes over from inertia in controlling the evolution of the velocity field (one might call this “Stokes,” or “Aristotelian” dynamics), while magnetic field is still happily frozen into this viscous flow and free to have interesting MHD behaviour all the way down to the resistive scale, which, at $\text{Pm} \gg 1$, is much smaller than the viscous one. The velocity perturbations below the viscous scale will be very small compared to the magnetic ones, so this is another MHD turbulent state that features an imbalance between the two fields.

Below, I am going to present a somewhat updated qualitative theory of the subviscous

⁴⁷It has also recently turned out, somewhat unexpectedly, that something very similar to this regime might be relevant in the context of collisionless gyrokinetic turbulence and ion heating in high-beta plasmas (Kawazura *et al.* 2019).

cascade—with tearing disruption and the ubiquitous Kolmogorov cutoff yet again making a cameo appearance.

10.1. Viscous Cutoff

When $\text{Pm} \gg 1$, there are two possibilities for the nature of turbulence at the viscous cutoff.

The first is that Pm is so large that the condition (7.3) is broken ($\text{Pm} \gtrsim \text{Re}^{1/9}$), so there is no tearing disruption and the (aligned) inertial-range MHD cascade encounters viscosity at the Boldyrev cutoff scale (6.22)—for $\text{Pm} \gg 1$, let me rename it:

$$\lambda_\nu \sim \lambda_{\text{CB}} \text{Re}^{-2/3} \sim \frac{\nu^{3/4}}{\varepsilon^{1/4}} \text{Re}^{1/12} \quad \Rightarrow \quad \frac{\xi_\nu}{\lambda_{\text{CB}}} \sim \text{Re}^{-1/2}, \quad \frac{l_{\parallel\nu}}{L_{\parallel}} \sim \text{Re}^{-1/3}, \quad (10.1)$$

where λ_{CB} is given by (6.14) and Re by (6.21). The last two formulae follow via (6.29) (for the scale on which the perturbed fields vary along themselves) and via (6.20) (for the parallel scale), respectively.

The second (rather difficult to achieve) possibility is that $1 \ll \text{Pm} \ll \text{Re}^{1/9}$, so (7.3) does hold and we have a tearing-mediated turbulent cascade curtailed by the Kolmogorov cutoff (7.13)—for $\text{Pm} \gg 1$, it is

$$\lambda_\nu \sim \lambda_{\text{CB}} \text{Re}^{-3/4} \sim \frac{\nu^{3/4}}{\varepsilon^{1/4}}. \quad (10.2)$$

Either way, some finite fraction of ε is thermalised at λ_ν , and at $\lambda < \lambda_\nu$ velocity perturbations will have gradients that are smaller than the decorrelation rate at λ_ν . This decorrelation rate is

$$\tau_{\text{nl}}^{-1} \sim \frac{\delta u_{\lambda_\nu}}{\xi_\nu} \sim \tau_\nu^{-1} \sim \frac{\nu}{\lambda_\nu^2} \sim \left(\frac{\varepsilon}{\nu}\right)^{1/2} \text{Re}^{-1/6} \quad \text{or} \quad \left(\frac{\varepsilon}{\nu}\right)^{1/2} \quad (10.3)$$

for (10.1) and (10.2), respectively.

10.2. Magnetic Fields at Subviscous Scales

In contrast to velocities, magnetic fields are immune to viscosity and so can be pushed to scales much smaller than λ_ν . However, since velocity gradients are suppressed at these scales, these magnetic fields will be dominantly interacting with the viscous-scale velocities, in a nonlocal fashion. Presumably, since the viscous-scale motions are correlated on the parallel scale $l_{\parallel\nu}$, so will be these magnetic fields, i.e., there is no parallel cascade:

$$l_{\parallel} \sim l_{\parallel\nu} = \text{const}. \quad (10.4)$$

Numerical simulations (Cho *et al.* 2002a, 2003) confirm (10.4) and show a magnetic spectrum $\propto k^{-1}$. In the mind of any minimally erudite turbulence theorist, this cannot fail to trigger a strong temptation to consider the whole situation as a variant of Batchelor (1959) advection of a passive field: assuming a cascade of magnetic energy with cascade time τ_ν at every scale, one gets (see Cho *et al.* 2002a and figure 25a):

$$\delta b_\lambda^2 \sim \varepsilon_m \tau_\nu = \text{const} \quad \Rightarrow \quad E_b(k_\perp) \sim \varepsilon_m \tau_\nu k_\perp^{-1}, \quad (10.5)$$

where ε_m is the part of the turbulent flux that is not dissipated at the viscous cutoff (possibly about half of it, since velocity and magnetic fields have the same energies at the viscous scale and are pushed into viscous dissipation and subviscous structure, respectively, at the same rate τ_ν^{-1}). The spectrum (10.5) stretches all the way to the

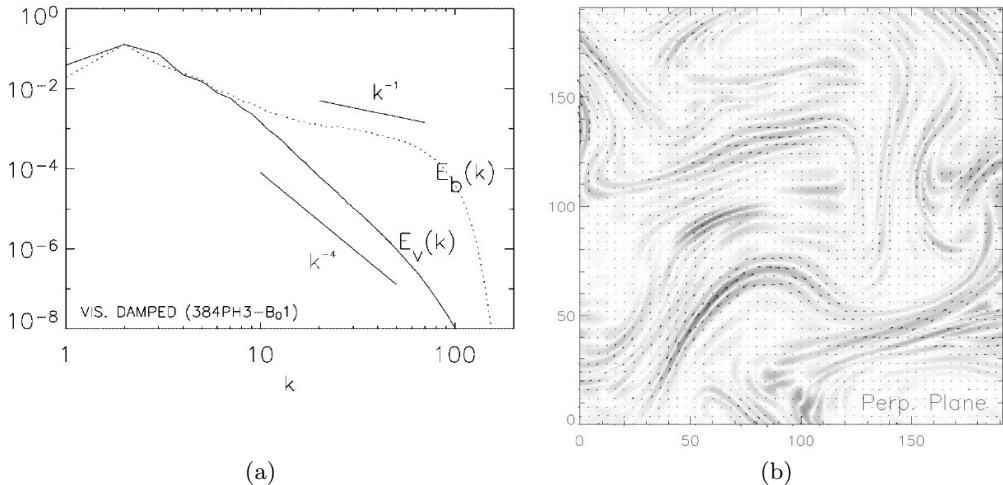


FIGURE 25. (a) Spectra of magnetic and kinetic energy for subviscous turbulence, taken from [Cho *et al.* \(2003\)](#). (b) Magnetic-field strength for the filtered $k > 20$ part of the field in the same simulation (from [Cho *et al.* 2002a](#)). Stripy field structure is manifest.

resistive scale, where Ohmic dissipation can rival advection:

$$\tau_\nu^{-1} \sim \frac{\eta}{\lambda_\eta^2} \Rightarrow \lambda_\eta \sim (\tau_\nu \eta)^{1/2} \sim \lambda_\nu \text{Pm}^{-1/2}. \quad (10.6)$$

The line of reasoning leading to (10.5) should perhaps be viewed with a degree of suspicion. In a regime where magnetic fields are nonlocally advected and stretched by the viscous-scale velocity field, while the latter experiences back reaction from them while constantly being dissipated by viscosity, why can one assume that magnetic energy is an independent invariant with a constant scale-to-scale flux? While this may be a plausible proposition, I do not know how to justify it beyond reasonable doubt—but I do believe the scaling (10.5) because it is bolstered by the following alternative argument of a more dynamical nature.

The situation at subviscous scales is not entirely dissimilar to a kind of dynamo (§ 12), or rather a 2D version of it in which the perturbed magnetic field \mathbf{b}_\perp is randomly stretched and sheared by the viscous-scale velocity and is excused from the 2D antidynamo theorem ([Zeldovich 1956](#)) by constant resupply from the inertial range. The the role of \mathbf{B}_0 is just to two-dimensionalise the dynamics approximately—maintaining all fields at the single parallel correlation scale $l_{\parallel\nu}$. The stretching and shearing of \mathbf{b}_\perp leads to a folded magnetic field (figure 28) forming a stripy pattern, with multiple reversals on small scales limited from below only by λ_η (figure 25b).⁴⁸

Just like in the case of dynamo-generated fields (§ 12.3.1), our stripy fields are spatially correlated along themselves on scales $\sim \xi_\nu$ and so can exert coherent Lorentz forces back on the viscous-scale velocity field. These forces are tension forces consisting of two parts:

$$\mathbf{F} = \mathbf{B}_0 \cdot \nabla \mathbf{b}_\perp + \mathbf{b}_\perp \cdot \nabla \mathbf{b}_\perp. \quad (10.7)$$

Here let us think of \mathbf{b}_\perp as just the part of \mathbf{B} that contains subviscous-scale variation

⁴⁸Subviscous-scale fields generated by randomly stirred and viscously damped flows in 2D were studied both analytically and numerically by [Kinney *et al.* \(2000\)](#), who found them to follow a k_\perp^{-1} spectrum (which is evident in their Fig. 11, even though they do not claim this scaling explicitly).

and absorb into \mathbf{B}_0 all inertial-range fields. The first term in (10.7) alternates sign on the scale λ_η (in the direction perpendicular to \mathbf{b}_\perp) and so its effect on the viscous-scale motions should cancel out. In contrast, the second term is quadratic in \mathbf{b}_\perp , and its size is $\sim b_\perp^2/\xi_\nu$. In order to be dynamically significant, it must be of the same order as the viscous and inertial forces, which are similar at the viscous scale:

$$\mathbf{b}_\perp \cdot \nabla \mathbf{b}_\perp \sim \nu \nabla_\perp^2 \mathbf{u}_\perp \sim \mathbf{u}_\perp \cdot \nabla \mathbf{u}_\perp \Rightarrow \frac{\delta b_\lambda^2}{\xi_\nu} \sim \frac{\delta u_{\lambda_\nu}^2}{\xi_\nu} \Rightarrow \delta b_\lambda^2 \sim \delta u_{\lambda_\nu}^2 \sim \varepsilon \tau_\nu. \quad (10.8)$$

On the face of it, this reproduces (10.5) (assuming $\varepsilon_m \sim \varepsilon$). However, we need not interpret this result as specifically vindicating a Batchelor-style cascade. Instead, we could think of the reversal scale as always being λ_η , the size of the reversing field as being $b_\perp \sim (\varepsilon \tau_\nu)^{1/2}$, and interpret δb_λ as the increment of a stripy field taken in two points separated by $\lambda_\eta \ll \lambda \ll \lambda_\nu$. The field difference between such two points will always be either $\delta b_\lambda \sim 2b_\perp$ or zero, with equal probabilities, and so $\langle \delta b_\lambda^2 \rangle \sim b_\perp^2 \sim \varepsilon \tau_\nu$ (this argument is due to [Yousef *et al.* 2007](#), who used it to posit a k^{-1} spectrum for dynamo-generated fields at large Pm, which will be visited in §12.4.1). In other words, cascade or no cascade, k_\perp^{-1} can be recovered as the spectrum of sharp, repeated stripes.⁴⁹

10.3. Velocity Field at Subviscous Scales

Numerical simulations ([Cho *et al.* 2003](#), shown in figure 25a) reveal that the velocity field at subviscous scales is very small and has an approximately k_\perp^{-4} spectrum. This can be recovered on the basis of the picture that I proposed in §10.2, in the following way. The balance between the viscous and magnetic forces at $k_\perp \lambda_\nu \gg 1$ gives us

$$\nu k_\perp^2 \mathbf{u}_\perp \mathbf{k} \sim (\mathbf{b}_\perp \cdot \nabla \mathbf{b}_\perp)_\mathbf{k} \Rightarrow E_u(k_\perp) \sim \frac{E_F(k_\perp)}{\nu^2 k_\perp^4} \sim \frac{\text{const}}{k_\perp^4}, \quad (10.9)$$

where $E_u(k_\perp)$ and $E_F(k_\perp)$ are the spectra of the velocity and of the tension force, respectively. Let me explain why $E_F(k_\perp) \sim \text{const}$. If \mathbf{b}_\perp consists of stripes of field alternating direction on the scale λ_η , then $\mathbf{b}_\perp \cdot \nabla \mathbf{b}_\perp \sim |\mathbf{b}_\perp|^2/\xi_\nu$ consists of a constant field interspersed by sharp downward spikes of width λ_η across the field and length ξ_ν along it. At $k_\perp \lambda_\eta \ll 1$ and $k_\perp \xi_\nu \gg 1$, these are effectively 1D delta functions, so $E_F(k_\perp) \sim \text{const}$, q.e.d.⁵⁰ Note that the contribution of the first term in (10.7) to E_F should scale the same as the spectrum of \mathbf{b}_\perp , viz., $\propto k_\perp^{-1}$ —or perhaps $k_\perp^{-1/2}$ from the cross-term, if it does not

⁴⁹To pre-empt a possible confusion, let me contrast this with the k_\perp^{-2} spectrum that is usually associated with a field consisting of sharp discontinuities, e.g., the Burgers turbulence of shocks ([Bec & Khanin 2007](#)) or an ensemble of current sheets (§9.4; see also [Dallas & Alexakis 2013a, 2014](#) and [Zhou *et al.* 2019](#)). The easiest way to get such a spectrum is to notice that it is the spectrum of a single Heaviside step function. It is also the spectrum of many random steps: if the field flips direction randomly, with the number of flips between two points separated by a distance λ increasing $\propto \lambda$, then the field increment will accumulate as a random walk: $\langle \delta b_\lambda^2 \rangle \propto \lambda$, giving again a k_\perp^{-2} spectrum. This is different from the stripy fields posited in this section, which are a repeated pattern, giving $\langle \delta b_\lambda^2 \rangle \sim \text{const}$.

⁵⁰A version of this argument was proposed by [Schekochihin *et al.* \(2004\)](#) for dynamo-generated fields. They simulated such fields (in 3D) directly and found the spectrum of tension to be flat and the velocity spectrum to satisfy (10.9) extremely well. [Kinney *et al.* \(2000\)](#) argued for, and saw, similar behaviour in 2D, although their E_u had a slope closer to $k_\perp^{-4.5}$. Interestingly, [Cho *et al.* \(2002a\)](#) also reported a steeper spectrum like this, although it was perhaps not fully numerically converged and so, in [Cho *et al.* \(2003\)](#), they changed their mind in favour of k_\perp^{-4} .

average to zero—this should produce steeper and, therefore, subdominant contributions to $E_u(k_\perp)$.⁵¹

10.4. Disruption by Tearing

A reader who still remembers the developments in §7 might wonder whether these stripy fields are safe against disruption by tearing. Setting $v_{Ay} \sim \delta b_\lambda$ in (7.1), let us ask whether there is a disruption scale $\lambda_{D,\text{subvisc}}$ at which the local tearing rate would be larger than the stretching rate by the viscous-scale eddies:

$$\gamma \sim \frac{\delta b_\lambda^{1/2}}{\lambda^{3/2}} \eta^{1/2} \text{Pm}^{-1/4} \gtrsim \tau_\nu^{-1} \quad \Rightarrow \quad \lambda \lesssim \varepsilon_m^{1/6} \tau_\nu^{5/6} \eta^{1/2} \nu^{-1/6} \equiv \lambda_{D,\text{subvisc}}, \quad (10.10)$$

where (10.5) was invoked for δb_λ . Using (10.6) to estimate the putative resistive cutoff, we get

$$\frac{\lambda_{D,\text{subvisc}}}{\lambda_\eta} \sim \varepsilon_m^{1/6} \tau_\nu^{1/3} \nu^{-1/6}. \quad (10.11)$$

If we are in the regime in which the tearing disruption already occurred in the inertial range ($\text{Pm} \lesssim \text{Re}^{1/9}$) and so (10.2) holds, then τ_ν is given by the second expression in (10.3), and (10.11) implies

$$\frac{\lambda_{D,\text{subvisc}}}{\lambda_\eta} \sim \left(\frac{\varepsilon_m}{\varepsilon} \right)^{1/6} \lesssim 1, \quad (10.12)$$

so no new disruption is possible in the subviscous range.

In contrast, if the inertial-range cascade was cut off in the aligned regime ($\text{Pm} \gtrsim \text{Re}^{1/9}$), so (10.1) and the first expression in (10.3) apply, then

$$\frac{\lambda_{D,\text{subvisc}}}{\lambda_\eta} \sim \left(\frac{\varepsilon_m}{\varepsilon} \right)^{1/6} \text{Re}^{1/18} \gg 1. \quad (10.13)$$

Modulo factors of order unity and small fractional powers, this means that if the tearing disruption did not have the chance to occur in the inertial range, it will occur in the subviscous range, and that $\lambda_{D,\text{subvisc}}$ will be the field reversal scale, not λ_η . In terms of the viscous scale (10.1), which is $\lambda_\nu \sim \lambda_\eta \text{Pm}^{1/2}$,

$$\frac{\lambda_D}{\lambda_\nu} \sim \left(\frac{\varepsilon_m}{\varepsilon} \right)^{1/6} \text{Re}^{1/18} \text{Pm}^{-1/2}, \quad (10.14)$$

where I renamed $\lambda_{D,\text{subvisc}} \rightarrow \lambda_D$, since this is the only disruption scale there is.

At $\lambda \lesssim \lambda_D$, a local MHD cascade is again ignited, just like it was in §7.2. It should not seem strange that inertial motions are again possible: viscously dominated tearing of the magnetic sheets will produce λ_D -sized plasmoids whose turnover times are shorter than their viscous-dissipation times. Indeed, demanding that they pick up all the available energy flux ε_m , one gets their amplitude

$$\frac{\delta Z_{\lambda_D}^3}{\lambda_D} \sim \varepsilon_m \quad \Rightarrow \quad \delta Z_{\lambda_D} \sim (\varepsilon_m \lambda_D)^{1/3} \quad (10.15)$$

⁵¹The mismatch of the spectrum obtained this way ($E_u \propto k_\perp^{-5}$) and the one observed in numerical simulations led Lazarian *et al.* (2004) to propose an ingenious scheme whereby all fields and velocities at subviscous scales had a scale-dependent volume-filling fraction, whose scaling was then determined by an additional requirement that subviscous velocities had local shears comparable to τ_ν^{-1} . Although this did give the desired k_\perp^{-4} scaling, I do not see how such an assumption can be justified.

and the associated Reynolds number for the new cascade:

$$\text{Re}_{\lambda_D} = \frac{\delta Z_{\lambda_D} \lambda_D}{\nu} \sim \text{Re}^{5/27} \text{Pm}^{-2/3} \gg 1 \quad \text{if} \quad \text{Re} \gg \text{Pm}^{18/5}. \quad (10.16)$$

This cascade is cut off, as usual, at the scale (7.13), but with this new Re:

$$\lambda_{\nu, \text{new}} \sim \lambda_D \text{Re}_{\lambda_D}^{-3/4} \sim \frac{\nu^{3/4}}{\varepsilon_m^{1/4}}, \quad (10.17)$$

the Kolmogorov scale again proving its universal resilience.

Thus, the subviscous cascade turns out to be a complicated transitional arrangement for enabling tearing disruption and restoration of the Kolmogorov cutoff (10.17). Yet again, below this cutoff, at $\lambda < \lambda_{\nu, \text{new}}$, we are confronted with a purely magnetic, “second subviscous cascade,” but this time with the (new) viscous-scale turnover time given by the formula analogous to the second expression in (10.3), viz., $\tau_{\nu, \text{new}} \sim (\varepsilon_m/\nu)^{1/2}$. All the arguments of §§ 10.2 and 10.3 apply, but with no longer any danger of further disruption [see (10.12)].

A reader sceptical of the falsifiability of these arguments (given the proliferation of small fractional powers of Re and the piling up of twiddle algebra) might feel this is all a fiction—but it is a logical one!

11. Decaying MHD Turbulence

Decaying MHD turbulence belongs to this part of this review because it too tends to end up in “imbalanced” states dominated either by the magnetic field or by one of the Elsasser fields (and because it remains in certain important respects a “loose end”). On a very crude level, it is perhaps obvious that this should be so, because ideal MHD equations have two types of exact nonlinear solutions for which nonlinear interactions vanish: Elsasser states ($\mathbf{u} = \pm \mathbf{B}$, or $\mathbf{Z}^\mp = 0$) and static force-free magnetic fields ($\mathbf{B} \times \mathbf{J} = 0$, where $\mathbf{J} = \nabla \times \mathbf{B}$). If the system finds a way towards either of these solutions concentrated on scales large enough to make dissipation small, it may, subject to this small dissipation, be able to linger in those states (“may” because their stability is not guaranteed—regarding the force-free states, see, e.g., the discussion and references in Appendix A of Hosking *et al.* 2020). We shall see below that both scenarios are possible and that recent developments point to magnetic reconnection muscling its way into this topic as well, controlling certain types of decaying MHD turbulence.

11.1. Towards Elsasser States

The eventual convergence to pure Elsasser states was first mooted by Dobrowolny *et al.* (1980), in the context of such states being occasionally observed in the solar wind. Since \mathbf{Z}^+ and \mathbf{Z}^- advect each other, one can easily imagine that a fluctuation of the imbalance at the outer scale in one direction, say in favour of \mathbf{Z}^+ , will lead to \mathbf{Z}^+ decaying slower and \mathbf{Z}^- faster, thus increasing the imbalance further, until \mathbf{Z}^- disappears and \mathbf{Z}^+ is left in splendid isolation. The crudest model of this is as follows (Maron & Goldreich 2001): if L is the energy-containing (outer) scale and Z^\pm are the two fields’ amplitudes at this scale, then

$$\frac{dZ^\pm}{dt} \sim -\frac{Z^\mp Z^\pm}{L} \quad \Rightarrow \quad Z^+ - Z^- \sim \text{const}, \quad \frac{d}{dt} \ln \frac{Z^+}{Z^-} \sim \frac{Z^+ - Z^-}{L}. \quad (11.1)$$

Thus, an initial imbalance in either direction will cause the (fractional) imbalance to get worse with time, until the weaker field has decayed away. In other words, cross-helicity

$(Z^+)^2 - (Z^-)^2 \sim \text{const} \cdot (Z^+ + Z^-)$ decays more slowly than energy, hence the increasing imbalance. The asymptotic state is an Elsasser state with $Z^+(t \rightarrow \infty) \sim (Z^+ - Z^-)(t = 0)$. Note that this simple model, and its conclusion, depend on assuming that L is the same for both fields (and that any alignment effects on the strength of the nonlinear interaction can be ignored), which is far from obvious and can be hard to sustain (e.g., [Hossain *et al.* 1995](#); [Wan *et al.* 2012](#); [Bandyopadhyay *et al.* 2019](#))—perhaps a hint as to why the conclusion is not inevitable.

It did, nevertheless, appear to be confirmed (very slowly in time) in the decaying RMHD simulation by [Chen *et al.* \(2011\)](#), initialised by first creating a statistically steady, forced, balanced turbulence and then switching off the forcing, so the breaking of the symmetry in favour of one of the fields arose from an initial fluctuation of the imbalance. In full-MHD simulations with a strong mean field, the same result had been found in a number of earlier papers: [Oughton *et al.* \(1994\)](#), [Maron & Goldreich \(2001\)](#), and [Cho *et al.* \(2002b\)](#). The case without a mean field has a much longer paper trail (starting with the early papers cited in footnote 13)—I will return to it momentarily.

The usual theoretical attitude to decaying turbulence, dating back to [Kolmogorov \(1941b,c\)](#), is to assume that its energy would decay quite slowly compared to the nonlinear interactions at small scales (simply because turnover times τ_{nl} are shorter at smaller scales) and hence to expect the situation in the inertial range to be the same as in the forced case: a constant-flux energy cascade, etc. In the simulation of [Chen *et al.* \(2011\)](#), this seemed to be the case, except the perpendicular spectrum was steeper than $k_{\perp}^{-3/2}$ (and closer to $k_{\perp}^{-5/3}$) and the parallel one steeper than k_{\parallel}^{-2} —this might actually be consistent with what one would expect for a system that moved gradually towards greater imbalance (see §8.2). With the small scales thus taken care of, the remaining interesting question is the large-scale behaviour: how fast do various types of energy (kinetic, magnetic, Elsasser) decay? how does the outer scale evolve?

11.2. *Evolution of Large Scales and the Role of Invariants*

There is a long experience of thinking of such questions in the context of (various flavours of) hydrodynamic turbulence. A magisterial tutorial on this subject, with all the main ideas, fallacies, nuances, historical triumphs and setbacks narrated in a friendly and clear style, can be found in the book by [Davidson \(2013\)](#), start from Chapter 11), whose own contributions form a significant part of the emerging canon. The main underlying idea is this. The energy in the system evolves roughly according to

$$\frac{dU^2}{dt} \sim -\frac{U^3}{L}, \quad (11.2)$$

where L is again the energy-containing (outer) scale and U the velocity at that scale. Both of these quantities are functions of time, so we need a second equation to determine $L(t)$. This is provided by statements of conservation, exact or approximate, of certain large-scale quantities even as the energy decays. The best known example is the Loitsyansky invariant in hydrodynamic turbulence, whose conservation is a consequence of the conservation of angular momentum (see [Davidson 2013](#)):

$$I = - \int d^3\mathbf{r} r^2 \langle \mathbf{u}(\mathbf{r}) \cdot \mathbf{u}(0) \rangle = \text{const} \quad \Rightarrow \quad U^2 L^5 \sim \text{const}, \quad (11.3)$$

Together with (11.2), this gives ([Kolmogorov 1941c](#))

$$U^2 \propto t^{-10/7}, \quad L \propto t^{2/7}. \quad (11.4)$$

So, energy decays and the outer scale grows. Note that there is no implication that any energy is actually transferred to larger scales: motions at larger scales just take longer to decay. Indeed, it is possible to show by a purely kinematic calculation (analogous to one presented for RMHD in appendix B.3) that the spectrum of this turbulence at $kL \ll 1$ has the asymptotic form

$$E(k) \propto Ik^4, \quad (11.5)$$

where I is the Loitsyansky invariant, so the energy content at large k is frozen by the conservation of this quantity—this is illustrated in figure 26(a) (which also shows that the conservation of I is not precise—indeed, I is allowed to have some small transient growth, before settling into a conserved state asymptotically with time; see Davidson 2013).

If, instead of Loitsyansky’s invariant, something else is conserved, different decay laws follow—applying to various different types of turbulence with different initial conditions, dimensions (2D), external forces (rotating, stratified), etc., all covered by Davidson (2013). And if all these can be profitably treated in this way, why not MHD turbulence?

11.3. Decaying Helical MHD Turbulence

In MHD, there are more invariants than in hydrodynamics, e.g., in 3D, no-mean-field, ideal MHD, the magnetic helicity $H = \langle \mathbf{A} \cdot \mathbf{B} \rangle$ is conserved. Furthermore, in resistive MHD, H is “better conserved” than energy: assuming the latter decays with time in a manner independent of the dissipation coefficients, as is usually the case in turbulence [e.g., as just happened in (11.4)], implies $\eta \langle J^2 \rangle \rightarrow \text{const}$ as $\eta \rightarrow +0$; therefore, H decays very slowly indeed:

$$\frac{dH}{dt} = -2\eta \langle \mathbf{B} \cdot \mathbf{J} \rangle \sim O(\eta^{1/2}) \quad \text{as } \eta \rightarrow +0. \quad (11.6)$$

It is a well-known result that MHD systems are partial to static magnetic equilibria that minimise magnetic energy subject to constant helicity and consist of linear force-free fields (“J. B. Taylor relaxation”: see Taylor 1974 or the lectures by Taylor & Newton 2015). Linear force-free fields are one-scale ($\mathbf{B} \times \mathbf{J} = 0$ implies $\nabla^2 \mathbf{B} = -k^2 \mathbf{B}$, where k is a single number that depends on the initial H and boundary conditions), so can hardly be thought of as a proper turbulent state, but one could nevertheless imagine MHD turbulence decaying towards a magnetically dominated state featuring such fields at large scales, probably with some (small? small-scale?) flows constantly re-excited by the large-scale “equilibrium” fields going unstable. Indeed, decaying states with magnetic energy decaying slower than kinetic and the former dominating over the latter in a broad range of scales starting from the outer scale have been found numerically in MHD simulations with finite helicity by Biskamp & Müller (1999, 2000). In line with the expectation articulated at the end of § 11.1, there are indications from simulations with very large resolution that something resembling a universal regime, possibly not entirely dissimilar, locally, from turbulence in a mean field, might emerge at small scales (Mininni *et al.* 2006).

If one adopts $H = \text{const}$ as a constraint, a crude model of the magnetic-energy decay in the spirit of (11.2–11.4) is

$$\frac{dB^2}{dt} \sim -\frac{UB^2}{L}, \quad B^2 L \sim \text{const}. \quad (11.7)$$

The tricky question is what to do about the kinetic energy U^2 . Assuming $U^2 \propto B^2$ gives (Hatori 1984; Son 1999)

$$B^2 \propto U^2 \propto t^{-2/3}, \quad L \propto t^{2/3}, \quad (11.8)$$

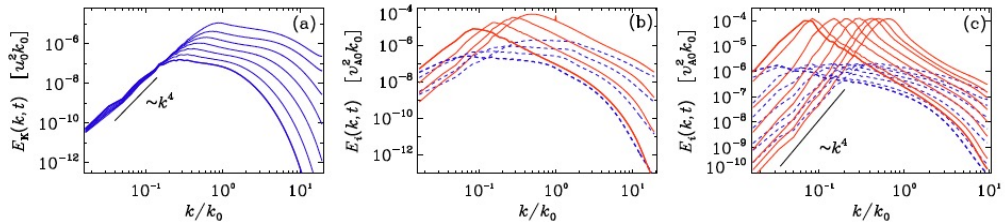


FIGURE 26. Spectra of kinetic (blue) and magnetic (red) energies in decaying turbulence: (a) pure hydrodynamic, (b) MHD with no mean field and zero helicity, (c) MHD with no mean field and finite helicity. The time evolution is from right to left (always towards larger scales). These plots are from [Brandenburg & Kahniashvili \(2017\)](#).

but this scaling disagrees with numerics ([Biskamp & Müller 1999, 2000](#)), and also, in fact, seems intuitively unlikely: if the system is trying to get into an approximately force-free, magnetically dominated state, this should probably mean that $U^2/B^2 \rightarrow 0$ as $t \rightarrow \infty$, i.e., that the kinetic energy decays faster than the magnetic one. Indeed, [Biskamp & Müller \(1999, 2000\)](#) spotted empirically in their simulations that $U^2 \propto B^4$, whence, via (11.7),

$$B^2 \propto t^{-1/2}, \quad U^2 \propto t^{-1}, \quad L \propto t^{1/2}. \quad (11.9)$$

These scalings did indeed appear to check out numerically, both in their simulations and in some later ones ([Christensson *et al.* 2001](#); [Banerjee & Jedamzik 2004](#); [Frick & Stepanov 2010](#); [Berera & Linkmann 2014](#); [Brandenburg *et al.* 2019](#)).⁵² I will discuss how to rationalise them in §§ 11.4.3 and 11.5.

The evolution of the magnetic spectrum in such a turbulence is shown in figure 26(c): while it has the same long-wavelength asymptotic as (11.5), the prefactor I now is manifestly *not* conserved, but rather grows robustly with time (in § 11.6, I will derive how), meaning that magnetic energy is quite vigorously transferred to larger scales—an “inverse cascade” (non necessarily local in k) associated with the conservation of magnetic helicity and its transfer to large scales, which is a well known phenomenon also in forced turbulence, often in the context of helical dynamo action ([Pouquet *et al.* 1976](#); [Brandenburg 2001](#); [Müller *et al.* 2012](#); [Rincon 2019](#)). In the dynamo case, forced ([Brandenburg 2001](#)) or decaying ([Brandenburg *et al.* 2019](#)), a helical velocity field generates a magnetic field from a small seed that initially has zero helicity. This field has helicity of one sign at small scales and of the opposite sign at large scales (larger than the scale of the velocity), keeping overall $H = 0$. The small-scale helicity is slowly destroyed by resistivity (which possibly makes the whole process very inefficient; see discussion in [Rincon 2019](#)), while the large-scale helicity is stuck at large scales and can, if forcing is switched off or absent from the beginning, serve as the starting point for a helical decaying regime—this scenario is nicely traced out in [Brandenburg *et al.* \(2019\)](#).

⁵²[Banerjee & Jedamzik \(2004\)](#), [Brandenburg & Kahniashvili \(2017\)](#) and [Brandenburg *et al.* \(2019\)](#) seem, nevertheless, to prefer the scalings (11.8). [Banerjee & Jedamzik \(2004\)](#) expect them to be recovered at greater resolution; [Brandenburg & Kahniashvili \(2017\)](#) deem their turbulence to evolve gradually towards (if not quite achieve) them; [Brandenburg *et al.* \(2019\)](#) think that (11.9) is a transient regime on the way to (11.8). I do not see why (11.8) should be viewed as more conceptually attractive than (11.9), but there is, admittedly, no rigorous proof that the ratio U^2/B^2 cannot tend to a small time-independent value even if the system is desperate for force-free field configurations.

11.4. Reconnection Takes Over Again?

Given that dynamo action by a helical flow can give rise to a helical magnetic field, MHD turbulence with finite helicity is a physically legitimate object of study. However, it requires mirror symmetry to be broken in the system, and one must at least consider the option of that not happening, i.e., $H = 0$. This destroys the usefulness of the $H = \text{const}$ constraint and re-opens the problem of the decay laws. The constant-helicity constraint is also absent when there is an external mean field, hence in RMHD, because there is no helicity conservation in this approximation. The non-helical decaying MHD turbulence has recently generated a flurry of excitement as inverse magnetic-energy transfer was discovered there numerically by Zrake (2014) and Brandenburg *et al.* (2015) (accompanied by Berera & Linkmann 2014 and followed by Reppin & Banerjee 2017, Park 2017, and Bhat *et al.* 2020)—figure 26(b) is from the non-helical simulation by Brandenburg *et al.* (2015) and shows healthy magnetic-energy growth at low wavenumbers. Zhou *et al.* (2020) found the same in RMHD: their system, initialised with an array of magnetic flux tubes, decayed not towards an Elsasser state, as the numerical experiments discussed in § 11.1 did, but to a state dominated by ever-larger-scale magnetic structures.

Their key contribution was to ask how those ever-larger magnetic structures might form dynamically from the initial collection of thin flux tubes and to conjecture, and then confirm, that (obviously!) they did so because reconnection caused these flux tubes to coalesce.

The distance from this realisation to specific scalings is quite short. Zhou *et al.* (2020) consider pairs of long flux tubes of radius $\sim L_\perp$, parallel to each other and to the mean field \mathbf{B}_0 , and reconnecting (coalescing) in the perpendicular plane. When that happens, their parallel (axial) fluxes $B_0 L_\perp^2$ add and, since $B_0 = \text{const}$, so do their areas L_\perp^2 , so their spatial scale increases. In the meanwhile, their perpendicular (poloidal) “2D flux” stays constant:⁵³

$$b_\perp L_\perp \sim \text{const}. \quad (11.10)$$

The time that full coalescence takes is the reconnection time:

$$t \sim \epsilon_{\text{rec}}^{-1} \frac{L_\perp}{b_\perp}, \quad \epsilon_{\text{rec}}^{-1} = (1 + \text{Pm})^{1/2} \min\{\tilde{S}_{L_\perp}^{1/2}, \tilde{S}_c^{1/2}\}, \quad \tilde{S}_{L_\perp} = \frac{u_\perp L_\perp}{\eta \sqrt{1 + \text{Pm}}}, \quad (11.11)$$

where ϵ_{rec} is the dimensionless reconnection rate, \tilde{S}_{L_\perp} is the Lundquist number (adjusted for a visco-Alfvénic outflow when $\text{Pm} \gg 1$) and $\tilde{S}_c \sim 10^4$ is its critical value above which reconnection switches from the Sweet–Parker regime (appendix C.3.1) to the fast, plasmoid-dominated regime (which is typically the threshold for the plasmoid instability: see appendix C.5).⁵⁴ But, in view of (11.10), $S_{L_\perp} \sim \text{const}$, so, in all circumstances,

$$t \propto \frac{L_\perp}{b_\perp} = \frac{L_\perp^2}{b_\perp L_\perp} \propto L_\perp^2 \quad \Rightarrow \quad L_\perp \propto t^{1/2}, \quad b_\perp^2 \propto t^{-1}, \quad (11.12)$$

where the last relation was obtained by applying (11.10) again. Since reconnection

⁵³This is an assumption, effectively equivalent to local conservation of anastrophy during 3D RMHD reconnection (see § 11.4.1). The 3D poloidal flux through the radial cross-section of the flux tube, $b_\perp L_\perp L_\parallel$, does *not* stay constant under this scheme. If it did, critical balance (11.13) would then imply $L_\perp \sim \text{const}$, which is clearly untrue.

⁵⁴If reconnection between flux tubes is stochastic in the sense advocated by Lazarian *et al.* (2020) (see appendix C.6), then, presumably, $\epsilon_{\text{rec}} \sim 1$. This does not appear to be the case in the simulations of Zhou *et al.* (2020), Bhat *et al.* (2020), and Hosking & Schekochihin (2021), viz., they see $\epsilon_{\text{rec}} \sim S_{L_\perp}^{-1/2}$, but there is no telling what might happen at higher resolutions.

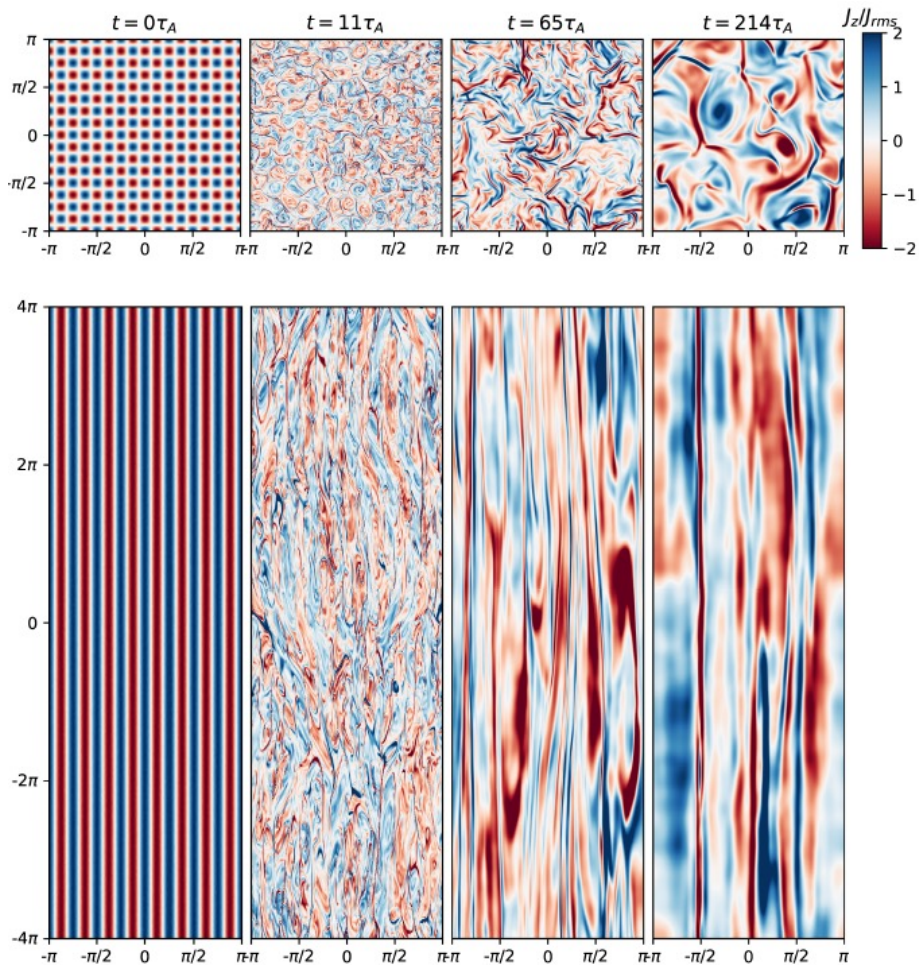


FIGURE 27. Snapshots of vertical (z) current density in the $(x, y, 0)$ (top row) and $(x, 0, z)$ (bottom row) planes, taken at a series of subsequent times in a decaying RMHD simulation by Zhou *et al.* (2020). This illustrates growth of $L_{\perp} \propto \sqrt{t}$ and $L_{\parallel} \propto t$ (the scalings confirmed quantitatively in their paper) and the presence of numerous current sheets.

involves (visco-)Alfvénic outflows, $u_{\perp} \sim b_{\perp}/\sqrt{1 + \text{Pm}}$ (see appendix C.3.1), i.e., the kinetic energy decays at the same rate as magnetic. The length of the tubes along the mean field is determined, as usual, by the CB condition:

$$\tau_A \sim \frac{L_{\parallel}}{v_A} \sim \frac{L_{\perp}}{b_{\perp}} \quad \Rightarrow \quad L_{\parallel} \propto t \quad (11.13)$$

(the reconnection time being generally longer than L_{\perp}/b_{\perp} and, therefore, τ_A , there should be plenty of time for the CB to establish itself).

They check all these scalings in their RMHD simulations (figure 27) and declare success. It is interesting to examine the ingredients of this success and assess to what degree it is non-accidental.

11.4.1. “Dimensional Reduction”: Is 3D Like 2D?

The argument leading to (11.12) is basically 2D and is indeed inherited from the 2D precursor paper by Zhou *et al.* (2019). In 2D, the scalings (11.12) have, in fact, been established for a long time (Biskamp & Welter 1989). They can be derived formally, without discussion of specific dynamics, in a manner analogous the scalings (11.8), but replacing the conservation of helicity with its 2D counterpart, the conservation of “anastrophy” $\langle A_z^2 \rangle$, where A_z is the out-of-plane component of the vector potential, which is “better conserved” than energy by an argument analogous to (11.6). Unlike helicity, anastrophy is a positive-definite quantity and cannot be zero, so there is only one regime. Since $\langle A_z^2 \rangle \sim B^2 L^2$, one gets (Hatori 1984)

$$\frac{dB^2}{dt} \sim -\frac{UB^2}{L}, \quad B^2 L^2 \sim \text{const}, \quad U^2 \sim B^2 \quad \Rightarrow \quad B^2 \propto U^2 \propto t^{-1}, \quad L \propto t^{1/2}. \quad (11.14)$$

The flux conservation in reconnection (11.10) is, as far as scaling laws are concerned, anastrophy conservation by a different name. The new thing in the 2D paper by Zhou *et al.* (2019) was not the scalings, but the attribution to reconnection of the controlling responsibility for the dynamics of turbulence decay—which they confirmed quite carefully by ascertaining that the time scale involved was the reconnection time scale (11.11), with its η dependence, rather than just the turnover time L_\perp/b_\perp (their S_{L_\perp} was small enough for their simulations to remain in the Sweet–Parker regime). This means that the first relation in (11.14) must, in fact, be written as

$$\frac{dB^2}{dt} \sim -\epsilon_{\text{rec}}^{-1} \frac{B^3}{L}, \quad (11.15)$$

where the decay time is the reconnection time, not just L/U . If $\epsilon_{\text{rec}} \sim \text{const}$, this does not change the decay laws, but one can check—successfully—that ϵ_{rec} is there either by including it into the rescaling of the time histories at different S_{L_\perp} , as Zhou *et al.* (2019) did, or by running numerical experiments with hyperresistivity, producing different decay laws (Hosking & Schekochihin 2021).

The extension of the above arguments to 3D RMHD implies that, modulo CB, decaying 3D RMHD turbulence is not all that different from the 2D one—at least if it is initialised in a state that is magnetically dominated (and, therefore, very well balanced; we saw in §11.1 that it can be quite different if initialised with some cross-helicity). Because the imposition of CB ensures that the parallel-propagation terms cannot be formally neglected, anastrophy is not conserved, but, if (11.10) is indeed the governing principle of dynamics, it seems to be conserved in some local and/or approximate sense. Olesen (2015) calls this “dimensional reduction” (in a slightly more formal context to which I will return in §11.5).

11.4.2. Decaying Non-Helical MHD Turbulence

What about 3D MHD turbulence with no mean field and zero helicity? There is ample numerical evidence that the scalings (11.14) work quite well—Mac Low *et al.* (1998) appear to have been the first to measure them in a 3D numerical simulation; they were confirmed with various degrees of certainty in all the numerical papers already cited in §§11.3–11.4. The 2D analogy did not escape their authors: e.g., Brandenburg *et al.* (2015) float “near conservation” of a local version of anastrophy as a promising idea. Bhat *et al.* (2020) make a long and careful empirical case that in this regime as well, coalescence of reconnecting structures is the dynamical driver of the increase of L_\perp and decay of B^2 . In fact, in an earlier paper, Reppin & Banerjee (2017) already mention (albeit gingerly and

amongst other options) the possibility that ever larger magnetic structures are generated via mergers of reconnecting flux ropes, an idea that they attribute to Müller *et al.* (2012), who in turn credit the 2D study by Biskamp & Bremer (1994). Reppin & Banerjee (2017) actually have quite nice circumstantial evidence for that: in their simulations, increasing Pm while holding Re constant kills the effect—as indeed it might do if reconnection, which slows down at higher Pm, were the culprit (note that in earlier, lower-resolution non-helical simulations by Banerjee & Jedamzik 2004, no inverse transfer was detected—presumably because Rm was not large enough for reconnection to get going properly).

11.4.3. Helical MHD Turbulence Revisited

Spotting that the scalings of U^2 and L in (11.14) and in the helical case (11.9) are the same, it is now tempting to rationalise the latter in the following way. Perhaps, with non-zero helicity present, the dynamics of decay are still controlled by reconnection, but the reconnecting component of magnetic field is systematically smaller than the non-reconnecting, force-free part that makes up most of $\langle B^2 \rangle$ —there might actually be a literal analogy between the mean field \mathbf{B}_0 in RMHD and this part of the field in helical MHD turbulence (the field is force-free, so does not have a dynamical influence, and is a kind of background equilibrium, although not necessarily scale-separated from the reconnecting fields). Then $B^2 \sim B_0^2 + \delta B^2$, where $\delta B^2 \ll B_0^2$ is the energy of the reconnecting field. Now $U \sim \delta B$ because reconnection creates outflows that are Alfvénic with respect to the reconnecting field. By the Zhou *et al.* (2020) argument (11.10–11.12),

$$\delta B L \sim \text{const}, \quad L \propto t^{1/2} \quad \Rightarrow \quad U^2 \sim \delta B^2 \propto t^{-1}, \quad (11.16)$$

and, by helicity conservation,

$$B_0^2 L \sim \text{const} \quad \Rightarrow \quad B^2 \sim B_0^2 \propto t^{-1/2}. \quad (11.17)$$

The scalings (11.9) are recovered.

11.5. Self-Similar Decay

Let me now introduce a clever formal way of thinking of decaying turbulence, pioneered by Olesen (1997). Whether it helps one derive anything conceptually new remains to be seen, but it is worth having this language in one’s vocabulary. Olesen (1997) starts by observing that MHD (and, indeed, also HD) equations have the following rescaling symmetry: $\forall a$ and h ,

$$\mathbf{r} \rightarrow a\mathbf{r}, \quad t \rightarrow a^{1-h}t, \quad \mathbf{u} \rightarrow a^h\mathbf{u}, \quad \mathbf{B} \rightarrow a^h\mathbf{B}, \quad \nu \rightarrow a^{1+h}\nu, \quad \eta \rightarrow a^{1+h}\eta. \quad (11.18)$$

He then posits that decaying MHD turbulence will simply go through a sequence of these transformation, with the rescaling parameter being a power of time, $a = (t/t_0)^{1/(1-h)}$, where t_0 is some reference (not necessarily initial) time. Then

$$U^2 \propto B^2 \propto t^{2h/(1-h)}, \quad L \propto t^{1/(1-h)}. \quad (11.19)$$

The tricky part is to find the right value of h . Conservation of helicity, $B^2 L \sim \text{const}$, would require $h = -1/2$, which gives the (probably) wrong solution (11.8). To get something else, one observes that the force-free magnetic field falls out of the momentum equation and, the induction equation being linear, can, in fact, be rescaled by an arbitrary constant: $\mathbf{B} \rightarrow a^m\mathbf{B}$, where m need not be the same as h (Campanelli 2004). Conservation of helicity then fixes m :

$$B^2 L \sim \text{const} \quad \Rightarrow \quad m = -\frac{1}{2} \quad \Rightarrow \quad B^2 \propto t^{-1/(1-h)}, \quad (11.20)$$

with h still undetermined.

Campanelli (2004) argued that $h = -1$ because the dissipation coefficients should stay constant. This got him both the helical scalings (11.9) and the non-helical ones (11.14).⁵⁵ Olesen (2015) commented that under this self-similarity, $\langle A^2 \rangle = \text{const}$, so anastrophy is conserved regardless of the dimensionality of the problem (“dimensional reduction”). It is then unsurprising that the same argument works in 2D, again returning the scalings (11.14).

Campanelli’s argument looks neat, but, on reflection, it is counterintuitive that everything should depend on the specific form of dissipation: indeed, if one were formally to replace viscosity and resistivity with hyperviscosity and hyperresistivity, $\eta\Delta \rightarrow \eta_m\Delta^n$, then keeping η_m unchanged by the scaling (11.18) would require a different value of h . Should we then expect different decay laws? This seems unlikely in the limit $\eta_m \rightarrow +0$.

Is the reconnection argument better? If reconnection is fast, either because it is plasmoid-dominated or because it is “stochastic” (see appendix C.6), (11.12) works regardless of the dissipation physics. If, on the other hand, it is standard Sweet–Parker reconnection (see appendix C.3.1), η (or η_m) does come in. It turns out that decay laws derived by generalising the Zhou *et al.* (2019, 2020) argument to a “hyper-resistive plasma” do indeed agree with numerical evidence, while those derived using the Campanelli (2004) principle do not (Hosking & Schekochihin 2021). So yes, the reconnection argument is better.

11.6. Self-Similar Spectra and Inverse Energy Transfer

It is very easy to see in this approach that most self-similar decay scenarios must involve inverse energy transfer from small to large scales. Let us follow Olesen (1997) and work out what the symmetry (11.18) implies for the spectrum of any of the fields that have it. For example, for the magnetic field, the spectrum satisfies

$$E(k, t) = 4\pi k^2 \int \frac{d^3\mathbf{r}}{(2\pi)^3} e^{-i\mathbf{k}\cdot\mathbf{r}} \langle \mathbf{B}(\mathbf{r}, t) \cdot \mathbf{B}(0, t) \rangle = a^{-1-2m} E(a^{-1}k, a^{1-h}t), \quad (11.21)$$

where I used the more general rescaling $\mathbf{B} \rightarrow a^m \mathbf{B}$ ($m = -1/2$ for a helical magnetic field, $m = h$ for a non-helical one, or for the velocity field). A self-similarly evolving solution of (11.21) is (entirely independently of the dimension of space)

$$E(k, t) = k^{-1-2m} f(kt^{1/(1-h)}), \quad (11.22)$$

where $f(x)$ is some function, which needs to be integrable in an appropriate way in order for the total energy to be finite:

$$\langle B^2 \rangle = \int_0^\infty dk E(k, t) = t^{2m/(1-h)} \int_0^\infty dx x^{-1-2m} f(x). \quad (11.23)$$

⁵⁵Christensson *et al.* (2005) have an argument for $L \propto t^{1/2}$ that is essentially a version of Campanelli’s (but their original publication in preprint form predated his paper). It is based on the self-similar solution (11.22) for the energy spectrum. It is hard-wired into this solution that $L \propto t^{1/(1-h)}$, but if one now assumes self-similarity all the way down to the dissipation scales, the dissipative cutoff must have the same scaling, so $\lambda_\eta \propto t^{1/(1-h)}$. In a nutshell, Christensson *et al.* (2005) then set $\lambda_\eta \sim (\eta t)^{1/2}$ by dimensional analysis and hence conclude that $h = -1$. This again relies on the notion that dissipation physics sets the decay law (see further discussion in this section). This is far from obvious, as is that λ_η depends only on η and t and, not, e.g., on η , L , B and/or U (and, therefore, on the initial energy and scale of the turbulence), as the Kolmogorov scale does in a turbulence with constant energy flux ($\varepsilon \sim B^2/t$ for the decaying case).

The familiar decay laws (11.9) and (11.14) are recovered for $(m, h) = (-1/2, -1)$ and $m = h = -1$, respectively [and the hydrodynamic decay (11.4) for $m = h = -5/2$].

Since magnetic field is solenoidal, its spectrum must be $\propto k^4$ [cf. (11.5)] at large scales ($kL \ll 1$). This requires $f(x) \propto x^{5+2m}$, whence

$$E(k) \propto t^{(5+2m)/(1-h)} k^4. \quad (11.24)$$

Thus, as long as $m > -5/2$ and $h < 1$, the energy content of low wavenumbers grows with time, implying not just selective decay (as for $m = h = -5/2$) but some form of inverse energy transfer, which is indeed observed numerically in both helical and non-helical cases: see figure 26(b,c). Note that (11.22) also implies that the peak of the spectrum, at $kL \sim 1$, is $E_{\max} \propto t^{(1+2m)/(1-h)} \sim \text{const}$ for the helical case (manifestly true in figure 26c) and $E_{\max} \propto t^{-1/2}$ for the non-helical one (figure 26b). Brandenburg & Kahniashvili (2017) show that rescaling their time-dependent spectra in line with (11.22), or, to be precise, with the equivalent expression $E(k, t) = L(t)^{1+2m} g(kL(t))$, where $L(t)$ is measured directly at every t , collapses them all onto a single curve, confirming self-similarity.

Let me observe, finally, that if the prefactor of the low- k asymptotic of $E(k)$ changes with time, as it does in (11.24), i.e., if there is no conserved quantity like the Loitsyansky invariant (11.3) that effectively freezes the spectrum at low k , I see no reason to expect that the long-term self-similar evolution should be tied to the low- k scaling baked into the initial condition, as many authors, starting with Olesen (1997), seem to believe. The self-similar solution need not start at $t = 0$, and it is perfectly possible that it is preceded by some initial non-self-similar rearrangement. There appears to be some convincing numerical evidence that this is indeed what happens (e.g., Brandenburg & Kahniashvili 2017; Brandenburg *et al.* 2019; Hosking & Schekochihin 2021). This said, it is not as yet entirely clear whether any Loitsyansky-style invariants might, in fact, exist in MHD (as they do, e.g., at $\text{Rm} \ll 1$; see Davidson 2013)—an open question worth looking into further.

11.7. Self-Similar Decay in RMHD

The reader who remembers the RMHD symmetry (3.5) has been straining at the leash to apply it to the decay problem. It is, of course, the same symmetry as (11.18) if one lets $\epsilon = a^h$, except now perpendicular and parallel gradients and, therefore, distances transform differently from each other:⁵⁶

$$\mathbf{r}_\perp \rightarrow a\mathbf{r}_\perp, \quad r_\parallel \rightarrow a^{1-h}r_\parallel. \quad (11.25)$$

This is just because v_A is now assumed to be an immutable constant, so r_\parallel transforms as time, rather than as distance (cf. Beresnyak 2015, and §5.2). At $h = -1$, these scalings instantly reproduce the Zhou *et al.* (2020) results (11.12) and (11.13).

In the same vein as (11.21) and (11.22), one finds, this time for the 2D spectra:

$$E_{2D}(k_\perp, k_\parallel, t) = a^{-2-h} E_{2D}(a^{-1}k_\perp, a^{-1+h}k_\parallel, a^{1-h}t). \quad (11.26)$$

The self-similar solution is, therefore,

$$E_{2D}(k_\perp, k_\parallel, t) = k_\perp^{-2-h} f(k_\perp t^{1/(1-h)}, k_\parallel t), \quad (11.27)$$

with some unknown function $f(x, y)$. The 1D perpendicular spectrum $E(k_\perp, t)$ is found

⁵⁶Note that this scaling of the parallel distances is correct both for distances along the global and the local mean field (cf. §5.3), because $\mathbf{b}_\perp \cdot \nabla_\perp \rightarrow a^{h-1}\mathbf{b}_\perp \cdot \nabla_\perp$.

by integrating (11.27) over all k_{\parallel} , predictably leading to the same result as (11.22). Integrating (11.27) over k_{\perp} instead, one gets the 1D parallel spectrum:

$$E(k_{\parallel}, t) = t^{(1+h)/(1-h)} g(k_{\parallel} t), \quad (11.28)$$

where $g(y) = \int_0^{\infty} dx x^{-2-h} f(x, y)$.

This result is interesting for the following reason. $E(k_{\parallel}, t)$ is the spectrum of a random field reflecting its dependence on a single scalar spatial coordinate, the distance along the field. The long-wavelength, $k_{\parallel} L_{\parallel} \ll 1$, asymptotic of this spectrum describes the absence of correlations at point separations $r_{\parallel} \gg L_{\parallel}$, so it is just the spectrum of a 1D white noise (cf. appendix B.1). Therefore, $g(y) \rightarrow \text{const}$ as $y \rightarrow 0$. But (11.28) then implies that the energy content of low k_{\parallel} is frozen in time if $h = -1$. This suggests that, if indeed $h = -1$, RMHD turbulence might have a Loitsyansky-like (or, rather, Saffman-like; see Davidson 2013) invariant I , so $E(k_{\parallel}, t) \approx I k_{\parallel}^0 = \text{const}$ at $k_{\parallel} L_{\parallel} \ll 1$ (cf. § 11.2). This invariant should have the form⁵⁷

$$I = \int dr_{\parallel} \langle \mathbf{b}_{\perp}(r_{\parallel}) \cdot \mathbf{b}_{\perp}(0) \rangle \quad (11.29)$$

(instead of \mathbf{b}_{\perp} , it may involve some other linear combination of the fields \mathbf{b}_{\perp} and \mathbf{u}_{\perp} , or \mathbf{Z}_{\perp}^{\pm}). If such a quantity were proven to be conserved, exactly or approximately, setting $h = -1$ would become a very solidly justified step—this would be another way of proving (11.10), which is, indeed, equivalent to $b_{\perp}^2 L_{\parallel} \sim \text{const}$ if the CB condition (11.13) is satisfied.

11.8. Inertial-Range Spectra

Finally, the philosophy articulated at the end of § 11.1 with regard to the inertial-range spectra does appear to be vindicated in the RMHD simulations of Zhou *et al.* (2020): they report $k_{\perp}^{-3/2}$ spectra of both magnetic and kinetic energy, presumably of the same origin as those derived in § 6. In the currently available decaying MHD simulations without a mean field, with or without helicity, there might not yet be sufficient resolution to tell what the asymptotic inertial-range spectra are (see, e.g., figure 26 and note particularly that there is no scale-by-scale equipartition between magnetic and kinetic energy at these resolutions)—or indeed whether they are universal with respect to initial conditions (Lee *et al.* 2010), a somewhat disconcerting prospect. An oft-reported “non-universal” spectrum is k^{-2} (e.g., by Lee *et al.* 2010; Brandenburg *et al.* 2015, 2019), which might actually be another signature of reconnection (rather than of the WT regime, as some of these authors suggest): Dallas & Alexakis (2013a) and Zhou *et al.* (2019, in 2D) interpret this spectrum geometrically as describing an ensemble of current sheets, which are step-like “discontinuities” of the magnetic field (this is the same argument as I mooted for the residual energy in § 9.4). According to Dallas & Alexakis (2013b, 2014), however, this scaling gives way to a shallower $k^{-5/3}$ or $k^{-3/2}$ slope at sufficiently small scales in simulations with sufficiently high resolution, as current sheets curl up and/or break up, so perhaps small-scale universality is safe after all.

11.9. Summary

To sum up, there appear to be at least three qualitatively different regimes of decaying MHD turbulence (although it is formally possible to imagine that there are many more: see, e.g., Stribling & Matthaeus 1991; Wan *et al.* 2012).

⁵⁷Intriguingly, (11.29) is the one-point correlator between the field and its $k_{\parallel} = 0$ part, evoking the special role of the “2D condensate” (see §§ 4.4 and 9.3).

(i) RMHD states with some initial imbalance tend towards enduring (i.e., decaying on the viscous/resistive time scale) pure Elsasser solutions, due to relatively slower decay of the cross-helicity compared to energy (§ 11.1).

(ii) RMHD turbulence starting in very balanced configurations—e.g., purely magnetic ones—settles into a reconnection-dominated decay towards ever-larger-scale magnetic structures accompanied by flows whose kinetic energy is a finite fraction of the magnetic one (§ 11.4). This resembles what happens in 2D MHD (§ 11.4.1) and in non-helical 3D MHD with no mean field (§ 11.4.2).

(iii) 3D MHD turbulence with no mean field but finite helicity ends up in a decaying state dominated by an approximately force-free magnetic field and some weaker motions, the latter decaying faster than the former (§ 11.3). Reconnection may well again be playing a controlling role in setting the decay rate (§ 11.4.3).

The different regimes are distinguished by different scalings with time of the decaying magnetic and kinetic energies and of the growing energy-containing scale (or, in the presence of a mean field, of the perpendicular and parallel coherence scales). As far as I am aware, it is not currently known what is the precise threshold value of the initial cross-helicity that separates regimes (i) and (ii) or of the initial helicity that separates regimes (ii) and (iii).

The evolution is self-similar (§§ 11.5 and 11.7) and usually features not just selective decay but also some transfer of energy to larger scales (§ 11.6). Whether this evolution is constrained by any non-obvious large-scale invariants, like it is in hydrodynamics (§ 11.2), remains to be seen (§§ 11.4.1 and 11.7).

At small (inertial-range) scales, all these different types of decaying turbulence probably behave similarly to their forced counterparts, although it remains a challenging computational task to confirm this definitively (§§ 11.1 and 11.8).

12. MHD Dynamo Meets Reconnection

An interesting and distinct type of MHD turbulence about which I have so far said anything only in the context of turbulence decay (§ 11) is the case of no mean field: starting with a steady-state, forced hydrodynamic turbulence and a dynamically weak, randomly tangled magnetic field, one observes exponential growth of the latter, a phenomenon known as *small-scale dynamo* (or *fluctuation dynamo*). The system eventually saturates with magnetic energy comparable to kinetic, but not, it seems, necessarily equal to it scale by scale—what the final state is remains an unsolved problem, both numerically (due to lack of resolution) and theoretically (due to lack of theoreticians). Furthermore, it matters whether the turbulence possesses net helicity (injected by the forcing) and/or has a large-scale shear superimposed on it—if it does, small-scale dynamo is accompanied by a *mean-field dynamo*, leading to growth of a large-scale field (the large scale in question being generally larger than the outer scale of the turbulence). Saturated states of such dynamos are also poorly understood, for the same reasons as stated above.

Turbulent dynamos deserve a separate review—and they have recently received a superb one, by Rincon (2019), to which I enthusiastically refer all interested public. This said, the ideas associated with the role of tearing in RMHD turbulence, reviewed in § 7, turn out to have some direct bearing on the “purest” (homogeneous, non-helical, unshered) small-scale dynamo problem. This is, therefore, a natural place for some discussion of it.

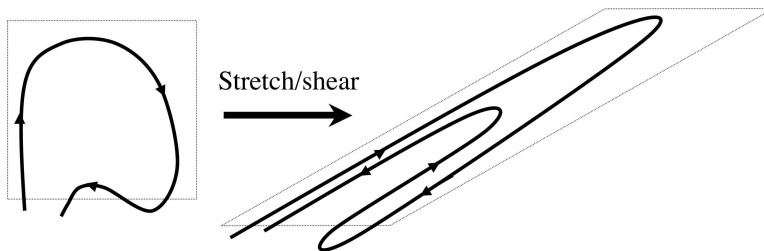


FIGURE 28. Stretching/shearing a field line produces direction reversals (cartoon from Schekochihin & Cowley 2007).

12.1. Old Arguments About Saturated Dynamo at Large Pm

In regimes with $\text{Pm} > 1$,⁵⁸ small-scale dynamo can be understood as the process of a velocity field, restricted to scales above the viscous cutoff, randomly stretching and shearing the magnetic field, which is allowed to go to smaller scales, limited only by the Ohmic resistivity. Intuitively, it is not hard to see that embedding a tangled field line into an “eddy” will lead to the field line being stretched and folded, resulting in a configuration featuring field reversals on ever smaller scales (figure 28). A combination of numerical evidence and theoretical arguments (see Schekochihin & Cowley 2007, Rincon 2019, and references therein) confirms that this process does indeed lead to net amplification of magnetic energy, with that energy residing preferentially in “folds”—magnetic fields that reverse direction across themselves on the resistive scale and remain approximately straight along themselves up to the scale of the velocity field. When the dynamo saturates, it does so in some not-very-well-understood way involving these bundles of alternating fields back-reacting on the turbulent flow and arresting further amplification. Whereas in the kinematic-dynamo stage (i.e., when the field is dynamically weak), the spectrum

⁵⁸After I first worked on this problem, I grew quite sceptical about the relevance of the $\text{Pm} \gg 1$ MHD dynamo to any real-world situations: plasmas that formally have high Pm (e.g., the hot interstellar medium or the intergalactic medium in galaxy clusters) tend to be very hot and tenuous and, therefore, not very collisional, so MHD with Laplacian viscosity cannot possibly apply there (see, e.g., Schekochihin & Cowley 2006, and further discussion in § 13.4). However, recent kinetic simulations of dynamo in such plasmas (Rincon *et al.* 2016; Kunz *et al.* 2016; St-Onge & Kunz 2018; St-Onge *et al.* 2020) appear to be showing many familiar large-Pm features, perhaps because plasma microphysics conspire to produce an effectively collisional medium, which might not be entirely dissimilar from a large-Pm MHD fluid. Furthermore, the first laboratory plasma dynamos, achieved in laser-plasma experiments, have turned out to be right in the collisional, $\text{Pm} \gtrsim 1$ regime (Tzeferacos *et al.* 2018; Bott *et al.* 2020). Thus, it seems that my scepticism was premature and we ought to tackle the large-Pm dynamo with renewed vigour and sense of relevance. In contrast with $\text{Pm} \gg 1$, the limit of $\text{Pm} \ll 1$ is much more straightforwardly relevant: liquid metals and plasmas in convective zones of stars *are* comfortably collisional MHD fluids, and there are many other examples. This case appears, however, to be quite different physically, at least in the kinematic regime, and even less well understood, although numerically we do know that there is dynamo (Iskakov *et al.* 2007; Schekochihin *et al.* 2007; Brandenburg *et al.* 2018) and that it has some kind of saturated state (Brandenburg 2011; Sahoo *et al.* 2011)—conclusions to obtain which, one still has to push at the resolution limits of currently achievable MHD simulations. A massive paper by Sahoo *et al.* (2011) contains a wealth of sophisticated statistical information but does not answer any of the more basic questions (their one distinctive physical conclusion is that the low-Pm case is less intermittent than the high-Pm one, which is plausible). I am not aware of any other systematic numerical study of how low-Pm dynamo saturates—an opportunity for a definitive contribution that some enterprising researcher with an MHD code and a large allocation of computing time should seize (there is a promise of that in McKay *et al.* 2019).

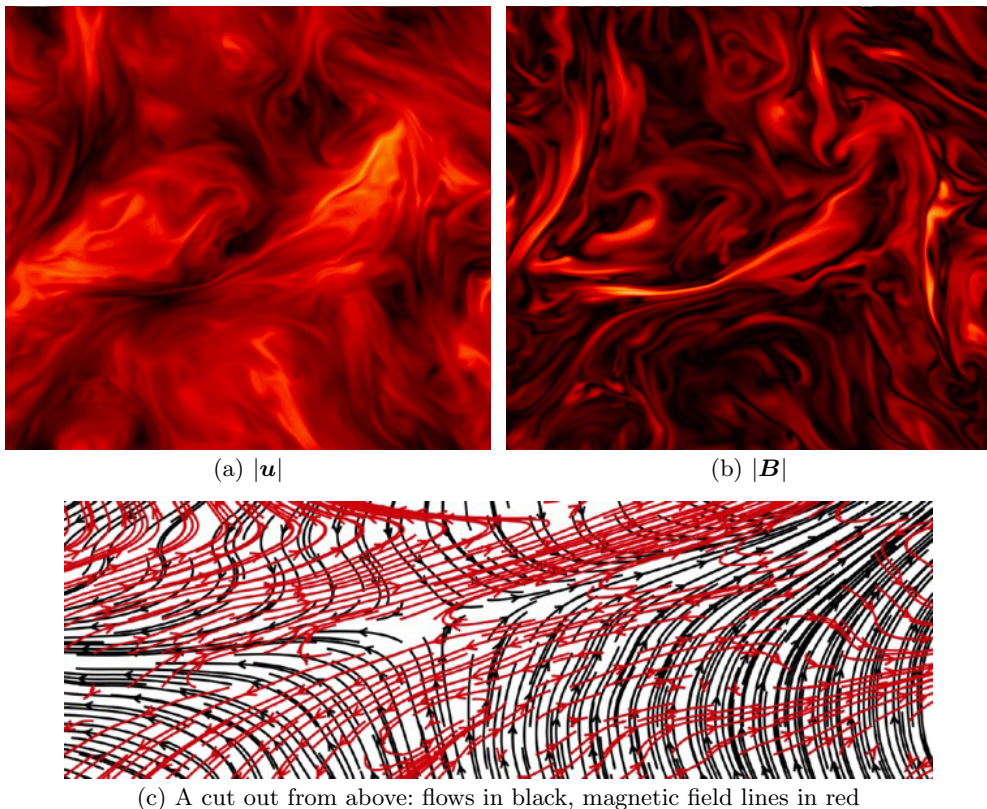
of the magnetic energy certainly peaks at the resistive scale (Schekochihin *et al.* 2004), what exactly happens in the saturated state is a matter of some debate. It is tempting to argue, with Kraichnan (1965), that the system will sort itself out into a state where the magnetic energy is at the outer scale, while the smaller scales behave in exactly the same way as they do in the presence of a strong mean field. Whether numerical evidence confirms this view is, at any resolutions achieved so far, in the eye of the beholder (Kida *et al.* 1991; Haugen *et al.* 2003, 2004; Cho & Ryu 2009; Beresnyak & Lazarian 2009a; Beresnyak 2012c; Teaca *et al.* 2011; Eyink *et al.* 2013; Porter *et al.* 2015; Grete *et al.* 2017, 2020; McKay *et al.* 2019; Bian & Aluie 2019; Brandenburg & Rempel 2019; Seta *et al.* 2020; see figure 31b). The alternative possibility is that the magnetic energy stays at small scales—not quite as small as in the kinematic regime, but still determined by resistivity (Schekochihin *et al.* 2002, 2004; Maron *et al.* 2004). The claim is that the folded field structure persists in saturation, with the folds elongating to the outer scale (L) of the turbulence and direction reversals within folds occurring on the scale $\lambda_\eta \sim L \text{Rm}^{-1/2}$, where the stretching rate ($\sim \delta u_L/L$) balances the Ohmic-diffusion rate ($\sim \eta/\lambda_\eta^2$).

Despite being associated with the latter point of view, I am not going to defend it here in its original form because of certain little known but consequential numerical developments, described in § 12.2, that occurred after that debate had its heyday. Instead, drawing on the ideas of § 7, I will propose, in §§ 12.3 and 12.4, an amended view of the saturated state of turbulent dynamo, in which reconnection and MHD turbulence will again meet and collaborate.

12.2. Numerical Evidence: Reconnection Strikes Again

Existence of turbulent dynamo was definitively established by Meneguzzi *et al.* (1981) in what was then a “hero” 64^3 MHD simulation—one of those *bona fide* numerical discoveries that make computer simulations worthwhile. 20 years later, when the debate about the nature of the saturated dynamo state focused on interpreting newly accessible, improved numerical evidence (Kinney *et al.* 2000; Schekochihin *et al.* 2004; Maron *et al.* 2004; Haugen *et al.* 2003, 2004), everyone was staring at not very conclusive magnetic spectra with some pronounced excess of the magnetic over kinetic energy at small scales, and at visualisations of magnetic fields organised in folds (especially at large Pm). One could be a believer in universality and think of this as a non-asymptotic state that would, at infinite resolution, turn into the usual Kolmogorov-style turbulence spectrum, with magnetic energy shifting to the outer scales (Haugen *et al.* 2003, 2004; Beresnyak & Lazarian 2009a; Beresnyak 2012c)—or one could rely on a different kind of physical intuition and argue that there was no obvious physical mechanism for unwrapping fields folded at the resistive scale (that was my view).

In more recent, sadly unfinished, work, Isakov & Schekochihin (2008) discovered, however, that, in simulations with moderate $\text{Pm} \geq 1$ and large Re (the former being the only affordable possibility compatible with the latter), magnetic folds in the nonlinear regime became current sheets, with very clear inflow–outflow patterns around the field reversals (figure 29). One might say that this should have been obvious from the start, although perhaps less so in the case of $\text{Pm} \gg 1$ (see § 12.3.3). We also found that the folds became corrugated and plasmoid-like structures (probably flux ropes) formed, with an approximately circularised cross-section. Larger simulations by Beresnyak (2012b), also unpublished (except for some bits in Beresnyak & Lazarian 2009a and Beresnyak 2012c), revealed the same feature, with the numerical box now teaming with small plasmoid-like structures and rippled folds (figure 30), a result confirmed at even higher resolutions by Galishnikova *et al.* (2020). Thus, while the folds could not perhaps be literally



(c) A cut out from above: flows in black, magnetic field lines in red

FIGURE 29. From unpublished work by [Iskakov & Schekochihin \(2008\)](#): a 512^3 incompressible-MHD simulation of saturated fluctuation dynamo, $\text{Pm} = 1$, $\text{Re} = 1360$ (defined $= u_{\text{rms}}/\nu k_0$, where $k_0 = 2\pi$ is the forcing wavenumber, corresponding to the box size; this is the same numerical set up as in [Schekochihin et al. 2007](#)). These are 2D cuts from instantaneous snapshots of absolute values of (a) velocity, (b) magnetic field. Panel (c) is a cut out from these snapshots, zooming in on the horizontal fold just down towards the left from the centre of the snapshot. Stream lines are in black and field lines are in red. A reconnecting-sheet structure, with field reversal, inflows and outflows is manifest. Very pretty 3D pictures of this kind of reconnecting structure extracted from an MHD turbulence simulation can be found in [Lalescu et al. \(2015\)](#).

unwrapped, they did turn out to be prone to breaking up and seeding populations of smaller structures.⁵⁹

There is little definitive analysis of all this available in print. There is, however, an intriguing finding by [Brandenburg \(2014\)](#), who analysed his own simulations and those of [Sahoo et al. \(2011\)](#) and discovered that the ratio of energy dissipated resistively to that dissipated viscously decreased at larger Pm ([Beresnyak 2012b](#) also had this result; [McKay et al. 2019](#), however, raise a degree of doubt as to whether it will survive at larger Rm). One might plausibly argue that something like this could happen if kinetic energy, first converted into magnetic one as fields were amplified and folded by large-

⁵⁹Note that neither [Iskakov & Schekochihin \(2008\)](#) nor [Beresnyak \(2012b\)](#) saw any of this happen in the “Stokes” regime $\text{Re} \sim 1$, $\text{Pm} \gg 1$, which is the only numerically accessible case if one wants very large Pm , and on which much of the previous physical intuition ([Schekochihin et al. 2004](#)) had been based: there, the saturated state just consisted of magnetic fields smoothly folded on the resistive scale. I shall argue in § 12.3.3 that this makes sense.



FIGURE 30. From unpublished work by [Beresnyak \(2012b\)](#) (reproduced with kind permission of the author): snapshot of the absolute value of magnetic field in a $Pm = 10$ and $Re \approx 500$ simulation at 1024^3 (the same numerical set up as in [Beresnyak & Lazarian 2009a](#) and [Beresnyak 2012c](#); note that Beresnyak defines his Re in terms of the “true” integral scale of the flow calculated from its spectrum). Plasmoids/fold corrugations galore. In his other simulations within this sequence, there are even more plasmoid-like-looking features at $Pm = 1$ and $Re \approx 6000$, with some sign of them breaking up into even smaller structures (cf. §12.3.3). In contrast, they start disappearing at $Pm = 10^2$ and $Re \approx 80$ and are gone completely in the “Stokes” regime $Pm = 10^4$ and $Re \approx 2$.

scale turbulent flows, were then to be recovered from magnetic energy at smaller scales as fluid motions were generated by reconnection and instabilities (presumably, tearing instabilities) in the folds. [Brandenburg & Rempel \(2019\)](#), while they do not engage with the notion of reconnecting folds, do confirm explicitly that, in larger- Pm simulations,

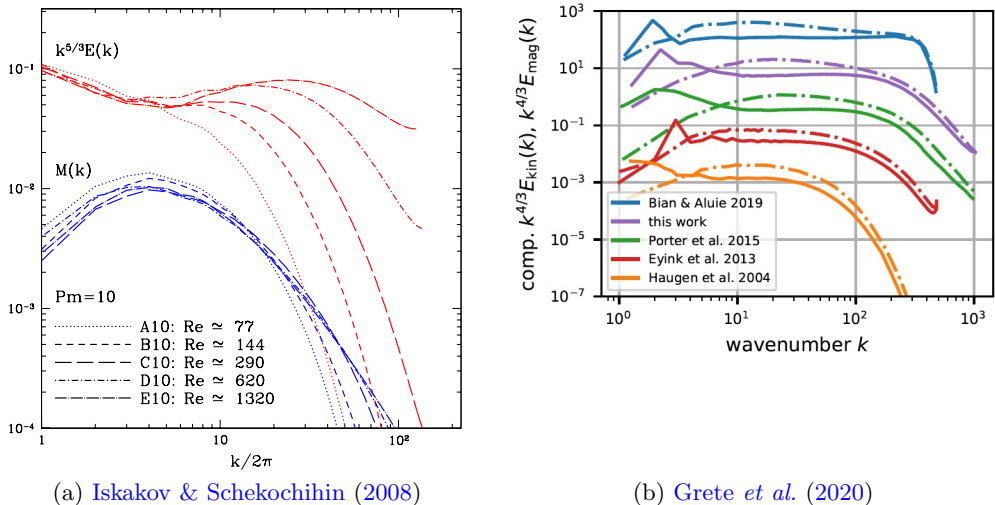


FIGURE 31. (a) Spectra of saturated MHD dynamo: kinetic-energy (red, compensated by $k^{5/3}$) and magnetic-energy (blue) spectra from a series of incompressible-MHD simulations with $Pm = 10$ and increasing Re by [Iskakov & Schekochihin \(2008\)](#). The numerical set up is the same as in [Schekochihin et al. \(2007\)](#); the resolution is 512^3 (so the highest- Re run may be numerically suspect). (b) A summary plot from [Grete et al. \(2020\)](#) of their and several other numerical studies, viz., from top to bottom, [Bian & Aluie \(2019\)](#); [Grete et al. \(2020\)](#); [Porter et al. \(2015\)](#); [Eyink et al. \(2013\)](#); [Haugen et al. \(2004\)](#). The kinetic-energy (solid lines) and magnetic-energy (dot-dashed lines) spectra are all compensated by $k^{4/3}$ to highlight the shallow kinetic-energy spectrum at small scales.

there is increasing net transfer of magnetic to kinetic energy at small scales, with kinetic energy’s viscous thermalisation increasingly dominating the overall dissipation rate.

A signature of this behaviour is discernible if one examines the magnetic- and, especially, kinetic-energy spectra in saturated dynamo simulations at relatively high resolutions (512^3 and up), without attempting to see what one might want to see, e.g., scale-by-scale equipartition or $k^{-5/3}$. Figure 31(a), taken from the unpublished simulations by [Iskakov & Schekochihin \(2008\)](#), shows that the kinetic-energy spectrum steepens at large scales compared to the hydrodynamic case (the empirical slope is $k^{-7/3}$; see [Schekochihin et al. 2004](#) and [St-Onge et al. 2020](#)), but picks up around the same wavenumber where the magnetic-energy spectrum has its peak and becomes shallower than Kolmogorov—[Grete et al. \(2020\)](#) find $k^{-4/3}$ to be a good fit, both in their simulations and, in retrospect, in many previous ones (figure 31b). By analysing energy transfers, they attribute this to significant transfer of energy from magnetic to kinetic, by means of the tension force—this is analogous to the result of [Brandenburg & Rempel \(2019\)](#) and again entirely consistent with (although does not amount to a definitive confirmation of) the idea that reconnection in the folds drives small-scale motions, which come to dominate the kinetic-energy spectrum at those scales. This is perhaps reinforced by their ([Grete et al. 2020](#)) observation (in disagreement with [Bian & Aluie 2019](#)) that the energy cascade at small scales is almost entirely controlled by magnetic forces, rather than by hydrodynamic advection. The paper by [Grete et al. \(2020\)](#) appears to be the first one for well over a decade that, having measured different kinetic- and magnetic-energy spectra, dares to consider the possibility that this might mean something physical, rather than just insufficient resolution for expected asymptotic recovery of $k^{-5/3}$ or $k^{-3/2}$.

Thus, reconnection appears to have caught up with dynamo, just as it did with Alfvénic

turbulence in § 7, the general principle at work in both cases being that while large-scale motions push magnetic fields into small-scale, direction-reversing configurations, resistive effects invariably manage to break those up.

12.3. Towards a New Theory of Reconnecting Dynamo

12.3.1. Kinematic Dynamo and Onset of Tearing

Consider first a weak, tangled magnetic field being stretched by fluid motions whose scale is ℓ (why I call it ℓ rather than λ is about to become obvious). Let us imagine that these fluid motions are part of vanilla Kolmogorov turbulence, described, inevitably, by (2.2):

$$\delta u_\ell \sim (\varepsilon \ell)^{1/3}. \quad (12.1)$$

Balancing the associated stretching rate with the Ohmic-diffusion rate gives one the resistive scale:

$$\tau_{\text{nl}}^{-1} \sim \frac{\delta u_\ell}{\ell} \sim \frac{\varepsilon^{1/3}}{\ell^{2/3}} \sim \tau_\eta^{-1} \sim \frac{\eta}{\lambda_\eta^2} \quad \Rightarrow \quad \lambda_\eta \sim (\eta \tau_{\text{nl}})^{1/2} \sim \ell \text{Rm}_\ell^{-1/2}, \quad \text{Rm}_\ell = \frac{\delta u_\ell \ell}{\eta}. \quad (12.2)$$

The scale λ_η is the reversal scale of the dynamo-generated magnetic field, whose typical coherence scale *along itself* will be ℓ .

Imagine now a general configuration in which magnetic field B_λ (as usual, in velocity units) reverses direction on some scale λ , not necessarily equal to λ_η . It will be subject to tearing at the rate (7.1), but with v_{Ay} replaced by B_λ :

$$\gamma \sim \frac{B_\lambda}{\lambda} S_\lambda^{-1/2} (1 + \text{Pm})^{-1/4} \sim \frac{B_\lambda^{1/2}}{\lambda^{3/2}} \eta^{1/2} (1 + \text{Pm})^{-1/4}. \quad (12.3)$$

When B_λ is infinitesimally small, as it would be in the kinematic stage of the dynamo, the tearing rate is small, $\gamma \ll \tau_\eta^{-1}$. It will become comparable to the resistive-diffusion rate at $\lambda = \lambda_\eta$ when the fields reversing at this scale grow to be at least

$$B_{\lambda_\eta} \sim \frac{\eta}{\lambda_\eta} (1 + \text{Pm})^{1/2} \sim \delta u_\ell \widetilde{\text{Re}}_\ell^{-1/2}, \quad \widetilde{\text{Re}}_\ell = \frac{\delta u_\ell \ell}{\nu + \eta} = \frac{\text{Rm}_\ell}{1 + \text{Pm}}. \quad (12.4)$$

Here $\widetilde{\text{Re}}_\ell$ is the usual Reynolds number Re_ℓ when $\text{Pm} \gtrsim 1$ and Rm_ℓ when $\text{Pm} \ll 1$ [cf. (6.22)]. In the former case, since the stretching rate τ_{nl}^{-1} at the viscous scale $\ell \sim \ell_\nu = \varepsilon^{-1/4} \nu^{3/4}$ is the largest, it is the viscous-scale eddies that will play the dominant role in amplifying an infinitesimally small field, but the dynamo will go nonlinear as soon as the field's energy becomes comparable to the energy of the viscous-scale motions, $B_{\lambda_\eta} \sim \delta u_{\ell_\nu}$. Since, by definition of ℓ_ν , $\text{Re}_{\ell_\nu} \sim 1$, the estimate (12.4) also turns into $B_{\lambda_\eta} \sim \delta u_{\ell_\nu}$, i.e., tearing in the folds will start outpacing Ohmic diffusion at exactly the same moment as the nonlinearity kicks in (this is perhaps obvious because tearing needs Lorentz force: see appendix C.1). Thus, a nonlinear dynamo is also a reconnecting dynamo.

In the limit of $\text{Pm} \ll 1$, the fastest eddies capable of field amplification are at the resistive scale, $\ell \sim \lambda_\eta$ (e.g., Boldyrev & Cattaneo 2004). Since $\text{Re}_{\lambda_\eta} \sim \text{Rm}_{\lambda_\eta} \sim 1$, the estimate (12.4) becomes $B_{\lambda_\eta} \sim \delta u_{\lambda_\eta}$, so it again tells us that the nonlinearity and tearing become important at the same time. Admittedly, there is no longer a scale separation between ℓ and λ_η in this situation, so the magnetic field is not, strictly speaking, “folded” (this is quite obvious from the snapshots of growing fields in Schekochihin *et al.* 2007), although one might still speculate that tearing is possible across generic X -point configurations. I shall keep my discussion general, but it might be easier for a doubtful reader just to think of large Pm in all cases.

12.3.2. Self-Similar Dynamo

It has been argued by [Schekochihin *et al.* \(2002, 2004\)](#) and [Maron *et al.* \(2004\)](#) (with later variants by [Beresnyak 2012c](#) and [Xu & Lazarian 2016](#)) and numerically confirmed in a conclusive fashion by [Cho *et al.* \(2009\)](#) and [Beresnyak \(2012c\)](#) that, once the dynamo goes nonlinear, the field will continue to be amplified, but by ever larger-scale motions that are, at a given time, just as energetic as the field.⁶⁰ That is, the scale $\ell(t)$ of the motions amplifying the field at any given time in its evolution is set by the condition

$$\delta u_{\ell(t)} \sim B_{\lambda}(t). \quad (12.5)$$

This leads, neatly, to a self-similar amplification regime:

$$\frac{dB_{\lambda}^2}{dt} \sim \frac{\delta u_{\ell}}{\ell} B_{\lambda}^2 \sim \frac{\delta u_{\ell}^3}{\ell} \sim \varepsilon \quad \Rightarrow \quad B_{\lambda}(t) \sim (\varepsilon t)^{1/2}, \quad \ell(t) \sim \varepsilon^{1/2} t^{3/2}. \quad (12.6)$$

After one outer-scale eddy-turnover time, $t \sim L/\delta u_L$, the field’s energy becomes comparable to that of the flow, $B_{\lambda} \sim \delta u_L$, and the dynamo saturates. At any time during the self-similar growth, the cascade below ℓ presumably looks just like the cascade in the saturated state, whereas above ℓ , the turbulence is still hydrodynamic.

12.3.3. Reconnecting Dynamo: Universality Regained

[Schekochihin *et al.* \(2002, 2004\)](#) calculated the field-reversal scale λ in the self-similar and saturated dynamo regimes by balancing $\delta u_{\ell}/\ell$ with the Ohmic-dissipation rate η/λ^2 . We now know, thanks to the argument in § 12.3.1 (obvious in retrospect!), that the folds generated by this process will in fact tear faster than they diffuse. So let me therefore balance the tearing rate (12.3) with $\delta u_{\ell}/\ell$ and obtain a scale familiar from the “ideal-tearing” condition (C 56) ([Pucci & Velli 2014](#); [Tenerani *et al.* 2015a](#)):

$$\lambda(\ell) \sim \ell \text{Rm}_{\ell}^{-1/3} (1 + \text{Pm})^{-1/6} \sim \varepsilon^{-1/9} \ell^{5/9} \eta^{1/3} (1 + \text{Pm})^{-1/6}. \quad (12.7)$$

In order for tearing to supersede Ohmic diffusion, we must have⁶¹

$$\lambda(\ell) \gg \lambda_{\eta}(\ell) \quad \Leftrightarrow \quad \widetilde{\text{Re}}_{\ell}^{1/6} \gg 1, \quad (12.8)$$

where $\lambda_{\eta}(\ell)$ was taken from (12.2). Note that $\lambda \ll \ell$ always, except, for low Pm, at the start of the self-similar regime, when $\text{Rm}_{\ell} \sim 1$ (this seems to suggest that even a low-Pm dynamo may form reconnecting folds in the nonlinear regime).

Let us imagine for now that that the self-similar evolution (12.6) has run its course and the dynamo has saturated in a state where the only motions that are responsible for (re)generation of the folds are on the outer scale, viz., $\ell \sim L$, while the motions below

⁶⁰There is a nice direct demonstration of that in the paper by [Brandenburg & Rempel \(2019\)](#), who measure the energy transfer from the velocity to the magnetic field and show that the sign of this transfer reverses at a scale that increases with time: the eddies above that scale act as a dynamo, while below that scale, the dynamo-generated fields drive some secondary flows, which then dissipate viscously. Analogous conclusions, by analogous means, were reached by [Bian & Aluie \(2019\)](#), [St-Onge *et al.* \(2020\)](#), and [Grete *et al.* \(2020\)](#).

⁶¹This condition means that the “Stokes” ($\text{Re} \lesssim 1$) simulations of [Kinney *et al.* \(2000\)](#) and [Schekochihin *et al.* \(2004\)](#) could not have captured this effect. In the simulations of [Iskakov & Schekochihin \(2008\)](#) and [Beresnyak \(2012b\)](#), one can see very clearly that when Pm is increased, which, at finite resolution, has to happen at the expense of Re, the magnetic folds become ever smoother and plasmoids/fold corrugations ever fewer, until they disappear entirely. Interestingly, at a given Re, larger values of Pm appear to promote the break up of the folds—perhaps because their aspect ratio λ/ℓ is, according to (12.7), larger when Pm is larger, and so is the number of islands (12.10) produced by the fastest-growing tearing mode.

this scale no longer affect the magnetic field (I will relax this assumption in §12.4.1). The reversal scale of the folds is then set by (12.7) with $\ell \sim L$. I shall call it

$$\lambda_R = \lambda(L) \sim L \text{Rm}_L^{-1/3} (1 + \text{Pm})^{-1/6}. \quad (12.9)$$

Consider a reconnecting fold of length L and width λ_R . Its tearing will produce islands whose number can be inferred from (7.4):

$$N \sim k_* L \sim \frac{L}{\lambda_R} S_{\lambda_R}^{-1/4} (1 + \text{Pm})^{1/8} \sim \text{Rm}_L^{1/6} (1 + \text{Pm})^{1/3}. \quad (12.10)$$

Just as I did at the end of §7.1, I can argue here that these islands will grow, circularise and turn into plasmoids (flux ropes) of diameter λ_R . Similarly to §7.2, I can entertain the possibility that they are the outer-scale structures of a new turbulent cascade, seeded by the reconnecting fold at the scale λ_R . At scales below λ_R , this new cascade is of the usual RMHD kind considered in §§5–7—the mean field now is B_{λ_R} , assuming that fields that make up the folds are unlikely to be exactly anti-parallel and so there is some component of the folded field, generally of the same order as its reversing component, pointing in the direction perpendicular both to the latter and to the direction of reversal.⁶²

Let the flux rope have a circulation velocity δu_{λ_R} and a perturbed field $\delta b_{\lambda_R} \sim \delta u_{\lambda_R}$. One can estimate these quantities by the same logic as led to (7.9): if this new cascade is to carry (a finite fraction of) the same energy flux as produced the fold,⁶³ then

$$\frac{\delta u_{\lambda_R}^3}{\lambda_R} \sim \varepsilon \quad \Rightarrow \quad \delta u_{\lambda_R} \sim (\varepsilon \lambda_R)^{1/3} \sim \delta u_L \left(\frac{\lambda_R}{L} \right)^{1/3} \sim \delta u_L \text{Rm}_L^{-1/9} (1 + \text{Pm})^{-1/18} \sim \delta b_{\lambda_R}. \quad (12.11)$$

Finally, the length of the flux rope (its “parallel” scale) is set by critical balance: the scale over which coherence can be maintained by propagating information at the Alfvén speed $\sim B_{\lambda_R} \sim \delta u_L$ is

$$l_{\parallel} \sim \frac{B_{\lambda_R} \lambda_R}{\delta u_{\lambda_R}} \sim L^{1/3} \lambda_R^{2/3} \sim L \text{Rm}_L^{-2/9} (1 + \text{Pm})^{-1/9}. \quad (12.12)$$

Thus, we have got ourselves a critically balanced RMHD-type cascade, with $\delta u_L \sim B_{\lambda_R}$ being the Alfvén speed, λ_R given by (12.9) playing the role of λ_{CB} , l_{\parallel} given by (12.12) in the role of the parallel outer scale L_{\parallel} , and the outer-scale amplitude δu_{λ_R} given by (12.11). The RMHD ordering parameter for this cascade is, therefore,

$$\epsilon \sim \frac{\delta u_{\lambda_R}}{\delta u_L} \sim \frac{\lambda_R}{l_{\parallel}} \sim \text{Rm}_L^{-1/9} (1 + \text{Pm})^{-1/18} \ll 1, \quad (12.13)$$

not terribly small in any real-world situation, but perfectly legitimate in principle. The Reynolds number of this cascade can be large:

$$\widetilde{\text{Re}}_{\lambda_R} \sim \frac{\delta u_{\lambda_R} \lambda_R}{\nu + \eta} \sim \text{Rm}_L^{5/9} (1 + \text{Pm})^{-11/9} \gg 1 \quad \Leftrightarrow \quad \widetilde{\text{Re}}_L \gg (1 + \text{Pm})^{6/5}. \quad (12.14)$$

⁶²There is perhaps a whiff of evidence for this in Schekochihin *et al.* (2004), who found that $\langle |\mathbf{B} \cdot \mathbf{J}|^2 \rangle$ in the nonlinear regime of the dynamo had the same Rm scaling as $\langle |\mathbf{B} \times \mathbf{J}|^2 \rangle$, where $\mathbf{J} = \nabla \times \mathbf{B}$. Precisely anti-parallel fields would have had $\mathbf{B} \cdot \mathbf{J} = 0$.

⁶³I am assuming here that reconnection, while destroying the folds, does not dissipate a significant amount of energy directly: the role of resistivity in the process of tearing is to break magnetic field lines, not to remove magnetic energy. This is not necessarily obvious, but is perhaps backed up by the following unsurprising estimate of the fraction of energy dissipated by resistivity in magnetic structures of width λ_R : $\varepsilon_{\lambda_R} / \varepsilon \sim \eta B_{\lambda_R}^2 / \lambda^2 \varepsilon \sim (L / \lambda_R)^2 \text{Rm}_L^{-1} \sim \widetilde{\text{Re}}_L^{-1/3} \ll 1$ (cf. footnote 33).

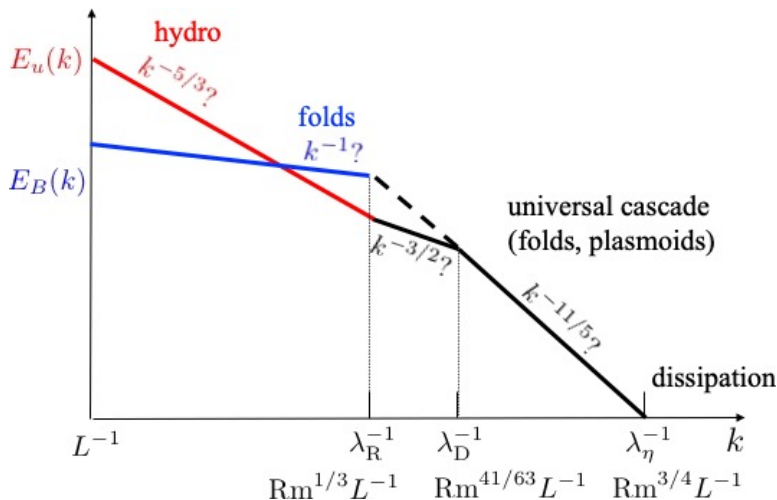


FIGURE 32. Spectrum of isotropic MHD turbulence, which is the saturated state of small-scale dynamo. The universal cascade below the fold-reversal scale λ_R [see (12.9)] is described in § 12.3.3; the various options for the spectrum at $k\lambda_R < 1$ are discussed in § 12.4. The disruption (λ_D) and dissipation (λ_η) scales are given by (12.15) and (12.16), respectively. Whether the $k^{-11/5}$ spectrum starts at λ_R (§ 12.4.1) or at λ_D (§ 12.3.3) is not obvious because how the spectra at scales below and above λ_R are connected remains an open question.

The latter condition might not always be satisfied when $\text{Pm} \gg 1$, but again is a perfectly legitimate limit. When it is *not* satisfied, the motions produced by the tearing of the folds will be quickly dissipated by viscosity and thus cannot seed a proper cascade; one option then is to invoke § 12.4.1 to deal with the sub- λ_R structure.

The RMHD cascade seeded by the production of flux ropes in reconnecting folds, as just described, will do what an RMHD cascade does: push energy to smaller scales, become aligned and be eventually disrupted by tearing. The arguments of § 7.2 apply: a succession of mini-cascades will be seeded, etc., as per figure 14. One expects a $k^{-3/2}$ spectrum (6.23) down to the disruption scale set by (7.2), viz.,

$$\lambda_D \sim \lambda_R \text{Rm}_{\lambda_R}^{-4/7} (1 + \text{Pm})^{-2/7} \sim L \text{Rm}_L^{-41/63} (1 + \text{Pm})^{-41/126}. \quad (12.15)$$

Below this scale, the mini-cascades will have a $k^{-11/5}$ spectral envelope described by (7.16) (figure 32). The final resistive cut-off is then determined by (7.13):

$$\lambda_\eta \sim \lambda_R \widetilde{\text{Re}}_{\lambda_R}^{-3/4} \sim \lambda_R \text{Rm}_L^{-5/12} (1 + \text{Pm})^{11/12} \sim L \widetilde{\text{Re}}_L^{-3/4}, \quad (12.16)$$

the Kolmogorov scale again—reassuringly, some things in the world never change.

Thus, turbulence in the saturated state of dynamo is, at scales below λ_R , likely to be similar to the tearing-mediated turbulence of § 7.2, the only difference being that the direction of the “local mean field” will be fluctuating strongly and all the statistics will be isotropic overall (although certainly not isotropic with respect to this fluctuating local mean field, as indeed spotted by Beresnyak & Lazarian 2009a).

This argument might be another example of a prediction of a tearing-mediated cascade that is unlikely to become falsifiable, either numerically or observationally, any time soon (if this new scheme is right, the state-of-the-art numerical spectra shown in figure 31 would have to describe a still non-asymptotic situation, perhaps only just starting to capture reconnection in the folds). This said, an aesthetically pleasing conclusion from

it is that universality is regained at small scales: even without the crutch of the mean field, MHD turbulence manages to turn itself into RMHD (Alfvénic) turbulence, at least in local patches where it is seeded by reconnecting folds.

The question still remains as to what happens in the scale range $[\lambda_R, L]$ and, most importantly, whether there is some further step in nonlinear evolution that is able to bring magnetic energy from λ_R to L . The short answer is that I do not know—but I am able to offer some speculations about plausible scenarios. Section 12.4 presents a menu of these—note that they are not necessarily all mutually exclusive and may coexist in a saturated dynamo state, perhaps in different spatial patches or at different times.

12.4. Saturation Scenarios

Wenn es aber Wirklichkeitssinn gibt, und niemand wird bezweifeln, daß er seine Daseinsberichtigung hat, dann muß es auch etwas geben, das man Möglichkeitssinn nennen kann. Wer ihn besitzt, sagt beispielweise nicht: Hier ist dies oder das geschehet, wird geschehen, muß geschehen; sondern er erfindet: Hier könnte, sollte oder müßte geschehen; und wenn man ihm von irgend etwas erklärt, daß es so sei, wie es sei, dann denkt er: Nun, es könnte wahrscheinlich auch anders sein. So ließe sich der Möglichkeitssinn geradezu als die Fähigkeit definieren, alles, was ebensogut sein könnte, zu denken und das, was ist, nicht wichtiger zu nehmen als das, was nicht ist. Man sieht, daß die Folgen solcher schöpferischen Anlage bemerkenswert sein können...

Robert Musil, *Der Mann ohne Eigenschaften*⁶⁴

12.4.1. Multiscale Folds?

In § 12.3.3, I assumed that in the saturated state, the only motions capable of stretching magnetic fields into folds were the outer-scale motions and that, consequently, all folds had length L and reversal scale $\lambda_R = \lambda(L)$ [see (12.7) and (12.9)]. Let me now relax this assumption and inquire what would happen if motions across some scale range $\ell < L$ produced different, independent folds. As I argued in § 12.3.2, the fields produced by any given motion cannot be stronger than this motion, so let us take a bold leap and guess that, for $\lambda < \lambda_R$,

$$B_\lambda \sim \delta u_{\ell(\lambda)} \sim [\varepsilon \ell(\lambda)]^{1/3} \sim \varepsilon^{2/5} \eta^{-1/5} (1 + \text{Pm})^{1/10} \lambda^{3/5}, \quad (12.17)$$

where $\ell(\lambda)$ is obtained by inverting the $\lambda(\ell)$ dependence (12.7). In a triumph of dimensional inevitability, this is just the same as the scaling (7.15), leading to the familiar $k^{-11/5}$ spectrum (7.16). One can now again fantasise about these folds breaking up into flux ropes as described by § 12.3.3, seeding mini-cascades similar to those produced by the successive disruptions of the RMHD cascade—those too have a $k^{-11/5}$ upper envelope,

⁶⁴ “But if there is a sense of reality,—and no one will doubt that it has every right to exist,—then there must also be something that one could call a sense of possibility. A person who possesses it does not, for example, say: here this or that has happened, will happen, must happen; no, he rather starts inventing: here might, should, or could happen something or other; and if he is explained about something that it is so and so, and how it is, then he thinks: well, it could have probably also been different. Thus, one may define the sense of possibility as the ability to perceive everything that can be, and not to attach more importance to what is than to what is not. It is evident that the consequences of such creative faculty can be quite remarkable...” —Robert Musil, *The Man Without Qualities*.

so perhaps this scaling emerges as an inevitable outcome at small scales of pretty much any scenario that involves resistivity.

Note that in the scheme leading to (12.17), interactions between velocities and magnetic fields are nonlocal in scale: velocities at scale ℓ interact with magnetic fields at scale $\lambda(\ell) \ll \ell$, and vice versa.⁶⁵ This nonlocality is more extreme than, e.g., Beresnyak (2012c) would have it, because λ/ℓ in (12.7) scales with Rm_ℓ and Pm , asymptotically large numbers (although it scales with quite modest fractional powers of them). Below λ_R , however, this nonlocality should get swamped by the local RMHD cascade proposed in §12.3.3.

Within the narrative advanced so far, there is no mechanism (absent mean-field dynamo) for magnetic structures at scales longer than λ_R to emerge dynamically, unless plasmoids/flux ropes coalesce very purposefully (see §12.4.3), or unless creation of folds is entirely stymied by very efficient stochastic reconnection of field lines, as, I expect, Eyink (2011) would argue (I cannot rule this out definitively without a clear dynamical picture of the turbulence in the presence of dynamically significant dynamo-generated fields;⁶⁶ stochastic reconnection is reviewed in appendix C.6). If we put these possibilities to one side, the magnetic spectrum at scales above λ_R should reflect the volume-filling properties of folds and the distribution of their reversal scales (all of this is certain to be highly intermittent). The simplest, probably too simple, guess is that it will be k^{-1} (Yousef *et al.* 2007), which follows if we assume that magnetic increments across any point separation $> \lambda_R$ will tend to have, in an averaged sense, the same value, roughly equal to the rms field B_{λ_R} , i.e., there is the same magnetic energy at every scale $\in [\lambda_R, L]$ (cf. §10.2).

This leaves us with the question of what velocities do in the interval $[\lambda_R, L]$. In (12.17), I blithely assumed that they continued to obey the Kolmogorov scaling (12.1). If this were true, that would connect nicely onto the flux-rope amplitude (12.11) (and hence onward to the universal tearing-mediated cascade). Admittedly, however, the justification for a Kolmogorov scaling in that case is difficult as (12.17) implies energy exchanges with the folds at smaller scales and thus undermines the assumption of a constant flux through the

⁶⁵It is easy to see how a large-scale flow directly produces small-scale fields (figure 28). Since the fields' *parallel* scale is ℓ , these formally smaller-scale fields can in turn exert ℓ -scale Lorentz forces: these are quadratic in the field, $\sim \mathbf{B} \cdot \nabla \mathbf{B}$, and do not know about direction reversals but do depend on the parallel scale (Schekochihin *et al.* 2004)—so they can fight back coherently against the ℓ -scale flow. This is, of course, only a heuristic argument and one could legitimately wonder if it might be simplistic and misleading. It might be, but not, it seems to me, for any of the reasons that have so far been aired in the literature. The most categorical statement of locality in MHD turbulence can be found in Aluie & Eyink (2010). Their proof depends on the assumption that both velocity and magnetic spectra have scaling exponents in the range $(-3, -1)$ —equivalently, that $\delta u_\lambda \propto \lambda^{\gamma^u}$ and $B_\lambda \propto \lambda^{\gamma^B}$ with $\gamma^u, \gamma^B \in (0, 1)$ (it is probably also true, conversely, that if interactions are local, the scaling exponents should be in this range). This makes sense because, in very simple terms, the contribution from field increments at a larger scale (Λ) to those at a smaller scale (λ) is $\delta u_{\Lambda \rightarrow \lambda} \sim \lambda \delta u_\Lambda / \Lambda \sim \delta u_\lambda (\lambda/\Lambda)^{1-\gamma} \ll \delta u_\lambda$ (provided $\gamma < 1$) and the contribution from the smaller-scale increments to the larger-scale ones is $\delta u_{\lambda \rightarrow \Lambda} \sim \delta u_\lambda \sim \delta u_\lambda (\lambda/\Lambda)^\gamma \ll \delta u_\Lambda$ (provided $\gamma > 0$). In RMHD turbulence, all this holds and interactions are indeed likely local (as I always assumed them to be in §§4–7). In the case of saturated dynamo, however, the unresolved issue is precisely whether velocity and magnetic field have scaling exponents $\in (0, 1)$ in the same range of scales—and also whether velocities at every scale are of the kind, dynamically, that can stretch magnetic fields at the same scale.

⁶⁶It may, however, be worth observing that, according to the numerical results reported by Busse *et al.* (2007), Lagrangian particles in MHD turbulence without a mean field tend to separate along the local field direction, rather than across it. An enthusiast of field-line folding might interpret this as an indication that stochastic reconnection fails to prevent fold creation.

scale range between L and λ_R . If the energy flux ε were depleted in favour of the folds at each scale ℓ on the same typical time scale $\ell/\delta u_\ell$ as the cascade of δu_ℓ proceeded, then δu_ℓ would have a steeper-than-Kolmogorov spectrum, leading, via a calculation analogous to (12.17), to a steeper-than- $k^{-11/5}$ spectrum of folds. This would mean that folds with reversal scales smaller than λ_R would get swamped by the tearing-mediated cascade originating from the longest, λ_R -scale folds, and we would be back to the scenario described in § 12.3.3. Cho *et al.* (2009) and Beresnyak (2012*c*) report, however, that the fraction of the energy flux transferred into magnetic fields during the self-similar regime described in § 12.3.2 is numerically quite small—between 0.04 and 0.07.⁶⁷ This suggests that the steepening of the velocity spectrum compared to the Kolmogorov scaling might be very slight.

12.4.2. Magnetoelastic Turbulence?

Let us now explore what happens in the scale interval $[\lambda_R, L]$ if we abandon (12.17) and return to the scenario in which the velocity field at the outer scale L constantly passes a certain fraction of the injected power ε to the folds with reversals at λ_R and hence into the tearing-mediated cascade, while the rest of the injected power goes into some motions on scales $[\lambda_R, L]$ that do not exchange energy with that cascade, i.e., do not stretch the field or cause it to develop sub- λ_R structure. What kind of motions can these be?

In search of the answer to this question, I wish to resurrect the old idea (Moffatt 1986; Gruzinov & Diamond 1996; Chandran 1997; Schekochihin *et al.* 2002; Maron *et al.* 2004) that a tangled mess of small-scale magnetic fields provides an elastic background through

⁶⁷Xu & Lazarian (2016) derive this number quite precisely from a theory containing adjustable constants of order unity. Putting aside this bold quantitative claim, here might be an opportune place to comment on the qualitative dynamo-evolution scenario that they have proposed (recently reviewed and put to some astrophysical use by McKee *et al.* 2020). They believe that, once the magnetic energy has grown to be comparable to the energy of the viscous-scale eddies ($B_{\lambda_\eta} \sim \delta u_{\ell_\nu}$; cf. § 12.3.1), its spectrum will embark on a rearrangement exercise in which its peak moves to the viscous scale while the overall magnetic energy stays constant (I will discuss in a moment why this is dubious). Once it reaches the viscous scale, a self-similar secular regime follows, of the kind described in § 12.3.2, except the scale of B_λ is now the same as the scale of the motions that are performing the dynamo action, $\lambda \sim \ell(t)$, whereas below that scale, a GS95-type turbulent cascade forms, with $B_{\ell(t)}$ playing the role of the mean field. As time advances, $\ell(t) \rightarrow L$, and the dynamo saturates with scale-by-scale equipartitioned $k^{-5/3}$ magnetic and velocity spectra, just like everyone since Biermann & Schlüter (1951) has always wanted it to do. This pleasing outcome depends on the assumption, unproven, but not in principle impossible, that fast stochastic reconnection (discussed in appendix C.6) will always provide just enough turbulent magnetic diffusivity to prevent the dynamo-generated field from organising into folds with reversals at scales much below $\ell(t)$. Even if this proved true, the Xu & Lazarian (2016) scenario still needs the earlier transitional stage during which the magnetic energy moves from the resistive to the viscous scale. I do not think their justification for such a stage is satisfactory. They interpret the magnetic field associated with each wavenumber as an independent dynamical entity and argue that, since the spectrum of these fields is $\propto k^{3/2}$ at $k \ll \lambda_\eta^{-1}$ (Kazantsev 1968; Kulsrud & Anderson 1992), the modes with $k \ll \lambda_\eta^{-1}$ can continue being amplified by the viscous-scale motions after those with $k \sim \lambda_\eta^{-1}$ have reached energetic equipartition with those motions—if the overall magnetic energy is assumed to stay constant, this then leads to a gradual “overturning” of the spectrum and shifts its peak towards the viscous scale. However, the $k^{3/2}$ spectrum is not a superposition of independent structures—rather, it is a Fourier-space representation of the folded field, so it is, in my view, not possible to talk about different k modes interacting independently with the flow. Thus, the Xu & Lazarian (2016) scenario, while attractive if true, remains at least as much of a speculation—and, in my view, an unconvincing one—as anything my exasperated reader will find elsewhere in this section.

which larger-scale Alfvén waves can propagate isotropically. The relevant calculation is straightforward. Consider the equations of incompressible MHD without a mean field:

$$\partial_t u_i + u_j \partial_j u_i = -\partial_i p + \partial_j M_{ij}, \quad (12.18)$$

$$\partial_t B_i + u_n \partial_n B_i = B_n \partial_n u_i, \quad (12.19)$$

where the equation for pressure p is $\partial_i u_i = 0$ and $M_{ij} = B_i B_j$ is the Maxwell stress tensor (the magnetic field is in velocity units). We can recast the induction equation in terms of M_{ij} and forget about B_i :

$$\partial_t M_{ij} + u_n \partial_n M_{ij} = M_{nj} \partial_n u_i + M_{in} \partial_n u_j. \quad (12.20)$$

The information about magnetic fields' reversals is now hidden away and only their ability to exert Lorentz force, quadratic in B_i , is retained. Let us expand the flows and the Maxwell stresses around a time- and space-averaged state:

$$\langle u_i \rangle = 0, \quad \langle M_{ij} \rangle = v_A^2 \delta_{ij}, \quad v_A^2 = \frac{1}{3} \langle B^2 \rangle, \quad M_{ij} = \langle M_{ij} \rangle + \delta M_{ij}. \quad (12.21)$$

Linearising (12.18) and (12.20) around this “equilibrium” filled with tangled fields, we get isotropically propagating Alfvén waves whose dispersion relation and eigenvector are⁶⁸

$$\omega^2 = k^2 v_A^2, \quad \delta M_{ij} = v_A^2 (\partial_i \xi_j + \partial_j \xi_i), \quad (12.22)$$

where ξ_i is the displacement ($\partial_t \xi_i = u_i$). These can be dubbed magnetoelastic waves to highlight the formal mathematical (Ogilvie & Proctor 2003) and obvious physical analogy between a magnetised plasma and certain types of polymeric fluids. Admittedly, this analogy between magnetic field lines and polymer strands moving with the fluid and elastically back-reacting on it becomes precarious if one looks beyond the ideal description: there is no such thing as “antiparallel” polymers strands, and so there is no reconnection. It is not obvious whether fast reconnection of field lines can foil their ability to make plasma an elastic medium: do tangled fields spring back when pushed at or just reconnect quickly to accommodate the push? Here, I shall assume that they do spring back and explore the consequences.

One of the consequences appears to be a surprising return of the IK turbulence (§ 2.2), which I have so far thoroughly dismissed—perhaps an indication that a clever idea, however wrong, never goes to waste. The reason that the IK scheme was wrong in the presence of a strong mean magnetic field was that Alfvén waves could not be legitimately expected to run around isotropically at small scales. Well, according to (12.22), the magnetoelastic waves do run around isotropically, and so the IK theory is back in business. While Kraichnan’s dimensional argument leading to (2.5) may or may not be compelling, the version of the IK theory outlined in footnote 4 is perhaps sensible. Indeed, whereas at the outer scale L , the nonlinear time $\tau_{nl} \sim L/\delta u_L$ and the Alfvén time $\tau_A \sim L/v_A$ are certainly comparable (because $\langle B^2 \rangle \sim \delta u_L^2$ for saturated dynamo), the former will shorten less quickly than the latter at smaller scales ($\tau_A \propto \ell$, while $\tau_{nl} \propto$ a fractional power of ℓ). Thus, at scales $\ell \ll L$, the magnetoelastic turbulence might be expected to be weak. The cascade time is then worked out from the random-walk

⁶⁸Schekochihin *et al.* (2002) argued that if the small-scale magnetic fields were organised in long-scale folds, these Alfvén waves would propagate as a kind of ripple along these folds, thus making them locally anisotropic. Mathematically, this led to the disappearance of the factor of $1/3$ in v_A^2 , because the tensor of magnetic-field directions $B_i B_j / B^2$ was a long-scale object. Since, however, I now propose that the folds will break up into flux ropes, etc., it seems more logical to think of the resulting magnetic tangle as an isotropic mess, at least from the point of view of long-scale perturbations.

argument (4.5), and the spectrum follows from the constancy of flux:

$$\tau_c \sim \frac{\tau_{nl}^2}{\tau_A} \sim \frac{\ell v_A}{\delta u_\ell^2}, \quad \frac{\delta u_\ell^2}{\tau_c} \sim \varepsilon \quad \Rightarrow \quad \delta u_\ell \sim (\varepsilon v_A \ell)^{1/4} \quad \Leftrightarrow \quad E(k) \sim (\varepsilon v_A)^{1/2} k^{-3/2}. \quad (12.23)$$

Presumably, this cascade terminates when it hits the scale λ_R , where the scale separation between the magnetoelastic waves and the magnetic fields associated with the tearing-mediated cascade of § 12.3.3 breaks down.

There is some numerical evidence in favour of an isotropic $k^{-3/2}$ spectrum of perturbations with a sound-like isotropic dispersion relation $\omega \propto k$ —the MHD fast (magnetoacoustic) waves: see [Cho & Lazarian \(2002, 2003\)](#) (who were inspired by this scaling having been derived for weak turbulence of sound waves by [Zakharov & Sagdeev 1970](#); a later study by [Kowal & Lazarian 2010](#) appears to be less certain about the scaling exponent). One might have thought that some evidence as to how much of a fiction, or otherwise, the spectrum (12.23) might be in an elastic medium could be found in simulations of polymer-laden turbulence. Surprisingly, the state of the art in this area features much smaller resolutions than in MHD. The most recent relevant numerical paper appears to be [Valente *et al.* \(2016\)](#), see references therein for earlier studies). They record significant nonlinear energy transfer in the inertial range from the motions of the solvent fluid to the elastic polymer admixture and back; they also see spectra that they report as consistent with $k^{-5/3}$, although their resolution would not have been sufficient to distinguish between that and $k^{-3/2}$. They do not appear to be aware of, or interested in, the possibility of elastic waves. In contrast, [Balkovsky *et al.* \(2001\)](#) and [Fouxon & Lebedev \(2003\)](#) are fully aware of it, as well as of the MHD analogy with Alfvén waves. They have a theory of turbulence of these waves at scales where elasticity is important, below the so-called [Lumley \(1969\)](#) scale (this is set by the balance between the turbulent rate of strain and the polymer relaxation time, a quantity without a clear MHD analogue because magnetic field lines have no interest in curling up the way polymers do, entropically; in our problem, the corresponding scale should be the outer scale L). They think that in this scale range, the waves will be nonlocally advected by the Lumley-scale motions, resulting in spectra steeper than k^{-3} because otherwise the nonlocality assumption fails. I do not see why such an assumption should hold, either for polymer-laden turbulence or in MHD. Finally, it is worth mentioning the recent paper by [Varshney & Steinberg \(2019\)](#), who have, for the first time, it seems, managed to excite and measure elastic waves experimentally.

Whether the magnetoelastic cascade (12.23), or even the magnetoelastic waves, actually exist in MHD turbulence remains an open question. [Hosking *et al.* \(2020\)](#) have shown numerically that magnetoelastic waves do exist in certain tangled, force-free magnetic configurations, and are well described by (12.22) (there are some further nuances that can mean that v_A is somewhat reduced for tangled fields that are spatially intermittent). What is still unknown is whether they can propagate against the background of a saturated dynamo state or, rather, are quickly damped by small-scale motions and thus rendered irrelevant.

12.4.3. Inverse Magnetic-Energy Transfer via Sporadic Decay?

Let me now turn to what has been the central question of small-scale-dynamo theory since the founding papers of [Batchelor \(1950\)](#) and [Biermann & Schlüter \(1951\)](#): will magnetic energy get stuck at small scales [in my current scheme, at the reversal scale λ_R given by (12.9)] or will it make its way to the outer scale L ? The latter would be everyone's preferred outcome: astrophysicists could then have their cosmic magnetic fields at the

scales where they are observed to be,⁶⁹ while theoretical physicists could stop worrying about no-mean-field vs. strong-mean-field MHD upsetting their universalist dream by exhibiting different kinds of turbulence—the fluctuating field at L would just be the effective mean field in the inertial range, as Kraichnan (1965) prophesied.

As I already said in §§ 12.1 and 12.2, a definitive demonstration of an inverse cascade in forced, isotropic MHD turbulence has remained elusive, leaving space for disagreement over how to interpret insufficiently asymptotic simulations. An interesting recent development, however, came from simulations of *decaying* MHD turbulence without a mean field: as I already mentioned in § 11.4, Zrake (2014) and Brandenburg *et al.* (2015) discovered numerically that such a turbulence, even without net helicity, could support a certain amount of inverse transfer of magnetic energy from small to large scales (as indeed was expected theoretically: see § 11.6). The existence of such an inverse transfer (or inverse cascade) in the case of non-zero net helicity is well known and well simulated (see § 11.3), but is not relevant here because it is just a nonlinear counterpart of the helical mean-field dynamo, a topic reviewing which I leave to Rincon (2019). In the absence of net helicity, there is not necessarily an inverse *cascade*, because the net energy transfer might still be direct, and because there is no second invariant to cascade inversely, but large-scale magnetic fields can still be generated. What is the dynamical mechanism by which they are generated? In § 11.4, I discussed the recent proposal by Zhou *et al.* (2020) and Bhat *et al.* (2020) that they form by merger of reconnecting flux ropes.

Let me explore what would happen if the same mechanism were to apply locally to the magnetic structures at the reversal scale λ_R , which *are* flux ropes (plasmoids). Imagine that, instead of being continuously forced everywhere, our saturated dynamo were to be left alone for a period of time (and/or in a region of space)—this could be due to the natural spatio-temporal intermittency of the system or to a method of forcing leading to sporadic energy-injection events with quiescent periods of decaying turbulence in between (e.g., in galaxy clusters: Roh *et al.* 2019). With the arrival of each quiescent period, mergers between the flux ropes should push magnetic energy to larger scales.

The salient bit of theory that is needed to assess this effect is the law of evolution of the magnetic-energy-containing scale with time during the decay of the turbulence. As argued in §§ 11.3–11.6, it is $\propto t^{1/2}$ in virtually all conceivable circumstances. Thus, if the field starts at scale λ_R , its scale after a period of decay will be

$$\lambda_B \sim \lambda_R \left(\frac{t}{t_0} \right)^{1/2}, \quad t_0 \sim \epsilon_{\text{rec}}^{-1} \frac{\lambda_R}{\delta b_{\lambda_R}} \sim \epsilon_{\text{rec}}^{-1} \left(\frac{\lambda_R}{L} \right)^{2/3} \frac{L}{\delta u_L}, \quad (12.24)$$

where t_0 is the characteristic reconnection time (11.11) for the initial flux tubes, whose scale is λ_R given by (12.9) and whose amplitude is δb_{λ_R} given by (12.11). Two relevant questions may now be answered.

First, suppose the decay is allowed to proceed for about one outer-scale turnover time $L/\delta u_L$, what will be the magnetic field’s scale after that? Answer:

$$\lambda_B \sim \epsilon_{\text{rec}}^{1/2} L^{1/3} \lambda_R^{2/3} \sim L \epsilon_{\text{rec}}^{1/2} \text{Rm}_L^{-2/9} (1 + \text{Pm})^{-1/9}, \quad (12.25)$$

⁶⁹See Vacca *et al.* (2018) and references therein for magnetic fields in clusters of galaxies and beyond. Interestingly, laboratory dynamo, achieved in a laser plasma, also appears to have its magnetic energy at the outer scale, in contradiction with MHD simulations of the same experiment (Tzeferacos *et al.* 2018; Bott *et al.* 2020). The most recent theoretical scenario that puts magnetic field at the outer scale is by Xu & Lazarian (2016), critiqued in the extended footnote 67.

where the dimensionless reconnection rate is (see appendices C.3.1 and C.5)

$$\epsilon_{\text{rec}} \sim \frac{\max\{\tilde{S}_{\lambda_R}^{-1/2}, \tilde{S}_c^{-1/2}\}}{(1 + \text{Pm})^{1/2}} \sim \frac{\max\{\text{Rm}_L^{-5/18}(1 + \text{Pm})^{1/4}, \tilde{S}_c^{-1/2}\}}{(1 + \text{Pm})^{1/2}}, \quad (12.26)$$

or, optimistically, $\epsilon_{\text{rec}} \sim 1$ if reconnection is fully stochastic (appendix C.6). One immediate consequence is that if reconnection is in the Sweet–Parker regime, there will be no effect at all, as the above scalings give $\lambda_B \ll \lambda_R$ for $\text{Rm}_L \gg 1$. If reconnection is fast, (12.25) has a slightly weaker Rm_L scaling than λ_R , but it is not a triumph of inverse transfer.

Secondly, one may ask how long a decay it would take to get the magnetic field to the outer scale, $\lambda_R \sim L$. The answer is

$$t \sim t_0 \left(\frac{L}{\lambda_R} \right)^2 \sim \frac{L}{\delta u_L} \epsilon_{\text{rec}}^{-1} \text{Rm}_L^{4/9} (1 + \text{Pm})^{2/9}, \quad (12.27)$$

quite a long time, as expected, i.e., the forcing would have to be very sporadic to achieve this.

All this does not amount to much more than an initial “back-of-the-envelope” assessment, but, if even roughly adequate, suggests that inverse transfer achievable in a decaying regime is not a very promising route to large-scale fields.

12.4.4. Local Shear Dynamo?

Let me complete my catalogue of speculations regarding the structure of the saturated dynamo state by invoking another piece of dynamo physics that, despite being of potentially fundamental and ubiquitous nature, has emerged relatively late in the game. A combination of small-scale turbulence and a large-scale shear generically leads to the emergence of large-scale magnetic field, even when the turbulence has no net helicity—an effect known as the “shear dynamo”. This was mooted theoretically in several early mean-field dynamo schemes and then confirmed numerically by Yousef *et al.* (2008*b,a*) (see references therein for the precursor theories, numerics and counter-arguments). This result turned out to be due to a form of “stochastic α effect” (Heinemann *et al.* 2011; Jingade *et al.* 2018), depending, therefore, on fluctuating helicity in the flow. Interestingly, the shear dynamo turned out to work also when the small-scale turbulence was magnetic, i.e., by the combination of a large-scale shear and the saturated state of small-scale dynamo (Yousef *et al.* 2008*a*). More recently, Squire & Bhattacharjee (2015, 2016) made sense of that by discovering semi-analytically the “magnetic shear-current effect” and showing that small-scale magnetic fields were actively helpful in enabling the shear dynamo.

The outcome of §12.3.3 was a situation in which outer-scale (L) field-stretching motions (plus possibly some sort of kinetic-energy cascade to smaller scales) coexisted with MHD turbulence produced by the break up of the folds, with an effective outer scale $\lambda_R \ll L$ [see (12.9)]. It seems to be an attractive speculation that the combination of this turbulence with the local shears associated with the “hydrodynamic” scales $> \lambda_R$ might act as a local shear dynamo and create “local mean fields” on scales $> \lambda_R$. It would be interesting to investigate whether such a mechanism exists and, if it does, whether it can push the magnetic-energy-containing scale closer to L —finally making it independent of Rm .

To conclude, there are plenty of potential theories—far too many, so no convincing one theory yet. Hero numerics reaching for asymptoticity, and intelligently analysed, might

help pair down this field and finally give our understanding of the saturated MHD dynamo a modicum of completeness to match what has been achieved for MHD turbulence with a mean field.

13. Next Frontier: Kinetic Turbulence

We can measure the globula of matter and the distances between them, but Space plasm itself is incomputable.

Vladimir Nabokov, *Ada, or Ardor*

13.1. Sundry Microphysics at Low Collisionality

I ended the first part of this review with a proclamation in § 7.4 that the story of MHD turbulence looked reasonably complete (before spending five chapters on the loose ends!). Since the main reason for this triumphalism was that MHD cascade finally made sense at the dissipation scales—and the key role in making it make sense belonged to reconnection, a dissipative phenomenon,—it is an inevitable complication that microphysics of dissipation may matter. The visco-resistive MHD description adopted above does apply to some natural plasmas, e.g., stellar convective zones or colder parts of accretion discs. These are mostly low-Pm environments. Whereas I have made an effort to keep all results general and applicable to the high-Pm limit, it is, in fact, quite hard to find naturally occurring high-Pm plasmas for which the standard visco-resistive MHD equations are a good model: this would require the particles' collision rate to be larger than their Larmor frequency, which rarely happens at high temperatures and low densities needed to achieve high Pm (one increasingly popular exception is some plasmas created in laser experiments: see, e.g., [Bott et al. 2020](#)). In fact, most of the interesting (and observed) plasmas in this hot, rarefied category are either “dilute” (an apt term coined by [Balbus 2004](#) to describe plasmas where turbulence is on scales larger than the mean free path, but the Larmor motion is on smaller scales than it—a good example is galaxy clusters; see, e.g., [Melville et al. 2016](#) and references therein) or downright collisionless (i.e., everything happens on scales smaller than the mean free path; the most obvious example is the solar wind: see the mega-review by [Bruno & Carbone 2013](#) or a human-sized one by [Chen 2016](#)). In either case, between the “ideal-MHD scales” and the resistive scale, there is a number of other scales at which the physics changes. These changes are of two distinct kinds.

The first is the appearance of dispersion in the wave physics: Alfvén waves become kinetic Alfvén waves (KAWs), with a different linear response and, therefore, a different variety of critically balanced cascade ([Cho & Lazarian 2004](#); [Schekochihin et al. 2009, 2019](#); [Boldyrev & Perez 2012](#); [Boldyrev et al. 2013](#); [Chen & Boldyrev 2017](#); [Passot et al. 2017](#)). The culprits here are the ion inertial scale (at which the Hall effect comes in), the ion sound scale (at which the electron-pressure-gradient force becomes important in Ohm's law), and the ion Larmor scale (at which the finite size of ion Larmor orbits starts playing a role). Which of these matters most depends on plasma beta and on the ratio of the ion and electron temperatures, but they all are essentially ion-electron decoupling effects and lead to more or less similar kinds of turbulence, at least in what concerns the KAW cascade. Note that the subviscous regime (§ 10) is, of course, irrelevant for such plasmas—except possibly, in a somewhat exotic way, at high beta ([Kawazura et al. 2019](#)).

The second important modification of MHD is that reconnection in a collisionless plasma need not be done by resistivity, but can be due to other physics that breaks flux conservation, viz., electron inertia, electron finite Larmor radius (FLR) and, more

generally, other kinetic features of the electron pressure tensor. Tearing modes are different in such plasmas, with a double ion-electron layer structure and a variety of scalings in a variety of parameter regimes.⁷⁰ Since tearing is important for rounding off the MHD cascade, all these effects must be considered and appropriate modifications worked out for the theory of tearing-mediated turbulence described in §7—this has been done by Mallet *et al.* (2017a) and by Loureiro & Boldyrev (2017a). It is going to be interesting to find out whether, where, and when any of this matters or if perhaps the aligned MHD cascade just segues directly into the KAW cascade (see, however, a discussion in a moment as to what that means). Since there are some mysteries still outstanding with regard to the scale at which the spectrum of solar-wind turbulence has a spectral break between the inertial range and the “kinetic” (KAW) range (Chen *et al.* 2014a; Boldyrev *et al.* 2015), perhaps something interesting can be done here (e.g., is the break set by onset of reconnection, rather than by the Larmor scale?—see Vech *et al.* 2018).

Furthermore, KAW turbulence in the kinetic range and *its* relationship with reconnection is a topic that is rapidly becoming very popular with both numerical modellers (e.g., TenBarge & Howes 2013; Bañón Navarro *et al.* 2016; Cerri & Califano 2017; Franci *et al.* 2017, 2018) and observational space physicists (e.g., Greco *et al.* 2016). There is a promise of interesting physics—interesting both conceptually and because it is eminently measurable in space. In the context of the prominent role that was given in §7 to the break up of MHD sheets in setting up the tail end of the MHD cascade, I want to highlight an intriguing suggestion (implicitly) contained in the paper by Cerri & Califano (2017) and further fleshed out by Franci *et al.* (2017). They look (numerically) at the formation of current sheets in kinetic turbulence and the disruption of these sheets by tearing (plasmoid) instabilities—and discover that it is precisely these processes that appear to seed the sub-Larmor-scale cascade with a steep (steeper than in the inertial range) energy spectrum usually associated with KAW turbulence. One might wonder then if such a KAW cascade is an entirely distinct phenomenon from a collisionless version of tearing-mediated turbulence in the disruption range. If we allow ourselves to get excited about this question, we might speculate that it rhymes nicely with the idea on which Boldyrev & Perez (2012) relied to advocate a steeper ($-8/3$) slope of KAW turbulence than the $-7/3$ implied by the standard CB-based theory (Cho & Lazarian 2004; Schekochihin *et al.* 2009). They argued that the energetically dominant perturbations at each scale were concentrated in 2D structures, thus making turbulence non-volume-filling (and perhaps monofractal; cf. Kiyani *et al.* 2009 and Chen *et al.* 2014b). While Boldyrev & Perez (2012) did not appear to think of these 2D structures as reconnecting sheets, an interpretation of them as such does not seem *a priori* unreasonable. So perhaps this is what happens in collisionless turbulence: sheet-like structures form in the usual (MHD) way, get disrupted by collisionless tearing and/or related instabilities and seed sub-Larmor turbulence,⁷¹ which stays mostly concentrated in those sheets or their remnants, with an effectively 2D filling fraction. Another possibility—or a version of this scheme—is to abandon the

⁷⁰Appendix B.3 of Zocco & Schekochihin (2011) has a review of standard results for collisionless and semicollisional tearing modes at low beta (using a convenient minimalist set of dynamical equations as a vehicle), as well as all the relevant references of which we were aware at the time. There is a huge literature on semicollisional and collisionless reconnection and, short of dedicating this review to name-checking it all (which would be a noble ambition, but a doomed one, as the literature is multiplying faster than one can keep track), I cannot give proper credit to everyone who deserves it. A useful recent treatment of electron-only tearing done with applications to space turbulence in mind is Mallet (2020).

⁷¹See Mallet *et al.* (2017a) for a discussion of what else they seed.

old KAW cascade altogether and declare sub-Larmor turbulence to be entirely controlled by (collisionless) tearing in a similar way to the tearing-mediated cascade of §7.2, with spectral slopes between -3 and $-8/3$, still consistent with observations and simulations (Loureiro & Boldyrev 2017a; Boldyrev & Loureiro 2019).

What I have said about kinetic physics so far might not sound like a true conceptual leap: basically, at small scales, we have different linear physics and a zoo of possibilities, depending on parameter regimes; one could work productively on porting some of the basic ideas developed in the preceding sections to these situations. There are, however, ways in which kinetic physics does bring in something altogether new. Three examples of that, chosen in a very biased way, are discussed in what follows.

13.2. Failed Cascades

FLR effects do not just change how linear waves propagate at sub-Larmor scales. They also change the nature of the second conserved quantity (the first being energy) possessed by the plasma: (R)MHD cross-helicity (imbalance) becomes magnetic helicity in the transition from the inertial to the sub-Larmor scale range. The trouble is that the KAW helicity is a quantity that naturally wants to cascade inversely, from small scales to large (Schekochihin *et al.* 2009; Cho 2011; Kim & Cho 2015; Cho & Kim 2016; Miloshevich *et al.* 2020). In low-beta plasmas, there is no dissipation at the Larmor scale, so an imbalanced cascade arriving from the inertial range would get thoroughly “confused” by the sudden need to reverse the direction of the helicity cascade. The result, it turns out, is a mighty blow back from the small scales to large and a failure to achieve a constant-flux steady state, at least within the RMHD approximation (Meyrand *et al.* 2020; some evidence of strange behaviour of energy fluxes in imbalanced solar-wind turbulence does appear to exist: see, e.g., Smith *et al.* 2009).

This means that in space or astrophysical environments where this applies (low beta, high Elsasser imbalance), we must either abandon the fluid approximation even at the outer scale or drop the assumption that we are observing a steady state with a constant flux—or both. This would be quite a change in attitude—in response to a rare example of plasma microphysics seriously upsetting system-scale macrophysics. Sadly, this renders §8 quite irrelevant for such plasmas.

13.3. Phase-Space Turbulence

What is turbulence? Some energy is injected into some part of the phase space of a nonlinear system (in fluid systems, that simply means position or wavenumber space), which is, generally speaking, not the part of the phase space where it can be efficiently thermalised. So turbulence is a process whereby this energy finds its way from where it is injected to where it can be dissipated, and its means of doing this is nonlinear coupling, usually from large to small scales (I am now putting to one side the upsetting example of the failure of this process discussed in §13.2). What kind of coupling is possible and at what rate the energy can be transferred from scale to scale then determines such things as energy spectra in a stationary state with a constant flux of energy.

The same principle applies to kinetic turbulence, but now the phase space is 6D rather than 3D: the particle distribution depends on positions and velocities, and energy transfer can be from large to small scales (or vice versa) in all six coordinates. The transfer of (free) energy to small scales in velocity space, leading ultimately to activation of collisions, however small the collision rate, is known as “phase mixing”. It is not always a nonlinear phenomenon: the simplest (although not necessarily very simple) phase-mixing process is the linear Landau (1946) damping. In a magnetised plasma, this is the *parallel* (to

\mathbf{B}_0) phase mixing, whereas the *perpendicular* phase mixing is nonlinear and has to do with particles on Larmor orbits experiencing different electromagnetic fields depending on the radius of the orbit (the Larmor radius is a kinetic variable, being proportional to v_\perp). The latter phenomenon leads to an interesting phase-space “entropy cascade” (Schekochihin *et al.* 2008, 2009; Tatsuno *et al.* 2009; Plunk *et al.* 2010; Cerri *et al.* 2018; Eyink 2018; Kawazura *et al.* 2019; cf. Pezzi *et al.* 2018), which is one of the more exotic phenomena that await a curious researcher at sub-Larmor scales. Its importance in the grand scheme of things is that it channels turbulent energy into ion heat, while the KAW cascade heats electrons—the question of which dissipation channel is the more important one, and when, being both fundamental and “applied” (in the astrophysical sense of the word—e.g., to accretion flows: see Quataert & Gruzinov 1999, Event Horizon Telescope Collaboration 2019). Understanding how energy is transferred between scales in phase space requires thinking somewhat outside the standard turbulence paradigm and so perhaps counts as conceptual novelty. Not much of it has been done so far and it is worth doing more.

Returning to parallel phase mixing, this too turns out to be interesting in a nonlinear setting, even though it is a linear phenomenon itself. First theoretical (Schekochihin *et al.* 2016; Adkins & Schekochihin 2018) and numerical (Parker *et al.* 2016; Meyrand *et al.* 2019) analyses suggest that, in a turbulent system, parallel phase mixing is effectively suppressed by the stochastic plasma echo, perhaps rendering kinetic systems that are notionally subject to Landau damping effectively fluid, at least in terms of their energy-flow budgets. In the context of inertial-range MHD turbulence, this is relevant to the compressive (“slow-mode”) perturbations, which, in a collisionless plasma, are energetically decoupled from, and nonlinearly slaved to, the Alfvénic ones, while the latter are still governed by RMHD (Schekochihin *et al.* 2009; Kunz *et al.* 2015). Linearly, these compressive perturbations must be damped—but nonlinearly they are not (Meyrand *et al.* 2019), thus accounting for them exhibiting a healthy power-law spectrum and other fluid features in the solar wind (Chen 2016; Verscharen *et al.* 2017). In this vein, one might also ask whether the Landau damping of KAWs at sub-Larmor scales is always efficient or even present at all—and if it is, as TenBarge & Howes (2013), Bañón Navarro *et al.* (2016), Kobayashi *et al.* (2017), and Chen *et al.* (2019) all say, then what is different at these scales (given that Loureiro *et al.* 2013*b* see a characteristic signature of phase mixing in collisionless reconnection, reconnection might yet again turn out to be the key player, as indeed it has been conjectured to be at these scales—see § 13.1).

The broader question is whether there is generally Landau damping in turbulent systems and whether, therefore, to put it crudely, “all turbulence is fluid.” While it might be a little disappointing if it is, the way and the sense in which this seems to be achieved are surprising and pleasingly nontrivial—and possibly soon to be amenable to direct measurement if the first MMS results on velocity-space (Hermite) spectra in the Earth’s magnetosheath (Servidio *et al.* 2017) are a good indication of the possibilities that are opening up.

13.4. Macro- and Microphysical Consequences of Pressure Anisotropy

Another line of inquiry pregnant with conceptual novelty concerns the effect of self-generated pressure anisotropy on MHD dynamics. Pressure anisotropies are generated in response to any motion in a magnetised collisionless or weakly collisional plasma as long as this motion leads to a change in the strength of the magnetic field. The conservation of the magnetic moment ($\propto v_\perp^2/B \propto$ the angular momentum of Larmor-gyrating particles) then causes positive (if the field grows) or negative (if it decreases) pressure anisotropy to arise (see, e.g., Schekochihin *et al.* 2010). This is usually quite small—in an Alfvén wave,

it is of order $(\delta b/v_A)^2$ —but it becomes relevant at high beta, when even small anisotropies (of order $1/\beta$) can have a dramatic effect, in two ways. Dynamically, pressure anisotropy supplies additional stress, which, when the anisotropy is negative ($p_\perp < p_\parallel$), can cancel Maxwell’s stress and thus remove magnetic tension—the simplest way to think of this is in terms of the Alfvén speed being modified so:

$$v_A \rightarrow \sqrt{v_A^2 + \frac{p_\perp - p_\parallel}{\rho}}. \quad (13.1)$$

Kinetically, pressure anisotropy is a source of free energy and will trigger fast, small-scale instabilities, most notably mirror and firehose (see [Kunz *et al.* 2014](#) and references therein). The firehose corresponds to the Alfvén speed (13.1) turning imaginary, i.e., it is an instability caused by negative tension; the mirror is not quite as simple to explain, but is fundamentally a result of effective magnetic pressure going negative by means of some subtle resonant-particle dynamics (see [Southwood & Kivelson 1993](#), [Kunz *et al.* 2015](#) and references therein). These instabilities in turn can regulate the anisotropy by scattering particles or by subtler, more devious means (see [Melville *et al.* 2016](#) and references therein).

In a recent investigation of the dynamics of a simple finite-amplitude Alfvén wave in a collisionless, high-beta plasma, [Squire *et al.* \(2016, 2017b,a\)](#) showed that both of these effects did occur and altered the wave’s behaviour drastically: it first slows down to a near halt due to the removal of magnetic tension, transferring much of its kinetic energy into heat and then, having spawned a colony of particle-scattering Larmor-scale perturbations, dissipates as if it were propagating in a plasma with a large [Braginskii \(1965\)](#) parallel viscosity. Sound waves in a collisionless plasma get similarly infested by firehoses and mirrors, except the effect of the resulting effective collisionality is to help them propagate in a medium that they thus render more fluid and, therefore, incapable of Landau damping (a different mechanism than discussed in §13.3, but a similar outcome; see [Kunz *et al.* 2020](#)).

These effects occur provided the amplitude of the waves is above a certain limit that scales with plasma beta: this is because pressure anisotropy must be large enough to compete with tension in (13.1) and the amount of anisotropy that can be generated is of the order of the field-strength perturbation. For an Alfvén wave, the latter is quadratic in the wave’s amplitude:

$$\left(\frac{\delta b}{v_A}\right)^2 \sim \frac{p_\perp - p_\parallel}{p} \gtrsim \frac{v_A^2}{p/\rho} \sim \frac{1}{\beta}. \quad (13.2)$$

In formal terms, this means that in high-beta collisionless plasmas, the small-amplitude and high-beta limits do not commute. The picture of Alfvénic turbulence simply obeying RMHD equations, even in a collisionless plasma ([Schekochihin *et al.* 2009](#); [Kunz *et al.* 2015](#)), must then be seriously revised. We can probably live with the current theory for most instances of the solar wind, where $\beta \sim 1$ (or, closer to the Sun, $\beta \ll 1$), but a conventional Alfvénic picture for turbulence in galaxy clusters, for example, and, generally, high-beta plasmas clearly needs a close re-examination (a first step in this direction has been taken by [Squire *et al.* 2019](#), who found that MHD turbulence with Braginskii viscosity, while looking in many respects similar to the usual Alfvénic turbulence, nevertheless manages to minimise changes in the magnetic-field strength to a much greater extent—a property they dubbed “magneto-immutability”; cf. [Tenerani](#)

& Velli 2020a, who do not like the term, but explore useful dynamical scenarios for achieving just such a state).⁷²

Existing understanding of another basic high-beta MHD process, the small-scale dynamo, which I discussed at length in § 12, is also potentially endangered by ubiquitous pressure anisotropies—but has survived the first contact with direct numerical experimentation, which required extra-large, “hero” kinetic simulations (Rincon *et al.* 2016; Kunz *et al.* 2016; St-Onge & Kunz 2018). So far it appears that in this problem as well, changing magnetic fields render plasma more collisional in some effective sense and so large-Pm dynamo remains a relevant paradigm. The same conclusion was reached by St-Onge *et al.* (2020), who simulated dynamo action and saturation in MHD with Braginskii stress (the collisional limit of pressure-anisotropic dynamics).

This line of investigation may be particularly rich in surprises because pressure-anisotropy stress undermines much of our basic intuition for ideal-MHD dynamics, not just modifies microscale plasma physics. This said, it is not entirely inconceivable that, at the end of the day (or of the decade), in some grossly coarse-grained sense, turbulent plasmas will just turn out to supply their own effective collisionality even where Coulomb collisions are rare—and so astrophysicists, with their focus on large-scale motions, need not be too worried about the validity of fluid models. I hope life is not quite so boring, although, as a theoretical physicist and, therefore, a believer in universality, I should perhaps be pleased by such an outcome.

14. Conclusion

Let us stop here. The story of MHD turbulence is a fascinating one—both the story of what happens physically and the story of how it has been understood. It is remarkable how long it takes to figure out simple things, obvious in retrospect. It is even more remarkable (and reassuring) that we get there after all, in finite time. This story now looks reasonably complete, at least in broad-brush outline (§ 7.4) and modulo some loose ends (§§ 8–12). Is this an illusion? Is it all wrong again? We shall know soon enough, but in the meanwhile, the siren call of kinetic physics is too strong to resist and the unexplored terrain seems vast and fertile (§ 13). Is everything different there? Or will it all, in the end, turn out to be the same, with Nature proving itself a universalist bore and contriving to supply effective collisions where nominally there are few? Is turbulence always basically fluid or do subtle delights await us in phase space? Even if we are in danger of being disappointed by the answers to these questions, getting there is proving to be a journey of amusing twists and turns.

For a topic as broad as this, it is difficult to list all the people from whom I have learned what I know (or think I know) of this subject. The most important such influence has been Steve Cowley. The views expressed in the first part of this paper (§§ 5–7) were informed largely by my collaboration with Alfred Mallet and Ben Chandran and by conversations with Nuno Loureiro and Dmitri Uzdensky. I have learned most of what I know of reconnection from Nuno and Dmitri and of the solar wind from Chris Chen, Tim Horbury, and Rob Wicks. The contents of § 12 were inspired by discussions with Andrey Beresnyak, François Rincon, and Matt Kunz, re-examining my views on small-scale dynamo that had been formed in the early 2000s. Ben, Nuno,

⁷²Let me mention parenthetically that at the small-scale end of the turbulent cascade, electron pressure anisotropies lie in wait to mess with the way in which reconnection occurs. I will not go into this here, referring the reader to a review by Egedal *et al.* (2013). This is another microphysical effect that may need to be inserted into the sub-Larmor dynamics (see § 13.1).

and Andrey have also helped me think coherently of imbalanced turbulence—without necessarily endorsing the outcome (§ 8). I owe the first epigraph of this paper to the erudition of Richard McCabe and the second (as well as the epigraph of § 7) to that of Matt Kunz. Besides the colleagues and friends mentioned above, conversations with Axel Brandenburg, Daniele Del Sarto, Thomas Foster, David Hosking, Henrik Latter, Alex Lazarian, Romain Meyrand, Maurizio Ottaviani, Felix Parra, Jono Squire, Marco Velli, and Muni Zhou have helped me work out what to say, and how to say it, in various bits of this review. I would like to thank the authors whose figures appear in the text for giving me permission to reproduce their art. I am grateful to the participants of the 1st JPP Frontiers of Plasma Physics Conference at the Abbazia di Spineto in 2017 for some lively discussions of this paper, which started as an “opinion piece” written for that conference, then ballooned and took four years to complete. I am pleased to acknowledge the hospitality of the Wolfgang Pauli Institute, Vienna, where, in meetings held annually for 12 years, many key interactions took place and ideas were hatched. My extended stay in 2018 at the Niels Bohr International Academy, Copenhagen, where some nontrivial i 's were dotted and t 's crossed, was supported by the Simons Foundation (and I am grateful to Martin Pessah for offering me NBIA's hospitality). Another place whose hospitality, in 2019, proved germane to making progress with this review was the Kavli Institute of Theoretical Physics, Santa Barbara, and its programme on “Multiscale Phenomena in Plasma Astrophysics” led by Anatoly Spitkovsky. In the UK, my work was supported in part by grants from STFC (ST/N000919/1) and EPSRC (EP/M022331/1 and EP/R034737/1). The manuscript was finally completed during the Covid-19 lockdown and its aftermath, but I offer no thanks to the virus.

Appendices

Appendix A. Successes and Failures of WT Theory

A.1. RMHD in Scalar Form

It is convenient to rewrite the RMHD equations (3.1) in terms of two scalar fields, so-called Elsasser potentials ζ^\pm , which are the stream functions for the 2D-solenoidal fields \mathbf{Z}_\perp^\pm (Schekochihin *et al.* 2009), viz.,

$$\mathbf{Z}_\perp^\pm = \hat{\mathbf{z}} \times \nabla_\perp \zeta^\pm, \quad (\text{A } 1)$$

where $\hat{\mathbf{z}} = \mathbf{B}_0/B_0$. Then ζ^\pm satisfy, as shown by taking the curl of (3.1) and using (A 1),

$$\frac{\partial \omega^\pm}{\partial t} \mp v_A \nabla_\parallel \omega^\pm = - \{ \zeta^\mp, \omega^\pm \} + \{ \partial_j \zeta^\pm, \partial_j \zeta^\mp \}, \quad (\text{A } 2)$$

where $\omega^\pm = \hat{\mathbf{z}} \cdot (\nabla_\perp \times \mathbf{Z}_\perp^\pm) = \nabla_\perp^2 \zeta^\pm$ are Elsasser vorticities, dissipative terms have been dropped, and

$$\{ \zeta^\mp, \omega^\pm \} = \frac{\partial \zeta^\mp}{\partial x} \frac{\partial \omega^\pm}{\partial y} - \frac{\partial \zeta^\mp}{\partial y} \frac{\partial \omega^\pm}{\partial x} = \mathbf{Z}_\perp^\mp \cdot \nabla_\perp \omega^\pm. \quad (\text{A } 3)$$

Note that I have written (A 2) in a slightly different (but equivalent) form than in Schekochihin *et al.* (2009). The present version emphasises that the two physical influences of the nonlinearity on the Elsasser vorticities are advection by the other Elsasser field \mathbf{Z}_\perp^\mp (the first term on the right-hand side) and “vortex stretching” (the second term) (cf. Zhdankin *et al.* 2016b).

In Fourier space, (A 2) has a nicely generic form

$$\partial_t \zeta_{\mathbf{k}}^{\pm} \mp ik_{\parallel} v_A \zeta_{\mathbf{k}}^{\pm} = \sum_{pq} M_{\mathbf{k}pq} \delta_{\mathbf{k}, \mathbf{p}+\mathbf{q}} \zeta_{\mathbf{p}}^{\mp} \zeta_{\mathbf{q}}^{\pm}, \quad (\text{A } 4)$$

with the coupling coefficients

$$M_{\mathbf{k}pq} = \hat{\mathbf{z}} \cdot (\mathbf{k}_{\perp} \times \mathbf{q}_{\perp}) \frac{\mathbf{k}_{\perp} \cdot \mathbf{q}_{\perp}}{k_{\perp}^2} = q_{\perp}^2 \sin \phi \cos \phi, \quad (\text{A } 5)$$

where ϕ is the angle between \mathbf{k}_{\perp} and \mathbf{q}_{\perp} .

A.2. Classic WT Calculation

Our objective is to derive an evolution equation for the spectra $C_{\mathbf{k}}^{\pm} = \langle |\zeta_{\mathbf{k}}^{\pm}|^2 \rangle$. Multiplying (A 4) by $\zeta_{\mathbf{k}}^{\pm*}$ and adding to the resulting equation its complex conjugate, we get

$$\partial_t C_{\mathbf{k}}^{\pm} = 2\text{Re} \sum_{pq} M_{\mathbf{k}pq} \delta_{\mathbf{k}, \mathbf{p}+\mathbf{q}} \langle \zeta_{\mathbf{p}}^{\mp} \zeta_{\mathbf{q}}^{\pm} \zeta_{\mathbf{k}}^{\pm*} \rangle. \quad (\text{A } 6)$$

Similarly, the evolution equation for the triple correlator appearing in the right-hand side is

$$\begin{aligned} \partial_t \langle \zeta_{\mathbf{p}}^{\mp} \zeta_{\mathbf{q}}^{\pm} \zeta_{\mathbf{k}}^{\pm*} \rangle \mp i2p_{\parallel} v_A \langle \zeta_{\mathbf{p}}^{\mp} \zeta_{\mathbf{q}}^{\pm} \zeta_{\mathbf{k}}^{\pm*} \rangle &= \sum_{\mathbf{k}'\mathbf{k}''} [M_{\mathbf{p}\mathbf{k}'\mathbf{k}''} \delta_{\mathbf{p}, \mathbf{k}'+\mathbf{k}''} \langle \zeta_{\mathbf{k}'}^{\pm} \zeta_{\mathbf{k}''}^{\mp} \zeta_{\mathbf{q}}^{\pm} \zeta_{\mathbf{k}}^{\pm*} \rangle \\ &\quad + M_{\mathbf{q}\mathbf{k}'\mathbf{k}''} \delta_{\mathbf{q}, \mathbf{k}'+\mathbf{k}''} \langle \zeta_{\mathbf{p}}^{\mp} \zeta_{\mathbf{k}'}^{\mp} \zeta_{\mathbf{k}''}^{\pm} \zeta_{\mathbf{k}}^{\pm*} \rangle \\ &\quad + M_{\mathbf{k}\mathbf{k}'\mathbf{k}''} \delta_{\mathbf{k}, \mathbf{k}'+\mathbf{k}''} \langle \zeta_{\mathbf{p}}^{\mp} \zeta_{\mathbf{q}}^{\pm} \zeta_{\mathbf{k}'}^{\mp} \zeta_{\mathbf{k}''}^{\pm*} \rangle] \equiv A_{\mathbf{k}pq}, \end{aligned} \quad (\text{A } 7)$$

where, in working out the linear term, it was opportune to take account of $k_{\parallel} = p_{\parallel} + q_{\parallel}$. To lowest order in the WT expansion, with $A_{\mathbf{k}pq}$ approximated as constant in time, the solution to this equation is

$$\langle \zeta_{\mathbf{p}}^{\mp} \zeta_{\mathbf{q}}^{\pm} \zeta_{\mathbf{k}}^{\pm*} \rangle = \frac{1 - e^{\mp i2p_{\parallel} v_A t}}{\pm i2p_{\parallel} v_A} A_{\mathbf{k}pq} \rightarrow \frac{\pi \delta(p_{\parallel})}{2v_A} A_{\mathbf{k}pq} \quad \text{as } t \rightarrow \infty. \quad (\text{A } 8)$$

This is the moment when it turns out that every interaction must involve a $p_{\parallel} = 0$ mode, for which the WT approximation is, in fact, broken.

Pressing on regardless, let us adopt a random-phase approximation, as always in WT (Zakharov *et al.* 1992; Nazarenko 2011). Namely, to lowest order in the WT expansion, any wave field is only correlated with itself at the same \mathbf{k} , all odd correlators vanish [which is why we had to iterate from (A 6) to (A 7)], and all even correlators are split into products of quadratic ones, viz.,

$$\langle \zeta_{\mathbf{k}}^{\pm} \zeta_{\mathbf{k}'}^{\pm} \rangle = C_{\mathbf{k}}^{\pm} \delta_{\mathbf{k}, -\mathbf{k}'}, \quad (\text{A } 9)$$

$$\langle \zeta_{\mathbf{k}}^{\pm} \zeta_{\mathbf{k}'}^{\mp} \rangle = 0, \quad (\text{A } 10)$$

$$\langle \zeta_{\mathbf{k}'}^{\pm} \zeta_{\mathbf{k}''}^{\mp} \zeta_{\mathbf{q}}^{\pm} \zeta_{\mathbf{k}}^{\pm*} \rangle = 0, \quad (\text{A } 11)$$

$$\langle \zeta_{\mathbf{p}}^{\mp} \zeta_{\mathbf{k}'}^{\mp} \zeta_{\mathbf{k}''}^{\pm} \zeta_{\mathbf{k}}^{\pm*} \rangle = C_{\mathbf{p}}^{\mp} \delta_{\mathbf{p}, -\mathbf{k}'} C_{\mathbf{k}}^{\pm} \delta_{\mathbf{k}'', \mathbf{k}}, \quad (\text{A } 12)$$

$$\langle \zeta_{\mathbf{p}}^{\mp} \zeta_{\mathbf{q}}^{\pm} \zeta_{\mathbf{k}'}^{\mp} \zeta_{\mathbf{k}''}^{\pm*} \rangle = C_{\mathbf{p}}^{\mp} \delta_{\mathbf{p}, \mathbf{k}'} C_{\mathbf{q}}^{\pm} \delta_{\mathbf{q}, \mathbf{k}''}. \quad (\text{A } 13)$$

Therefore, noticing that $M_{\mathbf{q}, -\mathbf{p}, \mathbf{k}} = -M_{\mathbf{k}pq} k_{\perp}^2 / q_{\perp}^2$, we get

$$A_{\mathbf{k}pq} = M_{\mathbf{k}pq} \delta_{\mathbf{k}, \mathbf{p}+\mathbf{q}} C_{\mathbf{p}}^{\mp} \left(C_{\mathbf{q}}^{\pm} - \frac{k_{\perp}^2}{q_{\perp}^2} C_{\mathbf{k}}^{\pm} \right). \quad (\text{A } 14)$$

Combining (A 14) with (A 8) and putting the latter back into (A 6), we arrive at the classic WT equation derived by Galtier *et al.* (2000):

$$\partial_t N_{\mathbf{k}}^{\pm} = \frac{\pi}{v_A} \sum_{\mathbf{pq}} \frac{k_{\perp}^2 M_{\mathbf{kpq}}^2}{p_{\perp}^2 q_{\perp}^2} \delta_{\mathbf{k}, \mathbf{p}+\mathbf{q}} \delta(p_{\parallel}) N_{\mathbf{p}}^{\mp} (N_{\mathbf{q}}^{\pm} - N_{\mathbf{k}}^{\pm}), \quad (\text{A } 15)$$

where $N_{\mathbf{k}}^{\pm} = k_{\perp}^2 C_{\mathbf{k}}^{\pm} = \langle |\mathbf{Z}_{\perp \mathbf{k}}^{\pm}|^2 \rangle$.

A.3. Solution of WT Equation

The wavenumber sum in (A 15) is turned into an integral in the usual fashion: taking account of the restriction $\mathbf{k} = \mathbf{p} + \mathbf{q}$ and of the fact that the integrand is even in ϕ ,

$$\sum_{\mathbf{pq}} (\dots) = 2 \frac{V}{(2\pi)^3} \int_{-\infty}^{+\infty} dq_{\parallel} \int_0^{\infty} dq_{\perp} q_{\perp} \int_0^{\pi} d\phi (\dots), \quad (\text{A } 16)$$

where $V = L_{\perp}^2 L_{\parallel}$ is the volume of the box. The angle integral can be recast as an integral with respect to p_{\perp} :

$$p_{\perp}^2 = k_{\perp}^2 + q_{\perp}^2 - 2k_{\perp} q_{\perp} \cos \phi \quad \Rightarrow \quad \int_0^{\pi} d\phi \sin \phi (\dots) = \int_{|k_{\perp}-q_{\perp}|}^{k_{\perp}+q_{\perp}} \frac{dp_{\perp} p_{\perp}}{k_{\perp} q_{\perp}} (\dots). \quad (\text{A } 17)$$

Finally, defining the 2D spectra $E_{2\text{D}}^{\pm}(k_{\perp}, k_{\parallel}) = k_{\perp} N_{\mathbf{k}}^{\pm} V / (2\pi)^2$, we get

$$\begin{aligned} \partial_t E_{2\text{D}}^{\pm}(k_{\perp}, k_{\parallel}) &= \frac{1}{v_A} \int_0^{\infty} dq_{\perp} \int_{|k_{\perp}-q_{\perp}|}^{k_{\perp}+q_{\perp}} dp_{\perp} \frac{k_{\perp}^2 q_{\perp}^2}{p_{\perp}} \sin \phi \cos^2 \phi \\ &\quad \times \frac{E_{2\text{D}}^{\mp}(p_{\perp}, 0)}{p_{\perp}} \left[\frac{E_{2\text{D}}^{\pm}(q_{\perp}, k_{\parallel})}{q_{\perp}} - \frac{E_{2\text{D}}^{\pm}(k_{\perp}, k_{\parallel})}{k_{\perp}} \right], \end{aligned} \quad (\text{A } 18)$$

where $\cos \phi = (k_{\perp}^2 + q_{\perp}^2 - p_{\perp}^2) / 2k_{\perp} q_{\perp}$ and $\sin \phi = (1 - \cos^2 \phi)^{1/2}$.

Let us now, as anticipated in (4.9), assume

$$E_{2\text{D}}^{\pm}(k_{\perp}, k_{\parallel}) = f^{\pm}(k_{\parallel}) k_{\perp}^{\mu_{\perp}^{\pm}}, \quad E_{2\text{D}}^{\mp}(k_{\perp}, 0) = f^{\mp}(0) k_{\perp}^{\mu_0^{\mp}}, \quad (\text{A } 19)$$

substitute these into the right-hand side of (A 18) and non-dimensionalise the integral by changing the integration variables to $x = q_{\perp}/k_{\perp}$ and $y = p_{\perp}/k_{\perp}$:

$$\partial_t E^{\pm}(k_{\perp}, k_{\parallel}) = \frac{f^{\mp}(0) f^{\pm}(k_{\parallel})}{v_A} I(\mu^{\pm}, \mu_0^{\mp}) k_{\perp}^{\mu^{\pm} + \mu_0^{\mp} + 3} \equiv - \frac{\partial \Pi^{\pm}(k_{\perp}, k_{\parallel})}{\partial k_{\perp}}, \quad (\text{A } 20)$$

$$I(\mu, \mu_0) = \int_0^{\infty} dx \int_{|1-x|}^{1+x} dy y^{-2+\mu_0} x^2 (x^{\mu-1} - 1) \sin \phi \cos^2 \phi, \quad (\text{A } 21)$$

where $\cos \phi = (1 + x^2 - y^2) / 2x$. The energy flux formally introduced in (A 20) is

$$\Pi^{\pm}(k_{\perp}, k_{\parallel}) = - \frac{f^{\mp}(0) f^{\pm}(k_{\parallel})}{v_A} \frac{I(\mu^{\pm}, \mu_0^{\mp})}{\mu^{\pm} + \mu_0^{\mp} + 4} k_{\perp}^{\mu^{\pm} + \mu_0^{\mp} + 4}. \quad (\text{A } 22)$$

It is assumed here that the flux in $(k_{\perp}, k_{\parallel})$ space is in the k_{\perp} direction only (no parallel cascade in WT). In order for (A 22) to be independent of k_{\perp} , it must be the case that⁷³

$$\mu^{\pm} + \mu_0^{\mp} = -4, \quad (\text{A } 23)$$

⁷³Or $\mu^{\pm} = 1$, in which case $I = 0$, so $\Pi^{\pm} = 0$. This is a (UV-divergent) thermal equilibrium spectrum, irrelevant in a forced problem.

but then, in order for the expression in (A 22) to have a finite value, it must also be the case that $I(\mu, \mu_0) \rightarrow 0$ when $\mu + \mu_0 + 4 \rightarrow 0$. That this is indeed the case is shown by changing the integration variables to $\xi = 1/x$, $\eta = y/x$, a change that leaves the domain of integration in (A 21) the same (a *Zakharov transformation*; see Zakharov *et al.* 1992). In these new variables,

$$I(\mu, \mu_0) = - \int_0^\infty d\xi \int_{|1-\xi|}^{1+\xi} d\eta \eta^{-2+\mu_0} \xi^{-\mu-\mu_0-2} (\xi^{\mu-1} - 1) \sin \phi \cos^2 \phi, \quad (\text{A } 24)$$

where $\cos \phi = (1 + \xi^2 - \eta^2)/2\xi$. When $\mu + \mu_0 = -4$, this is exactly the same integral as (A 21), except with a minus sign, so $I = -I = 0$, q.e.d.

The problem with this otherwise respectable-looking calculation is that $E_{2D}^\mp(p_\perp, 0)$, which plays a key role in (A 18), is the spectrum of zero-frequency, $p_\parallel = 0$ modes, for which the WT approximation cannot be used, so μ_0^\mp is certainly not determinable within WT, the random-phase approximation should not have been used for these modes (and has been explicitly shown not to hold for them by Meyrand *et al.* 2015), and so it is at the very least doubtful that (A 18) can be used for the determination of μ^\pm , the scaling exponents for the waves, either. For the moment, let me put aside the latter doubt and act on the assumption that if I can deduce μ_0^\mp in some way, μ^\pm will follow by (A 23).

A.4. Case of Broad-Band Forcing: Spectral Continuity

The argument that is about to be presented here is heuristic and routed in the ideas about the treatment of strong turbulence described in §§ 2.3 and 5—it turns out that, to understand weak turbulence, one must understand strong turbulence first. I will, therefore, not attempt to deal with imbalanced WT—because, even though I did, in § 8.2, attempt to construct a coherent picture of strong imbalanced turbulence, it is too tentative and too fiddly to be inserted into what follows, which will be tentative and fiddly in its own right. Thus, the “ \pm ” tags are now dropped everywhere.

In reality, the delta function $\delta(p_\parallel)$ in (A 8) has a width equal to the characteristic broadening of the frequency resonance due to nonlinear interactions, $\Delta k_\parallel \sim \tau_{\text{nl}}^{-1}/v_A$, to wit,

$$\delta(p_\parallel) = \frac{\Delta k_\parallel}{\pi} \frac{1}{p_\parallel^2 + \Delta k_\parallel^2} \quad (\text{A } 25)$$

(in the WT approximation, $\Delta k_\parallel \rightarrow 0$). At $p_\parallel \lesssim \Delta k_\parallel$, the “ $p_\parallel = 0$ ” condensate resides, whose turbulence is strong (figure 33). Let us work out the structure of this turbulence.

Let us assume that our WT is forced in a broad band of parallel wavenumbers $k_\parallel \in (0, 2\pi/L_\parallel)$ (obviously, the parallel size of “the box” must be $\gg L_\parallel$). This can happen, e.g., if the forcing is completely random with parallel coherence length L_\parallel , in which case its k_\parallel spectrum at $k_\parallel < 2\pi/L_\parallel$ is flat (a white noise). Thus, the same amount of energy is injected into each k_\parallel , this energy is cascaded weakly in k_\perp (by the still-to-be-worked-out condensate) without change in k_\parallel until it arrives at the CB scale associated with this k_\parallel , i.e., at the k_\perp for which $\Delta k_\parallel(k_\perp) \sim k_\parallel$ (equivalently, $\tau_{\text{nl}}^{-1} \sim k_\parallel v_A$), where it joins the condensate. Therefore, the flux of energy into, and via, the condensate is not scale-independent: at any given k_\perp , it is

$$\int_0^{\Delta k_\parallel(k_\perp)} dk_\parallel \Pi(k_\perp, k_\parallel) \sim \varepsilon L_\parallel \Delta k_\parallel(k_\perp), \quad \Delta k_\parallel(k_\perp) \sim \frac{\tau_{\text{nl}}^{-1}}{v_A}, \quad (\text{A } 26)$$

where I have assumed that $\Pi(k_\perp, k_\parallel) \sim \varepsilon L_\parallel$ is a constant in both of its arguments (constant in k_\perp because the WT cascade is a constant-flux one and constant in k_\parallel because

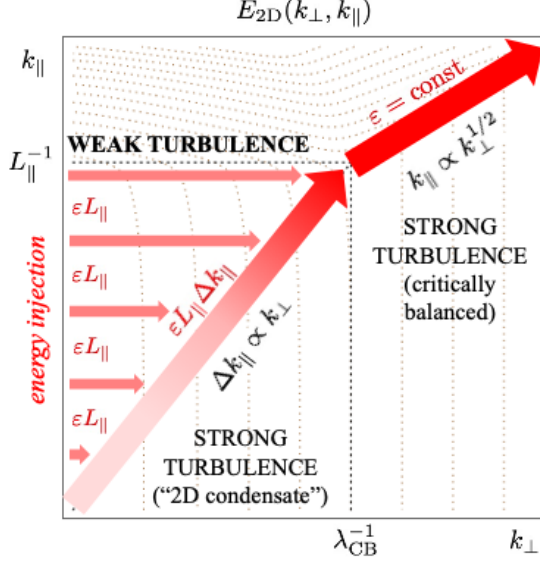


FIGURE 33. Cartoon of the 2D spectrum of broad-band-forced weak turbulence. Schematic contour lines of $E_{2D}(k_{\perp}, k_{\parallel})$ are the brown dotted lines. Red arrows are energy fluxes: $\Pi(k_{\perp}, k_{\parallel}) \sim \varepsilon L_{\parallel}$ arriving from the forcing wavenumbers to the “2D condensate” at each k_{\parallel} , $\varepsilon L_{\parallel} \Delta k_{\parallel}$ flowing through the condensate [see (A 26)], and $\varepsilon = \text{const}$ after the transition to critically balanced cascade (cf. figure 35a).

the amount of energy injection is the same at every k_{\parallel}). Then, for the condensate at scale $\lambda \sim k_{\perp}^{-1}$,

$$\frac{\delta Z_{\lambda}^2}{\tau_{\text{nl}}} \sim \varepsilon L_{\parallel} \Delta k_{\parallel}(k_{\perp}) \sim \frac{\varepsilon L_{\parallel}}{\tau_{\text{nl}} v_A} \Rightarrow \delta Z_{\lambda} \sim \left(\frac{\varepsilon L_{\parallel}}{v_A} \right)^{1/2} \Rightarrow E_0(k_{\perp}) \sim \frac{\varepsilon L_{\parallel}}{v_A} k_{\perp}^{-1}, \quad (\text{A } 27)$$

where $E_0(k_{\perp})$ is the condensate’s 1D spectrum.

This 1D spectrum is the 2D spectrum $E_0(k_{\perp}, k_{\parallel})$ integrated over all parallel wavenumbers belonging to the condensate, viz.,

$$E_0(k_{\perp}) \sim \int_0^{\Delta k_{\parallel}(k_{\perp})} dk_{\parallel} E_0(k_{\perp}, k_{\parallel}) \sim E_0(k_{\perp}, k_{\parallel}) \Delta k_{\parallel}(k_{\perp}). \quad (\text{A } 28)$$

The last step is valid on the assumption that $E_0(k_{\perp}, k_{\parallel})$ is, in fact, independent of k_{\parallel} , because by the usual CB assumption, there cannot be any correlations at parallel scales $k_{\parallel}^{-1} > v_A \tau_{\text{nl}} \sim \Delta k_{\parallel}^{-1}(k_{\perp})$ and so the corresponding k_{\parallel} spectrum is that of a white noise (cf. appendix B.1).

The cascade time for the condensate (which advects itself) is

$$\tau_{\text{nl}}^{-1} \sim \frac{\delta Z_{\lambda}}{\lambda} \sim \left(\frac{\varepsilon L_{\parallel}}{v_A} \right)^{1/2} \lambda^{-1} \Rightarrow \Delta k_{\parallel}(k_{\perp}) \sim \frac{(\varepsilon L_{\parallel})^{1/2}}{v_A^{3/2}} k_{\perp}. \quad (\text{A } 29)$$

I am assuming that there is no dynamic alignment (§ 6) for the condensate because the condensate is effectively forced at every scale by the WT cascade—this is not a proof, but a conjecture, adopted for its simplicity and plausibility. Finally, (A 29), via (A 28)

and (A 27), leads to

$$E_{0,2D}(k_{\perp}, k_{\parallel}) \sim (\varepsilon L_{\parallel} v_A)^{1/2} k_{\perp}^{-2}, \quad k_{\parallel} \lesssim \Delta k_{\parallel}(k_{\perp}). \quad (\text{A } 30)$$

Thus, $\mu_0 = -2$ for reasons that have little to do with weak interactions, and, therefore, by (A 23), $\mu = -2$ as well (in appendix B.5, the same results are rederived in a slightly different way, which may or may not shed more light).

Thus, there is, in fact, no difference between the WT spectrum at $k_{\parallel} > \Delta k_{\parallel}(k_{\perp})$ and the condensate's spectrum at $k_{\parallel} < \Delta k_{\parallel}(k_{\perp})$, even though the nature of turbulence in these two regions is quite different. The above construction can thus be viewed as a physical argument in support of spectral continuity. It does not make the derivation of the WT equation in appendix A.2 *formally* correct but it does perhaps lend it some credibility.

A.5. Residual Energy in WT

If one takes this appearance of WT credibility seriously, there is another result that can be “derived” within it. The random-phase approximation for Alfvén waves implied the absence of correlations between the counterpropagating Elsasser fields, (A 10). What if we relax this assumption—and only this assumption!—while still splitting fourth-order correlators into second-order ones? Namely, let us set

$$k_{\perp}^2 \langle \zeta_{\mathbf{k}}^{\pm} \zeta_{\mathbf{k}'}^{\mp} \rangle = R_{\mathbf{k}}^{\pm} \delta_{\mathbf{k}, -\mathbf{k}'}, \quad (\text{A } 31)$$

where, obviously, $R_{\mathbf{k}}^{-*} = R_{\mathbf{k}}^{+} \equiv R_{\mathbf{k}}$, and work out the WT evolution equation for $R_{\mathbf{k}}$. This is interesting, *inter alia*, because $\text{Re} R_{\mathbf{k}}$ is the 3D residual-energy spectrum and so the derivation I am about to present (which is a version of what Wang *et al.* 2011 did) has a claim to providing theoretical backing to the presence of negative residual energy both in observed and in numerically simulated MHD turbulence (see § 9).

From the field equation (A 4), straightforwardly,

$$\partial_t R_{\mathbf{k}} - 2ik_{\parallel} v_A R_{\mathbf{k}} = k_{\perp}^2 \sum_{\mathbf{p}\mathbf{q}} M_{\mathbf{k}\mathbf{p}\mathbf{q}} \delta_{\mathbf{k}, \mathbf{p}+\mathbf{q}} \left(\langle \zeta_{\mathbf{p}}^{-} \zeta_{\mathbf{q}}^{+} \zeta_{\mathbf{k}}^{-*} \rangle + \langle \zeta_{\mathbf{p}}^{+*} \zeta_{\mathbf{q}}^{-*} \zeta_{\mathbf{k}}^{+} \rangle \right). \quad (\text{A } 32)$$

Following the same protocol as in appendix A.2, let us write the evolution equation for the third-order correlators in (A 32) in terms of fourth-order correlators and then split the latter into second-order ones, but now allowing non-zero correlations between different Elsasser fields according to (A 31):

$$\begin{aligned} \partial_t \langle \zeta_{\mathbf{p}}^{\mp} \zeta_{\mathbf{q}}^{\pm} \zeta_{\mathbf{k}}^{\mp*} \rangle \mp i2q_{\parallel} v_A \langle \zeta_{\mathbf{p}}^{\mp} \zeta_{\mathbf{q}}^{\pm} \zeta_{\mathbf{k}}^{\mp*} \rangle &= \delta_{\mathbf{k}, \mathbf{p}+\mathbf{q}} \frac{\hat{\mathbf{z}} \cdot (\mathbf{k}_{\perp} \times \mathbf{q}_{\perp})}{k_{\perp}^2 p_{\perp}^2 q_{\perp}^2} [\mathbf{k}_{\perp} \cdot \mathbf{p}_{\perp} N_{\mathbf{q}}^{\pm} (N_{\mathbf{k}}^{\mp} - N_{\mathbf{p}}^{\mp}) \\ &+ \mathbf{k}_{\perp} \cdot \mathbf{q}_{\perp} (R_{\mathbf{p}}^{\mp} R_{\mathbf{q}}^{\pm} - R_{\mathbf{k}}^{\pm} N_{\mathbf{p}}^{\mp}) + \mathbf{p}_{\perp} \cdot \mathbf{q}_{\perp} (R_{\mathbf{k}}^{\pm} R_{\mathbf{q}}^{\pm} - R_{\mathbf{p}}^{\mp} N_{\mathbf{k}}^{\mp})]. \end{aligned} \quad (\text{A } 33)$$

The presence of the first term is proof that $R_{\mathbf{k}} = 0$ is, generally speaking, not a sustainable solution. However, since growth of correlations between counterpropagating Elsasser fields contradicts the random-phase approximation and thus undermines WT, perhaps we could hope (falsely, as I will show shortly) that $R_{\mathbf{k}}$ might be small and so the terms containing $R_{\mathbf{k}}$ in (A 33) could be neglected for the time being. Then the solution of (A 33) is

$$\langle \zeta_{\mathbf{p}}^{\mp} \zeta_{\mathbf{q}}^{\pm} \zeta_{\mathbf{k}}^{\mp*} \rangle = \frac{1 - e^{\pm i2q_{\parallel} v_A t}}{\mp i2q_{\parallel} v_A} \delta_{\mathbf{k}, \mathbf{p}+\mathbf{q}} \frac{\hat{\mathbf{z}} \cdot (\mathbf{k}_{\perp} \times \mathbf{q}_{\perp}) \mathbf{k}_{\perp} \cdot \mathbf{p}_{\perp}}{k_{\perp}^2 p_{\perp}^2 q_{\perp}^2} N_{\mathbf{q}}^{\pm} (N_{\mathbf{k}}^{\mp} - N_{\mathbf{p}}^{\mp}). \quad (\text{A } 34)$$

Substituting this into (A 32), solving that in turn, and denoting

$$B_{\mathbf{k}p\mathbf{q}} = \frac{|\mathbf{k}_\perp \times \mathbf{q}_\perp|^2 \mathbf{k}_\perp \cdot \mathbf{p}_\perp}{k_\perp^2 p_\perp^2 q_\perp^2} [N_{\mathbf{q}}^+ (N_{\mathbf{k}}^- - N_{\mathbf{p}}^-) + N_{\mathbf{q}}^- (N_{\mathbf{k}}^+ - N_{\mathbf{p}}^+)], \quad (\text{A } 35)$$

we find

$$\begin{aligned} \text{Re}R_{\mathbf{k}} &= \text{Re} \sum_{p\mathbf{q}} \delta_{\mathbf{k},p+\mathbf{q}} \frac{1}{i2q_\parallel v_A} \left(\frac{1 - e^{i2k_\parallel v_A t}}{i2k_\parallel v_A} - e^{i2q_\parallel v_A t} \frac{1 - e^{i2p_\parallel v_A t}}{i2p_\parallel v_A} \right) B_{\mathbf{k}p\mathbf{q}}, \\ &\rightarrow \frac{\pi^2}{4v_A^2} \sum_{p\mathbf{q}} \delta_{\mathbf{k},p+\mathbf{q}} \delta(p_\parallel) \delta(q_\parallel) B_{\mathbf{k}p\mathbf{q}} \quad \text{as } t \rightarrow \infty. \end{aligned} \quad (\text{A } 36)$$

The 2D spectrum of residual energy is, therefore,

$$\begin{aligned} E_{\text{res},2\text{D}}(k_\perp, k_\parallel) &= \frac{V k_\perp \text{Re}R_{\mathbf{k}}}{(2\pi)^2} = -\frac{\pi \delta(k_\parallel)}{4v_A^2} \int_0^\infty dq_\perp \int_{|k_\perp - q_\perp|}^{k_\perp + q_\perp} dp_\perp \frac{k_\perp^2 q_\perp^2}{p_\perp} \sin \phi \cos^2 \phi \\ &\times \left\{ \frac{E^+(q_\perp, 0)}{q_\perp} \left[\frac{E^-(k_\perp, 0)}{k_\perp} - \frac{E^-(p_\perp, 0)}{p_\perp} \right] + \frac{E^-(q_\perp, 0)}{q_\perp} \left[\frac{E^+(k_\perp, 0)}{k_\perp} - \frac{E^+(p_\perp, 0)}{p_\perp} \right] \right\}, \end{aligned} \quad (\text{A } 37)$$

where the wavenumber integrals have been manipulated in exactly the same way as they were in appendix A.2, in the lead-up to (A 18). Again assuming the power-law solutions (A 19), we get

$$E_{\text{res},2\text{D}}(k_\perp, k_\parallel) = -\text{const} \frac{f^+(0)f^-(0)}{v_A^2} k_\perp^{\mu_0^+ + \mu_0^- + 3} \delta(k_\parallel). \quad (\text{A } 38)$$

What does this result tell us? Primarily, it tells us that the WT calculation that led to it is formally invalid and can, at best, be interpreted as a qualitative indication of what is going on. All the action has turned out to be concentrated in the $k_\parallel = 0$ condensate, while for Alfvén waves with $k_\parallel \neq 0$, there is no residual energy. That we were going to end up with $\delta(k_\parallel)$ was, in fact, already obvious from the presence of the oscillatory term in (A 32). Nevertheless, without a claim to mathematical rigour, one can, as I did in appendix A.4, interpret the delta function in (A 38) as having a width $\Delta k_\parallel \sim \tau_{\text{nl}}^{-1}/v_A$, where $\tau_{\text{nl}} \propto k_\perp^{-1}$ is the cascade time for the condensate, worked out in (A 29). Taking $\mu_0^+ + \mu_0^- = -4$ and $\delta(k_\parallel) \sim \Delta k_\parallel^{-1} \propto k_\perp^{-1}$ in (A 38) gets us

$$E_{\text{res},2\text{D}}(k_\perp, k_\parallel) \propto -k_\perp^{-2}, \quad (\text{A } 39)$$

whereas the 1D spectrum can be calculated either by integrating out the delta function in (A 38) or by integrating its broadened version in (A 39) over its width $\Delta k_\parallel \propto k_\perp^{-1}$:

$$E_{\text{res}}(k_\perp) = \int dk_\parallel E_{\text{res},2\text{D}}(k_\perp, k_\parallel) = -\text{const} \frac{f^+(0)f^-(0)}{v_A^2} k_\perp^{-1}. \quad (\text{A } 40)$$

This is the result of Wang *et al.* (2011), who, however, go to slightly greater lengths in setting up a quasi-quantitative calculation in which they introduce by hand a nonlinear relaxation rate $\tau_{\text{nl}}^{-1} \propto k_\perp$ into (A 32) and thus get their $\delta(k_\parallel)$ to acquire the Lorentzian shape (A 25).⁷⁴

Note that (A 40) is, in fact, the same result as (A 27)—comparing (A 19) with (A 30), or

⁷⁴They attribute this relaxation to the $R_{\mathbf{k}}$ -dependent terms in (A 33), which is qualitatively correct, but quantitatively just as invalid as is generally the application of the WT approximation (i.e., correlator splitting) to the strongly turbulent condensate.

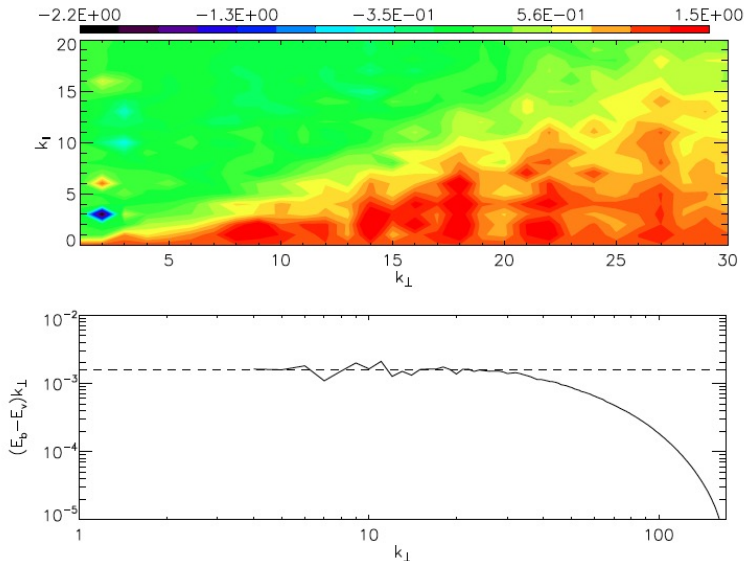


FIGURE 34. The 2D spectrum, $E_{\text{res},2\text{D}}(k_{\perp}, k_{\parallel})/E_{\text{res},2\text{D}}(k_{\perp}, 0)$ (upper panel) and the 1D, k_{\perp}^{-1} -compensated spectrum (lower panel) of residual energy from WT simulations by Wang *et al.* (2011) (512^3 , broad-band forced at $k_{\parallel} = 1, \dots, 16$ and $k_{\perp} = 1, 2$).

just simple dimensional analysis, confirms that $f^{\pm}(0) \sim (\varepsilon L_{\parallel} v_A)^{1/2}$, so the dimensional prefactors match. Thus, all we have learned from the above calculation is that the condensate has residual energy and that the amount of the latter is comparable, at every scale, to the amount of energy in the condensate. One might argue that the added value of the WT calculation was in confirming that this residual energy was negative—although the negativity of the prefactor in (A 38) is a quantitative result, not a qualitative one (one just has to calculate the appropriate integral and discover it to be negative, as Wang *et al.* 2011 did), and so cannot be guaranteed to hold for the true, strongly turbulent condensate. I find the qualitative argument for the development of negative vorticity correlation $\langle \omega^+ \omega^- \rangle < 0$ explained in § 9.4 more compelling. The WT calculation above basically just confirms that growth of residual energy is a strong-turbulence effect.

The qualitative considerations presented above are given some credence by the numerical simulations of WT reported by Wang *et al.* (2011): their residual energy does indeed have a k_{\perp}^{-1} spectrum and concentrates in a wedge of wavenumber space $k_{\parallel} \lesssim \Delta k_{\parallel} \propto k_{\perp}$, quite convincingly (figure 34).

A.6. Imbalanced WT

As I acknowledged in § 4.3, I do not know how to construct a good theory of imbalanced WT. If imbalanced WT, like the balanced one, spawns a 2D condensate that is predominantly magnetic, that may be a helpful insight, as the presence of significant residual energy would impose geometric constraints (§ 8.1.2) on the “+” and “−” components of the condensate. Boldyrev & Perez (2009) do find a magnetic condensate in an imbalanced simulation, but they only have results for order-unity imbalance. They also point out that if the cross-correlations (A 31) are retained in the derivation of the WT equation (A 15) for $N_{\mathbf{k}}$, this makes the evolution equation (A 18) for $E_{2\text{D}}^{\pm}(k_{\perp}, 0)$ acquire terms under the integral containing $E_{2\text{D}}^{\pm}(k_{\perp}, 0)E_{\text{res},2\text{D}}(p_{\perp}, 0) + E_{2\text{D}}^{\pm}(p_{\perp}, 0)E_{\text{res},2\text{D}}(k_{\perp}, 0)$. Steady-state

solutions then turn out to be possible only if

$$E_{\text{res},2\text{D}}(k_{\perp}, 0) \propto k_{\perp}^{-2}, \quad E_{2\text{D}}^{\pm}(k_{\perp}, 0) \propto k_{\perp}^{-2}, \quad (\text{A } 41)$$

i.e., the degeneracy of the $\mu_0^+ + \mu_0^- = -4$ solution is lifted and all scalings are fixed. Perhaps this points us in the right direction, despite the fact that the WT equation for $E_{2\text{D}}^{\pm}(k_{\perp}, 0)$, whose derivation requires correlator splitting etc., is not, in fact, quantitatively valid for the condensate.

In their mildly imbalanced WT simulation, [Boldyrev & Perez \(2009\)](#) find that $E^+(k_{\perp})$ and $E^-(k_{\perp})$ have, respectively, a steeper and a shallower slope than k_{\perp}^{-2} , but the spectra appear to be pinned at the dissipation scale and thus get closer to each other with increased resolution. Thus, if one wants a theory that describes finite-resolution simulations, some scheme like the one I proposed in §8.2 would need to be invented for the WT regime, generalising appendix A.4 to the imbalanced case.

Appendix B. 2D Spectra of RMHD Turbulence

As we trade in k_{\perp} (or λ) and k_{\parallel} (or l_{\parallel}) scalings, it is only natural that we might wish to have 2D spectra of RMHD turbulence, $E_{2\text{D}}(k_{\perp}, k_{\parallel})$. It is quite easy to work them out, given the information we already have about the λ and l_{\parallel} scalings of the Elsasser increments.

Since, as I explained in §5.3, the physically meaningful parallel correlations are along the local mean field, we should think of our Elsasser fields \mathbf{Z}_{\perp}^{\pm} as being mapped on a grid of values of $(\mathbf{r}_{\perp}, r_{\parallel})$, where r_{\parallel} is the distance measured along the exact field line (what matters here is not that the parallel distances are slightly longer than their projection on the z axis—the difference is small in the RMHD ordering—but that we probe correlations along the exact field line rather than slipping off it; see figure 8). The Fourier transform of $\mathbf{Z}_{\perp}^{\pm}(\mathbf{r}_{\perp}, r_{\parallel})$ is a function of k_{\perp} and k_{\parallel} , $\mathbf{Z}_{\perp}^{\pm}(\mathbf{k}_{\perp}, k_{\parallel})$, and the 2D spectrum is defined to be

$$E_{2\text{D}}(k_{\perp}, k_{\parallel}) = 2\pi k_{\perp} \langle |\mathbf{Z}_{\perp}^{\pm}(\mathbf{k}_{\perp}, k_{\parallel})|^2 \rangle. \quad (\text{B } 1)$$

Let us start with the premise that $E_{2\text{D}}(k_{\perp}, k_{\parallel})$ will be a product of power laws in both of its arguments and that the scaling exponents of these power laws will be different depending on where we are in the $(k_{\perp}, k_{\parallel})$ space vis-à-vis the line of critical balance, which is also a power-law relation, between k_{\perp} and k_{\parallel} :

$$\tau_{\text{nl}} \sim \tau_{\text{A}} \quad \Leftrightarrow \quad k_{\parallel} \sim k_{\perp}^{\sigma}. \quad (\text{B } 2)$$

We shall treat the wavenumbers as dimensionless, $k_{\parallel} L_{\parallel} \rightarrow k_{\parallel}$, $k_{\perp} \lambda_{\text{CB}} \rightarrow k_{\perp}$; according to (6.20),

$$\sigma = \frac{1}{2}. \quad (\text{B } 3)$$

Thus, we shall look for the 2D spectrum in the form

$$E_{2\text{D}}(k_{\perp}, k_{\parallel}) \sim \begin{cases} k_{\parallel}^{-\alpha} k_{\perp}^{\beta}, & k_{\parallel} \gtrsim k_{\perp}^{\sigma}, \\ k_{\parallel}^{\delta} k_{\perp}^{-\gamma}, & k_{\parallel} \lesssim k_{\perp}^{\sigma}. \end{cases} \quad (\text{B } 4)$$

The four exponents α , β , γ , and δ can be determined by the following argument, analogous to one proposed by [Schekochihin *et al.* \(2016\)](#) for drift-kinetic turbulence.

B.1. Determining δ

At long parallel wavelengths, $k_{\parallel} \ll k_{\perp}^{\sigma}$, the k_{\parallel} spectrum measures correlation between points along the field line that are separated by longer distances than an Alfvén wave can travel in one nonlinear time ($\tau_A \gg \tau_{nl}$) and, consequently, are causally disconnected (§ 5.1). Therefore, their parallel correlation function is that of a 1D white noise and the corresponding spectrum is flat:

$$\delta = 0. \quad (\text{B5})$$

It may be worth belabouring this point: the flat k_{\parallel} spectrum at $k_{\parallel} \lesssim k_{\perp}^{\sigma}$ (figure 35b) is the Fourier-space signature of CB turbulence, not an indication of the presence of quasi-2D motions or of failure of local-in-scale interactions (as, e.g., Meyrand *et al.* 2016 appear to imply). This highlights the fact that the wavenumbers where energy is present are not quite the same thing as the correlation scales of the turbulent field (and so one should not expect that CB requires a spectrum peaked at $k_{\parallel} \sim k_{\perp}^{\sigma}$ —a fallacy that has made it into a number of published texts, rigorous peer review notwithstanding). The same argument applies to frequency spectra, should one want to plot them: there must be a flat spectrum at $\omega \lesssim \tau_{nl}^{-1}$ because instances separated by times longer than τ_{nl} are uncorrelated and will, therefore, have white-noise statistics.

B.2. Determining γ

Let us calculate the 1D k_{\perp} spectrum: if we assume (and promise to check later) that $\alpha > 1$, then the k_{\parallel} integral over $E_{2D}(k_{\perp}, k_{\parallel})$ is dominated by the region $k_{\parallel} \lesssim k_{\perp}^{\sigma}$ and the 1D spectrum is mostly determined by the CB scales $k_{\parallel} \sim k_{\perp}^{\sigma}$ (as is indeed argued in the GS95 theory and its descendants reviewed in the main text):

$$E(k_{\perp}) \sim \int_0^{k_{\perp}^{\sigma}} dk_{\parallel} E_{2D}(k_{\perp}, k_{\parallel}) \sim k_{\perp}^{-\gamma+\sigma}. \quad (\text{B6})$$

Then the amplitude of an Elsasser field at scale $\lambda = k_{\perp}^{-1}$ is

$$\delta Z_{\lambda}^2 \sim \int_{k_{\perp}}^{\infty} dk'_{\perp} E(k'_{\perp}) \sim k_{\perp} E(k_{\perp}) \sim k_{\perp}^{-\gamma+\sigma+1}, \quad (\text{B7})$$

assuming $\gamma - \sigma > 1$. On the other hand, the usual Kolmogorov constant-flux condition coupled with the CB conjecture gives us

$$\frac{\delta Z_{\lambda}^2}{\tau_{nl}} \sim \text{const}, \quad \tau_{nl}^{-1} \sim \tau_A^{-1} \propto k_{\parallel} \sim k_{\perp}^{\sigma} \quad \Rightarrow \quad \delta Z_{\lambda}^2 \sim k_{\perp}^{-\sigma}. \quad (\text{B8})$$

Comparing this with (B7), we get

$$\gamma = 2\sigma + 1 = 2. \quad (\text{B9})$$

The 1D spectral exponent in (B6) is then $-\gamma + \sigma = -3/2$, as it should be [see (6.20)].

B.3. Determining β

This calculation is purely kinematic. Let us write the desired spectrum (B1) as

$$\begin{aligned} \langle |\mathbf{Z}_{\perp}^{\pm}(\mathbf{k}_{\perp}, k_{\parallel})|^2 \rangle &= \int \frac{d^2 \mathbf{r}_{\perp}}{(2\pi)^2} e^{-i\mathbf{k}_{\perp} \cdot \mathbf{r}_{\perp}} \langle \mathbf{Z}_{\perp}^{\pm}(\mathbf{r}_{\perp}, k_{\parallel}) \cdot \mathbf{Z}_{\perp}^{\pm*}(0, k_{\parallel}) \rangle \\ &= \frac{1}{2\pi} \int_0^{\infty} dr_{\perp} r_{\perp} J_0(k_{\perp} r_{\perp}) C^{\pm}(r_{\perp}, k_{\parallel}), \end{aligned} \quad (\text{B10})$$

where $C^\pm(r_\perp, k_\parallel)$ is the two-point correlation function of $\mathbf{Z}_\perp^\pm(\mathbf{r}_\perp, k_\parallel)$. It is only a function of the point separation r_\perp because of statistical homogeneity and isotropy in the perpendicular plane. For any given k_\parallel , we may assume that, by the CB conjecture, the correlation length of the field is $\lambda \sim k_\parallel^{-1/\sigma}$. The integral in (B 10) is then effectively restricted by $C^\pm(r_\perp, k_\parallel)$ to $r_\perp \lesssim \lambda$. If we now let $k_\perp \lambda \ll 1$ (equivalently, $k_\perp^\sigma \ll k_\parallel$), then the Bessel function can be expanded in small argument: $J_0(k_\perp r_\perp) = 1 - k_\perp^2 r_\perp^2 / 4 + \dots$. The spectrum (B 1) is then

$$E_{2D}(k_\perp, k_\parallel) = \frac{k_\perp}{2\pi} (C_0 + C_2 k_\perp^2 + \dots), \quad (\text{B } 11)$$

$$C_0 = 2\pi \int_0^\infty dr_\perp r_\perp C^\pm(r_\perp, k_\parallel), \quad C_2 = -\frac{\pi}{2} \int_0^\infty dr_\perp r_\perp^3 C^\pm(r_\perp, k_\parallel). \quad (\text{B } 12)$$

The first of these coefficients, $C_0 = \int d^2\mathbf{r}_\perp \langle \mathbf{Z}_\perp^\pm(\mathbf{r}_\perp, k_\parallel) \cdot \mathbf{Z}_\perp^{\pm*}(0, k_\parallel) \rangle$, vanishes if $\int d^2\mathbf{r}_\perp \mathbf{Z}_\perp^\pm(\mathbf{r}_\perp, k_\parallel) = 0$, which should be a safe enough assumption for a solenoidal field [see (A 1)] in a box. This leaves us with the series (B 11) for E_{2D} starting at the second term and so $E_{2D} \propto k_\perp^3$ to lowest order. Thus,

$$\beta = 3. \quad (\text{B } 13)$$

B.4. Determining α

Finally, α is determined simply by the requirement that the 2D spectra match along the CB line: substituting $k_\parallel \sim k_\perp^\sigma$ into (B 4) and equating powers of k_\perp , we get

$$\alpha = \frac{\beta + \gamma}{\sigma} - \delta = 10. \quad (\text{B } 14)$$

This ridiculous exponent⁷⁵ suggests that there is very little energy indeed in wave-like perturbations with $\tau_A \ll \tau_{nl}$.

Note that the consistency of what I have done above can be checked by calculating the 1D k_\parallel spectrum:

$$E(k_\parallel) = \int dk_\perp E_{2D}(k_\perp, k_\parallel) \sim \int_0^{k_\parallel^{1/\sigma}} dk_\perp k_\parallel^{-\alpha} k_\perp^\beta + \int_{k_\parallel^{1/\sigma}}^\infty dk_\perp k_\parallel^\delta k_\perp^{-\gamma} \sim k_\parallel^{-\zeta}, \quad (\text{B } 15)$$

where

$$\zeta = \alpha - \frac{\beta + 1}{\sigma} = \frac{\gamma - 1}{\sigma} - \delta = 2, \quad (\text{B } 16)$$

as it should be (see § 5.2).

To summarise, the 2D spectrum (B 4) of critically balanced Alfvénic turbulence is

$$E_{2D}(k_\perp, k_\parallel) \sim \begin{cases} k_\parallel^{-10} k_\perp^3, & k_\parallel \gtrsim k_\perp^{1/2}, \\ k_\parallel^0 k_\perp^{-2}, & k_\parallel \lesssim k_\perp^{1/2}, \end{cases} \quad (\text{B } 17)$$

leading to 1D spectra $E(k_\perp) \sim k_\perp^{-3/2}$ and $E(k_\parallel) \sim k_\parallel^{-2}$. The spectra (B 17) are sketched in figure 35.

⁷⁵Such a steep scaling is probably unmeasurable in practice. Indeed, one would need to follow the perturbed field line very precisely—much more precisely than is recommended in § 5.3—in order to detect the lack of energy at large k_\parallel ; slipping off a field line even slightly would access the perpendicular variation of the turbulent fields.

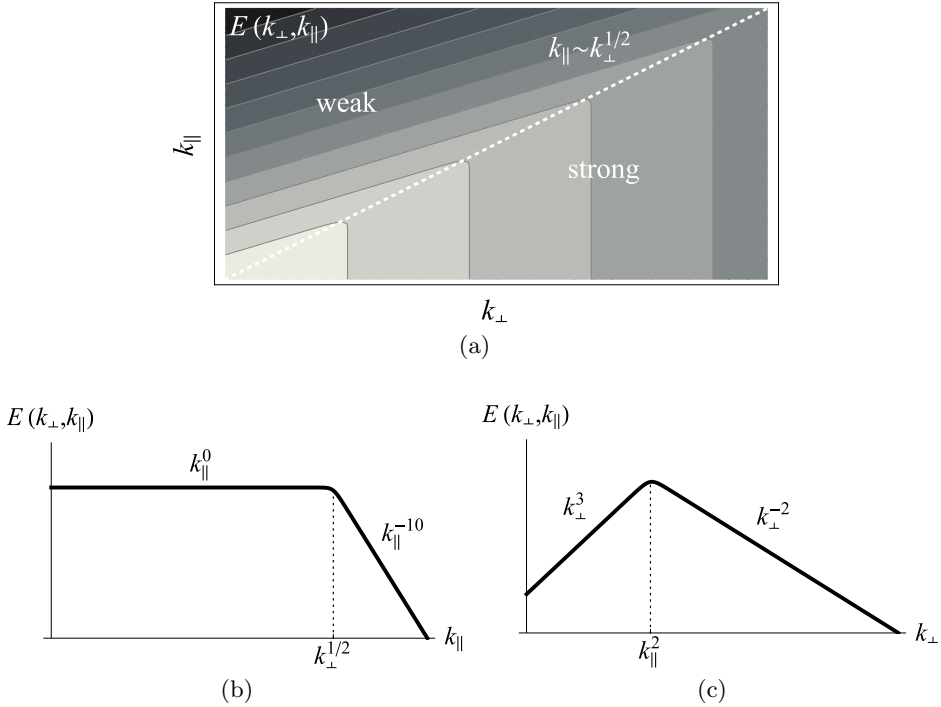


FIGURE 35. Sketch of the 2D spectra (B 17) of RMHD turbulence: (a) in the 2D wave-number plane; (b) at constant k_{\perp} ; (c) at constant k_{\parallel} . Note that k_{\parallel} here is measured along the perturbed field, not the z axis (see discussion in § 5.3).

I leave it as an exercise for the reader to show that if the same scheme is applied to the tearing-mediated turbulence described in § 7.2, the exponents in (B 4) are

$$\sigma = \frac{6}{5}, \quad \delta = 0, \quad \gamma = \frac{17}{5}, \quad \beta = 3, \quad \alpha = \frac{16}{3}, \quad \zeta = 2. \quad (\text{B } 18)$$

B.5. 2D Spectrum of WT

The 2D spectrum of broad-band-forced WT determined in appendix A.4 can easily be obtained by arguments analogous to the above:

$$\delta = 0 \quad (\text{B } 19)$$

for the same reason as in appendix B.1,

$$\gamma = \sigma + 1 \quad (\text{B } 20)$$

similarly to appendix B.2, but now employing the non-constant-flux argument (A 27),

$$\beta = -4 + \gamma = \sigma - 3 \quad (\text{B } 21)$$

by the WT condition (A 23) (where $\mu_0 = -\gamma$, $\mu = \beta$) instead of the kinematic calculation of appendix B.3, and, finally, matching the spectra as in appendix B.4, we get

$$\beta + \gamma = (\alpha + \delta)\sigma \quad \Rightarrow \quad 2(\sigma - 1) = \alpha\sigma. \quad (\text{B } 22)$$

Here we can either set $\sigma = 1$ by assuming a nonaligned cascade of the condensate, as in (A 29), and hence get $\alpha = 0$, or set $\alpha = 0$ by assuming no parallel cascade and equal forcing at all k_{\parallel} in the WT regime, in which case the matching condition (B 22) requires

$\sigma = 1$ (and so I would have had to contend with discontinuous spectra if, in appendix A.4, I had allowed the condensate to have alignment). Thus,

$$\sigma = 1, \quad \delta = 0, \quad \gamma = 2, \quad \beta = -2, \quad \alpha = 0. \quad (\text{B } 23)$$

Note that the 2D spectrum in the strongly nonlinear region $k_{\parallel} \lesssim k_{\perp}^{\sigma}$ does not actually change at the transition from the WT to the CB turbulence—spectral continuity vindicated.

Appendix C. A Reconnection Primer

Since it is now clear that reconnection phenomena play an essential role in MHD turbulence, it is useful to provide a series of shortcuts to the key results. I will not do any precise calculations of the kind that make the theory of resistive MHD instabilities such a mathematically accomplished subject (what better example on which to teach an undergraduate class to solve ODEs with boundary layers than the many incarnations of the tearing mode!), but will instead go for “quick and dirty” ways of getting at the right scalings. Readers yearning for more exactitude will find it, e.g., in a recent treatment by [Boldyrev & Loureiro \(2018\)](#).

When dealing with resistive MHD instabilities, it is convenient to write the RMHD equations in their original form ([Strauss 1976](#)), in terms of the stream (flux) functions for the velocity and magnetic fields:

$$\mathbf{u}_{\perp} = \hat{\mathbf{z}} \times \nabla_{\perp} \Phi, \quad \mathbf{b}_{\perp} = \hat{\mathbf{z}} \times \nabla_{\perp} \Psi. \quad (\text{C } 1)$$

Since $\zeta^{\pm} = \Phi \pm \Psi$, we can recover these equations from (A 2) or, indeed, use (C 1) and derive them directly from the momentum and induction equations of MHD (see [Schekochihin et al. 2009](#), [Oughton et al. 2017](#) and references therein):

$$\frac{\partial}{\partial t} \nabla_{\perp}^2 \Phi + \{\Phi, \nabla_{\perp}^2 \Phi\} = v_A \nabla_{\parallel} \nabla_{\perp}^2 \Psi + \{\Psi, \nabla_{\perp}^2 \Psi\} + \nu \nabla_{\perp}^4 \Phi, \quad (\text{C } 2)$$

$$\frac{\partial}{\partial t} \Psi + \{\Phi, \Psi\} = v_A \nabla_{\parallel} \Phi + \eta \nabla_{\perp}^2 \Psi, \quad (\text{C } 3)$$

where the difference between the Ohmic diffusivity η and viscosity ν has been restored.

C.1. Tearing Instability

Let us ignore parallel derivatives in (C 2–C 3) and consider small perturbations of a simple static equilibrium in which the in-plane magnetic field points in the y direction and reverses direction at $x = 0$:

$$\Phi = \phi(x, y)e^{\gamma t}, \quad \Psi = \Psi_0(x) + \psi(x, y)e^{\gamma t} \quad \Rightarrow \quad \mathbf{b}_{\perp} = \hat{\mathbf{y}}b_0(x) + \hat{\mathbf{z}} \times \nabla_{\perp} \psi e^{\gamma t}, \quad (\text{C } 4)$$

where $b_0(x) = \Psi_0'(x)$ is an odd function (the equilibrium field reverses direction at $x = 0$) and γ is the rate at which perturbations will grow (if they are interesting). Now linearise the RMHD equations (C 2–C 3) and Fourier-transform them in the y direction:

$$[\gamma - \nu(\partial_x^2 - k_y^2)] (\partial_x^2 - k_y^2)\phi = ik_y [b_0(x)(\partial_x^2 - k_y^2) - b_0''(x)] \psi, \quad (\text{C } 5)$$

$$[\gamma - \eta(\partial_x^2 - k_y^2)] \psi = ik_y b_0(x)\phi. \quad (\text{C } 6)$$

When η is small, this system has a boundary layer around $x = 0$, of width δ_{in} , outside which the solution is an ideal-MHD one and inside which resistivity is important and reconnection occurs.

C.1.1. *Outer Solution*

If we assume that the outer-region solution has scale λ and

$$\tau_\eta^{-1} \equiv \frac{\eta}{\lambda^2} \sim \tau_\nu^{-1} \equiv \frac{\nu}{\lambda^2} \ll \gamma \ll \tau_{A_y}^{-1} \equiv \frac{v_{A_y}}{\lambda}, \quad (\text{C7})$$

where $v_{A_y} \equiv \lambda b'_0(0)$, then the outer solution satisfies

$$\partial_x^2 \psi = \left[k_y^2 + \frac{b''_0(x)}{b_0(x)} \right] \psi, \quad \phi = -\frac{i\gamma}{k_y b_0(x)} \psi. \quad (\text{C8})$$

Since ψ is even and the magnetic field $b_y = \partial_x \psi$ must reverse direction at $x = 0$, ψ has a discontinuous derivative (figure 36). This corresponds to a singular current that is developed by the ideal-MHD solution as it approaches the boundary layer—with the singularity resolved inside the layer by resistivity. The solutions outside and inside the layer are matched to each other by equating the discontinuity in the former to the total change in $\partial_x \psi$ calculated from the latter:

$$\Delta' = \frac{[\partial_x \psi_{\text{out}}]_{-0}^{+0}}{\psi_{\text{out}}(0)} = \frac{2}{\delta_{\text{in}}} \int_0^\infty dX \frac{\partial_X^2 \psi_{\text{in}}(X)}{\psi_{\text{in}}(0)}, \quad (\text{C9})$$

where $\psi_{\text{out}}(x) = \psi(x)$ is the outer solution, $\psi_{\text{in}}(X) = \psi(X\delta_{\text{in}})$ is the inner one, and $X = x/\delta_{\text{in}}$ is the “inner” variable, rescaled to the current layer’s width δ_{in} .

To find Δ' from the outer solution, one must solve (C8) for some particular form of $b_0(x)$. For our purposes, all we need is the asymptotic behaviour of Δ' in the limit of $k_y \lambda \ll 1$, where λ is the characteristic scale of $b_0(x)$. While in general this asymptotic depends on the functional form of $b_0(x)$, it is (see appendix C.1.2)

$$\Delta' \sim \frac{1}{k_y \lambda^2} \quad (\text{C10})$$

if one can assume that $b_0(x)$ varies faster at $|x| \lesssim \lambda$, in the region where it reverses direction, than at $|x| \gg \lambda$, where it might be approximately flat. An example of such a situation is the exactly solvable and ubiquitously useful Harris (1962) sheet $b_0(x) = v_{A_y} \tanh(x/\lambda)$. This situation might be particularly relevant because in ideal MHD, field-reversing configurations of the kind that we need to support a tearing mode tend to be collapsing sheets, with λ shrinking dynamically compared to the characteristic scales in the y direction or indeed in the x direction away from the field-reversal region (see further discussion in appendix C.4).

C.1.2. *Scaling of Δ'*

A reader who is happy to accept (C10) can now skip to appendix C.1.3. For those who would like to see a more detailed derivation leading to (C10), let me put forward the following argument, which is adapted from Loureiro *et al.* (2007, 2013a).

Consider first $|x| \lesssim \lambda$. Since $b''_0/b_0 \sim 1/\lambda^2 \gg k_y^2$, we may neglect the k_y^2 term in (C8) and seek a solution in the form $\psi = b_0(x)\chi(x)$. This allows us to integrate the equation directly, with the result

$$\psi = b_0(x) \left[C_1^\pm + C_2^\pm \int_{\pm x_0}^x \frac{dx'}{b_0^2(x')} \right], \quad (\text{C11})$$

where \pm refer to solutions at positive and negative x , respectively, $C_{1,2}^\pm$ are integration constants and $x_0 \sim \lambda$ is some integration limit, whose precise value does not matter (any

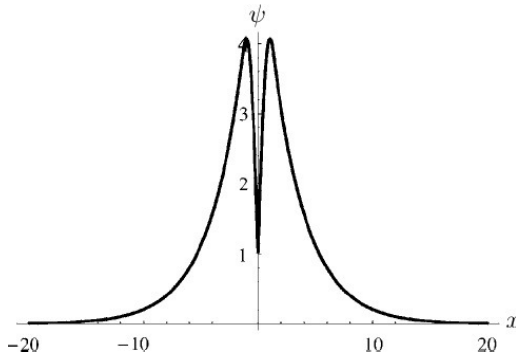


FIGURE 36. The outer solution for a tearing mode in a large-aspect-ratio sheet (adapted from Loureiro *et al.* 2007). Δ' measures the discontinuity of $\partial_x \psi$ at $x = 0$ [see (C9)].

difference that it makes can be absorbed into C_1^\pm). Since $b_0(x)$ is an odd function,

$$b_0(x) \approx \frac{x}{\lambda} v_{Ay} \quad \text{at } |x| \ll \lambda. \quad (\text{C12})$$

Taking $x \rightarrow 0$ in (C11), we can, therefore, fix the constant C_2^\pm via

$$\psi(0) = -C_2^\pm \frac{\lambda}{v_{Ay}}. \quad (\text{C13})$$

Considering now $|x| \gg \lambda$ and assuming that $b_0(x) \rightarrow \pm v_{Ay}^{(\infty)} = \text{const}$ as $x \rightarrow \pm\infty$, we find that the solution (C11) asymptotes to

$$\psi \approx \pm C_1^\pm v_{Ay}^{(\infty)} \mp \psi(0) \frac{v_{Ay}}{v_{Ay}^{(\infty)}} \frac{x}{\lambda}. \quad (\text{C14})$$

But in this limit $b_0''/b_0 \rightarrow 0$ by assumption, so we must solve (C8) neglecting the b_0''/b_0 terms while retaining k_y^2 and then match the resulting solution to (C14). The solution that vanishes at infinity is

$$\psi = C_3^\pm e^{\mp k_y x} \quad (\text{C15})$$

and its $k_y x \ll 1$ asymptotic is

$$\psi \approx C_3^\pm \mp C_3^\pm k_y x. \quad (\text{C16})$$

Demanding that this match (C14), we get

$$C_3^\pm = \frac{v_{Ay}}{v_{Ay}^{(\infty)}} \frac{\psi(0)}{k_y \lambda}, \quad C_1^\pm = \pm \frac{C_3^\pm}{v_{Ay}^{(\infty)}}. \quad (\text{C17})$$

Finally, returning to (C11) and using (C12), we obtain, for $k_y \lambda \ll 1$,

$$\Delta' = \frac{\psi'(+0) - \psi'(-0)}{\psi(0)} \approx \frac{v_{Ay}}{\lambda} \frac{C_1^+ - C_1^-}{\psi(0)} = 2 \left(\frac{v_{Ay}}{v_{Ay}^{(\infty)}} \right)^2 \frac{1}{k_y \lambda^2} \sim \frac{1}{k_y \lambda^2}, \quad \text{q.e.d.} \quad (\text{C18})$$

Pending detailed insight into the functional form of the aligned fluctuations in MHD turbulence, I am going to treat this scaling of Δ' with k_y and λ as generic. A formally more general scaling

$$\Delta' \lambda \sim \frac{1}{(k_y \lambda)^n} \quad (\text{C19})$$

corresponds, for $n > 1$, to $b_0(x)$ decaying to zero at large x on the same scale as it reverses

direction around $x = 0$: e.g., one gets $n = 2$ for $b_0(x) = v_{Ay} \tanh(x/\lambda)/\cosh^2(x/\lambda)$ (Porcelli *et al.* 2002), or for a simple sinusoidal profile. There is some space for discussion as to whether $n = 1$ or $n = 2$ is the best model for what happens in a typical MHD-turbulent structure (cf. Walker *et al.* 2018). Generalising all the scalings derived throughout this review to arbitrary n is a tedious but straightforward exercise (Del Sarto *et al.* 2016; Loureiro & Boldyrev 2017a; Pucci *et al.* 2018; Singh *et al.* 2019), which I have opted to forgo, to avoid bulky n -dependent exponents everywhere. A meticulous reader who wishes to do this exercise will find the tearing-mode scalings for arbitrary n in appendix C.1.5.

C.1.3. Inner Solution

In the inner region, whose width is δ_{in} , we can approximate the equilibrium magnetic field's profile by (C12). Since $k_y \ll \partial_x \sim \delta_{\text{in}}^{-1}$, the equations (C5) and (C6) for the tearing perturbation become

$$(\gamma - \nu \partial_x^2) \partial_x^2 \phi = ik_y \frac{x}{\lambda} v_{Ay} \partial_x^2 \psi, \quad (\text{C20})$$

$$(\gamma - \eta \partial_x^2) \psi = ik_y \frac{x}{\lambda} v_{Ay} \phi. \quad (\text{C21})$$

Combining them, we get

$$\partial_x^2 \psi = - \left(\frac{\gamma \lambda}{k_y v_{Ay}} \right)^2 \frac{1}{x} \left(1 - \frac{\nu}{\gamma} \partial_x^2 \right) \partial_x^2 \frac{1}{x} \left(1 - \frac{\eta}{\gamma} \partial_x^2 \right) \psi. \quad (\text{C22})$$

This immediately tells us what the width of the boundary layer is:

$$\frac{\nu}{\gamma \delta_{\text{in}}^2} \ll 1 \quad \Rightarrow \quad \left(\frac{\gamma \lambda}{k_y v_{Ay}} \right)^2 \frac{\eta}{\gamma \delta_{\text{in}}^4} \sim 1 \quad \Rightarrow \quad \frac{\delta_{\text{in}}}{\lambda} \sim \left(\frac{\gamma \tau_{Ay}^2}{\tau_\eta} \right)^{1/4} \frac{1}{(k_y \lambda)^{1/2}}, \quad (\text{C23})$$

$$\frac{\nu}{\gamma \delta_{\text{in}}^2} \gg 1 \quad \Rightarrow \quad \left(\frac{\gamma \lambda}{k_y v_{Ay}} \right)^2 \frac{\eta \nu}{\gamma^2 \delta_{\text{in}}^6} \sim 1 \quad \Rightarrow \quad \frac{\delta_{\text{in}}}{\lambda} \sim \left(\frac{\tau_{Ay}^2}{\tau_\eta \tau_\nu} \right)^{1/6} \frac{1}{(k_y \lambda)^{1/3}}. \quad (\text{C24})$$

The latter regime, in which viscosity is large, is a slightly less popular version of the tearing mode, but it can be treated together with the classic limit (C23) at little extra cost.

Let us now rescale $x = X \delta_{\text{in}}$ in (C22). Then $\psi_{\text{in}}(X) = \psi(X \delta_{\text{in}})$ satisfies

$$\frac{\nu}{\gamma \delta_{\text{in}}^2} \ll 1 \quad \Rightarrow \quad \partial_X^2 \psi_{\text{in}} = -\frac{1}{X} \partial_X^2 \frac{1}{X} (A - \partial_X^2) \psi_{\text{in}}, \quad A = \left(\frac{\gamma \lambda}{k_y v_{Ay}} \right)^2 \frac{1}{\delta_{\text{in}}^2}, \quad (\text{C25})$$

$$\frac{\nu}{\gamma \delta_{\text{in}}^2} \gg 1 \quad \Rightarrow \quad \partial_X^2 \psi_{\text{in}} = \frac{1}{X} \partial_X^4 \frac{1}{X} (A - \partial_X^2) \psi_{\text{in}}, \quad A = \left(\frac{\gamma \lambda}{k_y v_{Ay}} \right)^2 \frac{\nu}{\gamma \delta_{\text{in}}^4}. \quad (\text{C26})$$

In both cases, the inner solution depends on a single dimensionless parameter A (the eigenvalue). In view of (C23–C24), this parameter is, in both cases, just the ratio of the growth rate of the mode to the rate of resistive diffusion across a layer of width δ_{in} , with

the appropriate scaling of δ_{in} :

$$\Lambda \sim \frac{\gamma \delta_{\text{in}}^2}{\eta} \sim \begin{cases} \frac{\gamma^{3/2} \tau_\eta^{1/2} \tau_{\text{Ay}}}{k_y \lambda} \sim \frac{(\gamma \tau_{\text{Ay}})^{3/2}}{k_y \lambda} S_\lambda^{1/2}, & \frac{\nu}{\gamma \delta_{\text{in}}^2} \sim \frac{\text{Pm}}{\Lambda} \ll 1, \\ \frac{\gamma \tau_\eta^{2/3} \tau_\nu^{-1/3} \tau_{\text{Ay}}^{2/3}}{(k_y \lambda)^{2/3}} \sim \left[\frac{(\gamma \tau_{\text{Ay}})^{3/2}}{k_y \lambda} (S_\lambda \text{Pm})^{1/2} \right]^{2/3}, & \frac{\nu}{\gamma \delta_{\text{in}}^2} \sim \frac{\text{Pm}}{\Lambda} \gg 1, \end{cases} \quad (\text{C } 27)$$

where the Lundquist number (associated with scale λ) and the magnetic Prandtl number are defined as follows:

$$S_\lambda = \frac{\tau_\eta}{\tau_{\text{Ay}}} = \frac{v_{\text{Ay}} \lambda}{\eta}, \quad \text{Pm} = \frac{\tau_\eta}{\tau_\nu} = \frac{\nu}{\eta}. \quad (\text{C } 28)$$

C.1.4. Peak Growth Rate and Wavenumber

Whatever the specific form of the solution of (C 25) (Coppi *et al.* 1976) or (C 26), Δ' calculated from it according to (C 9) (and non-dimensionalised) must be a function only of Λ :

$$\Delta' \delta_{\text{in}} = f(\Lambda). \quad (\text{C } 29)$$

Equating this to the the value (C 10) calculated from the outer solution, we arrive at an equation for Λ :

$$f(\Lambda) \sim \frac{\delta_{\text{in}}}{k_y \lambda^2} \sim \begin{cases} \frac{\gamma^{1/4} \tau_{\text{Ay}}^{1/2} \tau_\eta^{-1/4}}{(k_y \lambda)^{3/2}} \sim \Lambda^{1/6} (k_y \lambda S_\lambda^{1/4})^{-4/3}, & \text{Pm} \ll \Lambda, \\ \frac{\tau_{\text{Ay}}^{1/3} (\tau_\eta \tau_\nu)^{-1/6}}{(k_y \lambda)^{4/3}} \sim (k_y \lambda S_\lambda^{1/4} \text{Pm}^{-1/8})^{-4/3}, & \text{Pm} \gg \Lambda. \end{cases} \quad (\text{C } 30)$$

Since the function $f(\Lambda)$ does not depend on any parameters apart from Λ , one might argue that the maximum growth of the tearing mode should occur at $\Lambda \sim 1$, when $f(\Lambda) \sim 1$. Using these estimates in (C 30) and (C 27), we find

$$k_y \lambda \sim S_\lambda^{-1/4} (1 + \text{Pm})^{1/8} \equiv k_* \lambda \quad \Rightarrow \quad \gamma \tau_{\text{Ay}} \sim S_\lambda^{-1/2} (1 + \text{Pm})^{-1/4}, \quad (\text{C } 31)$$

where Pm only matters if it is large. Note that if $S_\lambda \gg (1 + \text{Pm})^{1/2}$, the assumption $k_y \lambda \ll 1$ is confirmed. These are the maximum growth rate and the corresponding wavenumber of the tearing mode.⁷⁶ Note that, for this solution, since $f(\Lambda) \sim 1$, (C 30) gives us

$$\frac{\delta_{\text{in}}}{\lambda} \sim k_* \lambda. \quad (\text{C } 32)$$

If setting $\Lambda \sim 1$, $f(\Lambda) \sim 1$ does not feel inevitable to the reader, perhaps the following considerations will help solidify the case for it. Let us consider two physically meaningful limits that do not satisfy these assumptions.

First, let us ask what happens if $\Lambda \ll 1$. This means that the mode grows slowly compared to the Ohmic diffusion rate in the current layer, $\gamma \ll \eta / \delta_{\text{in}}^2$, a situation that corresponds, in a sense that is to be quantified in a moment, to small Δ' . In this limit, $f(\Lambda) \sim \Lambda$ to lowest order in the expansion. Putting this into (C 30) and using (C 27) to

⁷⁶I picked up the general idea of this argument from J. B. Taylor (2010, private communication); it is a slight generalisation of his treatment of the tearing mode in Taylor & Newton (2015).

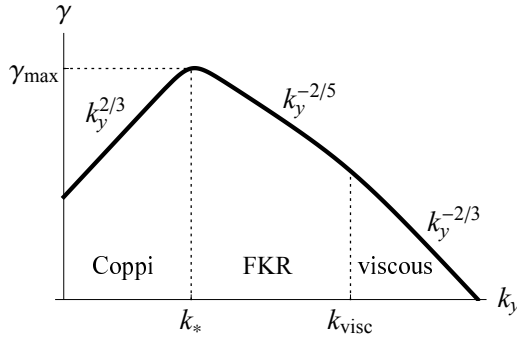


FIGURE 37. Tearing growth rate γ vs. k_y : the Coppi *et al.* (1976) solution (C 35) for $k_y \ll k_*$, where k_* is given in (C 31), and the FKR solution (C 33) at $k_y \gg k_*$. The viscous version of the latter takes over at $k_y \gg k_{\text{visc}}$, where $k_{\text{visc}}\lambda \sim S_\lambda^{-1/4}\text{Pm}^{-5/8}$. This cartoon is for $\text{Pm} \ll 1$; if $\text{Pm} \gg 1$, the viscous-FKR scaling starts at k_* .

unpack Λ , we find

$$\gamma\tau_{Ay} \sim \begin{cases} S_\lambda^{-3/5}(k_y\lambda)^{-2/5}, & k_y\lambda \ll S_\lambda^{-1/4}\text{Pm}^{-5/8}, \\ S_\lambda^{-2/3}\text{Pm}^{-1/6}(k_y\lambda)^{-2/3}, & k_y\lambda \gg S_\lambda^{-1/4}\text{Pm}^{-5/8}. \end{cases} \quad (\text{C } 33)$$

This is the famous FKR solution (Furth *et al.* 1963; see also Porcelli 1987 for the large-Pm case). Since, to get it, $\Lambda \ll 1$ was assumed, substituting (C 33) into (C 27) tells us that the approximation is valid at wavenumbers exceeding the wavenumber (C 31) of peak growth, $k_y \gg k_*$. Note that this imposes an upper bound on Δ' :

$$\Delta'\lambda \sim \frac{1}{k_y\lambda} \ll \frac{1}{k_*\lambda}. \quad (\text{C } 34)$$

This is sometimes (perhaps misleadingly) called the “small- Δ' ” (or weakly driven) limit.

Let us now consider the limit opposite to (C 34), i.e., when Δ' is very large and $k_y \ll k_*$. In (C 30), this corresponds to $f(\Lambda) \rightarrow \infty$ and we argue that this limit must be reached for some value $\Lambda \sim 1$ (it is not physically reasonable to expect that $\Lambda \gg 1$, i.e., that the growth rate of the mode can be much larger than the Ohmic diffusion rate in the current layer; this reasoning is confirmed by the exact solution—see Coppi *et al.* 1976). This implies, with the aid of (C 27),

$$\gamma\tau_{Ay} \sim S_\lambda^{-1/3}(1 + \text{Pm})^{-1/3}(k_y\lambda)^{2/3}. \quad (\text{C } 35)$$

This long-wavelength (“infinite- Δ' ,” or strongly driven) limit of the tearing mode was first derived by Coppi *et al.* (1976) (and by Porcelli 1987 for the large-Pm case).

We see that the small- k_y asymptotic (C 35) is an ascending and the large- k_y one (C 33) a descending function of k_y (figure 37). The wavenumber k_* of peak growth lies in between, where these two asymptotics meet, which is quite obviously the solution (C 31).

The applicability of this solution is subject to an important caveat. The Harris-like equilibrium that was used to obtain it is a 1D configuration, implicitly assumed to extend as far in the y direction as the mode requires to develop. In reality, any sheet-like configuration forming as a result of (ideal) MHD dynamics will have a length, as well as width: $\xi \gg \lambda$, but still finite. The finiteness of ξ will limit the wavenumbers of the tearing perturbations that can develop. The fastest-growing mode (C 31) will only fit into the

sheet if

$$k_* \xi \gtrsim 1 \quad \Leftrightarrow \quad \frac{\xi}{\lambda} \gtrsim S_\lambda^{1/4} (1 + \text{Pm})^{-1/8}. \quad (\text{C } 36)$$

If this condition fails to be satisfied, i.e., if the aspect ratio of the sheet is too small, the fastest-growing mode will be the FKR mode (C 33) with the smallest possible allowed wavenumber $k_y \xi \sim 1$. Thus, low-aspect-ratio sheets will develop tearing perturbations comprising just one or two islands, whereas the high-aspect-ratio ones will spawn whole chains of them, consisting of $N \sim k_* \xi$ islands.

C.1.5. Case of Arbitrary Scaling of Δ'

As promised at the end of appendix C.1.2, here is the generalisation of the main tearing-mode scalings to the case of Δ' scaling according to (C 19). For $\Lambda \sim 1$, (C 27), which is independent of n , implies

$$\gamma \tau_{Ay} \sim (k_* \lambda)^{2/3} S_\lambda^{-1/3} (1 + \text{Pm})^{-1/3}, \quad \frac{\delta_{\text{in}}}{\lambda} \sim (k_* \lambda)^{-1/3} S_\lambda^{-1/3} (1 + \text{Pm})^{1/6}. \quad (\text{C } 37)$$

Using (C 19) in (C 29) and setting $f(\Lambda) \sim 1$ gets us, instead of (C 32),

$$\frac{\delta_{\text{in}}}{\lambda} \sim (k_* \lambda)^n. \quad (\text{C } 38)$$

Combining this with (C 37) leads to the generalised version of (C 31):

$$k_* \lambda \sim S_\lambda^{-1/(3n+1)} (1 + \text{Pm})^{1/2(3n+1)}, \quad \gamma \tau_{Ay} \sim S_\lambda^{-(n+1)/(3n+1)} (1 + \text{Pm})^{-n/(3n+1)}. \quad (\text{C } 39)$$

C.2. Onset of Nonlinearity and Saturation of the Tearing Mode

The tearing mode normally enters a nonlinear regime when the width w of its islands becomes comparable to δ_{in} . The islands then grow secularly (Rutherford 1973) until $w \Delta' \sim 1$. As we saw in appendix C.1.4, for the fastest-growing Coppi mode, $\Delta' \sim \delta_{\text{in}}^{-1}$, so the secular-growth stage is skipped. The width of the islands at the onset of the nonlinear regime is, therefore,

$$\frac{w}{\lambda} \sim \frac{\delta_{\text{in}}}{\lambda} \sim \frac{1}{\Delta' \lambda} \sim (k_* \lambda)^n. \quad (\text{C } 40)$$

There is little overhead here for keeping n general, so I will.

The amplitudes δb_x and δb_y of the tearing perturbation at the onset of nonlinearity can be worked out by observing that the typical angular distortion of a field line due to the perturbation is

$$w k_* \sim \frac{\delta b_x}{b_0(x \sim w)}. \quad (\text{C } 41)$$

Since, from (C 12), $b_0(x \sim w) \sim (w/\lambda) v_{Ay}$, and, by solenoidality, $\delta b_y \sim \delta b_x / w k_*$, we have

$$\frac{\delta b_x}{v_{Ay}} \sim \frac{w^2 k_*}{\lambda} \sim (k_* \lambda)^{2n+1}, \quad \frac{\delta b_y}{v_{Ay}} \sim \frac{w}{\lambda} \sim (k_* \lambda)^n. \quad (\text{C } 42)$$

Note that the second of these relations implies $\delta b_y \sim b_0(x \sim w)$, i.e., the perturbed field is locally (at $x \sim w$) as large as the equilibrium field.

Let us confirm that (C 40) was a good estimate for the onset of nonlinearity, i.e., that, once it is achieved, the characteristic rate of the nonlinear evolution of the tearing perturbation becomes comparable to its linear growth rate (C 39). The nonlinear evolution rate can be estimated as $k_* \delta u_y$, where δu_y is the outflow velocity from the tearing region. When $\text{Pm} \lesssim 1$, this is obviously Alfvénic, $\delta u_y \sim \delta b_y$. When $\text{Pm} \gg 1$, the situation is

more subtle as the viscous relaxation of the flows is in fact faster than their Alfvénic evolution (as we are about to see). Then the outflow velocity must be determined from the force balance between viscous and magnetic stresses: using (C 42),

$$\frac{\nu}{w^2} \delta u_y \sim k_* \delta b_y^2 \quad \Rightarrow \quad \frac{\delta u_y}{\delta b_y} \sim \frac{k_* w^2 \delta b_y}{\nu} \sim \frac{k_* w^3 v_{Ay}}{\lambda \nu} \sim (k_* \lambda)^{3n+1} \frac{S_\lambda}{\text{Pm}} \sim \frac{1}{\sqrt{\text{Pm}}}. \quad (\text{C } 43)$$

Combining the small- and large-Pm cases, we get

$$\delta u_y \sim \frac{\delta b_y}{\sqrt{1 + \text{Pm}}} \quad \Rightarrow \quad k_* \delta u_y \sim \frac{(k_* \lambda)^{n+1} v_{Ay} / \lambda}{\sqrt{1 + \text{Pm}}} \sim \gamma. \quad (\text{C } 44)$$

In the last expression, (C 42) was used to express the perturbation amplitude and then (C 39) to ascertain that the nonlinear and linear rates are indeed the same.

Once nonlinear effects come in, the tearing perturbation becomes subject to ideal-MHD evolution (for $\text{Pm} \gg 1$, also to viscous forces). This leads to collapse of the X -points separating the islands of the tearing perturbation into current sheets (Waelbroeck 1993; Jemella *et al.* 2003, 2004). The time scale for this process is the same as that for the Coppi mode’s growth (Loureiro *et al.* 2005) (which, as we have just seen, is the same as the ideal-MHD time scale for a perturbation that is gone nonlinear). If we now assume that, as a result, the islands circularise while preserving their area in the perpendicular plane, we find the saturated island size to be

$$\frac{w_{\text{sat}}}{\lambda} \sim (w k_*^{-1})^{1/2} \sim (k_* \lambda)^{(n-1)/2}. \quad (\text{C } 45)$$

For $n = 1$, this means that, at the end of the tearing mode’s evolution, the associated perturbation finally breaks its scale separation with the equilibrium. If $n > 1$, presumably it does so later on, in the course of further reconnection within the island chain (or the assumption of area-preserving circularisation is wrong).

C.3. Sweet–Parker Sheet

Let me flesh out what was meant by the X -point collapse at the end of appendix C.2. The idea is that, once the nonlinearity takes hold and Alfvénic (or visco-Alfvénic) outflows from the reconnection region develop, the reconnecting site will suck plasma in, carrying the magnetic field with it, thus leading to formation of an extended sheet, which is a singularity from the ideal-MHD viewpoint, resolved, of course, by resistivity and acting as a funnel both for magnetic flux and plasma (figure 38). After the collapse has occurred and a sheet has been formed, the magnetic field just outside the resistive layer (the “upstream field”) is now the full equilibrium field, brought in by the incoming flow u_x of plasma. In terms of the discussion in appendix C.2, this means $\delta b_y \sim v_{Ay}$ and so the islands at the ends of the sheet are large: $w \sim \lambda$, according to (C 45) with $n = 1$. Note that for this situation, it is certainly true that $n = 1$, as the scale of the equilibrium field’s reversal within the sheet is much smaller than that of its variation outside it (and so the derivation in appendix C.1.2 applies).

C.3.1. Sweet–Parker Reconnection

The flux brought in by this flow must be destroyed by resistivity (reconnected and turned into b_x). This translates into what formally is just a statement of balance between the advective and resistive terms in the induction equation:

$$u_x v_{Ay} \sim \eta j_z \sim \eta \frac{v_{Ay}}{\delta} \quad \Rightarrow \quad \delta \sim \frac{\eta}{u_x} \sim \frac{\ell}{S_\ell} \frac{v_{Ay}}{u_x}, \quad S_\ell = \frac{v_{Ay} \ell}{\eta}, \quad (\text{C } 46)$$

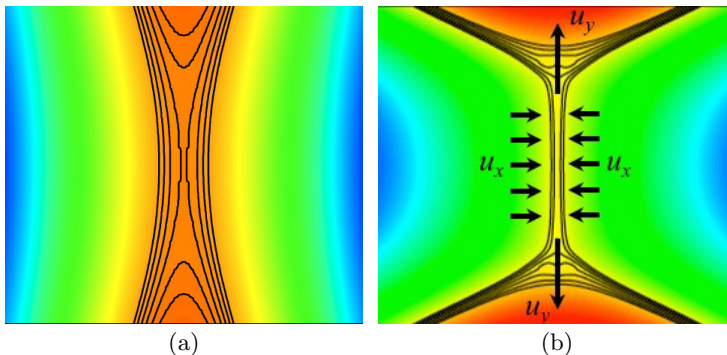


FIGURE 38. (a) An X-point, shown during the nonlinear stage of tearing mode, (b) SP current sheet, formed later on, upon collapse of that X-point (adapted from a 2D RMHD numerical simulation by Loureiro *et al.* 2005). The black lines are magnetic-field lines (constant-flux contours). The in-plane field reverses direction along the middle of the domain that is shown. In the notation of appendix C.3.1, the length of the sheet is ℓ and its width is δ .

where δ is the resistive layer’s width and u_x the inflow velocity. I have, in line with the prevailing convention (and physics) of the reconnection theory, introduced a Lundquist number based on the sheet length ℓ (in the context of a sheet formed between two islands of a tearing perturbation, this length is $\ell \sim k_*^{-1}$).

Since the sheet has to process matter as well as flux and since matter must be conserved, we may balance its inflow (u_x) and outflow (u_y):

$$u_x \ell \sim u_y \delta \quad \Rightarrow \quad u_x \sim \frac{\delta}{\ell} u_y \quad \Rightarrow \quad \delta \sim \frac{\ell}{\sqrt{S_\ell}} \left(\frac{v_{Ay}}{u_y} \right)^{1/2}, \quad (\text{C } 47)$$

where the third equation is the result of combining the second with (C 46).

Finally, the outflow velocity is inevitably Alfvénic in the absence of viscosity: this follows by balancing Reynolds and Maxwell stresses (inertia and tension) in the momentum equation (in either y or x direction; note that $b_x \sim v_{Ay} \delta / \ell$). Physically, this is just saying that the tension in the “parabolic”-shaped freshly reconnected magnetic field line (manifest in figure 38a) will accelerate plasma and propel it out of the sheet. In the presence of viscosity, i.e., when $\text{Pm} \gg 1$, we must balance the magnetic stress with the viscous one, exactly like we did in (C 43), but with a narrower channel and a greater upstream field:

$$\frac{\nu}{\delta^2} u_y \sim \frac{v_{Ay}^2}{\ell} \quad \Rightarrow \quad \frac{u_y}{v_{Ay}} \sim \frac{v_{Ay} \delta^2}{\ell \nu} \sim \frac{1}{\sqrt{\text{Pm}}}. \quad (\text{C } 48)$$

To get the last expression, δ had to be substituted from (C 47). Just as we have done everywhere else, let us combine the low- and high-Pm cases [cf. (C 44)]:

$$u_y \sim \frac{v_{Ay}}{\sqrt{1 + \text{Pm}}} \quad \Rightarrow \quad \frac{\delta}{\ell} \sim \frac{(1 + \text{Pm})^{1/4}}{\sqrt{S_\ell}} \equiv \frac{1}{\sqrt{\tilde{S}_\ell}}, \quad \tilde{S}_\ell = \frac{u_y \ell}{\eta}, \quad (\text{C } 49)$$

where \tilde{S}_ℓ , the Lundquist number based on the outflow velocity, is an obviously useful shorthand.⁷⁷ Other relevant quantities can now be calculated, e.g., the rate at which flux

⁷⁷Note that replacing in this argument $\ell \rightarrow k_*^{-1}$, $u_y \rightarrow \delta u_y$, $v_{Ay} \rightarrow \delta b_y \sim v_{Ay} w / \lambda \sim v_{Ay} k_* \lambda$ gives us back the scalings associated with the tearing mode at the onset of nonlinearity (appendix C.2), with $\delta \sim \delta_{\text{in}}$. This is, of course, inevitable as both theories are based on the same balances in the reconnection region, except the tearing before X-point collapse has a smaller upstream field δb_y .

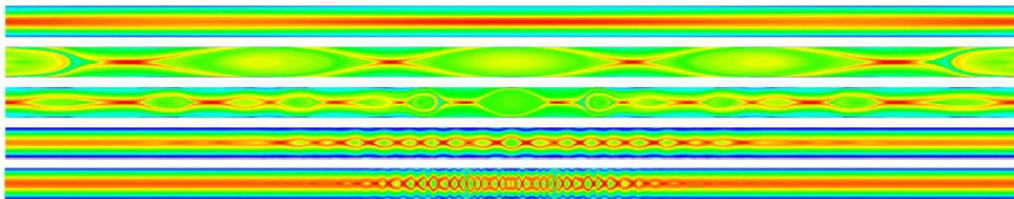


FIGURE 39. Plasmoid instability in current sheets with, from top to bottom, $S_\xi = 10^4, 10^5, 10^6, 10^7, 10^8$. The domain shown is 0.12 of the full length of the sheet. This plot is adapted from Samtaney *et al.* (2009), who confirmed the scalings (C 51) numerically.

is reconnected:

$$\frac{\partial \Psi}{\partial t} \sim u_x v_{Ay} \sim \frac{u_y v_{Ay}}{\sqrt{\tilde{S}_\ell}} \sim \frac{v_{Ay}^2}{(1 + \text{Pm})^{1/4} \sqrt{S_\ell}}. \quad (\text{C } 50)$$

The argument that I have just presented is one of the enduring classics of the genre and is due to Sweet (1958) and Parker (1957) (hereafter SP; the large-Pm extension was done by Park *et al.* 1984). While the argument is qualitative, it does work, in the sense both that one can construct unique solutions of the SP kind, in a manner pleasing to rigorous theoreticians (Uzdensky *et al.* 1996; Uzdensky & Kulsrud 2000), and that SP reconnection has been measured and confirmed experimentally (Ji *et al.* 1998, 1999) (figure 40 shows an SP sheet measured in their MRX experiment at Princeton).

C.3.2. Plasmoid Instability

However, an SP sheet is a sheet like any other and so, like for any sheet, one can work out a tearing instability for it (this is not the same tearing instability that might have given rise to the sheet as suggested at the beginning of appendix C.3—the SP sheet is the new underlying equilibrium; I will return to the idea of secondary, or recursive, tearing in appendix C.4.2). The results of appendix C.1.4 can be ported directly to this situation, by identifying $\delta = \lambda$ and $\ell = \xi$. This gives instantly

$$\gamma \sim \frac{u_y}{\xi} \tilde{S}_\xi^{1/4}, \quad k_* \xi \sim \tilde{S}_\xi^{3/8}, \quad \frac{\delta_{\text{in}}}{\delta} \sim \tilde{S}_\xi^{-1/8}. \quad (\text{C } 51)$$

This is the so-called *plasmoid instability* (Tajima & Shibata 1997; Loureiro *et al.* 2007, 2013a; Bhattacharjee *et al.* 2009; Comisso & Grasso 2016; see figure 39). The realisation that SP sheets must be unstable can be traced back to Bulanov *et al.* (1978, 1979), with the first numerical demonstration achieved by Biskamp (1986) (see also Biskamp 1982, Steinolfson & van Hoven 1984, Matthaeus & Lamkin 1985, Dahlburg *et al.* 1986, Lee & Fu 1986, and Malara *et al.* 1992). However, this knowledge did not seem to have impacted the field as much as it should have done⁷⁸ until the appearance of the analytical paper by Loureiro *et al.* (2007) and the rise of the plasmoid-chain simulation industry in 2D (Lapenta 2008; Daughton *et al.* 2009b,a; Cassak *et al.* 2009; Huang & Bhattacharjee 2010, 2012, 2013; Huang *et al.* 2017; Bárta *et al.* 2011; Loureiro *et al.* 2012; Shen *et al.* 2013; Tenerani *et al.* 2015b; Tenerani & Velli 2020b), followed, more recently, by its more turbulent counterpart in 3D (Oishi *et al.* 2015; Huang & Bhattacharjee 2016; Beresnyak 2017; Kowal *et al.* 2017; Stanier *et al.* 2019; Yang *et al.* 2020)⁷⁹ and even

⁷⁸A reader interested in history will find a useful review of secondary-tearing literature in Appendix B of Del Sarto & Ottaviani (2017).

⁷⁹In 3D, plasmoids become flux ropes, which are prone to going kink-unstable and breaking up. Their coherence length along the mean field should then be set by a CB-style argument—a

some experimental undertakings (Moser & Bellan 2012; Jara-Almonte *et al.* 2016; Hare *et al.* 2017*b,a*, 2018; Peterson *et al.* 2019). Perhaps this was because plasmoids had to wait for their moment in the sun until they could be properly resolved numerically and that required relatively large simulations. Indeed, for an SP sheet to start spawning plasmoids, a sizable Lundquist number is needed: asking for $\delta_{\text{in}}/\delta$ to be a reasonably small number, say, at least 1/3, (C 51) gives us

$$\tilde{S}_\xi \gtrsim \tilde{S}_{\xi,c}^{(\text{plasmoid})} \sim 10^4, \quad (\text{C } 52)$$

the critical Lundquist number for the plasmoid instability (Samtaney *et al.* 2009; Ni *et al.* 2010; Shi *et al.* 2018).

Arguably the most important conclusion from (C 51) is that the plasmoid instability of an SP sheet is massively supercritical: at large enough \tilde{S}_ξ , it is nowhere near marginal stability and so the question really is whether we should expect SP sheets ever to be formed in natural circumstances. This brings us to our next topic.

C.4. Formation and Disruption of Sheets

Let us put SP sheets aside and talk more generally about MHD sheets of the kind envisioned in appendix C.1 as the background equilibrium for tearing. The naturally occurring tearing-unstable ideal-MHD solutions are, in fact, not static equilibria: they arise, basically, because of the dynamical tendency in MHD for X -points to collapse into sheets (which I invoked at the transition between appendices C.2 and C.3), illustrated in figure 40. An elementary example is the classic Chapman & Kendall (1963) collapsing solution of MHD equations:

$$\Phi_0 = \Gamma(t)xy, \quad \Psi_0 = \frac{v_{\text{Ay}}}{2} \left[\frac{x^2}{\lambda(t)} - \frac{y^2}{\xi(t)} \right]. \quad (\text{C } 53)$$

Here $\Gamma(t)$ can be specified arbitrarily and then $\lambda(t)$ and $\xi(t)$ follow upon direct substitution of (C 53) into the RMHD equations (C 2–C 3) (with $\eta = 0$). The original Chapman & Kendall (1963) version of this was the exponential collapse:

$$\Gamma(t) = \Gamma_0 = \text{const}, \quad \lambda(t) = \lambda_0 e^{-2\Gamma_0 t}, \quad \xi(t) = \xi_0 e^{2\Gamma_0 t}. \quad (\text{C } 54)$$

A later, perhaps more physically relevant example, due to Uzdensky & Loureiro (2016), is obtained by fixing the outflow velocity at the end of the sheet to be a constant parameter: $u_y = \partial\Phi_0/\partial x = u_0 y/\xi$ and so

$$\Gamma(t) = \frac{u_0}{\xi(t)}, \quad \lambda(t) = \frac{\lambda_0 \xi_0}{\xi_0 + 2u_0 t}, \quad \xi(t) = \xi_0 + 2u_0 t. \quad (\text{C } 55)$$

In this, or any other conceivable model of sheet formation, the aspect ratio increases with time as the sheet's width λ decreases and its length ξ increases.

The traditional thinking about sheets in MHD held that an ideal collapsing solution such as (C 53) (or an explosively collapsing one obtained by Syrovatskii 1971 for compressible MHD) would culminate in a steady-state current sheet, which, from the ideal-MHD point of view, would be a singularity, but resolved in resistive MHD by Ohmic diffusion, leading to an SP sheet. One could then discuss magnetic reconnection in such a sheet (appendix C.3.1). However, as we saw in appendix C.3.2, an examination of the stability

balance between the Alfvénic propagation time along the field and some typical perpendicular circulation time. This has not, to my knowledge, been carefully checked (except, in a different set up, by Zhou *et al.* 2020), and all of the 3D simulations cited above were outside the RMHD regime of strong guide field—see discussion in § 7.3.2.

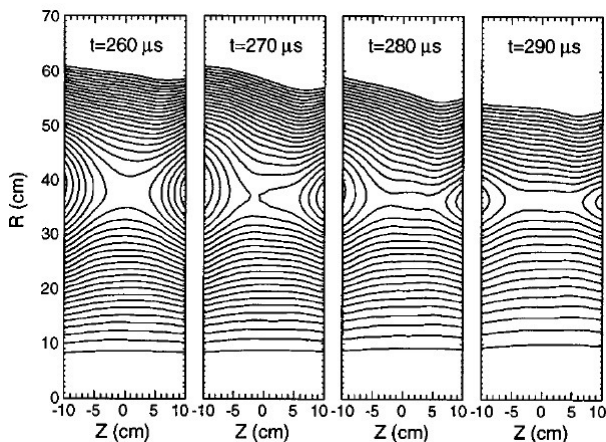


FIGURE 40. Formation of a sheet from an X -point in the MRX experiment at Princeton (plot taken from Yamada *et al.* 1997).

of this object to tearing perturbations shows that it is massively unstable and will break up into a multitude of islands (“plasmoids”). Uzdensky & Loureiro (2016) and Pucci & Velli (2014) argued that it would never form anyway as tearing perturbations growing against the background of a collapsing ideal-MHD solution will disrupt it before it reaches its steady-state, resistive SP limit.

The detailed demonstration of this result involves realising that not only does the instantaneous aspect ratio of a forming sheet decide what types of tearing perturbations are allowed (single-island FKR modes or multi-island fastest-growing, “Coppi” modes; see appendix C.1.4), but that, in principle, this can change as the sheet evolves, that many different modes can coexist and that these perturbations will grow on different time scales not only linearly but also nonlinearly (the FKR modes having to go through the secular Rutherford 1973 regime, the Coppi ones not). A careful analysis of all this can be found in the paper by Uzdensky & Loureiro (2016); the summary that will suffice for our purposes here is that if the fastest-growing linear mode (C 31) fits into the sheet, it will also be the one that first reaches the nonlinear regime and disrupts the formation of the sheet—with the moment of disruption defined as the moment when the width w of the islands associated with the perturbation becomes comparable to the width λ of the sheet.

Let us focus on the last point a little more closely. At the onset of the nonlinear regime of the tearing mode, the width of the islands is given by (C 40). Since $w \ll \lambda$, islands of this size are, in fact, short of what is needed to disrupt the sheet. Uzdensky & Loureiro (2016) argue that the collapse of the inter-island X -points, already mooted at the end of appendix C.2, will produce saturated islands of size λ [see (C 45)], just right to be properly disruptive. This is a key ingredient for the discussion of “tearing-mediated turbulence” in § 7.2.

C.4.1. “Ideal Tearing”

So what kind of sheets can form before disruption occurs? Namely, what aspect ratio can a sheet reach before the growth rate of the tearing mode triggered in the sheet becomes larger than the rate at which the sheet is collapsing via its ideal-MHD evolution? The former rate is given by (C 31) and the latter is $\Gamma \sim v_{Ay}/\xi$, as is illustrated by the

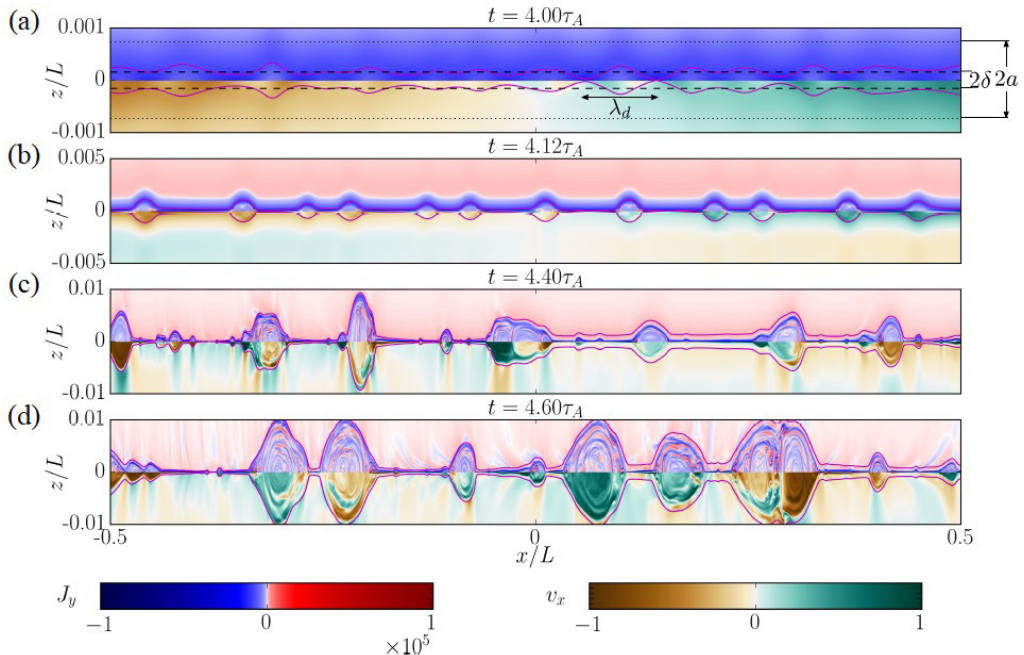


FIGURE 41. This is a plot from [Huang *et al.* \(2017\)](#) illustrating the evolution of tearing perturbations of an evolving sheet in a 2D MHD simulation with $S_\xi \sim 10^6$ and $\text{Pm} \ll 1$. Their (x, y, z) are our (y, z, x) , their L is our ξ (sheet length), their a is our λ (sheet width), their τ_A is our $\Gamma^{-1} \sim \xi/v_A$ (characteristic time of the sheet evolution), their δ is our δ_{in} (width of the tearing inner layer). The colour in the upper halves of their plots shows out-of-page current (colour bar “ J_y ”) and in the lower halves the outflow velocity along the sheet (colour bar “ v_x ”). The solid magenta lines are separatrices demarcating two “global” coalescing islands that they set up to form the sheet. The four snapshots are (a) at the moment the tearing mode goes nonlinear ($w \sim \delta_{\text{in}}$; see appendix C.2), (b) a little later, showing formation of secondary sheets (and so collapse of inter-island X -points), (c) later on, with secondary instability of these sheets manifesting itself as more plasmoids appear (cf. appendix C.4.2), and (d) in saturation, which for them is the period of stochastic but statistically steady and fast (with rate independent of S_ξ) reconnection and which obviously also corresponds to islands reaching the width of the sheet and starting to form a stochastic chain, moving and coalescing (see [Uzdensky *et al.* 2010](#) and appendix C.5). Note that all of this evolution happens within one Alfvén time, although the initial-growth stage does need a few Alfvén times to get going.

Uzdensky–Loureiro solution (C 55).⁸⁰ Then

$$\gamma \gtrsim \Gamma \quad \Leftrightarrow \quad \frac{\xi}{\lambda} \gtrsim S_\lambda^{1/2} (1 + \text{Pm})^{1/4} \quad \Leftrightarrow \quad \frac{\xi}{\lambda} \gtrsim S_\xi^{1/3} (1 + \text{Pm})^{1/6}. \quad (\text{C } 56)$$

The last expression contains the Lundquist number referred to the length ξ rather than to the width λ of the sheet, as it customarily done in magnetic-reconnection theory (cf. appendix C.3). Note that the assumption that it is the fastest-growing Coppi mode (C 31) that should be used in this estimate is confirmed *a posteriori* by checking that the

⁸⁰Assuming an Alfvénic outflow. This is fine even when $\text{Pm} \gg 1$ as long as the sheet is macroscopic, i.e., viscosity is unimportant at scale λ . If instead one is considering a microscopic “equilibrium,” like the secondary X -points between the islands of a tearing perturbation (appendix C.2), one should use $\Gamma \sim u_y/\xi$, where u_y is the visco-Alfvénic outflow: see (C 49). The condition (C 56) then becomes $\xi/\lambda \gtrsim \hat{S}_\lambda^{1/2} = S_\lambda^{1/2} (1 + \text{Pm})^{-1/4}$.

mode does fit into the sheet [cf. (C36)]: for ξ satisfying the equality in (C56),

$$k_* \xi \sim S_\lambda^{1/4} (1 + \text{Pm})^{3/8} \sim S_\xi^{1/6} (1 + \text{Pm})^{1/3} \gg 1. \quad (\text{C57})$$

The scaling (C56) of the aspect ratio of the sheet with S_ξ was proposed by Pucci & Velli (2014) to be the maximum possible attainable one before the sheet is destroyed by what they termed “ideal tearing,” i.e., by tearing modes that grow on the same time scale as the ideal-MHD sheet evolves (this result was extended to $\text{Pm} \gg 1$ by Tenerani *et al.* 2015a, then generalised by Del Sarto *et al.* 2016 and Pucci *et al.* 2018 to the case of arbitrary scaling of Δ' with k_y that I dealt with in appendix C.1.5). The conclusion that the sheet is indeed destroyed depends on the X -point-collapse argument described above, because the tearing modes by themselves do not produce islands as wide as the sheet.

The argument in §7.1 about the disruption of MHD turbulence by tearing is essentially the application of the criterion (C56) to the aligned structures of which Boldyrev’s MHD turbulent cascade consists.

Since the aspect ratio of the sheet described by (C49) is smaller than that of the SP sheet ($S_\xi^{1/3}$, rather than $S_\xi^{1/2}$), Pucci & Velli (2014) argued that global SP sheets can never form. A recent extensive numerical study by Huang *et al.* (2017) of the instability of forming current sheets has indeed confirmed explicitly that the plasmoid-instability scalings (C51) derived for an SP sheet only survive up to a certain critical value

$$S_{\xi,c}^{(\text{ideal})} \sim 10^5 - 10^6 \quad (\text{C58})$$

[which obviously has to be bigger than the critical Lundquist number (C52) for the plasmoid instability itself], with the “ideal-tearing” scalings (C56) and (C57) taking over at $S_\xi \gtrsim S_{\xi,c}^{(\text{ideal})}$.⁸¹ Figure 41, taken from their paper, is an excellent illustration of the evolution of tearing perturbations and plasmoid chains.

C.4.2. Recursive Tearing

It is not a difficult leap to realise that if a collapsing “global” MHD sheet-like configuration (which, the way it was introduced at the beginning of appendix C.4, was manifestly an X -point configuration) is unstable to tearing, the secondary X -points generated by the tearing can also be unstable to (secondary) tearing and thus might not “complete” the collapse into “proper” SP sheets that was posited for them above. This can happen if the secondary tearing has a shorter growth time than the primary one,

⁸¹They also find that $S_{\xi,c}^{(\text{ideal})}$ gets smaller when larger initial background noise is present in the system and that the onset of tearing instability (and, therefore, of fast reconnection) is generally facilitated by such noise (the same is true for the plasmoid instability of SP sheets: see Loureiro *et al.* 2009). Their paper is written in a way that might give one the impression that they disagree profoundly with both Uzdensky & Loureiro (2016) and Pucci & Velli (2014): the main point of disagreement is their observation that the disruption of the sheet happens when γ is equal a few times Γ , rather than $\gamma/\Gamma \approx 1$ [see (C56)], and that exactly how many times Γ it must be depends on the initial noise level. In the context of the turbulence-disruption arguments advanced in §7, this may be a useful practical caveat pointing to the value of λ_D [see (7.2)] possibly being an overestimate by a factor of a few. However, all theory in this review is order-unity-inaccurate “twiddle” theory, so I am not as bothered by this complication as someone attempting a quantitative numerical study might be. In any event, the fact that the disruption of the sheet is helped by more noise is surely a good thing for the validity of $\gamma/\Gamma \sim 1$ as the disruption criterion in a turbulent environment, where there is noise aplenty. Another (related) complication that matters quantitatively but probably not qualitatively is the possible presence of logarithmic corrections and other subtleties in the tearing-instability scalings for time-dependent sheets (Comisso *et al.* 2016, 2017, 2018; Huang *et al.* 2019).

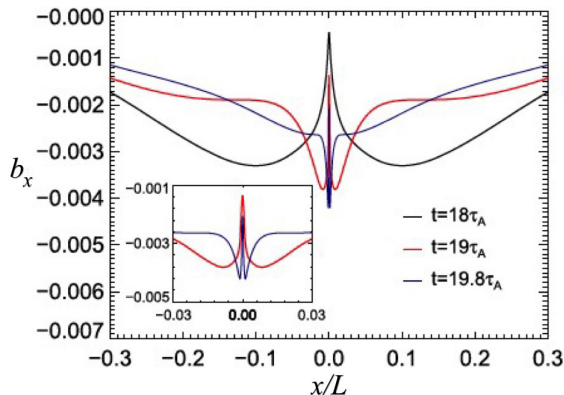


FIGURE 42. A plot, adapted from [Tenerani *et al.* \(2015b\)](#), of the $b_x = -ik_y\psi(x)$ profiles (cf. figure 36) for nested tearing modes: primary (black), secondary (red) and tertiary (blue). They extracted these from a direct numerical simulation of a recursively tearing sheet. This is a remarkably clean example of the similarity of tearing at ever smaller scales.

which, as we are about to see, is always the case. This conjures up an image of recursive tearings proceeding *ad infinitum* ([Shibata & Tanuma 2001](#); [Tenerani *et al.* 2015b, 2016](#)) or, rather, until the inter-island sheets become short enough to be stable [see (C 52)]. At that point, they can all collapse properly into reconnecting mini-SP-sheets and we are left with a multiscale population of islands, which now have time to circularise and finally break up the “mother sheet” (and/or interact with each other). For the purposes of the discussion in the main text (§ 7.2), the issue is whether we should be concerned that the outcome of this break up is not just a number of flux ropes of one size (C 45), but a whole multiscale distribution of them.

Let us work on the assumption that the secondary tearing of an inter-island X -point works in the same way as the primary tearing described in appendix C.1.4 (see figure 42), except the width of the “equilibrium” is now the island width (C 40) of the primary tearing mode at the onset of nonlinearity (cf. [Cassak & Drake 2009](#); [Del Sarto & Ottaviani 2017](#)) and the length of the secondary sheet is the wavelength k_*^{-1} of the primary mode, given by (C 31)—we already saw in appendix C.2 that fields associated with this new “equilibrium” are locally at least of the same size as the original equilibrium field. We now assign our old equilibrium parameters to the i -th level of tearing and the perturbation’s parameters (worked out in appendix C.2) to the $(i + 1)$ -st:

$$v_i \equiv v_{Ay}, \quad v_{i+1} \equiv \delta b_y, \quad \lambda_i \equiv \lambda, \quad \lambda_{i+1} \equiv w, \quad \xi_i \equiv \xi, \quad \xi_{i+1} \equiv k_*^{-1}, \quad (\text{C } 59)$$

with $i = 0$ corresponding to the mother sheet. Then

$$\gamma_i \sim \frac{u_i}{\lambda_i} \tilde{S}_i^{-1/2}, \quad \frac{v_{i+1}}{v_i} \sim \frac{\lambda_{i+1}}{\lambda_i} \sim \frac{\xi_i}{\xi_{i+1}} \sim \tilde{S}_i^{-1/4}, \quad (\text{C } 60)$$

where [cf. (C 44)]

$$u_i = \frac{v_i}{\sqrt{1 + \text{Pm}}}, \quad \tilde{S}_i = \frac{S_i}{\sqrt{1 + \text{Pm}}}, \quad S_i = \frac{v_i \lambda_i}{\eta}. \quad (\text{C } 61)$$

Using the second relation in (C 60),

$$\frac{\tilde{S}_{i+1}}{\tilde{S}_i} = \frac{v_{i+1} \lambda_{i+1}}{v_i \lambda_i} \sim \tilde{S}_i^{-1/2} \quad \Rightarrow \quad \tilde{S}_{i+1} \sim \tilde{S}_i^{1/2} \quad \Rightarrow \quad \tilde{S}_i \sim \tilde{S}_0^{(1/2)^i}. \quad (\text{C } 62)$$

If there is some critical Lundquist number \tilde{S}_c required for tearing modes to be unstable, (C 62) allows us to work out the maximum number of times that the recursive tearing will be iterated before X -points can collapse unimpeded into proper, stable, reconnecting current sheets:

$$i_{\max} \sim \ln \frac{\ln \tilde{S}_0}{\ln \tilde{S}_c}. \quad (\text{C } 63)$$

It is obvious that in practice this will not be a large number at all. However, this detail does not matter for our purposes and, in any event, thinking in wildly asymptotic terms is what theoretical physicists do, so let us press on.

The second relation in (C 60) tells us that the amplitude of the i -th perturbation is proportional to its transverse scale:

$$\frac{v_i}{\lambda_i} \sim \text{const} \sim \frac{v_0}{\lambda_0}. \quad (\text{C } 64)$$

When translated into a spectral slope, this gives k_{\perp}^{-3} , i.e., while islands at all scales below λ_0 are produced, they do not contain much energy. If this is true, we should be allowed to dismiss recursive tearing as a side show in the context of the disruption-range turbulence described in § 7.

The result (C 64) follows from the relation between the island width and the amplitude of the tearing perturbation at the onset of nonlinearity [see (C 42)]. In order for this to be usable, it must be the case that the $(i + 1)$ -st tearing starts right at the onset of nonlinearity and outperforms the collapse of the i -th tearing perturbation's X -point. This appears to be easy: in view of (C 44) and (C 60),

$$\frac{\gamma_{i+1}}{u_{i+1}/\xi_{i+1}} \sim \frac{\gamma_{i+1}}{\gamma_i} \sim \left(\frac{v_{i+1}}{v_i}\right)^{1/2} \left(\frac{\lambda_{i+1}}{\lambda_i}\right)^{-3/2} \sim \frac{\lambda_i}{\lambda_{i+1}} \sim \tilde{S}_i^{1/4} \gg 1. \quad (\text{C } 65)$$

Let us check also that the fastest-growing mode always fits into its sheet: using (C 60) and (C 62),

$$\frac{\xi_{i+1}}{\xi_i} \sim \frac{\xi_{i+1}}{\lambda_i} \frac{\lambda_i}{\lambda_{i-1}} \frac{\lambda_{i-1}}{\xi_i} \sim \tilde{S}_i^{1/4} \tilde{S}_{i-1}^{-1/2} \sim \tilde{S}_i^{-3/4} \ll 1. \quad (\text{C } 66)$$

While this all looks good, let me hedge by acknowledging that it may be a bit of a bold leap to assume that the local “equilibrium” set up by the i -th tearing perturbation, which features flows as well as fields, will be tearing unstable in exactly the same way as a very simple equilibrium used in appendix C.1. It appears, however, that the flows are only expected to be seriously stabilising if $u_{i+1}/\xi_{i+1} \sim \gamma_{i+1}$ (Bulanov *et al.* 1978, 1979; Biskamp 1986; Shi *et al.* 2018), so perhaps we are safe in that regard.

Another wrinkle in my argument is as follows. According to (C 65), the $(i + 1)$ -st tearing calculated at the onset of nonlinearity is already very fast. One might wonder how it can get to be so fast without first going through a marginal level $\gamma_{i+1} \sim u_{i+1}/\xi_{i+1}$ at an earlier stage in the evolution—which would mean (counter-intuitively and, surely, incorrectly!) that the i -th tearing perturbation should give rise to a secondary instability already in its linear regime, when it modifies its background equilibrium only slightly. I do not know how to construct a theory of this sort (the extant theories that do assume marginally unstable tearing at each level, summarised in appendix C.4.3, in fact require the secondary instability to wait till later, not earlier, in the primary's evolution). For now, I will leave this issue open, with the understanding that if the secondary tearing starts even earlier than I assumed, this will mean that the amplitudes of the secondary islands will be even lower than (C 64) implies and so my conclusion that all of this is just a side show will survive.

With these caveats duly noted, here are the explicit expressions for everything, for completeness: using (C 62) and the recursion relations given above, one gets

$$\gamma_i \sim \frac{u_0}{\lambda_0} \tilde{S}_0^{-(1/2)^{i+1}} \rightarrow \frac{u_0}{\lambda_0}, \quad (\text{C } 67)$$

$$\frac{v_i}{v_0} \sim \frac{\lambda_i}{\lambda_0} \sim \tilde{S}_0^{-[1-(1/2)^i]/2} \rightarrow \tilde{S}_0^{-1/2}, \quad (\text{C } 68)$$

$$\frac{\xi_i}{\lambda_0} \sim \tilde{S}_0^{-[1-3(1/2)^i]/2} \rightarrow \tilde{S}_0^{-1/2}. \quad (\text{C } 69)$$

The limits are all for $i \rightarrow \infty$. Note that the relationship between ξ_0 and λ_0 does not satisfy (C 69) because the first sheet in the sequence was not itself produced by tearing and ξ_0 could have been anything. Taking this first sheet to satisfy the “ideal-tearing” criterion (C 56), we find that $\xi_\infty/\xi_0 \sim S_0^{-1}$, i.e., the total number of islands generated at all levels of recursive tearing scales as S_0 .

All of this happens very quickly (on the γ_0^{-1} time scale), then the islands circularise, with only the largest ones being energetically of any consequence [see (C 64)], and the sheet breaks up. Were it to persist for a long time, everything would change in the course of the subsequent dynamics of its plasmoid (island) population: plasmoid shapes (they circularise), their number (they travel along the sheet, coalesce, and eventually get ejected from the sheet), field amplitudes in them (reconnection continues via elementary inter-plasmoid current sheets that are short enough to be stable).⁸² Such stochastic plasmoid chains have been studied numerically by many people (see references in appendix C.3.2). The statistical steady state of such a chain is, I believe, correctly described by the theoretical model of Uzdensky *et al.* (2010) (see appendix C.5). Whether it matters in tearing-mediated turbulence is discussed in § 7.3.

C.4.3. Variants of Recursive Tearing

The key difference between the “naïve” recursive model described in appendix C.4.2 and those of Shibata & Tanuma (2001) and Tenerani *et al.* (2015*b*, 2016) (both usefully reviewed by Singh *et al.* 2019) is that they assume effectively that, before any secondary tearing occurs, the X -point collapse proceeds at least far enough that the reconnecting field can be assumed the same at all levels of tearing:

$$v_i \sim v_0. \quad (\text{C } 70)$$

Secondly, they assume that the tearing at each level only just outperforms the X -point collapse, or, equivalently, the outflows:

$$\gamma_i \sim \frac{u_i}{\xi_i} \Rightarrow \frac{\lambda_i}{\xi_i} \sim \tilde{S}_i^{-1/2}. \quad (\text{C } 71)$$

This is the “ideal-tearing” threshold (C 56), except, for $\text{Pm} \gg 1$, the Alfvénic outflow is tempered by viscosity, because secondary-sheet dynamics, as well as tearing, happen at scales where viscosity matters. Finally, Shibata & Tanuma (2001) assume that the length of the sheet at the $(i + 1)$ -st level ξ_{i+1} is the wave length k_*^{-1} of the tearing mode at the

⁸²The notion that all this happens *after* recursive tearing has run its course may be a gross idealisation. I assumed implicitly (as other recursive-tearing models discussed in appendix C.4.3 do as well) that secondary tearing would be the first instability to kick in once the tearing mode becomes nonlinear—and thus ignored, e.g., the possibility, raised some time ago by Malara *et al.* (1992), that the islands produced by tearing might start coalescing *before* secondary tearing destabilises the inter-island X -points. I have not seen this scenario revisited in recent literature.

i -th level (which I also do), viz.,

$$\xi_{i+1} \sim \lambda_i \tilde{S}_i^{1/4}, \quad (\text{C } 72)$$

but let the width λ_{i+1} be determined from (C 71) (one only needs three equations for the three unknowns v_{i+1} , ξ_{i+1} , λ_{i+1}). Then, instead of (C 62), one gets

$$\frac{\tilde{S}_{i+1}}{\tilde{S}_i} \sim \frac{\lambda_{i+1}}{\lambda_i} \sim \frac{\xi_{i+1} \tilde{S}_{i+1}^{-1/2}}{\lambda_i} \sim \tilde{S}_i^{1/4} \tilde{S}_{i+1}^{-1/2} \Rightarrow \tilde{S}_{i+1} \sim \tilde{S}_i^{5/6}, \quad \text{etc.} \quad (\text{C } 73)$$

This means that the $(i+1)$ -st tearing starts only when islands grow a bit larger than δ_{in} of the i -th tearing:

$$\frac{\lambda_{i+1}}{\delta_{\text{in},i}} \sim \frac{\lambda_{i+1}}{\lambda_i \tilde{S}_i^{-1/4}} \sim \tilde{S}_i^{1/12} \gg 1. \quad (\text{C } 74)$$

In contrast, [Tenerani *et al.* \(2015b, 2016\)](#) assume (based on their simulations) that the width of the sheet at the $(i+1)$ -st level λ_{i+1} is the island width $w \sim \delta_{\text{in}}$ [see (C 40)] of the tearing mode at the i -th level (which, again, I also do), viz.,

$$\lambda_{i+1} \sim \lambda_i \tilde{S}_i^{-1/4}, \quad (\text{C } 75)$$

but let ξ_{i+1} be determined from (C 71). Then, instead of (C 73),

$$\frac{\tilde{S}_{i+1}}{\tilde{S}_i} \sim \frac{\lambda_{i+1}}{\lambda_i} \sim \tilde{S}_i^{-1/4} \Rightarrow \tilde{S}_{i+1} \sim \tilde{S}_i^{3/4}, \quad \text{etc.} \quad (\text{C } 76)$$

This effectively implies that the i -th tearing must somehow produce more, smaller islands than allowed by the wavenumber k_* of its fastest-growing mode:

$$k_{*,i} \xi_{i+1} \sim \tilde{S}_i^{-1/4} \tilde{S}_{i+1}^{1/2} \frac{\lambda_{i+1}}{\lambda_i} \sim \tilde{S}_i^{-1/8} \ll 1. \quad (\text{C } 77)$$

I do not see why the local X -point “equilibria” produced in the nonlinear stage of the primary tearing should stay stable until X -point collapse makes $v_i \sim v_0$ [which, according to (C 65), it will do slower than the notional secondary tearing perturbation would grow], but determining definitely whether they do so clearly requires a careful quantitative theory of the secondary tearing.

Note that my model can be viewed as a version of the earlier model by [Cassak & Drake \(2009\)](#), who posit that the width λ_{i+1} of the secondary sheet is the SP width δ given by (C 49) with $l \rightarrow \xi_{i+1}$ but with reduced upstream field

$$v_{Ay} \rightarrow v_{i+1} \sim v_i \frac{\lambda_{i+1}}{\lambda_i} \quad (\text{C } 78)$$

(a recent paper by [Del Sarto & Ottaviani 2017](#) takes the same view; this is sometimes referred to as the “embedding effect”). But then λ_{i+1} is nothing but δ_{in} (and, therefore, w) for a tearing mode at the onset of nonlinearity (see appendix C.2 and footnote 77). The simulations of [Cassak & Drake \(2009\)](#) appear to support the notion that secondary tearing gets going in these circumstances, but such simulations are perhaps in the eye of the beholder—thus, [Tenerani *et al.* \(2015b, 2016\)](#) claim that their simulations support their picture instead.

Do these differences matter? Not for the qualitative picture of recursive tearing quickly leading to the formation of a fully nonlinear sheet hosting a plasmoid chain—the outcome alluded to at the end of appendix C.4.2. Once this has happened, i.e., once all X -points have fully collapsed, (C 70) is certainly true at all levels ([Uzdensky *et al.* 2010](#); [Loureiro *et al.* 2012](#)). However, if it were also true and, consequently, (C 64) untrue

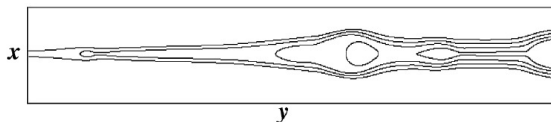


FIGURE 43. Contour plot of the magnetic flux function illustrating the open flux. This is taken from a section of a 2D MHD simulation of a plasmoid chain, reproduced from [Uzdensky *et al.* \(2010\)](#). The centre of the sheet is somewhere far away on the left.

during the initial recursive tearing, then I would not be able to disregard the role of the secondary islands in the disruption process, as I did in §7.3.1. There would then be a legitimate question of how all these islands might modify, or even completely determine, the disruption-range statistics. [Tenerani & Velli \(2020b\)](#) engaged with this question and came up with a scheme, involving their recursion relations for secondary tearing and a model of intermittency of the reconnecting sheets, to derive the spectrum of turbulence on this basis—getting $k_{\perp}^{-11/5}$ again!

C.5. Fast MHD Reconnection

I have referred several times already to the fully nonlinear plasmoid chain being the end result of recursive tearing (appendix C.4.2) and making reconnection fast (§7.3). Let me reproduce here, in broad brush, the [Uzdensky *et al.* \(2010\)](#) explanation of this regime.

Once all the X -points at all levels of recursive tearing have collapsed, the current sheet becomes a chain of plasmoids of different sizes connected by the longest SP sheets that can remain stable, i.e., ones whose “critical” length and width are

$$\ell_c \sim \frac{\tilde{S}_c \eta}{u_y}, \quad \delta_c \sim \ell_c \tilde{S}_c^{-1/2}, \quad (\text{C } 79)$$

where $u_y \sim v_{Ay}/\sqrt{1 + \text{Pm}}$ is the outflow velocity [see (C 49)] and \tilde{S}_c is the critical Lundquist number (C 52) for the plasmoid instability. The inter-plasmoid sheets cannot be any longer than ℓ_c because the moment they get stretched longer they go unstable and break up into more plasmoids. Thus, the number of plasmoids typically found in a sheet of length ℓ , in steady state, is $N \sim \ell/\ell_c \sim \tilde{S}_\ell/\tilde{S}_c$. These plasmoids are all of different sizes, having been generated at various levels of recursive tearing or as a result of coalescence of earlier-generation plasmoids. One can think of them as belonging to many hierarchical levels, with plasmoids of the n -th level living in “local” sheets bounded by pairs of $(n - 1)$ -st-level plasmoids. At every level, they are all moving along their local sheet with a mean (visco-)Alfvénic outflow u_y , the same at every level, eventually getting ejected into (coalesced with) the previous-level plasmoids.

It is surprisingly easy to argue that reconnection in such a system (illustrated by the lowest panel of figure 41) is fast. First notice that if the plasmoids travelling along the sheet and eventually ejected from it would carry no reconnected flux (no δb_x) if they only contained closed field lines. However, since the upstream (reconnecting) field v_{Ay} decreases gently from the centre of the sheet ($y = 0$) outwards along y , the reconnection on the smaller- $|y|$ side of each plasmoid is slightly faster than on the larger- $|y|$ side of it. Therefore, each plasmoid carries some open flux (figure 43) and it is the ejection of this open flux that contributes to the overall reconnection rate. At every level n in the plasmoid hierarchy, reconnection in a sheet containing n -th-and-higher-level plasmoids and bounded by two $(n - 1)$ -st-level ones adds to the open flux enveloping the $(n - 1)$ -st-level plasmoid on the larger- $|y|$ side and subtracts from the one on the smaller- $|y|$ side.

The overall reconnected flux is the sum over these contributions, all of which cancel each other except for the one from the centre of the sheet. Thus, the overall reconnection rate is just the reconnection rate in the central elementary sheet, given by (C 50) with the critical Lundquist number \tilde{S}_c :

$$\frac{\partial \Psi}{\partial t} \sim \tilde{S}_c^{-1/2} u_y v_{Ay} \sim 10^{-2} (1 + \text{Pm})^{-1/2} v_{Ay}^2, \quad (\text{C } 80)$$

independent of the actual Lundquist number \tilde{S}_ℓ and the same at every level in the hierarchy.

This result can be rederived (or re-interpreted) as a modification of the SP reconnection (proposed by Shibata & Tanuma 2001) in which the effective width $\delta_{\text{eff}}^{(n-1)}$ of the sheet (whose length is $\ell^{(n-1)}$) connecting the $(n-1)$ -st-level plasmoids, for the purposes of mass (and with it, flux) ejection, is the width of the largest plasmoids in that sheet, which are the n -th-level plasmoids. Then the reconnection rate in such a sheet, i.e., the rate of growth of the flux $\Psi^{(n-1)}$ in the $(n-1)$ -st-level plasmoids, is

$$\frac{\partial \Psi^{(n-1)}}{\partial t} \sim u_x^{(n-1)} v_{Ay} \sim \frac{\delta_{\text{eff}}^{(n-1)}}{\ell^{(n-1)}} u_y v_{Ay}, \quad \delta_{\text{eff}}^{(n-1)} \sim w^{(n)}, \quad (\text{C } 81)$$

where the inflow velocity $u_x^{(n-1)}$ has been calculated from mass conservation, as in (C 47), and the (visco-)Alfvénic outflow u_y is the same at every level of the hierarchy, because the inter-plasmoid X -points are all fully collapsed, so the upstream field is v_{Ay} at every level. The n -th-level plasmoids' width is then found by letting the perturbed field inside them be comparable to that upstream field:

$$\delta b_y^{(n)} \sim \frac{\Psi^{(n)}}{w^{(n)}} \sim v_{Ay} \quad \Rightarrow \quad w^{(n)} \sim \frac{\Psi^{(n)}}{v_{Ay}}. \quad (\text{C } 82)$$

Finally, the flux typically contained inside the n -th-level plasmoid can be estimated as the reconnection rate at that level times the time that an n -th-level plasmoid will take to travel out of the $(n-1)$ -st-level sheet:⁸³

$$\Psi^{(n)} \sim \frac{\ell^{(n-1)}}{u_y} \frac{\partial \Psi^{(n)}}{\partial t}. \quad (\text{C } 83)$$

Combining (C 81–C 83), we get

$$\frac{\partial \Psi^{(n-1)}}{\partial t} \sim \frac{\partial \Psi^{(n)}}{\partial t}, \quad (\text{C } 84)$$

so the reconnection rate is the same at every level and thus equal to the reconnection rate (C 80) at $n \rightarrow \infty$, i.e., in the most elementary sheet, q.e.d.

Thus, the basic reason for reconnection becoming fast in this way is that plasmoids make the SP sheet effectively fatter, relieving the severe constraint that pumping mass and flux through a narrow funnel would otherwise impose. The only remaining constraint is the need to get the SP sheet to be at least as long as ℓ_c in order for it to be able to break up into plasmoids.

⁸³This estimate, combined with (C 80), immediately allows one to determine the distribution function of the plasmoid fluxes—not necessary for the purposes of the present argument, but a nice falsifiable result. The number of plasmoids with $\Psi > \Psi^{(n)}$ in the sheet of overall length ℓ is $N(\Psi^{(n)}) \sim \ell/\ell^{(n-1)} \propto 1/\Psi^{(n)}$. Therefore, the plasmoid-flux distribution function is $f(\Psi) \propto \Psi^{-2}$ and, by (C 82), the plasmoid-width distribution function is $f(w) \propto w^{-2}$. These scalings are indeed corroborated numerically (Loureiro *et al.* 2012, see figure 44b).

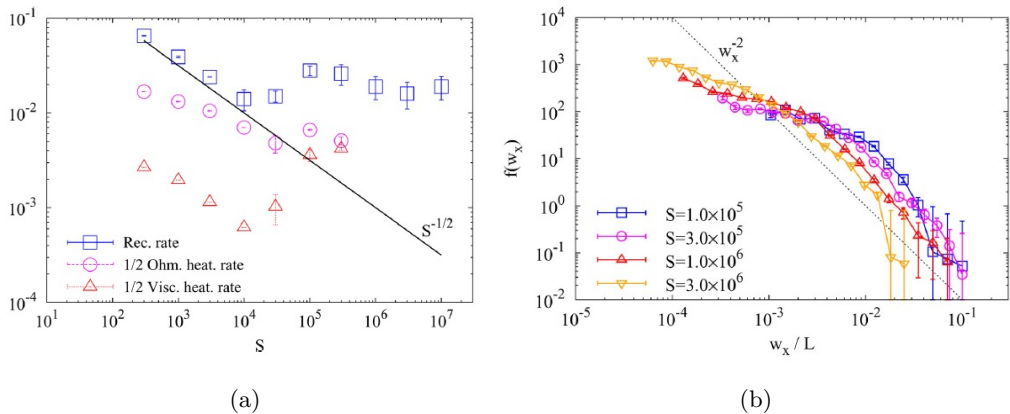


FIGURE 44. (a) Reconnection rate (blue squares), normalised, in my notation, to $u_y v_{Ay}$, in 2D MHD $\text{Pm} = 1$ simulations by Loureiro *et al.* (2012), from whose paper these plots are reproduced. Transition at $S_\ell \sim 10^4$ from the SP scaling to the fast-reconnection regime (C 80) is manifest. (b) Plasmoid-width distribution function in the same simulations, from the same paper, confirming the scaling predicted by Uzdensky *et al.* (2010) (see footnote 83).

The fact that SP reconnection transitions to a fast, plasmoid-dominated regime at $S_\ell \gtrsim S_c \sim 10^4$, with the reconnection rate set by S_c , was confirmed numerically by Bhattacharjee *et al.* (2009), Loureiro *et al.* (2012, see figure 44a) and in numerous subsequent simulations (many of them cited in appendix C.3.2).

In the next section, I will discuss another, quite different, way in which reconnection can be fast, when it is submerged in a turbulent environment.

C.6. Stochastic Reconnection and MHD Turbulence

In this busy world, writing one’s own papers tends to take precedence over reading other people’s. And so the developments that I described in §§ 6–7 appear to have been, for the most part, intellectually decoupled from another strand of thinking, vaguely anticipated by Matthaeus & Lamkin (1985, 1986) and properly launched by Lazarian & Vishniac (1999) when they put forward the notion of “stochastic reconnection”—a widely cited paper, which, however, has acquired the reputation of being rather hard to understand. Eyink *et al.* (2011) seem to me to have succeeded in explaining it with a degree of clarity by adopting somewhat different terms, based on a sizable body of precursor work by Eyink (2009, 2011). There are many self-reviews of this school of thought, of which the most recent and comprehensive one is Lazarian *et al.* (2020), so my exposition will focus only on the direct implications for the models of turbulence discussed in the main part of this review. The idea is roughly as follows.

First, let us note that, instead of (C 46), we may follow Kulsrud (2005) and start our consideration of an SP sheet by stating that the width of the sheet must be equal to the typical distance that the field lines would diffuse resistively in the direction (x) transverse to the upstream field over the time that it takes the plasma to transit through the sheet and be ejected out of it, viz.,

$$\delta \sim (\eta t_{\text{out}})^{1/2}, \quad t_{\text{out}} \sim \frac{\ell}{u_y} \quad \Rightarrow \quad \delta \sim \left(\frac{\eta \ell}{u_y} \right)^{1/2} \sim \frac{\ell}{\sqrt{S_\ell}} \left(\frac{v_{Ay}}{u_y} \right)^{1/2}, \quad (\text{C } 85)$$

which is the same expression as in (C 47).

Lazarian & Vishniac (1999), as interpreted by Eyink *et al.* (2011),⁸⁴ argue that if the sheet is embedded in a turbulent environment, δ should instead be calculated as the distance by which two magnetic field lines initially starting arbitrarily close-by separate after time t_{out} and that this distance is the same as the distance by which two Lagrangian fluid particles separate. It is this identification between stochastic particle trajectories and field lines that requires all the work contained in Eyink (2009, 2011). In formal terms, he is able to prove that, in the presence of resistivity, the magnetic field at any point in space and time is an average over the realisations of a stochastic field that end up at that point after evolving as “virtual” magnetic fields “frozen” into a stochastic flow that is the superposition of the Lagrangian turbulent velocity field and a white noise with the diffusion constant η . However small is η , such fields diverge in the same way as Lagrangian trajectories do. Eyink *et al.* (2013) successfully tested this proposition in a large numerical simulation of MHD turbulence.

In fluid dynamics, the stochastic separation of Lagrangian trajectories is known as Richardson diffusion, and one argues, with Richardson (1926), that the rate of change of the typical square distance Δr^2 between them is the turbulent diffusivity associated with velocities at the scale Δr :

$$\frac{d\Delta r^2}{dt} \sim D(\Delta r) \sim \delta u_{\Delta r}^2 \tau_c \sim \delta u_{\Delta r} \Delta r \sim \varepsilon^{1/3} \Delta r^{4/3}. \quad (\text{C } 86)$$

The last two steps follow from $\tau_c \sim \Delta r / \delta u_{\Delta r}$ and might appear to be valid only for standard K41 or GS95 turbulence (2.9). In fact, they are also valid for the aligned turbulence because the velocities in (C 86) must be in the direction of the particle separation Δr , so we must use the scaling of δu with ξ , not with λ —and that is always the Kolmogorov scaling, both for the aligned cascade [see (6.29)] and even for the tearing-mediated one (see § 7.2.3). Integrating (C 86) gets us

$$\Delta r(t) \sim \varepsilon^{1/2} t^{3/2}, \quad (\text{C } 87)$$

as long as $\Delta r(t) < \lambda_{\text{CB}}$ (the outer scale of the strong turbulence), or, equivalently, as long as t is shorter than the nonlinear time at scale λ_{CB} . A salient feature here is that $\Delta r(t)$ is independent of the initial separation, which can be arbitrarily small. Therefore, the width of the reconnecting sheet and the inflow speed are

$$\delta \sim \Delta r(t_{\text{out}}) \sim \varepsilon^{1/2} \left(\frac{\ell}{u_y} \right)^{3/2} \Rightarrow u_x \sim \frac{\delta}{\ell} u_y \sim \left(\frac{\varepsilon \ell}{u_y} \right)^{1/2}. \quad (\text{C } 88)$$

In their simulations of a macroscopic magnetic field reconnecting in the presence of externally injected turbulence, Kowal *et al.* (2009, 2012) (usefully summarised by Lazarian *et al.* 2015) do indeed see the scaling $u_x \propto \varepsilon^{1/2}$, independent of η (figure 45).⁸⁵

⁸⁴For the connoisseurs, there is, in fact, not complete equivalence between the argument of Lazarian & Vishniac (1999) and its interpretation by Eyink *et al.* (2011). The former paper and many of its successors believe that their stochastic-reconnection mechanism can only work in 3D, because magnetic-field lines are too topologically constrained in 2D. For Eyink *et al.* (2011), there is no problem in 2D as Lagrangian trajectories in 2D MHD turbulence still separate quickly. Loureiro *et al.* (2009) did report fast reconnection in an SP sheet buffeted by 2D turbulence, although Kulpa-Dybel *et al.* (2010) disagreed. I am not aware of the issue having been looked into since then.

⁸⁵Yang *et al.* (2020), who have recently revisited this problem, seem to see a weaker scaling, not clear why.

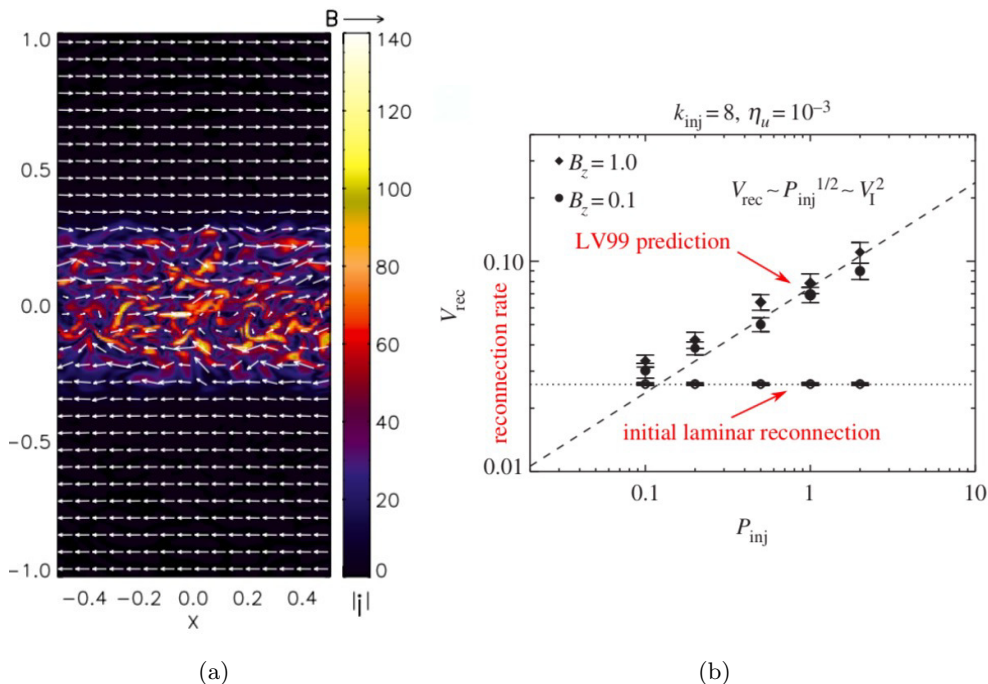


FIGURE 45. Simulations of stochastic reconnection by Kowal *et al.* (2009): (a) arrows are magnetic fields, colour shows (turbulent) currents; (b) reconnection rate V_{rec} vs. injected power P_{inj} , which, in my notation, are u_x and ε , respectively—this plot, taken from Lazarian *et al.* (2015), shows $u_x \propto \varepsilon^{1/2}$, in accordance with (C 88).

C.6.1. Stochastic Reconnection and GS95 Turbulence

Let us now apply this result to a typical turbulent structure in which $\ell = \xi$ and $u_y \sim \delta u_\xi \sim (\varepsilon \xi)^{1/3}$. This instantly implies

$$\delta \sim \xi, \quad u_x \sim \delta u_\xi. \quad (\text{C } 89)$$

For GS95 turbulence ($\xi \sim \lambda$), this implies that reconnection of field lines within each “eddy” occurs on the same time scale as the “eddy” turns over—this is, I think, what Lazarian *et al.* (2015) mean when they say that stochastic reconnection makes GS95 turbulence “self-consistent”.

C.6.2. Stochastic Reconnection and Aligned Turbulence

What if the turbulence is aligned? According to my argument above, in view of (6.29), it might seem that (C 89) remains valid. This is worrisome: indeed this tells us that the width of the layer over which stochastic reconnection would be happening is larger than the width of the aligned structure: $\delta \sim \xi \gg \lambda$! If this were true, writing this review would have been a waste of time: aligned structures would be quickly broken up by stochastic reconnection, so there would be no aligned cascade. This would invalidate all of § 6 and, consequently, obviate any consideration of tearing-mediated turbulence in § 7—the cascade would just be GS95 all the way to the dissipation scale. Lazarian *et al.* (2015) (and their previous papers referenced therein) might then be excused for (politely) ignoring all the newfangled turbulence theory postdating GS95, and Beresnyak (2011, 2012a, 2014b, 2019) would be vindicated much more completely than I could offer to do

at the end of § 7.2.1. I cannot prove formally that this does not or cannot happen, but I can show that aligned turbulence is, in fact, not ruled out by stochastic reconnection.

Let us imagine that an aligned structure has emerged with transverse (to fluctuating fields) scale λ and longitudinal (fluctuation-direction) scale $\xi \gg \lambda$. In order for stochastic reconnection to destroy it quickly, there must be turbulent structures within the layer of width λ whose longitudinal scales can be as large as $\sim \lambda$. But within this layer, there is an intense shear $\sim \delta u_\lambda / \lambda$, which should suppress any turbulent motions whose typical nonlinear time scales are longer than the inverse of this shear. For small enough structures, the nonlinear times will be short and eventually overcome the shear. Let us find the longitudinal scale ξ' of the largest possible such motions: their nonlinear decorrelation rate is

$$\frac{\delta u_{\xi'}}{\xi'} \sim \frac{\delta u_\lambda}{\lambda} \Rightarrow \frac{\xi'}{\lambda} \sim \left(\frac{\lambda}{\xi}\right)^{1/2} \sim \left(\frac{\lambda}{\lambda_{\text{CB}}}\right)^{1/8} \ll 1, \quad (\text{C } 90)$$

where I have used (6.29) for $\delta u_{\xi'} \sim (\varepsilon \xi')^{1/3}$ and $\delta u_\lambda = \delta u_\xi \sim (\varepsilon \xi)^{1/3}$.⁸⁶ If these motions are aligned in the usual way, with transverse scale λ' , then, using (6.29) again, $\lambda'/\lambda \sim (\lambda/\lambda_{\text{CB}})^{1/2}$.

Going back to (C 86), one must now integrate this equation up to time $t_{\text{out}} \sim \xi/\delta u_\xi \sim \varepsilon^{-1/3} \xi^{2/3}$, which is longer than the nonlinear time $\xi'/\delta u_{\xi'} \sim \varepsilon^{-1/3} \xi'^{2/3}$ of the largest turbulent structures within our layer. This gives conventional turbulent diffusion:

$$\delta \sim \Delta r(t_{\text{out}}) \sim \left(\varepsilon^{1/3} \xi'^{4/3} t_{\text{out}}\right)^{1/2} \sim \xi'^{2/3} \xi^{1/3} \sim \lambda, \quad (\text{C } 91)$$

where the last step follows from (C 90). Just like in (C 89), the width of the stochastically reconnecting layer is the same as the width of the (now aligned) structure, so the magnetic fields in the aligned cascade reconnect just as fast as the turbulent structures decorrelate. The aligned cascade too is consistent with stochastic reconnection.

The same is going to be true of the tearing-mediated cascade of § 7.2 because, in the argument leading to (C 91), all I needed was the Kolmogorov scaling of the turbulent velocities in the fluctuation direction, which is always preserved (§ 7.2.3). The competition between the nonlinear decorrelation rate and the tearing rate that leads to disruption (§ 7.1) is unaffected by all this because disruption happens precisely at the scale where tearing becomes “ideal”. Any smaller-scale turbulence, ambient or created by the tearing, can presumably be viewed as providing seed perturbations for the instability.

The overall conclusion appears to be that stochastic reconnection, while a useful notion in the treatment of large-scale magnetic-field configurations, does not undermine (or modify) the existing theory of the aligned or tearing-mediated turbulence, but rather plays an interpretative role: it provides a further insight into the behaviour of magnetic field in a turbulent environment and reassures us that whatever topological rearrangements are necessary for the cascade to proceed can always occur on the time scales of the cascade.

REFERENCES

- ADKINS, T. & SCHEKOCHIHIN, A. A. 2018 A solvable model of Vlasov-kinetic plasma turbulence in Fourier-Hermite phase space. *J. Plasma Phys.* **84**, 905840107.
- ALEXANDROVA, O., SAUR, J., LACOMBE, C., MANGENEY, A., MITCHELL, J., SCHWARTZ, S. J. & ROBERT, P. 2009 Universality of solar-wind turbulent spectrum from MHD to electron scales. *Phys. Rev. Lett.* **103**, 165003.

⁸⁶NB: ξ is a function of λ ; by δu_ξ , I mean δu_λ expressed in terms of ξ , not δu_λ taken at $\lambda = \xi$.

- ALFVÉN, H. 1942 Existence of electromagnetic-hydrodynamic waves. *Nature* **150**, 405.
- ALUIE, H. & EYINK, G. L. 2010 Scale locality of magnetohydrodynamic turbulence. *Phys. Rev. Lett.* **104**, 081101.
- BAÑÓN NAVARRO, A., TEACA, B., TOLD, D., GROŠELJ, D., CRANDALL, P. & JENKO, F. 2016 Structure of plasma heating in gyrokinetic Alfvénic turbulence. *Phys. Rev. Lett.* **117**, 245101.
- BALBUS, S. A. 2004 Viscous shear instability in weakly magnetized, dilute plasmas. *Astrophys. J.* **616**, 857.
- BALKOVSKY, E., FOUXON, A. & LEBEDEV, V. 2001 Turbulence of polymer solutions. *Phys. Rev. E* **64**, 056301.
- BANDYOPADHYAY, R., MATTHAEUS, W. H., OUGHTON, S. & WAN, M. 2019 Evolution of similarity lengths in anisotropic magnetohydrodynamic turbulence. *J. Fluid Mech.* **876**, 5.
- BANERJEE, R. & JEDAMZIK, K. 2004 Evolution of cosmic magnetic fields: From the very early Universe, to recombination, to the present. *Phys. Rev. D* **70**, 123003.
- BÁRTA, M., BÜCHNER, J., KARLICKÝ, M. & SKÁLA, J. 2011 Spontaneous current-layer fragmentation and cascading reconnection in solar flares. I. Model and analysis. *Astrophys. J.* **737**, 24.
- BATCHELOR, G. K. 1950 On the spontaneous magnetic field in a conducting liquid in turbulent motion. *Proc. R. Soc. London A* **201**, 405.
- BATCHELOR, G. K. 1959 Small-scale variation of convected quantities like temperature in turbulent fluid. Part 1. General discussion and the case of small conductivity. *J. Fluid Mech.* **5**, 113.
- BEC, J. & KHANIN, K. 2007 Burgers turbulence. *Phys. Rep.* **447**, 1.
- BERERA, A. & LINKMANN, M. 2014 Magnetic helicity and the evolution of decaying magnetohydrodynamic turbulence. *Phys. Rev. E* **90**, 041003.
- BERESNYAK, A. 2011 The spectral slope and Kolmogorov constant of MHD turbulence. *Phys. Rev. Lett.* **106**, 075001.
- BERESNYAK, A. 2012a Basic properties of magnetohydrodynamic turbulence in the inertial range. *Mon. Not. R. Astron. Soc.* **422**, 3495.
- BERESNYAK, A. 2012b Simulations of nonlinear small-scale dynamo. Unpublished.
- BERESNYAK, A. 2012c Universal nonlinear small-scale dynamo. *Phys. Rev. Lett.* **108**, 035002.
- BERESNYAK, A. 2013 Comment on Perez et al [PRX 2, 041005 (2012), arXiv:1209.2011]. *E-print* arXiv:1301.7425.
- BERESNYAK, A. 2014a Reply to Comment on “Spectra of strong magnetohydrodynamic turbulence from high-resolution simulations”. *E-print* arXiv:1410.0957.
- BERESNYAK, A. 2014b Spectra of strong magnetohydrodynamic turbulence from high-resolution simulations. *Astrophys. J.* **784**, L20.
- BERESNYAK, A. 2015 On the parallel spectrum in magnetohydrodynamic turbulence. *Astrophys. J.* **801**, L9.
- BERESNYAK, A. 2017 Three-dimensional spontaneous magnetic reconnection. *Astrophys. J.* **834**, 47.
- BERESNYAK, A. 2019 MHD turbulence. *Living Rev. Comput. Astrophys.* **5**, 2.
- BERESNYAK, A. & LAZARIAN, A. 2006 Polarization intermittency and its influence on MHD turbulence. *Astrophys. J.* **640**, L175.
- BERESNYAK, A. & LAZARIAN, A. 2008 Strong imbalanced turbulence. *Astrophys. J.* **682**, 1070.
- BERESNYAK, A. & LAZARIAN, A. 2009a Comparison of spectral slopes of magnetohydrodynamic and hydrodynamic turbulence and measurements of alignment effects. *Astrophys. J.* **702**, 1190.
- BERESNYAK, A. & LAZARIAN, A. 2009b Structure of stationary strong imbalanced turbulence. *Astrophys. J.* **702**, 460.
- BERESNYAK, A. & LAZARIAN, A. 2010 Scaling laws and diffuse locality of balanced and imbalanced magnetohydrodynamic turbulence. *Astrophys. J.* **722**, L110.
- BHAT, P., ZHOU, M. & LOUREIRO, N. F. 2020 Inverse energy transfer in decaying, three dimensional, nonhelical magnetic turbulence due to magnetic reconnection. *E-prints*: arXiv:2007.07325.

- BHATTACHARJEE, A., HUANG, Y.-M., YANG, H. & ROGERS, B. 2009 Fast reconnection in high-Lundquist-number plasmas due to the plasmoid instability. *Phys. Plasmas* **16**, 112102.
- BHATTACHARJEE, A. & NG, C. S. 2001 Random scattering and anisotropic turbulence of shear Alfvén wave packets. *Astrophys. J.* **548**, 318.
- BIAN, X. & ALUIE, H. 2019 Decoupled cascades of kinetic and magnetic energy in magnetohydrodynamic turbulence. *Phys. Rev. Lett.* **122**, 135101.
- BIERMANN, L. & SCHLÜTER, A. 1951 Cosmic radiation and cosmic magnetic fields. II. Origin of cosmic magnetic fields. *Phys. Rev.* **82**, 863.
- BIGOT, B. & GALTIER, S. 2011 Two-dimensional state in driven magnetohydrodynamic turbulence. *Phys. Rev. E* **83**, 026405.
- BISKAMP, D. 1982 Effect of secondary tearing instability on the coalescence of magnetic islands. *Phys. Lett. A* **87**, 357.
- BISKAMP, D. 1986 Magnetic reconnection via current sheets. *Phys. Fluids* **29**, 1520.
- BISKAMP, D. & BREMER, U. 1994 Dynamics and statistics of inverse cascade processes in 2D magnetohydrodynamic turbulence. *Phys. Rev. Lett.* **72**, 3819.
- BISKAMP, D. & MÜLLER, W.-C. 1999 Decay laws for three-dimensional magnetohydrodynamic turbulence. *Phys. Rev. Lett.* **83**, 2195.
- BISKAMP, D. & MÜLLER, W.-C. 2000 Scaling properties of three-dimensional isotropic magnetohydrodynamic turbulence. *Phys. Plasmas* **7**, 4889.
- BISKAMP, D. & WELTER, H. 1989 Dynamics of decaying two-dimensional magnetohydrodynamic turbulence. *Phys. Fluids B* **1**, 1964.
- BOLDYREV, S. 2002 Kolmogorov-Burgers model for star-forming turbulence. *Astrophys. J.* **569**, 841.
- BOLDYREV, S. 2005 On the spectrum of magnetohydrodynamic turbulence. *Astrophys. J.* **626**, L37.
- BOLDYREV, S. 2006 Spectrum of magnetohydrodynamic turbulence. *Phys. Rev. Lett.* **96**, 115002.
- BOLDYREV, S. & CATTANEO, F. 2004 Magnetic-field generation in Kolmogorov turbulence. *Phys. Rev. Lett.* **92**, 144501.
- BOLDYREV, S., CHEN, C. H. K., XIA, Q. & ZHDANKIN, V. 2015 Spectral breaks of Alfvénic turbulence in a collisionless plasma. *Astrophys. J.* **806**, 238.
- BOLDYREV, S., HORAITES, K., XIA, Q. & PEREZ, J. C. 2013 Toward a theory of astrophysical plasma turbulence at subproton scales. *Astrophys. J.* **777**, 41.
- BOLDYREV, S. & LOUREIRO, N. F. 2017 Magnetohydrodynamic turbulence mediated by reconnection. *Astrophys. J.* **844**, 125.
- BOLDYREV, S. & LOUREIRO, N. F. 2018 Calculations in the theory of tearing instability. *J. Phys. Conf. Ser.* **1100**, 012003.
- BOLDYREV, S. & LOUREIRO, N. F. 2019 Role of reconnection in inertial kinetic-Alfvén turbulence. *Phys. Rev. Res.* **1**, 012006(R).
- BOLDYREV, S., MASON, J. & CATTANEO, F. 2009 Dynamic alignment and exact scaling laws in magnetohydrodynamic turbulence. *Astrophys. J.* **699**, L39.
- BOLDYREV, S., NORDLUND, Å. & PADOAN, P. 2002 Supersonic turbulence and structure of interstellar molecular clouds. *Phys. Rev. Lett.* **89**, 031102.
- BOLDYREV, S. & PEREZ, J. C. 2009 Spectrum of weak magnetohydrodynamic turbulence. *Phys. Rev. Lett.* **103**, 225001.
- BOLDYREV, S. & PEREZ, J. C. 2012 Spectrum of kinetic-Alfvén turbulence. *Astrophys. J.* **758**, L44.
- BOLDYREV, S., PEREZ, J. C., BOROVSKY, J. E. & PODESTA, J. J. 2011 Spectral scaling laws in magnetohydrodynamic turbulence simulations and in the solar wind. *Astrophys. J.* **741**, L19.
- BOLDYREV, S., PEREZ, J. C. & ZHDANKIN, V. 2012 Residual energy in MHD turbulence and in the solar wind. *AIP Conf. Proc.* **1436**, 18.
- BOTT, A. F. A., TZEFERACOS, P., CHEN, L., PALMER, C. A. J., RIGBY, A., BELL, A., BINGHAM, R., BIRKEL, A., GRAZIANI, C., FROULA, D. H., KATZ, J., KOENIG, M., KUNZ, M. W., LI, C. K., MEINECKE, J., MINIATI, F., PETRASSO, R., PARK, H. S., REMINGTON, B. A., REVILLE, B., ROSS, J. S., RYU, D., RYUTOV, D., SÉGUIN, F., WHITE, T. G., SCHEKOCIHIN, A. A., LAMB, D. Q. & GREGORI, G. 2020 Time-resolved fast turbulent dynamo in a laser plasma. *E-print* arXiv:2007.12837.

- BOWEN, T. A., MALLETT, A., BONNELL, J. W. & BALE, S. D. 2018 Impact of residual energy on solar wind turbulent spectra. *Astrophys. J.* **865**, 45.
- BRAGINSKII, S. I. 1965 Transport processes in a plasma. *Rev. Plasma Phys.* **1**, 205.
- BRANDENBURG, A. 2001 The inverse cascade and nonlinear alpha-effect in simulations of isotropic helical hydromagnetic turbulence. *Astrophys. J.* **550**, 824.
- BRANDENBURG, A. 2011 Nonlinear small-scale dynamos at low magnetic Prandtl numbers. *Astrophys. J.* **741**, 92.
- BRANDENBURG, A. 2014 Magnetic Prandtl number dependence of the kinetic-to-magnetic dissipation ratio. *Astrophys. J.* **791**, 12.
- BRANDENBURG, A., HAUGEN, N. E. L., LI, X.-Y. & SUBRAMANIAN, K. 2018 Varying the forcing scale in low Prandtl number dynamos. *Mon. Not. R. Astron. Soc.* **479**, 2827.
- BRANDENBURG, A. & KAHNIASHVILI, T. 2017 Classes of Hydrodynamic and Magnetohydrodynamic Turbulent Decay. *Phys. Rev. Lett.* **118**, 055102.
- BRANDENBURG, A., KAHNIASHVILI, T., MANDAL, S., POL, A. R., TEVZADZE, A. G. & VACHASPATI, T. 2019 Dynamo effect in decaying helical turbulence. *Phys. Rev. Fluids* **4**, 024608.
- BRANDENBURG, A., KAHNIASHVILI, T. & TEVZADZE, A. G. 2015 Nonhelical inverse transfer of a decaying turbulent magnetic field. *Phys. Rev. Lett.* **114**, 075001.
- BRANDENBURG, A. & REMPEL, M. 2019 Reversed dynamo at small scales and large magnetic Prandtl number. *Astrophys. J.* **879**, 57.
- BRUNO, R. & CARBONE, V. 2013 The solar wind as a turbulence laboratory. *Living Rev. Solar Phys.* **10**, 2.
- BULANOV, S. V., SAKAI, J. & SYROVATSKII, S. I. 1979 Tearing-mode instability in approximately steady MHD configurations. *Sov. J. Plasma Phys.* **5**, 280.
- BULANOV, S. V., SYROVATSKII, S. I. & SAKAI, J. 1978 Stabilizing influence of plasma flow on dissipative tearing instability. *Sov. Phys.-JETP Lett.* **28**, 177.
- BUSSE, A., MÜLLER, W.-C., HOMANN, H. & GRAUER, R. 2007 Statistics of passive tracers in three-dimensional magnetohydrodynamic turbulence. *Phys. Plasmas* **14**, 122303.
- CAMPANELLI, L. 2004 Scaling laws in magnetohydrodynamic turbulence. *Phys. Rev. D* **70**, 083009.
- CARBONE, V., VELTRI, P. & MANGENEY, A. 1990 Coherent structure formation and magnetic field line reconnection in magnetohydrodynamic turbulence. *PFA* **2**, 1487.
- CASSAK, P. A. & DRAKE, J. F. 2009 The impact of microscopic magnetic reconnection on pre-flare energy storage. *Astrophys. J.* **707**, L158.
- CASSAK, P. A., SHAY, M. A. & DRAKE, J. F. 2009 Scaling of Sweet-Parker reconnection with secondary islands. *Phys. Plasmas* **16**, 120702.
- CERRI, S. S. & CALIFANO, F. 2017 Reconnection and small-scale fields in 2D-3V hybrid-kinetic driven turbulence simulations. *New J. Phys.* **19**, 025007.
- CERRI, S. S., KUNZ, M. W. & CALIFANO, F. 2018 Dual phase-space cascades in 3D hybrid-Vlasov-Maxwell turbulence. *Astrophys. J.* **856**, L13.
- CHANDRAN, B. D. G. 1997 *Ph. D. Thesis*. Princeton University.
- CHANDRAN, B. D. G. 2008 Strong anisotropic MHD turbulence with cross helicity. *Astrophys. J.* **685**, 646.
- CHANDRAN, B. D. G., LI, B., ROGERS, B. N., QUATAERT, E. & GERMASCHEWSKI, K. 2010 Perpendicular ion heating by low-frequency Alfvén-wave turbulence in the solar wind. *Astrophys. J.* **720**, 503.
- CHANDRAN, B. D. G. & PEREZ, J. C. 2019 Reflection-driven magnetohydrodynamic turbulence in the solar atmosphere and solar wind. *J. Plasma Phys.* **85**, 905850409.
- CHANDRAN, B. D. G., SCHEKOCHIHIN, A. A. & MALLETT, A. 2015 Intermittency and alignment in strong RMHD turbulence. *Astrophys. J.* **807**, 39.
- CHAPMAN, S. & KENDALL, P. C. 1963 Liquid instability and energy transformation near a magnetic neutral line: a soluble non-linear hydromagnetic problem. *Proc. R. Soc. London A* **271**, 435.
- CHEN, C. H. K. 2016 Recent progress in astrophysical plasma turbulence from solar wind observations. *J. Plasma Phys.* **82**, 535820602.
- CHEN, C. H. K., BALE, S. D., BONNELL, J. W., BOROVNIKOV, D., BOWEN, T. A., BURGESS, D., CASE, A. W., CHANDRAN, B. D. G., DUDOK DE WIT, T., GOETZ, K., HARVEY, P. R.,

- KASPER, J. C., KLEIN, K. G., KORRECK, K. E., LARSON, D., LIVI, R., MACDOWALL, R. J., MALASPINA, D. M., MALLET, A., MCMANUS, M. D., MONCUQUET, M., PULUPA, M., STEVENS, M. L. & WHITTLESEY, P. 2020 The evolution and role of solar wind turbulence in the inner heliosphere. *Astrophys. J. Suppl.* **246**, 53.
- CHEN, C. H. K., BALE, S. D., SALEM, C. S. & MARUCA, B. A. 2013a Residual energy spectrum of solar wind turbulence. *Astrophys. J.* **770**, 125.
- CHEN, C. H. K. & BOLDYREV, S. 2017 Nature of kinetic scale turbulence in the Earth's magnetosheath. *Astrophys. J.* **842**, 122.
- CHEN, C. H. K., BOLDYREV, S., XIA, Q. & PEREZ, J. C. 2013b Nature of subproton scale turbulence in the solar wind. *Phys. Rev. Lett.* **110**, 225002.
- CHEN, C. H. K., KLEIN, K. G. & HOWES, G. G. 2019 Evidence for electron Landau damping in space plasma turbulence. *Nature Comm.* **10**, 740.
- CHEN, C. H. K., LEUNG, L., BOLDYREV, S., MARUCA, B. A. & BALE, S. D. 2014a Ion-scale spectral break of solar wind turbulence at high and low beta. *Geophys. Res. Lett.* **41**, 8081.
- CHEN, C. H. K., MALLET, A., SCHEKOCIHIN, A. A., HORBURY, T. S., WICKS, R. T. & BALE, S. D. 2012a Three-dimensional structure of solar wind turbulence. *Astrophys. J.* **758**, 120.
- CHEN, C. H. K., MALLET, A., YOUSEF, T. A., SCHEKOCIHIN, A. A. & HORBURY, T. S. 2011 Anisotropy of Alfvénic turbulence in the solar wind and numerical simulations. *Mon. Not. R. Astron. Soc.* **415**, 3219.
- CHEN, C. H. K., SALEM, C. S., BONNELL, J. W., MOZER, F. S. & BALE, S. D. 2012b Density fluctuation spectrum of solar wind turbulence between ion and electron scales. *Phys. Rev. Lett.* **109**, 035001.
- CHEN, C. H. K., SORRISO-VALVO, L., ŠAFRÁNKOVÁ, J. & NĚMEČEK, Z. 2014b Intermittency of solar wind density fluctuations from ion to electron scales. *Astrophys. J.* **789**, L8.
- CHO, J. 2011 Magnetic helicity conservation and inverse energy cascade in electron magnetohydrodynamic wave packets. *Phys. Rev. Lett.* **106**, 191104.
- CHO, J. & KIM, H. 2016 Spectral evolution of helical electron magnetohydrodynamic turbulence. *J. Geophys. Res. A* **121**, 6157.
- CHO, J. & LAZARIAN, A. 2002 Compressible sub-Alfvénic MHD turbulence in low- β plasmas. *Phys. Rev. Lett.* **88**, 245001.
- CHO, J. & LAZARIAN, A. 2003 Compressible magnetohydrodynamic turbulence: mode coupling, scaling relations, anisotropy, viscosity-damped regime and astrophysical implications. *Mon. Not. R. Astron. Soc.* **345**, 325.
- CHO, J. & LAZARIAN, A. 2004 The anisotropy of electron magnetohydrodynamic turbulence. *Astrophys. J.* **615**, L41.
- CHO, J., LAZARIAN, A. & VISHNIAC, E. T. 2002a New regime of magnetohydrodynamic turbulence: Cascade below the viscous cutoff. *Astrophys. J.* **566**, L49.
- CHO, J., LAZARIAN, A. & VISHNIAC, E. T. 2002b Simulations of magnetohydrodynamic turbulence in a strongly magnetized medium. *Astrophys. J.* **564**, 291.
- CHO, J., LAZARIAN, A. & VISHNIAC, E. T. 2003 Ordinary and viscosity-damped magnetohydrodynamic turbulence. *Astrophys. J.* **595**, 812.
- CHO, J. & RYU, D. 2009 Characteristic lengths of magnetic field in magnetohydrodynamic turbulence. *Astrophys. J.* **705**, L90.
- CHO, J. & VISHNIAC, E. T. 2000 The anisotropy of magnetohydrodynamic Alfvénic turbulence. *Astrophys. J.* **539**, 273.
- CHO, J., VISHNIAC, E. T., BERESNYAK, A., LAZARIAN, A. & RYU, D. 2009 Growth of magnetic fields induced by turbulent motions. *Astrophys. J.* **693**, 1449.
- CHRISTENSSON, M., HINDMARSH, M. & BRANDENBURG, A. 2001 Inverse cascade in decaying three-dimensional magnetohydrodynamic turbulence. *Phys. Rev. E* **64**, 056405.
- CHRISTENSSON, M., HINDMARSH, M. & BRANDENBURG, A. 2005 Scaling laws in decaying helical hydromagnetic turbulence. *Astron. Nachr.* **326**, 393.
- COMISSO, L. & GRASSO, D. 2016 Visco-resistive plasmoid instability. *Phys. Plasmas* **23**, 032111.
- COMISSO, L., HUANG, Y.-M., LINGAM, M., HIRVIJOKI, E. & BHATTACHARJEE, A. 2018 Magnetohydrodynamic turbulence in the plasmoid-mediated regime. *Astrophys. J.* **854**, 103.

- COMISSO, L., LINGAM, M., HUANG, Y.-M. & BHATTACHARJEE, A. 2016 General theory of the plasmoid instability. *Phys. Plasmas* **23**, 100702.
- COMISSO, L., LINGAM, M., HUANG, Y.-M. & BHATTACHARJEE, A. 2017 Plasmoid instability in forming current sheets. *Astrophys. J.* **850**, 142.
- COPPI, B., GALVÃO, R., PELLAT, R., ROSENBLUTH, M. & RUTHERFORD, P. 1976 Resistive internal kink modes. *Sov. J. Plasma Phys.* **2**, 961.
- CORRSIN, S. 1963 Estimates of the relations between Eulerian and Lagrangian scales in large Reynolds number turbulence. *J. Atmos. Sci.* **20**, 115.
- DAHLBURG, R. B., ZANG, T. A. & MONTGOMERY, D. 1986 Unstable transition properties of the driven magnetohydrodynamic sheet pinch. *J. Fluid Mech.* **169**, 71.
- DALLAS, V. & ALEXAKIS, A. 2013a Origins of the k^{-2} spectrum in decaying Taylor-Green magnetohydrodynamic turbulent flows. *Phys. Rev. E* **88**, 053014.
- DALLAS, V. & ALEXAKIS, A. 2013b Symmetry breaking of decaying magnetohydrodynamic Taylor-Green flows and consequences for universality. *Phys. Rev. E* **88**, 063017.
- DALLAS, V. & ALEXAKIS, A. 2014 The signature of initial conditions on magnetohydrodynamic turbulence. *Astrophys. J.* **788**, L36.
- DAUGHTON, W., ROYTERSHTYEN, V., ALBRIGHT, B. J., KARIMABADI, H., YIN, L. & BOWERS, K. J. 2009a Influence of Coulomb collisions on the structure of reconnection layers. *Phys. Plasmas* **16**, 072117.
- DAUGHTON, W., ROYTERSHTYEN, V., ALBRIGHT, B. J., KARIMABADI, H., YIN, L. & BOWERS, K. J. 2009b Transition from collisional to kinetic regimes in large-scale reconnection layers. *Phys. Rev. Lett.* **103**, 065004.
- DAVIDSON, P. A. 2013 *Turbulence in Rotating, Stratified and Electrically Conducting Fluids*. Cambridge: Cambridge University Press.
- DEL SARTO, D. & OTTAVIANI, M. 2017 Secondary fast reconnecting instability in the sawtooth crash. *Phys. Plasmas* **24**, 012102.
- DEL SARTO, D., PUCCI, F., TENERANI, A. & VELLI, M. 2016 “Ideal” tearing and the transition to fast reconnection in the weakly collisional MHD and EMHD regimes. *J. Geophys. Res.* **121**, 1857.
- DOBROWOLNY, M., MANGENEY, A. & VELTRI, P. 1980 Fully developed anisotropic hydromagnetic turbulence in interplanetary space. *Phys. Rev. Lett.* **45**, 144.
- DONG, C., WANG, L., HUANG, Y.-M., COMISSO, L. & BHATTACHARJEE, A. 2018 Role of the plasmoid instability in magnetohydrodynamic turbulence. *Phys. Rev. Lett.* **121** (16), 165101.
- DUBRULLE, B. 1994 Intermittency in fully developed turbulence: Log-Poisson statistics and generalized scale covariance. *Phys. Rev. Lett.* **73**, 959.
- EGEDAL, J., LE, A. & DAUGHTON, W. 2013 A review of pressure anisotropy caused by electron trapping in collisionless plasma, and its implications for magnetic reconnection. *Phys. Plasmas* **20**, 061201.
- ELSASSER, W. M. 1950 The hydromagnetic equations. *Phys. Rev.* **79**, 183.
- EVENT HORIZON TELESCOPE COLLABORATION 2019 First M87 Event Horizon Telescope results. V. Physical origin of the asymmetric ring. *Astrophys. J.* **875**, L5.
- EYINK, G., VISHNIAC, E., LALESCU, C., ALUIE, H., KANOV, K., BÜRGER, K., BURNS, R., MENEVEAU, C. & SZALAY, A. 2013 Flux-freezing breakdown in high-conductivity magnetohydrodynamic turbulence. *Nature* **497**, 466.
- EYINK, G. L. 2009 Stochastic line motion and stochastic flux conservation for nonideal hydromagnetic models. *J. Math. Phys.* **50**, 083102.
- EYINK, G. L. 2011 Stochastic flux freezing and magnetic dynamo. *Phys. Rev. E* **83**, 056405.
- EYINK, G. L. 2018 Cascades and dissipative anomalies in nearly collisionless plasma turbulence. *Phys. Rev. X* **8**, 041020.
- EYINK, G. L., LAZARIAN, A. & VISHNIAC, E. T. 2011 Fast magnetic reconnection and spontaneous stochasticity. *Astrophys. J.* **743**, 51.
- FOUXON, A. & LEBEDEV, V. 2003 Spectra of turbulence in dilute polymer solutions. *Phys. Fluids* **15**, 2060.
- FRANCI, L., CERRI, S. S., CALIFANO, F., LANDI, S., PAPINI, E., VERDINI, A., MATTEINI, L., JENKO, F. & HELLINGER, P. 2017 Magnetic reconnection as a driver for a sub-ion-scale cascade in plasma turbulence. *Astrophys. J.* **850**, L16.

- FRANCI, L., LANDI, S., VERDINI, A., MATTEINI, L. & HELLINGER, P. 2018 Solar wind turbulent cascade from MHD to sub-ion scales: large-size 3D hybrid particle-in-cell simulations. *Astrophys. J.* **853**, 26.
- FRICK, P. & STEPANOV, R. 2010 Long-term free decay of MHD turbulence. *Europhys. Lett.* **92**, 34007.
- FRISCH, U. 1995 *Turbulence: The Legacy of A. N. Kolmogorov*. Cambridge: Cambridge University Press.
- FURTH, H. P., KILLEEN, J. & ROSENBLUTH, M. N. 1963 Finite-resistivity instabilities of a sheet pinch. *Phys. Fluids* **6**, 459.
- GALISHNIKOVA, A., KUNZ, M. W. & SCHEKOCIHIN, A. A. 2020 in preparation.
- GALTIER, S., NAZARENKO, S. V., NEWELL, A. C. & POUQUET, A. 2000 A weak turbulence theory for incompressible magnetohydrodynamics. *J. Plasma Phys.* **63**, 447.
- GOGOBERIDZE, G., CHAPMAN, S. C. & HNAT, B. 2012 Generation of residual energy in the turbulent solar wind. *Phys. Plasmas* **19**, 102310.
- GOLDREICH, P. & SRIDHAR, S. 1995 Toward a theory of interstellar turbulence. 2: Strong Alfvénic turbulence. *Astrophys. J.* **438**, 763.
- GOLDREICH, P. & SRIDHAR, S. 1997 Magnetohydrodynamic turbulence revisited. *Astrophys. J.* **485**, 680.
- GRAPPIN, R., FRISCH, U., POUQUET, A. & LEORAT, J. 1982 Alfvénic fluctuations as asymptotic states of MHD turbulence. *Astron. Astrophys.* **105**, 6.
- GRAPPIN, R., LEORAT, J. & POUQUET, A. 1983 Dependence of MHD turbulence spectra on the velocity field-magnetic field correlation. *Astron. Astrophys.* **126**, 51.
- GRAPPIN, R., MÜLLER, W.-C. & VERDINI, A. 2016 Alfvén-dynamo balance and magnetic excess in magnetohydrodynamic turbulence. *Astron. Astrophys.* **589**, A131.
- GRAUER, R., KRUG, J. & MARLIANI, C. 1994 Scaling of high-order structure functions in magnetohydrodynamic turbulence. *Phys. Lett. A* **195**, 335.
- GRECO, A., PERRI, S., SERVIDIO, S., YORDANOVA, E. & VELTRI, P. 2016 The complex structure of magnetic field discontinuities in the turbulent solar wind. *Astrophys. J.* **823**, L39.
- GRETE, P., O'SHEA, B. W. & BECKWITH, K. 2020 As a matter of tension—kinetic energy spectra in MHD turbulence. *E-print arXiv:2009.03342*.
- GRETE, P., O'SHEA, B. W., BECKWITH, K., SCHMIDT, W. & CHRISTLIEB, A. 2017 Energy transfer in compressible magnetohydrodynamic turbulence. *Phys. Plasmas* **24**, 092311.
- GROŠELJ, D., CHEN, C. H. K., MALLET, A., SAMTANEY, R., SCHNEIDER, K. & JENKO, F. 2019 Kinetic turbulence in astrophysical plasmas: waves and/or structures? *Phys. Rev. X* **9**, 031037.
- GRUZINOV, A. V. & DIAMOND, P. H. 1996 Nonlinear mean field electrodynamics of turbulent dynamos. *Phys. Plasmas* **3**, 1853.
- HARE, J. D., LEBEDEV, S. V., SUTTLE, L. G., LOUREIRO, N. F., CIARDI, A., BURDIAK, G. C., CHITTENDEN, J. P., CLAYSON, T., EARDLEY, S. J., GARCIA, C., HALLIDAY, J. W. D., NIASSE, N., ROBINSON, T., SMITH, R. A., STUART, N., SUZUKI-VIDAL, F., SWADLING, G. F., MA, J. & WU, J. 2017a Formation and structure of a current sheet in pulsed-power driven magnetic reconnection experiments. *Phys. Plasmas* **24**, 102703.
- HARE, J. D., SUTTLE, L., LEBEDEV, S. V., LOUREIRO, N. F., CIARDI, A., BURDIAK, G. C., CHITTENDEN, J. P., CLAYSON, T., GARCIA, C., NIASSE, N., ROBINSON, T., SMITH, R. A., STUART, N., SUZUKI-VIDAL, F., SWADLING, G. F., MA, J., WU, J. & YANG, Q. 2017b Anomalous heating and plasmoid formation in a driven magnetic reconnection experiment. *Phys. Rev. Lett.* **118**, 085001.
- HARE, J. D., SUTTLE, L. G., LEBEDEV, S. V., LOUREIRO, N. F., CIARDI, A., CHITTENDEN, J. P., CLAYSON, T., EARDLEY, S. J., GARCIA, C., HALLIDAY, J. W. D., ROBINSON, T., SMITH, R. A., STUART, N., SUZUKI-VIDAL, F. & TUBMAN, E. R. 2018 An experimental platform for pulsed-power driven magnetic reconnection. *Phys. Plasmas* **25**, 055703.
- HARRIS, E. G. 1962 On a plasma sheath separating regions of oppositely directed magnetic field. *Nuovo Cimento* **23**, 115.
- HATORI, T. 1984 Kolmogorov-style argument for the decaying homogeneous MHD turbulence. *J. Phys. Soc. Japan* **53**, 2539.

- HAUGEN, N. E., BRANDENBURG, A. & DOBLER, W. 2004 Simulations of nonhelical hydromagnetic turbulence. *Phys. Rev. E* **70**, 016308.
- HAUGEN, N. E. L., BRANDENBURG, A. & DOBLER, W. 2003 Is nonhelical hydromagnetic turbulence peaked at small scales? *Astrophys. J.* **597**, L141.
- HEINEMANN, T., MCWILLIAMS, J. C. & SCHEKOCIHIN, A. A. 2011 Large-scale magnetic field generation by randomly forced shearing waves. *Phys. Rev. Lett.* **107**, 255004.
- HIGDON, J. C. 1984 Density fluctuations in the interstellar medium: evidence for anisotropic magnetogasdynamic turbulence. I — Model and astrophysical sites. *Astrophys. J.* **285**, 109.
- HORBURY, T. S., FORMAN, M. & OUGHTON, S. 2008 Anisotropic scaling of magnetohydrodynamic turbulence. *Phys. Rev. Lett.* **101**, 175005.
- HOSKING, D. N. & SCHEKOCIHIN, A. A. 2021 Reconnection-controlled decay of magnetohydrodynamic turbulence. *J. Plasma Phys.*, in preparation.
- HOSKING, D. N., SCHEKOCIHIN, A. A. & BALBUS, S. A. 2020 Elasticity of tangled magnetic fields. *E-print arXiv:2006.15141*.
- HOSSAIN, M., GRAY, P. C., PONTIUS, JR., D. H., MATTHAEUS, W. H. & OUGHTON, S. 1995 Phenomenology for the decay of energy-containing eddies in homogeneous MHD turbulence. *Phys. Fluids* **7**, 2886.
- HUANG, S. Y., SAHRAOUI, F., DENG, X. H., HE, J. S., YUAN, Z. G., ZHOU, M., PANG, Y. & FU, H. S. 2014 Kinetic turbulence in the terrestrial magnetosheath: Cluster observations. *Astrophys. J.* **789**, L28.
- HUANG, Y.-M. & BHATTACHARJEE, A. 2010 Scaling laws of resistive magnetohydrodynamic reconnection in the high-Lundquist-number, plasmoid-unstable regime. *Phys. Plasmas* **17**, 062104.
- HUANG, Y.-M. & BHATTACHARJEE, A. 2012 Distribution of plasmoids in high-Lundquist-number magnetic reconnection. *Phys. Rev. Lett.* **109**, 265002.
- HUANG, Y.-M. & BHATTACHARJEE, A. 2013 Plasmoid instability in high-Lundquist-number magnetic reconnection. *Phys. Plasmas* **20**, 055702.
- HUANG, Y.-M. & BHATTACHARJEE, A. 2016 Turbulent magnetohydrodynamic reconnection mediated by the plasmoid instability. *Astrophys. J.* **818**, 20.
- HUANG, Y.-M., COMISSO, L. & BHATTACHARJEE, A. 2017 Plasmoid instability in evolving current sheets and onset of fast reconnection. *Astrophys. J.* **849**, 75.
- HUANG, Y.-M., COMISSO, L. & BHATTACHARJEE, A. 2019 Scalings pertaining to current sheet disruption mediated by the plasmoid instability. *Phys. Plasmas* **26**, 092112.
- IROSHNIKOV, R. S. 1963 Turbulence of a conducting fluid in a strong magnetic field. *Astron. Zh.* **40**, 742.
- ISKAKOV, A. B. & SCHEKOCIHIN, A. A. 2008 Saturated small-scale turbulent dynamo revisited. Unpublished.
- ISKAKOV, A. B., SCHEKOCIHIN, A. A., COWLEY, S. C., MCWILLIAMS, J. C. & PROCTOR, M. R. E. 2007 Numerical demonstration of fluctuation dynamo at low magnetic Prandtl numbers. *Phys. Rev. Lett.* **98**, 208501.
- JARA-ALMONTE, J., JI, H., YAMADA, M., YOO, J. & FOX, W. 2016 Laboratory observation of resistive electron tearing in a two-fluid reconnecting current sheet. *Phys. Rev. Lett.* **117**, 095001.
- JEMELLA, B. D., DRAKE, J. F. & SHAY, M. A. 2004 Singular structure of magnetic islands resulting from reconnection. *Phys. Plasmas* **11**, 5668.
- JEMELLA, B. D., SHAY, M. A., DRAKE, J. F. & ROGERS, B. N. 2003 Impact of frustrated singularities on magnetic island evolution. *Phys. Rev. Lett.* **91**, 125002.
- JI, H., YAMADA, M., HSU, S. & KULSRUD, R. 1998 Experimental test of the Sweet-Parker model of magnetic reconnection. *Phys. Rev. Lett.* **80**, 3256.
- JI, H., YAMADA, M., HSU, S., KULSRUD, R., CARTER, T. & ZAHARIA, S. 1999 Magnetic reconnection with Sweet-Parker characteristics in two-dimensional laboratory plasmas. *Phys. Plasmas* **6**, 1743.
- JINGADE, N., SINGH, N. K. & SRIDHAR, S. 2018 Generation of large-scale magnetic fields due to fluctuating α in shearing systems. *J. Plasma Phys.* **84**, 735840601.
- KADOMTSEV, B. B. & POGUTSE, O. P. 1974 Nonlinear helical perturbations of a plasma in the tokamak. *Soviet Phys. JETP* **38**, 283.

- KAWAZURA, Y., BARNES, M. & SCHEKOCIHIN, A. A. 2019 Thermal disequilibrium of ions and electrons by collisionless plasma turbulence. *Proc. Nat. Acad. Sci.* **116**, 771.
- KAZANTSEV, A. P. 1968 Enhancement of a magnetic field by a conducting fluid. *Sov. Phys.-JETP* **26**, 1031.
- KIDA, S., YANASE, S. & MIZUSHIMA, J. 1991 Statistical properties of MHD turbulence and turbulent dynamo. *Phys. Fluids A* **3**, 457.
- KIM, H. & CHO, J. 2015 Inverse cascade in imbalanced electron magnetohydrodynamic turbulence. *Astrophys. J.* **801**, 75.
- KINNEY, R. M., CHANDRAN, B., COWLEY, S. & MCWILLIAMS, J. C. 2000 Magnetic field growth and saturation in plasmas with large magnetic Prandtl number. I. The two-dimensional case. *Astrophys. J.* **545**, 907.
- KIYANI, K. H., CHAPMAN, S. C., KHOTYAINTEV, Y. V., DUNLOP, M. W. & SAHRAOUI, F. 2009 Global scale-invariant dissipation in collisionless plasma turbulence. *Phys. Rev. Lett.* **103**, 075006.
- KOBAYASHI, S., SAHRAOUI, F., PASSOT, T., LAVEDER, D., SULEM, P. L., HUANG, S. Y., HENRI, P. & SMETS, R. 2017 Three-dimensional simulations and spacecraft observations of sub-ion scale turbulence in the solar wind: influence of Landau damping. *Astrophys. J.* **839**, 122.
- KOLMOGOROV, A. N. 1941a Dissipation of energy in the locally isotropic turbulence. *Dokl. Acad. Nauk SSSR* **32**, 19.
- KOLMOGOROV, A. N. 1941b Local structure of turbulence in incompressible viscous fluid at very large Reynolds numbers. *Dokl. Acad. Nauk SSSR* **30**, 299.
- KOLMOGOROV, A. N. 1941c On the degeneration of isotropic turbulence in an incompressible viscous fluid. *Dokl. Acad. Nauk SSSR* **31**, 538.
- KOLMOGOROV, A. N. 1962 A refinement of previous hypotheses concerning the local structure of turbulence in a viscous incompressible fluid at high Reynolds number. *J. Fluid Mech.* **13**, 82.
- KOWAL, G., FALCETA-GONÇALVES, D. A., LAZARIAN, A. & VISHNIAC, E. T. 2017 Statistics of reconnection-driven turbulence. *Astrophys. J.* **838**, 91.
- KOWAL, G., FALCETA-GONÇALVES, D. A., LAZARIAN, A. & VISHNIAC, E. T. 2020 Kelvin-Helmholtz versus tearing instability: What drives turbulence in stochastic reconnection? *Astrophys. J.* **892**, 50.
- KOWAL, G. & LAZARIAN, A. 2010 Velocity field of compressible magnetohydrodynamic turbulence: wavelet decomposition and mode scalings. *Astrophys. J.* **720**, 742.
- KOWAL, G., LAZARIAN, A., VISHNIAC, E. T. & OTMIANOWSKA-MAZUR, K. 2009 Numerical tests of fast reconnection in weakly stochastic magnetic fields. *Astrophys. J.* **700**, 63.
- KOWAL, G., LAZARIAN, A., VISHNIAC, E. T. & OTMIANOWSKA-MAZUR, K. 2012 Reconnection studies under different types of turbulence driving. *Nonlin. Proc. Geophys.* **19**, 297.
- KRAICHNAN, R. H. 1965 Inertial-range spectrum of hydromagnetic turbulence. *Phys. Fluids* **8**, 1385.
- KUHN, T. S. 1962 *The Structure of Scientific Revolutions*. Chicago: University of Chicago Press.
- KULPA-DYBEL, K., KOWAL, G., OTMIANOWSKA-MAZUR, K., LAZARIAN, A. & VISHNIAC, E. 2010 Reconnection in weakly stochastic B-fields in 2D. *Astron. Astrophys.* **514**, A26.
- KULSRUD, R. M. 2005 *Plasma Physics for Astrophysics*. Princeton: Princeton University Press.
- KULSRUD, R. M. & ANDERSON, S. W. 1992 The spectrum of random magnetic fields in the mean field dynamo theory of the Galactic magnetic field. *Astrophys. J.* **396**, 606.
- KUNZ, M. W., SCHEKOCIHIN, A. A., CHEN, C. H. K., ABEL, I. G. & COWLEY, S. C. 2015 Inertial-range kinetic turbulence in pressure-anisotropic astrophysical plasmas. *J. Plasma Phys.* **81**, 325810501.
- KUNZ, M. W., SCHEKOCIHIN, A. A. & STONE, J. M. 2014 Firehose and mirror instabilities in a collisionless shearing plasma. *Phys. Rev. Lett.* **112**, 205003.
- KUNZ, M. W., SQUIRE, J., SCHEKOCIHIN, A. A. & QUATAERT, E. 2020 Self-sustaining sound in collisionless, high-beta plasma. *E-print arXiv:2006.08940*.
- KUNZ, M. W., STONE, J. M. & QUATAERT, E. 2016 Magnetorotational turbulence and dynamo in a collisionless plasma. *Phys. Rev. Lett.* **117**, 235101.
- LALESCU, C. C., SHI, Y.-K., EYINK, G. L., DRIVAS, T. D., VISHNIAC, E. T. & LAZARIAN,

- A. 2015 Inertial-range reconnection in magnetohydrodynamic turbulence and in the solar wind. *Phys. Rev. Lett.* **115**, 025001.
- LANDAU, L. 1946 On the vibration of the electronic plasma. *Zh. Eksp. Teor. Fiz.* **16**, 574.
- LANDAU, L. D. & LIFSHTIZ, E. M. 1987 *Fluid Mechanics*. Oxford: Pergamon Press.
- LAPENTA, G. 2008 Self-feeding turbulent magnetic reconnection on macroscopic scales. *Phys. Rev. Lett.* **100**, 235001.
- LAZARIAN, A., EYINK, G., VISHNIAC, E. & KOWAL, G. 2015 Turbulent reconnection and its implications. *Philos. Trans. R. Soc. London A* **373**, 20140144.
- LAZARIAN, A., EYINK, G. L., JAFARI, A., KOWAL, G., LI, H., XU, S. & VISHNIAC, E. T. 2020 3D turbulent reconnection: theory, tests and astrophysical implications. *Phys. Plasmas* **27**, 012305.
- LAZARIAN, A. & VISHNIAC, E. T. 1999 Reconnection in a weakly stochastic field. *Astrophys. J.* **517**, 700.
- LAZARIAN, A., VISHNIAC, E. T. & CHO, J. 2004 Magnetic field structure and stochastic reconnection in a partially ionized gas. *Astrophys. J.* **603**, 180.
- LEE, E., BRACHET, M. E., POUQUET, A., MININNI, P. D. & ROSENBERG, D. 2010 Lack of universality in decaying magnetohydrodynamic turbulence. *Phys. Rev. E* **81**, 016318.
- LEE, L. C. & FU, Z. F. 1986 Multiple X line reconnection. I. A criterion for the transition from a single X line to a multiple X line reconnection. *J. Geophys. Res.* **91**, 6807.
- LITHWICK, Y. & GOLDREICH, P. 2003 Imbalanced weak magnetohydrodynamic turbulence. *Astrophys. J.* **582**, 1220.
- LITHWICK, Y., GOLDREICH, P. & SRIDHAR, S. 2007 Imbalanced strong MHD turbulence. *Astrophys. J.* **655**, 269.
- LOMONOSOV, M. V. 1748 Letter to L. Euler, 5 July 1748. Source: <http://lomonosov.niv.ru/lomonosov/pisma/letter-12.htm>.
- LOUREIRO, N. F. & BOLDYREV, S. 2017a Collisionless reconnection in magnetohydrodynamic and kinetic turbulence. *Astrophys. J.* **850**, 182.
- LOUREIRO, N. F. & BOLDYREV, S. 2017b Role of magnetic reconnection in magnetohydrodynamic turbulence. *Phys. Rev. Lett.* **118**, 245101.
- LOUREIRO, N. F. & BOLDYREV, S. 2018 Turbulence in magnetized pair plasmas. *Astrophys. J.* **866**, L14.
- LOUREIRO, N. F. & BOLDYREV, S. 2020 Nonlinear reconnection in magnetized turbulence. *Astrophys. J.* **890**, 55.
- LOUREIRO, N. F., COWLEY, S. C., DORLAND, W. D., HAINES, M. G. & SCHEKOCHIHIN, A. A. 2005 X-point collapse and saturation in the nonlinear tearing mode reconnection. *Phys. Rev. Lett.* **95**, 235003.
- LOUREIRO, N. F., SAMTANEY, R., SCHEKOCHIHIN, A. A. & UZDENSKY, D. A. 2012 Magnetic reconnection and stochastic plasmoid chains in high-Lundquist-number plasmas. *Phys. Plasmas* **19**, 042303.
- LOUREIRO, N. F., SCHEKOCHIHIN, A. A. & COWLEY, S. C. 2007 Instability of current sheets and formation of plasmoid chains. *Phys. Plasmas* **14**, 100703.
- LOUREIRO, N. F., SCHEKOCHIHIN, A. A. & UZDENSKY, D. A. 2013a Plasmoid and Kelvin-Helmholtz instabilities in Sweet-Parker current sheets. *Phys. Rev. E* **87**, 013102.
- LOUREIRO, N. F., SCHEKOCHIHIN, A. A. & ZOCCO, A. 2013b Fast collisionless reconnection and electron heating in strongly magnetized plasmas. *Phys. Rev. Lett.* **111**, 025002.
- LOUREIRO, N. F., UZDENSKY, D. A., SCHEKOCHIHIN, A. A., COWLEY, S. C. & YOUSEF, T. A. 2009 Turbulent magnetic reconnection in two dimensions. *Mon. Not. R. Astron. Soc.* **399**, L146.
- LUMLEY, J. L. 1969 Drag reduction by additives. *Annu. Rev. Fluid Mech.* **1**, 367.
- LUO, Q. Y. & WU, D. J. 2010 Observations of anisotropic scaling of solar wind turbulence. *Astrophys. J.* **714**, L138.
- MAC LOW, M.-M., KLESSEN, R. S., BURKERT, A. & SMITH, M. D. 1998 Kinetic energy decay rates of supersonic and super-Alfvénic turbulence in star-forming clouds. *Phys. Rev. Lett.* **80**, 2754.
- MALARA, F., VELTRI, P. & CARBONE, V. 1992 Competition among nonlinear effects in tearing instability saturation. *Phys. Fluids B* **4**, 3070.
- MALLET, A. 2020 The onset of electron-only reconnection. *J. Plasma Phys.* **86**, 905860301.

- MALLET, A., KLEIN, K. G., CHANDRAN, B. D. G., GROŠELJ, D., HOPPOCK, I. W., BOWEN, T. A., SALEM, C. S. & BALE, S. D. 2019 Interplay between intermittency and dissipation in collisionless plasma turbulence. *J. Plasma Phys.* **85**, 175850302.
- MALLET, A. & SCHEKOCIHIN, A. A. 2011 Simulations of imbalanced RMHD turbulence. Unpublished.
- MALLET, A. & SCHEKOCIHIN, A. A. 2017 A statistical model of three-dimensional anisotropy and intermittency in strong Alfvénic turbulence. *Mon. Not. R. Astron. Soc.* **466**, 3918.
- MALLET, A., SCHEKOCIHIN, A. A. & CHANDRAN, B. D. G. 2015 Refined critical balance in strong Alfvénic turbulence. *Mon. Not. R. Astron. Soc.* **449**, L77.
- MALLET, A., SCHEKOCIHIN, A. A. & CHANDRAN, B. D. G. 2017*a* Disruption of Alfvénic turbulence by magnetic reconnection in a collisionless plasma. *J. Plasma Phys.* **83**, 905830609.
- MALLET, A., SCHEKOCIHIN, A. A. & CHANDRAN, B. D. G. 2017*b* Disruption of sheetlike structures in Alfvénic turbulence by magnetic reconnection. *Mon. Not. R. Astron. Soc.* **468**, 4862.
- MALLET, A., SCHEKOCIHIN, A. A., CHANDRAN, B. D. G., CHEN, C. H. K., HORBURY, T. S., WICKS, R. T. & GREENAN, C. C. 2016 Measures of three-dimensional anisotropy and intermittency in strong Alfvénic turbulence. *Mon. Not. R. Astron. Soc.* **459**, 2130.
- MARON, J., COWLEY, S. & MCWILLIAMS, J. 2004 The nonlinear magnetic cascade. *Astrophys. J.* **603**, 569.
- MARON, J. & GOLDREICH, P. 2001 Simulations of incompressible magnetohydrodynamic turbulence. *Astrophys. J.* **554**, 1175.
- MASON, J., CATTANEO, F. & BOLDYREV, S. 2006 Dynamic alignment in driven magnetohydrodynamic turbulence. *Phys. Rev. Lett.* **97**, 255002.
- MASON, J., CATTANEO, F. & BOLDYREV, S. 2008 Numerical measurements of the spectrum in magnetohydrodynamic turbulence. *Phys. Rev. E* **77**, 036403.
- MASON, J., PEREZ, J. C., BOLDYREV, S. & CATTANEO, F. 2012 Numerical simulations of strong incompressible magnetohydrodynamic turbulence. *Phys. Plasmas* **19**, 055902.
- MASON, J., PEREZ, J. C., CATTANEO, F. & BOLDYREV, S. 2011 Extended scaling laws in numerical simulations of magnetohydrodynamic turbulence. *Astrophys. J.* **735**, L26.
- MATTHAEUS, W. H., GHOSH, S., OUGHTON, S. & ROBERTS, D. A. 1996 Anisotropic three-dimensional MHD turbulence. *J. Geophys. Res.* **101**, 7619.
- MATTHAEUS, W. H. & GOLDSTEIN, M. L. 1982 Measurement of the rugged invariants of magnetohydrodynamic turbulence in the solar wind. *J. Geophys. Res.* **87**, 6011.
- MATTHAEUS, W. H. & LAMKIN, S. L. 1985 Rapid magnetic reconnection caused by finite amplitude fluctuations. *Phys. Fluids* **28**, 303.
- MATTHAEUS, W. H. & LAMKIN, S. L. 1986 Turbulent magnetic reconnection. *Phys. Fluids* **29**, 2513.
- MATTHAEUS, W. H., MONTGOMERY, D. C. & GOLDSTEIN, M. L. 1983 Turbulent generation of outward-traveling interplanetary Alfvénic fluctuations. *Phys. Rev. Lett.* **51**, 1484.
- MATTHAEUS, W. H., POUQUET, A., MININNI, P. D., DMITRUK, P. & BREECH, B. 2008 Rapid alignment of velocity and magnetic field in magnetohydrodynamic turbulence. *Phys. Rev. Lett.* **100**, 085003.
- MATTHAEUS, W. H., SERVIDIO, S., DMITRUK, P., CARBONE, V., OUGHTON, S., WAN, M. & OSMAN, K. T. 2012 Local anisotropy, higher order statistics, and turbulence spectra. *Astrophys. J.* **750**, 103.
- McKAY, M. E., BERERA, A. & HO, R. D. J. G. 2019 Fully resolved array of simulations investigating the influence of the magnetic Prandtl number on magnetohydrodynamic turbulence. *Phys. Rev. E* **99**, 013101.
- McKEE, C. F., STACY, A. & LI, P. S. 2020 Magnetic fields in the formation of the first stars. I. Theory vs. simulation. *E-print* arXiv:2006.14607.
- MELVILLE, S., SCHEKOCIHIN, A. A. & KUNZ, M. W. 2016 Pressure-anisotropy-driven microturbulence and magnetic-field evolution in shearing, collisionless plasma. *Mon. Not. R. Astron. Soc.* **459**, 2701.
- MENEGUZZI, M., FRISCH, U. & POUQUET, A. 1981 Helical and nonhelical turbulent dynamos. *Phys. Rev. Lett.* **47**, 1060.

- MEYRAND, R., GALTIER, S. & KIYANI, K. H. 2016 Direct evidence of the transition from weak to strong magnetohydrodynamic turbulence. *Phys. Rev. Lett.* **116**, 105002.
- MEYRAND, R., KANEKAR, A., DORLAND, W. & SCHEKOCIHIN, A. A. 2019 Fluidization of collisionless plasma turbulence. *Proc. Nat. Acad. Sci.* **116**, 1185.
- MEYRAND, R., KIYANI, K. H. & GALTIER, S. 2015 Weak magnetohydrodynamic turbulence and intermittency. *J. Fluid Mech.* **770**, R1.
- MEYRAND, R. & SQUIRE, J. 2020 private communication.
- MEYRAND, R., SQUIRE, J., SCHEKOCIHIN, A. A. & DORLAND, W. 2020 Violation of the zeroth law of turbulence in space plasmas. *E-print arXiv:2009.02828*.
- MILOSHEVICH, G., LAVEDER, D., PASSOT, T. & SULEM, P.-L. 2020 Inverse cascade and magnetic vortices in kinetic Alfvén-wave turbulence. *E-print arXiv:2007.06976*.
- MININNI, P. D., POUQUET, A. G. & MONTGOMERY, D. C. 2006 Small-scale structures in three-dimensional magnetohydrodynamic turbulence. *Phys. Rev. Lett.* **97**, 244503.
- MOFFATT, H. K. 1986 Magnetostatic equilibria and analogous Euler flows of arbitrarily complex topology. Part 2. Stability considerations. *J. Fluid Mech.* **166**, 359.
- MONTGOMERY, D. & TURNER, L. 1981 Anisotropic magnetohydrodynamic turbulence in a strong external magnetic field. *Phys. Fluids* **24**, 825.
- MOSER, A. L. & BELLAN, P. M. 2012 Magnetic reconnection from a multiscale instability cascade. *Nature* **482**, 379.
- MÜLLER, W.-C. & BISKAMP, D. 2000 Scaling properties of three-dimensional magnetohydrodynamic turbulence. *Phys. Rev. Lett.* **84**, 475.
- MÜLLER, W.-C., BISKAMP, D. & GRAPPIN, R. 2003 Statistical anisotropy of magnetohydrodynamic turbulence. *Phys. Rev. E* **67**, 066302.
- MÜLLER, W.-C. & GRAPPIN, R. 2005 Spectral energy dynamics in magnetohydrodynamic turbulence. *Phys. Rev. Lett.* **95**, 114502.
- MÜLLER, W.-C., MALAPAKA, S. K. & BUSSE, A. 2012 Inverse cascade of magnetic helicity in magnetohydrodynamic turbulence. *Phys. Rev. E* **85**, 015302.
- NAZARENKO, S. 2007 2D enslaving of MHD turbulence. *New J. Phys.* **9**, 307.
- NAZARENKO, S. 2011 *Wave Turbulence*. Berlin: Springer.
- NAZARENKO, S. V. & SCHEKOCIHIN, A. A. 2011 Critical balance in magnetohydrodynamic, rotating and stratified turbulence: towards a universal scaling conjecture. *J. Fluid Mech.* **677**, 134.
- NG, C. S. & BHATTACHARJEE, A. 1996 Interaction of shear-Alfvén wave packets: implication for weak magnetohydrodynamic turbulence in astrophysical plasmas. *Astrophys. J.* **465**, 845.
- NG, C. S. & BHATTACHARJEE, A. 1997 Scaling of anisotropic spectra due to the weak interaction of shear-Alfvén wave packets. *Phys. Plasmas* **4**, 605.
- NI, L., GERMASCHESKI, K., HUANG, Y.-M., SULLIVAN, B. P., YANG, H. & BHATTACHARJEE, A. 2010 Linear plasmoid instability of thin current sheets with shear flow. *Phys. Plasmas* **17**, 052109.
- Ogilvie, G. I. & PROCTOR, M. R. E. 2003 On the relation between viscoelastic and magnetohydrodynamic flows and their instabilities. *J. Fluid Mech.* **476**, 389.
- OISHI, J. S., MAC LOW, M.-M., COLLINS, D. C. & TAMURA, M. 2015 Self-generated turbulence in magnetic reconnection. *Astrophys. J.* **806**, L12.
- OLESEN, P. 1997 Inverse cascades and primordial magnetic fields. *Phys. Lett. B* **398**, 321.
- OLESEN, P. 2015 Dimensional reduction in freely decaying turbulent non-helical magnetic fields. *E-print arXiv:1511.05007*.
- OSMAN, K. T., MATTHAEUS, W. H., GOSLING, J. T., GRECO, A., SERVIDIO, S., HNAT, B., CHAPMAN, S. C. & PHAN, T. D. 2014 Magnetic reconnection and intermittent turbulence in the solar wind. *Phys. Rev. Lett.* **112**, 215002.
- OSMAN, K. T., WAN, M., MATTHAEUS, W. H., BREECH, B. & OUGHTON, S. 2011 Directional alignment and non-Gaussian statistics in solar wind turbulence. *Astrophys. J.* **741**, 75.
- OUGHTON, S., MATTHAEUS, W. H. & DMITRUK, P. 2017 Reduced MHD in astrophysical applications: two-dimensional or three-dimensional? *Astrophys. J.* **839**, 2.
- OUGHTON, S., PRIEST, E. R. & MATTHAEUS, W. H. 1994 The influence of a mean magnetic field on three-dimensional magnetohydrodynamic turbulence. *J. Fluid Mech.* **280**, 95.

- PARK, K. 2017 On the inverse transfer of (non-)helical magnetic energy in a decaying magnetohydrodynamic turbulence. *Mon. Not. R. Astron. Soc.* **472**, 1628.
- PARK, W., MONTICELLO, D. A. & WHITE, R. B. 1984 Reconnection rates of magnetic fields including the effects of viscosity. *Phys. Fluids* **27**, 137.
- PARKER, E. N. 1957 Sweet's mechanism for merging magnetic fields in conducting fluids. *J. Geophys. Res.* **62**, 509.
- PARKER, J. T., HIGHCOCK, E. G., SCHEKOCIHIN, A. A. & DELLAR, P. J. 2016 Suppression of phase mixing in drift-kinetic plasma turbulence. *Phys. Plasmas* **23**, 070703.
- PASSOT, T., SULEM, P. L. & TASSI, E. 2017 Electron-scale reduced fluid models with gyroviscous effects. *J. Plasma Phys.* **83**, 715830402.
- PEREZ, J. C. & BOLDYREV, S. 2008 On weak and strong magnetohydrodynamic turbulence. *Astrophys. J.* **672**, L61.
- PEREZ, J. C. & BOLDYREV, S. 2009 Role of cross-helicity in magnetohydrodynamic turbulence. *Phys. Rev. Lett.* **102**, 025003.
- PEREZ, J. C. & BOLDYREV, S. 2010a Numerical simulations of imbalanced strong magnetohydrodynamic turbulence. *Astrophys. J.* **710**, L63.
- PEREZ, J. C. & BOLDYREV, S. 2010b Strong magnetohydrodynamic turbulence with cross helicity. *Phys. Plasmas* **17**, 055903.
- PEREZ, J. C., MASON, J., BOLDYREV, S. & CATTANEO, F. 2012 On the energy spectrum of strong magnetohydrodynamic turbulence. *Phys. Rev. X* **2**, 041005.
- PEREZ, J. C., MASON, J., BOLDYREV, S. & CATTANEO, F. 2014a Comment on the numerical measurements of the magnetohydrodynamic turbulence spectrum by A. Beresnyak (Phys. Rev. Lett. 106 (2011) 075001; MNRAS 422 (2012) 3495; ApJ 784 (2014) L20). *E-print arXiv:1409.8106*.
- PEREZ, J. C., MASON, J., BOLDYREV, S. & CATTANEO, F. 2014b Scaling properties of small-scale fluctuations in magnetohydrodynamic turbulence. *Astrophys. J.* **793**, L13.
- PETERSON, E. E., ENDRIZZI, D. A., BEIDLER, M., BUNKERS, K. J., CLARK, M., EGEDAL, J., FLANAGAN, K., MCCOLLAM, K. J., MILHONE, J., OLSON, J., SOVINEC, C. R., WALEFFE, R., WALLACE, J. & FOREST, C. B. 2019 A laboratory model for the Parker spiral and magnetized stellar winds. *Nature Phys.* **15**, 1095.
- PEZZI, O., SERVIDIO, S., PERRONE, D., VALENTINI, F., SORRISO-VALVO, L., GRECO, A., MATTHAEUS, W. H. & VELTRI, P. 2018 Velocity-space cascade in magnetized plasmas: numerical simulations. *Phys. Plasmas* **25**, 060704.
- PLUNK, G. G., COWLEY, S. C., SCHEKOCIHIN, A. A. & TATSUNO, T. 2010 Two-dimensional gyrokinetic turbulence. *J. Fluid Mech.* **664**, 407.
- PODESTA, J. J. 2009 Dependence of solar-wind power spectra on the direction of the local mean magnetic field. *Astrophys. J.* **698**, 986.
- PODESTA, J. J. 2011 On the cross-helicity dependence of the energy spectrum in magnetohydrodynamic turbulence. *Phys. Plasmas* **18**, 012907.
- PODESTA, J. J. & BHATTACHARJEE, A. 2010 Theory of incompressible magnetohydrodynamic turbulence with scale-dependent alignment and cross-helicity. *Astrophys. J.* **718**, 1151.
- PODESTA, J. J. & BOROVSKY, J. E. 2010 Scale invariance of normalized cross-helicity throughout the inertial range of solar wind turbulence. *Phys. Plasmas* **17**, 112905.
- PODESTA, J. J., CHANDRAN, B. D. G., BHATTACHARJEE, A., ROBERTS, D. A. & GOLDSTEIN, M. L. 2009 Scale-dependent angle of alignment between velocity and magnetic field fluctuations in solar wind turbulence. *J. Geophys. Res.* **114**, A131107.
- POLITANO, H. & POUQUET, A. 1998a Dynamical length scales for turbulent magnetized flows. *Geophys. Res. Lett.* **25**, 273.
- POLITANO, H. & POUQUET, A. 1998b von Kármán-Howarth equation for magnetohydrodynamics and its consequences on third-order longitudinal structure and correlation functions. *Phys. Rev. E* **57**, R21.
- POLITANO, H., POUQUET, A. & SULEM, P. L. 1989 Inertial ranges and resistive instabilities in two-dimensional magnetohydrodynamic turbulence. *Phys. Fluids B* **1**, 2330.
- PORCELLI, F. 1987 Viscous resistive magnetic reconnection. *Phys. Fluids* **30**, 1734.
- PORCELLI, F., BORGOGNO, D., CALIFANO, F., GRASSO, D., OTTAVIANI, M. & PEGORARO, F. 2002 Recent advances in collisionless magnetic reconnection. *Plasma Phys. Control. Fusion* **44**, B389.

- PORTER, D. H., JONES, T. W. & RYU, D. 2015 Vorticity, shocks, and magnetic fields in subsonic, ICM-like turbulence. *Astrophys. J.* **810**, 93.
- POUQUET, A., FRISCH, U. & LEORAT, J. 1976 Strong MHD helical turbulence and the nonlinear dynamo effect. *J. Fluid Mech.* **77**, 321.
- POUQUET, A., FRISCH, U. & MENEGUZZI, M. 1986 Growth of correlations in magnetohydrodynamic turbulence. *Phys. Rev. A* **33**, 4266.
- POUQUET, A., SULEM, P. L. & MENEGUZZI, M. 1988 Influence of velocity-magnetic field correlations on decaying magnetohydrodynamic turbulence with neutral X points. *Phys. Fluids* **31**, 2635.
- PUCCI, F. & VELLI, M. 2014 Reconnection of quasi-singular current sheets: the “ideal” tearing mode. *Astrophys. J.* **780**, L19.
- PUCCI, F., VELLI, M., TENERANI, A. & DEL SARTO, D. 2018 Onset of fast “ideal” tearing in thin current sheets: dependence on the equilibrium current profile. *Phys. Plasmas* **25**, 032113.
- QUATAERT, E. & GRUZINOV, A. 1999 Turbulence and particle heating in advection-dominated accretion flows. *Astrophys. J.* **520**, 248.
- REPPIN, J. & BANERJEE, R. 2017 Nonhelical turbulence and the inverse transfer of energy: a parameter study. *Phys. Rev. E* **96**, 053105.
- RETINÒ, A., SUNDKVIST, D., VAIVADS, A., MOZER, F., ANDRÉ, M. & OWEN, C. J. 2007 In situ evidence of magnetic reconnection in turbulent plasma. *Nature Phys.* **3**, 236.
- RICHARDSON, L. F. 1926 Atmospheric diffusion shown on a distance-neighbour graph. *Proc. R. Soc. London A* **110**, 709.
- RINCON, F. 2019 Dynamo theories. *J. Plasma Phys.* **85**, 205850401.
- RINCON, F., CALIFANO, F., SCHEKOCHIHIN, A. A. & VALENTINI, F. 2016 Turbulent dynamo in a collisionless plasma. *Proc. Nat. Acad. Sci.* **113**, 3950.
- ROBERTS, D. A., GOLDSTEIN, M. L., KLEIN, L. W. & MATTHAEUS, W. H. 1987 Origin and evolution of fluctuations in the solar wind - HELIOS observations and Helios-Voyager comparisons. *J. Geophys. Res.* **92**, 12023.
- ROBINSON, D. C. & RUSBRIDGE, M. G. 1971 Structure of turbulence in the Zeta plasma. *Phys. Fluids* **14**, 2499.
- ROH, S., RYU, D., KANG, H., HA, S. & JANG, H. 2019 Turbulence dynamo in the stratified medium of galaxy clusters. *Astrophys. J.* **883**, 138.
- RUTHERFORD, P. H. 1973 Nonlinear growth of the tearing mode. *Phys. Fluids* **16**, 1903.
- SAHOO, G., PERLEKAR, P. & PANDIT, R. 2011 Systematics of the magnetic-Prandtl-number dependence of homogeneous, isotropic magnetohydrodynamic turbulence. *New J. Phys.* **13**, 013036.
- SAHRAOUI, F., HUANG, S. Y., BELMONT, G., GOLDSTEIN, M. L., RÉTINO, A., ROBERT, P. & DE PATOUL, J. 2013 Scaling of the electron dissipation range of solar wind turbulence. *Astrophys. J.* **777**, 15.
- SAMTANEY, R., LOUREIRO, N. F., UZDENSKY, D. A., SCHEKOCHIHIN, A. A. & COWLEY, S. C. 2009 Formation of plasmoid chains in magnetic reconnection. *Phys. Rev. Lett.* **103**, 105004.
- SCHEKOCHIHIN, A. A. 2020 *Lectures on Kinetic Theory and Magnetohydrodynamics of Plasmas*. Lecture Notes for the Oxford MMathPhys programme; URL: <http://www-thphys.physics.ox.ac.uk/people/AlexanderSchekochihin/KT/2015/KTLectureNotes.pdf>.
- SCHEKOCHIHIN, A. A. & COWLEY, S. C. 2006 Turbulence, magnetic fields, and plasma physics in clusters of galaxies. *Phys. Plasmas* **13**, 056501.
- SCHEKOCHIHIN, A. A. & COWLEY, S. C. 2007 Turbulence and magnetic fields in astrophysical plasmas. In *Magnetohydrodynamics: Historical Evolution and Trends* (ed. Molokov, S., Moreau, R., and Moffatt, H. K.), p. 85. Berlin: Springer.
- SCHEKOCHIHIN, A. A., COWLEY, S. C., DORLAND, W., HAMMETT, G. W., HOWES, G. G., PLUNK, G. G., QUATAERT, E. & TATSUNO, T. 2008 Gyrokinetic turbulence: a nonlinear route to dissipation through phase space. *Plasma Phys. Control. Fusion* **50**, 124024.
- SCHEKOCHIHIN, A. A., COWLEY, S. C., DORLAND, W., HAMMETT, G. W., HOWES, G. G., QUATAERT, E. & TATSUNO, T. 2009 Astrophysical gyrokinetics: kinetic and fluid turbulent cascades in magnetized weakly collisional plasmas. *Astrophys. J. Suppl.* **182**, 310.

- SCHEKOCHIHIN, A. A., COWLEY, S. C., HAMMETT, G. W., MARON, J. L. & MCWILLIAMS, J. C. 2002 A model of nonlinear evolution and saturation of the turbulent MHD dynamo. *New J. Phys.* **4**, 84.
- SCHEKOCHIHIN, A. A., COWLEY, S. C., RINCON, F. & ROSIN, M. S. 2010 Magnetofluid dynamics of magnetized cosmic plasma: firehose and gyrothermal instabilities. *Mon. Not. R. Astron. Soc.* **405**, 291.
- SCHEKOCHIHIN, A. A., COWLEY, S. C., TAYLOR, S. F., MARON, J. L. & MCWILLIAMS, J. C. 2004 Simulations of the small-scale turbulent dynamo. *Astrophys. J.* **612**, 276.
- SCHEKOCHIHIN, A. A., ISKAKOV, A. B., COWLEY, S. C., MCWILLIAMS, J. C., PROCTOR, M. R. E. & YOUSEF, T. A. 2007 Fluctuation dynamo and turbulent induction at low magnetic Prandtl numbers. *New J. Phys.* **9**, 300.
- SCHEKOCHIHIN, A. A., KAWAZURA, Y. & BARNES, M. A. 2019 Constraints on ion versus electron heating by plasma turbulence at low beta. *J. Plasma Phys.* **85**, 905850303.
- SCHEKOCHIHIN, A. A., NAZARENKO, S. V. & YOUSEF, T. A. 2012 Weak Alfvén-wave turbulence revisited. *Phys. Rev. E* **85**, 036406.
- SCHEKOCHIHIN, A. A., PARKER, J. T., HIGHCOCK, E. G., DELLAR, P. J., DORLAND, W. & HAMMETT, G. W. 2016 Phase mixing versus nonlinear advection in drift-kinetic plasma turbulence. *J. Plasma Phys.* **82**, 905820212.
- SERVIDIO, S., CHASAPIS, A., MATTHAEUS, W. H., PERRONE, D., VALENTINI, F., PARASHAR, T. N., VELTRI, P., GERSHMAN, D., RUSSELL, C. T., GILES, B., FUSELIER, S. A., PHAN, T. D. & BURCH, J. 2017 Magnetospheric Multiscale (MMS) observation of plasma velocity-space cascade: Hermite representation and theory. *Phys. Rev. Lett.* **119**, 205101.
- SERVIDIO, S., DMITRUK, P., GRECO, A., WAN, M., DONATO, S., CASSAK, P. A., SHAY, M. A., CARBONE, V. & MATTHAEUS, W. H. 2011a Magnetic reconnection as an element of turbulence. *Nonlin. Proc. Geophys.* **18**, 675.
- SERVIDIO, S., GRECO, A., MATTHAEUS, W. H., OSMAN, K. T. & DMITRUK, P. 2011b Statistical association of discontinuities and reconnection in magnetohydrodynamic turbulence. *J. Geophys. Res.* **116**, A09102.
- SERVIDIO, S., MATTHAEUS, W. H., SHAY, M. A., CASSAK, P. A. & DMITRUK, P. 2009 Magnetic reconnection in two-dimensional magnetohydrodynamic turbulence. *Phys. Rev. Lett.* **102**, 115003.
- SERVIDIO, S., MATTHAEUS, W. H., SHAY, M. A., DMITRUK, P., CASSAK, P. A. & WAN, M. 2010 Statistics of magnetic reconnection in two-dimensional magnetohydrodynamic turbulence. *Phys. Plasmas* **17**, 032315.
- SETA, A., BUSHBY, P. J., SHUKUROV, A. & WOOD, T. S. 2020 Saturation mechanism of the fluctuation dynamo at $\text{Pr}_M \geq 1$. *Phys. Rev. Fluids* **5**, 043702.
- SHE, Z.-S. & LEVEQUE, E. 1994 Universal scaling laws in fully developed turbulence. *Phys. Rev. Lett.* **72**, 336.
- SHE, Z.-S. & WAYMIRE, E. C. 1995 Quantized energy cascade and log-Poisson statistics in fully developed turbulence. *Phys. Rev. Lett.* **74**, 262.
- SHEBALIN, J. V., MATTHAEUS, W. H. & MONTGOMERY, D. 1983 Anisotropy in MHD turbulence due to a mean magnetic field. *J. Plasma Phys.* **29**, 525.
- SHEN, C., LIN, J., MURPHY, N. A. & RAYMOND, J. C. 2013 Statistical and spectral properties of magnetic islands in reconnecting current sheets during two-ribbon flares. *Phys. Plasmas* **20**, 072114.
- SHI, C., VELLI, M. & TENERANI, A. 2018 Marginal stability of Sweet–Parker type current sheets at low Lundquist numbers. *Astrophys. J.* **859**, 83.
- SHIBATA, K. & TANUMA, S. 2001 Plasmoid-induced-reconnection and fractal reconnection. *Earth, Planets, and Space* **53**, 473.
- SINGH, A., PUCCI, F., TENERANI, A., SHIBATA, K., HILLIER, A. & VELLI, M. 2019 Dynamic evolution of current sheets, ideal tearing, plasmoid formation and generalized fractal reconnection scaling relations. *Astrophys. J.* **881**, 52.
- SMITH, C. W., STAWARZ, J. E., VASQUEZ, B. J., FORMAN, M. A. & MACBRIDE, B. T. 2009 Turbulent cascade at 1 AU in high cross-helicity flows. *Phys. Rev. Lett.* **103**, 201101.
- SON, D. T. 1999 Magnetohydrodynamics of the early Universe and the evolution of primordial magnetic fields. *Phys. Rev. D* **59**, 063008.

- SOUTHWOOD, D. J. & KIVELSON, M. G. 1993 Mirror instability: 1. Physical mechanism of linear instability. *J. Geophys. Res. A* **98**, 9181.
- SQUIRE, J. & BHATTACHARJEE, A. 2015 Generation of large-scale magnetic fields by small-scale dynamo in shear flows. *Phys. Rev. Lett.* **115**, 175003.
- SQUIRE, J. & BHATTACHARJEE, A. 2016 The magnetic shear-current effect: generation of large-scale magnetic fields by the small-scale dynamo. *J. Plasma Phys.* **82**, 535820201.
- SQUIRE, J., KUNZ, M. W., QUATAERT, E. & SCHEKOCHIHIN, A. A. 2017a Kinetic simulations of the interruption of large-amplitude shear-Alfvén waves in a high- β plasma. *Phys. Rev. Lett.* **119**, 155101.
- SQUIRE, J., QUATAERT, E. & SCHEKOCHIHIN, A. A. 2016 A stringent limit on the amplitude of Alfvénic perturbations in high-beta low-collisionality plasmas. *Astrophys. J.* **830**, L25.
- SQUIRE, J., SCHEKOCHIHIN, A. A. & QUATAERT, E. 2017b Amplitude limits and nonlinear damping of shear-Alfvén waves in high-beta low-collisionality plasmas. *New J. Phys.* **19**, 055005.
- SQUIRE, J., SCHEKOCHIHIN, A. A., QUATAERT, E. & KUNZ, M. W. 2019 Magneto-immutable turbulence in weakly collisional plasmas. *J. Plasma Phys.* **85**, 905850114.
- SRIDHAR, S. & GOLDREICH, P. 1994 Toward a theory of interstellar turbulence. 1: Weak Alfvénic turbulence. *Astrophys. J.* **432**, 612.
- ST-ONGE, D. A. & KUNZ, M. W. 2018 Fluctuation dynamo in a collisionless, weakly magnetized plasma. *Astrophys. J.* **863**, L25.
- ST-ONGE, D. A., KUNZ, M. W., SQUIRE, J. & SCHEKOCHIHIN, A. A. 2020 Fluctuation dynamo in a weakly collisional plasma. *E-print* arXiv:2003.09760.
- STANIER, A., DAUGHTON, W., LE, A., LI, X. & BIRD, R. 2019 Influence of 3D plasmoid dynamics on the transition from collisional to kinetic reconnection. *Phys. Plasmas* **26** (7), 072121.
- STEINOLFSON, R. S. & VAN HOVEN, G. 1984 Nonlinear evolution of the resistive tearing mode. *Phys. Fluids* **27**, 1207.
- STRAUSS, H. R. 1976 Nonlinear, three-dimensional magnetohydrodynamics of noncircular tokamaks. *Phys. Fluids* **19**, 134.
- STRIBLING, T. & MATTHAEUS, W. H. 1991 Relaxation processes in a low-order three-dimensional magnetohydrodynamics model. *Phys. Fluids B* **3**, 1848.
- SUNDKVIST, D., RETINÒ, A., VAIVADS, A. & BALE, S. D. 2007 Dissipation in turbulent plasma due to reconnection in thin current sheets. *Phys. Rev. Lett.* **99**, 025004.
- SWEET, P. A. 1958 The neutral point theory of solar flares. In *Electromagnetic Phenomena in Cosmical Physics* (ed. B. Lehnert), *IAU Symposium*, vol. 6, p. 123.
- SYROVATSKIĬ, S. I. 1971 Formation of current sheets in a plasma with a frozen-in strong magnetic field. *Sov. Phys.-JETP* **33**, 933.
- TAJIMA, T. & SHIBATA, K. 1997 *Plasma Astrophysics*. Reading, MA: Addison-Wesley.
- TATSUNO, T., DORLAND, W., SCHEKOCHIHIN, A. A., PLUNK, G. G., BARNES, M., COWLEY, S. C. & HOWES, G. G. 2009 Nonlinear phase mixing and phase-space cascade of entropy in gyrokinetic plasma turbulence. *Phys. Rev. Lett.* **103**, 015003.
- TAYLOR, J. B. 1974 Relaxation of toroidal plasma and generation of reverse magnetic fields. *Phys. Rev. Lett.* **33**, 1139.
- TAYLOR, J. B. & NEWTON, S. L. 2015 Special topics in plasma confinement. *J. Plasma Phys.* **81**, 205810501.
- TEACA, B., LALESCU, C. C., KNAEPEN, B. & CARATI, D. 2011 Controlling the level of the ideal invariant fluxes for MHD turbulence using TURBO spectral solver. *E-print* arXiv:1108.2640.
- TENBARGE, J. M. & HOWES, G. G. 2013 Current sheets and collisionless damping in kinetic plasma turbulence. *Astrophys. J.* **771**, L27.
- TENERANI, A., RAPPAZZO, A. F., VELLI, M. & PUCCI, F. 2015a The tearing mode instability of thin current sheets: the transition to fast reconnection in the presence of viscosity. *Astrophys. J.* **801**, 145.
- TENERANI, A. & VELLI, M. 2018 Nonlinear firehose relaxation and constant-B field fluctuations. *Astrophys. J.* **867**, L26.
- TENERANI, A. & VELLI, M. 2020a Alfvénic fluctuations in the solar wind: nonlinearities and pressure anisotropy effects. *Plasma Phys. Control. Fusion* **62**, 014001.

- TENERANI, A. & VELLI, M. 2020*b* Spectral signatures of recursive magnetic field reconnection. *Mon. Not. R. Astron. Soc.* **491**, 4267.
- TENERANI, A., VELLI, M. & HELLINGER, P. 2017 The parametric instability of Alfvén waves: effects of temperature anisotropy. *Astrophys. J.* **851**, 99.
- TENERANI, A., VELLI, M., PUCCI, F., LANDI, S. & RAPPAZZO, A. F. 2016 “Ideally” unstable current sheets and the triggering of fast magnetic reconnection. *J. Plasma Phys.* **82**, 535820501.
- TENERANI, A., VELLI, M., RAPPAZZO, A. F. & PUCCI, F. 2015*b* Magnetic reconnection: recursive current sheet collapse triggered by ideal tearing. *Astrophys. J.* **813**, L32.
- TZEFERACOS, P., RIGBY, A., BOTT, A. F. A., BELL, A. R., BINGHAM, R., CASNER, A., CATTANEO, F., CHURAZOV, E. M., EMIG, J., FIUZA, F., FOREST, C. B., FOSTER, J., GRAZIANI, C., KATZ, J., KOENIG, M., LI, C.-K., MEINECKE, J., PETRASSO, R., PARK, H.-S., REMINGTON, B. A., ROSS, J. S., RYU, D., RYUTOV, D., WHITE, T. G., REVILLE, B., MINIATI, F., SCHEKOCIHIN, A. A., LAMB, D. Q., FROULA, D. H. & GREGORI, G. 2018 Laboratory evidence of dynamo amplification of magnetic fields in a turbulent plasma. *Nature Comm.* **9**, 591.
- UZDENSKY, D. A. & BOLDYREV, S. A. 2006 Unpublished.
- UZDENSKY, D. A. & KULSRUD, R. M. 2000 Two-dimensional numerical simulation of the resistive reconnection layer. *Phys. Plasmas* **7**, 4018.
- UZDENSKY, D. A., KULSRUD, R. M. & YAMADA, M. 1996 Theoretical analysis of driven magnetic reconnection experiments. *Phys. Plasmas* **3**, 1220.
- UZDENSKY, D. A. & LOUREIRO, N. F. 2016 Magnetic reconnection onset via disruption of a forming current sheet by the tearing instability. *Phys. Rev. Lett.* **116**, 105003.
- UZDENSKY, D. A., LOUREIRO, N. F. & SCHEKOCIHIN, A. A. 2010 Fast magnetic reconnection in the plasmoid-dominated regime. *Phys. Rev. Lett.* **105**, 235002.
- VACCA, V., MURGIA, M., GOVONI, F., ENSSLIN, T., OPPERMAN, N., FERETTI, L., GIOVANNINI, G. & LOI, F. 2018 Magnetic fields in galaxy clusters and in the large-scale structure of the Universe. *Galaxies* **6**, 142.
- VALENTE, P. C., DA SILVA, C. B. & PINHO, F. T. 2016 Energy spectra in elasto-inertial turbulence. *Phys. Fluids* **28**, 075108.
- VARSHNEY, A. & STEINBERG, V. 2019 Elastic Alfvén waves in elastic turbulence. *Nature Comm.* **10**, 652.
- VECH, D. & CHEN, C. H. K. 2016 Testing the effects of expansion on solar wind turbulence. *Astrophys. J.* **832**, L16.
- VECH, D., MALLET, A., KLEIN, K. G. & KASPER, J. C. 2018 Magnetic reconnection may control the ion-scale spectral break of solar wind turbulence. *Astrophys. J.* **855**, L27.
- VERDINI, A. & GRAPPIN, R. 2015 Imprints of expansion on the local anisotropy of solar wind turbulence. *Astrophys. J.* **808**, L34.
- VERDINI, A., GRAPPIN, R., ALEXANDROVA, O., FRANCI, L., LANDI, S., MATTEINI, L. & PAPINI, E. 2019 Three-dimensional local anisotropy of velocity fluctuations in the solar wind. *Mon. Not. R. Astron. Soc.* **486**, 3006.
- VERDINI, A., GRAPPIN, R., ALEXANDROVA, O. & LION, S. 2018 3D anisotropy of solar wind turbulence: tubes or ribbons? *Astrophys. J.* **853**, 85, erratum: *Astrophys. J.* **867**, 168 (2018).
- VERSCHAREN, D., CHEN, C. H. K. & WICKS, R. T. 2017 On kinetic slow modes, fluid slow modes, and pressure-balanced structures in the solar wind. *Astrophys. J.* **840**, 106.
- WALBROECK, F. L. 1993 Onset of the sawtooth crash. *Phys. Rev. Lett.* **70**, 3259.
- WALKER, J., BOLDYREV, S. & LOUREIRO, N. 2018 Influence of tearing instability on magnetohydrodynamic turbulence. *Phys. Rev. E* **98**, 033209.
- WAN, M., OUGHTON, S., SERVIDIO, S. & MATTHAEUS, W. H. 2012 von Kármán self-preservation hypothesis for magnetohydrodynamic turbulence and its consequences for universality. *J. Fluid Mech.* **697**, 296.
- WAN, M., RAPPAZZO, A. F., MATTHAEUS, W. H., SERVIDIO, S. & OUGHTON, S. 2014 Dissipation and reconnection in boundary-driven reduced magnetohydrodynamics. *Astrophys. J.* **797**, 63.
- WANG, Y., BOLDYREV, S. & PEREZ, J. C. 2011 Residual energy in magnetohydrodynamic turbulence. *Astrophys. J.* **740**, L36.

- WICKS, R. T., HORBURY, T. S., CHEN, C. H. K. & SCHEKOCIHIN, A. A. 2010 Power and spectral index anisotropy of the entire inertial range of turbulence in the fast solar wind. *Mon. Not. R. Astron. Soc.* **407**, L31.
- WICKS, R. T., HORBURY, T. S., CHEN, C. H. K. & SCHEKOCIHIN, A. A. 2011 Anisotropy of imbalanced Alfvénic turbulence in fast solar wind. *Phys. Rev. Lett.* **106**, 045001.
- WICKS, R. T., MALLETT, A., HORBURY, T. S., CHEN, C. H. K., SCHEKOCIHIN, A. A. & MITCHELL, J. J. 2013a Alignment and scaling of large-scale fluctuations in the solar wind. *Phys. Rev. Lett.* **110**, 025003.
- WICKS, R. T., ROBERTS, D. A., MALLETT, A., SCHEKOCIHIN, A. A., HORBURY, T. S. & CHEN, C. H. K. 2013b Correlations at large scales and the onset of turbulence in the fast solar wind. *Astrophys. J.* **778**, 177 [erratum: *Astrophys. J.* **782**, 118 (2014)].
- XU, S. & LAZARIAN, A. 2016 Turbulent dynamo in a conducting fluid and a partially ionized gas. *Astrophys. J.* **833**, 215.
- XU, S. & LAZARIAN, A. 2017 Magnetohydrodynamic turbulence and turbulent dynamo in partially ionized plasma. *New J. Phys.* **19**, 065005.
- YAGLOM, A. N. 1949 Local structure of temperature field in a turbulent flow. *Dokl. Acad. Nauk SSSR* **69**, 743.
- YAMADA, M., JI, H., HSU, S., CARTER, T., KULSRUD, R., BRETZ, N., JOBES, F., ONO, Y. & PERKINS, F. 1997 Study of driven magnetic reconnection in a laboratory plasma. *Phys. Plasmas* **4**, 1936.
- YANG, L., LI, H., GUO, F., LI, X., LI, S., HE, J., ZHANG, L. & FENG, X. 2020 Fast magnetic reconnection with turbulence in high Lundquist number limit. *Astrophys. J.* **901**, L22.
- YOUSEF, T. A., HEINEMANN, T., RINCON, F., SCHEKOCIHIN, A. A., KLEEORIN, N., ROGACHEVSKII, I., COWLEY, S. C. & MCWILLIAMS, J. C. 2008a Numerical experiments on dynamo action in sheared and rotating turbulence. *Astron. Nachr.* **329**, 737.
- YOUSEF, T. A., HEINEMANN, T., SCHEKOCIHIN, A. A., KLEEORIN, N., ROGACHEVSKII, I., ISKAKOV, A. B., COWLEY, S. C. & MCWILLIAMS, J. C. 2008b Generation of magnetic field by combined action of turbulence and shear. *Phys. Rev. Lett.* **100**, 184501.
- YOUSEF, T. A., RINCON, F. & SCHEKOCIHIN, A. A. 2007 Exact scaling laws and the local structure of isotropic magnetohydrodynamic turbulence. *J. Fluid Mech.* **575**, 111.
- YOUSEF, T. A. & SCHEKOCIHIN, A. A. 2009 Simulations of weak RMHD turbulence. Unpublished.
- ZAKHAROV, V. E., L'VOV, V. S. & FALKOVICH, G. 1992 *Kolmogorov Spectra of Turbulence I: Wave Turbulence*. Berlin: Springer.
- ZAKHAROV, V. E. & SAGDEEV, R. Z. 1970 Spectrum of acoustic turbulence. *Sov. Phys. Doklady* **15**, 439.
- ZELDOVICH, Y. B. 1956 The magnetic field in the two-dimensional motion of a conducting turbulent liquid. *Zh. Eksp. Teor. Fiz.* **31**, 154, English translation: *Sov. Phys. JETP* **4**, 460 (1957).
- ZHDANKIN, V., BOLDYREV, S. & CHEN, C. H. K. 2016a Intermittency of energy dissipation in Alfvénic turbulence. *Mon. Not. R. Astron. Soc.* **457**, L69.
- ZHDANKIN, V., BOLDYREV, S., PEREZ, J. C. & TOBIAS, S. M. 2014 Energy dissipation in magnetohydrodynamic turbulence: coherent structures or “nanoflares”? *Astrophys. J.* **795**, 127.
- ZHDANKIN, V., BOLDYREV, S. & UZDENSKY, D. A. 2016b Scalings of intermittent structures in magnetohydrodynamic turbulence. *Phys. Plasmas* **23**, 055705.
- ZHDANKIN, V., UZDENSKY, D. A. & BOLDYREV, S. 2015 Temporal analysis of dissipative structures in magnetohydrodynamic turbulence. *Astrophys. J.* **811**, 6.
- ZHDANKIN, V., UZDENSKY, D. A., PEREZ, J. C. & BOLDYREV, S. 2013 Statistical analysis of current sheets in three-dimensional magnetohydrodynamic turbulence. *Astrophys. J.* **771**, 124.
- ZHOU, M., BHAT, P., LOUREIRO, N. F. & UZDENSKY, D. A. 2019 Magnetic island merger as a mechanism for inverse magnetic energy transfer. *Phys. Rev. Res.* **1**, 012004(R).
- ZHOU, M., LOUREIRO, N. F. & UZDENSKY, D. A. 2020 Multi-scale dynamics of magnetic flux tubes and inverse magnetic energy transfer. *E-print* arXiv:2001.07291.
- ZOCCO, A. & SCHEKOCIHIN, A. A. 2011 Reduced fluid-kinetic equations for low-frequency

dynamics, magnetic reconnection, and electron heating in low-beta plasmas. *Phys. Plasmas* **18**, 102309.

ZRAKE, J. 2014 Inverse cascade of nonhelical magnetic turbulence in a relativistic fluid. *Astrophys. J.* **794**, L26.